Desregulación Génica en el Núcleo Epileptógeno de un Modelo Preclínico de Epilepsia: Implicaciones del Polimorfismo de Nucleótido Único p.His289Tyr en el Gen de la Subunidad 1 del Receptor de Kainato

---

Tesis doctoral de

Sandra Marcela Díaz Rodríguez

Directores

Ricardo Gómez-Nieto

Manuel Javier Herrero Turrión

Laboratorio de Trastornos Audiomotores

Instituto de Neurociencias de Castilla y León (INCyL)

Universidad de Salamanca

Salamanca, 2024

FINANCIACIÓN

La realización de este trabajo ha sido posible gracias a la obtención de un contrato de investigación predoctoral financiado por la Junta de Castilla y León (BOCYL, EDU/556/2019). Trabajo subvencionado por la Junta de Castilla y León a través del proyecto #SA075P20, cofinanciado con fondos FEDER, "una manera de hacer Europa".

AGRADECIMIENTOS

En primer lugar, quiero agradecer a la directora del laboratorio 12, la **Dra. Mª Dolores E. López** por su acogimiento en el laboratorio, constante apoyo y colaboración en la producción científica de este trabajo, al igual que a los directores de esta tesis, a los **Drs. Ricardo Gómez-Nieto y Javier Herrero-Turrión**, por su ayuda en la revisión y en la mejora científica de los artículos pertinentes para este trabajo de tesis doctoral.

Agradecerle también a los Drs. **Armando Die, Isabel Ivorra, Andrés Morales, José María Pereda y Javier Espinosa,** por su colaboración en la elaboración de los artículos científicos, sin su ayuda hubiera sido imposible concretar estos artículos.

A todos mis compañeros del laboratorio y compañeros del doctorado del INCYL, gracias por su compañía y la terapia de grupo en el café.

A mi quería Familia Española **Corrales Gómez**, ya no me imagino una vida sin ustedes… Gracias por acogerme todos estos años…convertirse en mis padres y hermanos…hoy solo puedo decirle que su generosidad me ha vuelto cada día mejor persona.

Mi mejor amigo, **Manuel Alejandro López**, te adoro, eres de mis personas favoritas del mundo. Gracias por escucharme desde la distancia y nunca dejarme desistir, darme ánimo cuando no podía más y hacerme reír siempre.

A mis amados padres, **José Manuel Diaz** y **Luz Yolanda Rodríguez**, por este sueño que me crearon desde niña y hoy lo cumplimos "Algún día vas a ser una exitosa profesional". Por ustedes, cada día me puse de pie a pesar de las adversidades. Los amo demasiado y siempre serán el amor de mi vida.

Mis queridas hermanas, **Nini** y **Mingus,** las amo infinitamente. Sois mi luz y mis estrellas, gracias por ser mis amigas y apoyarme desde la distancia.

A mi amado **David Corrales Gómez,** sin ti este sueño nunca hubiera podido empezar; cuando era pequeña soñé con ser investigadora y lo logre gracias a ti, "gracias por la financiación". Por caminar conmigo estos años, escuchar, llorar, reír y aguantarme cuando estaba enojada…gracias por ser tu mejor versión conmigo, por siempre gatitos.

LISTA DE PUBLICACIONES

Esta tesis corresponde a un compendio de tres artículos científicos publicados en revistas indexadas en Journal Citation Reports.

Díaz-Rodríguez SM [1,2,3], López-López D [1,2,3], Herrero-Turrión MJ [1,2,4], Gómez-Nieto R [1,2,3], Canal-Alonso A [5], López DE [1,2,3]. Inferior Colliculus Transcriptome After Status Epilepticus in the Genetically Audiogenic Seizure-Prone Hamster GASH/Sal. Frontiers in Neuroscience. 2020, 14:508. doi: 10.3389/fnins.2020.00508. FI: 4.67. Q2

Díaz-Rodríguez SM [1,2,3], Herrero-Turrión MJ [1,2,4], García-Peral C [1,2,3], Gómez-Nieto R [1,2,3]. Delving into the Significance of the His289Tyr Single-Nucleotide polymorphism in the Glutamate Ionotropic Receptor Kainate-1 (Grik1) Gene of a Genetically Audiogenic Seizure Model. *Frontiers in Molecular Neuroscience*. 2023. Volume 16. Doi: 10.3389/fnmol.2023.1322750. FI: 4.8. Q21

Díaz-Rodríguez SM [1,2,3], Ivorra I [6], Espinosa J [6], Vegar C [6], Herrero-Turrión MJ [1,2,4], López DE [1,2,3], Gómez-Nieto R [1,2,3], Alberola-Die A [6]. Enhanced Membrane Incorporation of H289Y Mutant GluK1 Receptors from the Audiogenic Seizure-Prone GASH/Sal Model: Functional and Morphological Impacts on *Xenopus* Oocytes. International Journal of Molecular Sciences. 2023 Nov 28;24(23):16852. doi: 10.3390/ijms242316852. Número especial "Epilepsy: From Molecular Basis to Therapy", de *International Journal of Molecular Sciences*, 2023, FI: 5.6. Q1

1. Institute of Neuroscience of Castilla and León, (INCYL). University of Salamanca, Salamanca, Spain
2. Institute of Biomedical Research of Salamanca (IBSAL). Salamanca, Spain
3. Dept Cell Biology and Pathology. University of Salamanca, Salamanca, Spain
4. Neurological Tissue Bank INCYL (BTN-INCYL).
5. *BISITE Research Group, University of Salamanca, Salamanca, Spain*
6. University of Alicante, Department of Physiology, Genetics and Microbiology., Alicante, Spain

RESUMEN

La epilepsia, un trastorno neurológico caracterizado por la predisposición sostenida a la generación de crisis convulsivas, engloba diversas manifestaciones comportamentales derivadas de la actividad neuronal aberrante en el cerebro. Comprender los complejos mecanismos subyacentes a estas crisis convulsivas es esencial para avanzar en la investigación y tratamiento de esta enfermedad neurológica. En las últimas décadas, la investigación en epilepsia se ha beneficiado notablemente de modelos animales diseñados para replicar los síntomas clave de la enfermedad. Estos modelos ofrecen una plataforma esencial para comprender aspectos genéticos y moleculares, contribuyendo significativamente al avance en el conocimiento y tratamiento de la epilepsia. El modelo animal empleado en esta tesis doctoral, conocido como como hámster con convulsiones audiogénicas de origen genético (GASH/Sal, del inglés *Genetic audiogenic seizures hamster* from Salamanca), se distingue por experimentar crisis convulsivas generalizadas de tipo tónico-clónico en respuesta a estímulos sonoros intensos, manifestando similitudes notables con las crisis de tipo Gran Mal observadas en humanos. Esta tesis doctoral tiene por objetivo ampliar la comprensión de los mecanismos genéticos y moleculares subyacentes a las convulsiones audiogénicas en el modelo GASH/Sal, proporcionando una plataforma valiosa para la investigación preclínica en epilepsia. Para ello, la tesis abarca diseños experimentales que involucran técnicas muy diversas como análisis *in silico* y modelaje de estructuras proteicas, técnicas moleculares para el análisis de expresión génica y de proteínas, así como inmunohistoquímica para la visualización de proteínas mediante microscopía de campo claro y microscopía láser confocal, junto con técnicas electrofisiológicas. La tesis doctoral se presenta por compendio de tres artículos científicos publicados en revistas indexadas en el *Journal Citation Reports.* El primer artículo tuvo como objetivo identificar las alteraciones en el patrón de expresión de genes en el colículo inferior (CI), el foco epileptogénico, del hámster GASH/Sal después del estado epiléptico. Empleando la técnica de secuenciación de ARN (RNA-Seq) se realizó un estudio comparativo entre el transcriptoma del CI de animales GASH/Sal frente al de animales control, hámsteres sirios dorados (*Mesocricetus auratus*), ambos sometidos a una estimulación sonora intensa, obteniendo un total de 36 genes diferencialmente expresados: 24 sobreexpresados (*Egr1-4*, factores de transcripción -*Fosb, JuncB*, *Fos* y *Npas4*-, genes involucrados en canales de potasio – *Kcns1* y *Kcnj13*-, transportador de nucleósido – *Slc28a1*-, *Gass45g* y *Ttr,* entre otros) y 12 infraexpresados (como dos genes relacionados con las rutas de señalización de calcio -*ATp2a3, Grin2c*- y la proteína del complemento *C6*). Este resultado fue posteriormente validado

mediante la técnica de retrotranscripción combinada con la PCR cuantitativa en tiempo real (RT-qPCR). Los genes diferencialmente expresados se clasificaron en categorías ontológicas asociadas con eventos epileptógenos similares a los producidos por las convulsiones tónicas generalizadas en humanos. Los análisis no solo revelaron cambios en la expresión génica asociados a las convulsiones audiogénicas sino también en la expresión de genes involucrados en rutas metabólicas, destacando las vías de señalización de interleucinas-4 y -13, así como las vías de transporte de nucleósidos y bases nitrogenadas en la membrana plasmática. En la vía glutamatérgica, identificamos varios genes diferencialmente expresados que correspondían con genes mutados previamente descritos, destacándose la mutación de un polimorfismo de nucleótido único en el gen *Grik1* (*del inglés, glutamate receptor ionotropic kainate-1*) que codifica la subunidad del receptor glutamato ionotrópico, de kainato tipo 1 (GluK1). Dicha mutación consiste en la sustitución de una citosina (C) por una timina (T) en la posición 9586732 de este gen *Grik1*, que implica el reemplazo en su proteína codificante del aminoácido histidina (His, H) en la posición 289 por una tirosina (Tyr, Y) (p.His289Tyr). El segundo artículo tuvo por objetivo explorar el impacto de esa mutación en la estructura y conformación de la proteína GluK1, así como en el patrón de expresión génica de *Grik1* y de su proteína GluK1 en las áreas cerebrales asociadas a las crisis convulsivas del modelo GASH/Sal. La predicción de la estructura tridimensional de GluK1 mostró una alteración en la conformación de la proteína en el dominio amino-terminal y una predicción correspondiente a un aumento en la estabilidad de la proteína. El análisis mediante RT-qPCR detectó alteraciones en el perfil de transcripción del gen *Grik1* dentro de la red neuronal asociada a las convulsiones audiogénicas. Adicionalmente, los resultados de Western blot mostraron modificaciones en los niveles de expresión de la proteína GluK1 en varias estructuras cerebrales, acompañadas por una distintiva isoforma de menor peso molecular en los colículos inferior y superior. Esto se correlaciona con disparidades en la distribución de la inmunoreactividad para GluK1 en múltiples regiones cerebrales, incluyendo el cerebelo, hipocampo, subdivisiones de los colículos inferior y superior, y la corteza prefrontal. Destacó la inmunoreactividad difusa que se acumulaba en el soma neuronal, fibras axonales y terminales nerviosos, exhibiendo una concentración prominente en proximidad al núcleo celular. Esto sugiere posibles alteraciones en el mecanismo de transporte de GluK1, que podría afectar posteriormente la transmisión sináptica de glutamato. Finalmente, el tercer artículo evaluó el impacto funcional de también la mutación p.His289Tyr, teniendo en cuenta su posible efecto en el dominio amino-terminal que está implicado en el ensamblaje del canal receptor y el tráfico citoplasmático a la membrana. Examinamos, mediante la técnica de fijación de voltaje de dos electrodos, las

corrientes evocadas por el kainato (I_{Ka}s) en receptores GluK1 de tipo silvestre (control) y mutados expresados heterólogamente en ovocitos de *Xenopus laevis*, identificando una mejora en el porcentaje de I_{Kas} en Gluk1_p.His289Tyr en comparación con el control, sin que se manifestarán afectadas sus propiedades funcionales. De acuerdo con estos resultados, también observamos que GluK1_p.His289Tyr presenta un mayor direccionamiento hacia la membrana plasmática en ovocitos de *X. laevis* y una mayor incorporación de la proteína en la membrana. Estos resultados corroboran los obtenidos en el segundo artículo, sugiriendo posibles trastornos en el mecanismo de transporte de GluK1, con impacto en la transmisión sináptica de glutamato. En conjunto, esta tesis doctoral respalda la relevancia del modelo GASH/Sal en la investigación de las crisis convulsivas, facilitando la identificación y caracterización de genes, sustratos moleculares y aspectos morfológicos asociados a este fenómeno. Estos hallazgos respaldan no solo futuras investigaciones en el campo de la epilepsia, sino que también sientan las bases para el desarrollo de estrategias terapéuticas dirigidas al sistema glutamatérgico en general y, de manera más específica, a los receptores de tipo kainato.

ÍNDICE

1. INTRODUCCIÓN

Sigo cruzando ríos
Andando selvas, amando el sol,
Cada día sigo sacando espinas
De lo profundo del corazón

Leonel García Núñez De Cáceres
María Natalia Lafourcade Silva

1. INTRODUCCIÓN

1.1 Epilepsia: Una Enfermedad Intrincada de Múltiples Dimensiones

La epilepsia, un trastorno cerebral caracterizado por episodios repetidos de convulsiones, emerge como una manifestación de actividad neuronal descontrolada y anormal. La complejidad de esta condición reside en su naturaleza heterogénea, presentando una variedad de trastornos que comparten la manifestación de crisis convulsivas, pero divergen en términos de origen, expresión clínica, respuesta terapéutica, pronóstico y comorbilidades asociadas (Gómez-Nieto et al., 2021). Es uno de los trastornos neurológicos más frecuentes, con un riesgo acumulado a lo largo de la vida del 1-2%. Diversos factores desencadenantes pueden subyacer a esta afección compleja, abarcando desde anomalías estructurales cerebrales, predisposición genética, influencias infecciosas, cambios metabólicos, respuestas inmunológicas y, en ocasiones, causas aún por identificar (WHO, 2006). Algunas estimaciones sugieren que una proporción significativa de la población mundial experimenta epilepsia debido a distintas combinaciones de estos factores (McCandless & Schwartzenburg, 1982). Destacable es el componente genético, evidente en aproximadamente un tercio de los casos de epilepsia (Ottman, 2005), incluso sugiriéndose la posibilidad de que hasta seis síndromes epilépticos diferentes se asocien con la herencia monogénica (Berkovic & Wiebe, 2019). La diversidad en las causas y manifestaciones clínicas de esta afección enfatiza la necesidad continua de investigación y la evolución constante en el tratamiento y manejo de la epilepsia dentro de la práctica médica.

La epilepsia, en su variabilidad etiológica, ha sido categorizada según el patrón fenotípico de las crisis epilépticas que manifiesta. La denominada **"crisis convulsiva"** se define por una secuencia abrupta y desordenada de movimientos corporales, acompañada por alteraciones en el comportamiento, como consecuencia de una actividad neuronal anómala en el cerebro. Este fenotipo se manifiesta con síntomas que abarcan desde la pérdida de conciencia hasta cambios emocionales, pérdida del control muscular y manifestaciones temblorosas (Liga Internacional contra la Epilepsia, según sus siglas en inglés, *ILAE*) (Scheffer et al., 2017). En relación con distintos términos utilizados para describir esta condición, como "**desorden convulsivo**", "**crisis epiléptica**" y "**crisis cerebrales**", todos se refieren a los episodios de actividad cerebral anormal que son repentinos, breves e intensos, características fundamentales de la epilepsia y conocidos como "episodios paroxísticos" (Scheffer et al., 2017). Por consiguiente, estos términos, incluyendo los desórdenes y las crisis epilépticas, se

caracterizan por una predisposición continua a experimentar una actividad neuronal anormal en el cerebro, la cual interrumpe de manera súbita y temporal su funcionamiento (Fisher et al., 2005; Kwan et al., 2009; Perucca, 2017). Esta anomalía da lugar a la alteración de señales inhibitorias y excitatorias en los circuitos neuronales, ya sea por hiperexcitabilidad o por la disminución de la inhibición, lo que en última instancia conduce al desencadenamiento de una crisis epiléptica (Boison, 2013). La predisposición a experimentar crisis epilépticas puede originarse por una disfunción en los sistemas excitatorios e inhibitorios del cerebro, en los que los neurotransmisores glutamato y GABA (ácido gamma aminobutírico) desempeñan un papel crucial (Garcia-Cairasco et al., 1996). Esta excitabilidad neuronal anormal involucra al glutamato como un neurotransmisor fundamental en las convulsiones, lo que conlleva a daño excitotóxico. Las convulsiones crónicas alteran la expresión de receptores y transportadores de glutamato, contribuyendo al desarrollo de la epilepsia (Barker-Haliski & White, 2015). Esta disfunción del glutamato está relacionada con trastornos del sistema nervioso central, como la depresión, frecuentemente observada en pacientes con epilepsia (Barker-Haliski & White, 2015). Por otro lado, estudios neurohistoquímicos en modelos animales han revelado un aumento en los niveles de GABA en el hipocampo de aquellos que padecen crisis convulsivas (Ilie et al., 2012). Esta alteración en el equilibrio entre neurotransmisores excitadores e inhibidores podría contribuir significativamente a la génesis y mantenimiento de la epilepsia, evidenciando la importancia crítica de un sistema glutamatérgico y GABAérgico funcional en la regulación de las crisis epilépticas. Las descargas eléctricas pueden producirse en diferentes regiones del sistema nervioso central (SNC), originando convulsiones que pueden iniciarse con episodios convulsivos breves o de contracciones musculares hasta convulsiones prolongadas y graves, pérdida de consciencia y del control de esfínteres (Boison, 2013; Löscher, 2017; Wada et al., 1970). Por otra parte, es de destacar el hecho de que gran parte del conocimiento actual sobre la epilepsia deriva de la investigación con modelos animales experimentales (Fisher et al., 2005). Estos modelos se emplean para inducir epilepsia mediante el uso controlado de drogas convulsionantes, la privación selectiva de metabolitos o la aplicación de estimulación eléctrica (Kandratavicius et al., 2014). Recientemente, se están empleando modelos animales con predisposición genética a este trastorno específico (Serikawa et al., 2015). Estos modelos genéticos de crisis convulsivas presentan algunas ventajas notables, como fundamentalmente la susceptibilidad hereditaria, evitando de este modo el uso de productos químicos para inducir esta patología, y garantizándose así la compatibilidad en los diseños experimentales. Además, empleando estos modelos animales se permite la inducción controlada de convulsiones mediante estimulación sensorial y ofrecen una amplia información a niveles molecular, celular y conductual, lo que los convierte en herramientas esenciales para

comprender los mecanismos subyacentes en el origen y propagación de las convulsiones (Kandratavicius et al., 2014; Ross & Coleman, 2000).

1.2 Modelos Experimentales de Epilepsias Reflejas

El uso de modelos animales con convulsiones y/o epilepsia es esencial para comprender los mecanismos subyacentes a esta enfermedad (Scheffer et al., 2017). El origen de dichos modelos es muy variado. Existen algunos modelos experimentales inducidos por agentes químicos como el kainato o la pilocarpina; físicos, como descargas eléctricas o estímulos repetitivos (*kindling*) o animales con epilepsia de origen genético. Se cree que el primer roedor con crisis convulsivas audiógenas (CCA) fue observado por Studenzov en 1924 estudiaba el condicionamiento por sonidos en ratones (Poletaeva et al., 2017; Ross & Coleman, 2000). Como se muestras en la Figura 1 en la actualidad existen una gran variedad de modelos animales utilizados en la investigación de la epilepsia, divididos principalmente en dos categorías: aquellos con una predisposición genética a esta patología y aquellos modelos de animales silvestres en los que se inducen crisis epilépticas de forma artificial y exógena mediante fármacos o estimulaciones eléctricas. Dentro del primer grupo existen tres cepas de ratas genéticamente predispuestas a experimentar crisis epilépticas: la rata Wistar Audiogénica (*WAR*), que desarrolla crisis tónico-clónicas generalizadas focalizadas en el tronco del encéfalo (Garcia-Cairasco, 2002; Garcia-Cairasco et al., 1996, 2017); las ratas genéticamente propensas a la epilepsia (*GEPRs*, por sus siglas en inglés "*genetically epilepsy-prone rat"*), criadas selectivamente y que son susceptibles a la epilepsia tanto por estímulos auditivos como por convulsivos químicos (p. ej. pilocarpina, pentilentetrazol, glutamato monosódico y ácido kaínico) , así como a padecer hipertermia e inflamación (Hirvonen et al., 2012; Jobe & Dailey, 2006), y finalmente, las ratas Estrasburgo con epilepsia genética de ausencia (*GAERS*, por sus siglas en inglés "*Genetic Absence Epilepsy Rat from Strasbourg*"), caracterizadas por presentar convulsiones tónicas (Franois et al., 2008). Por otra parte, dada la importancia en esta tesis doctoral del grupo de roedores genéticamente propensos a sufrir CCA, se mencionarán de forma más detallada en el siguiente apartado.

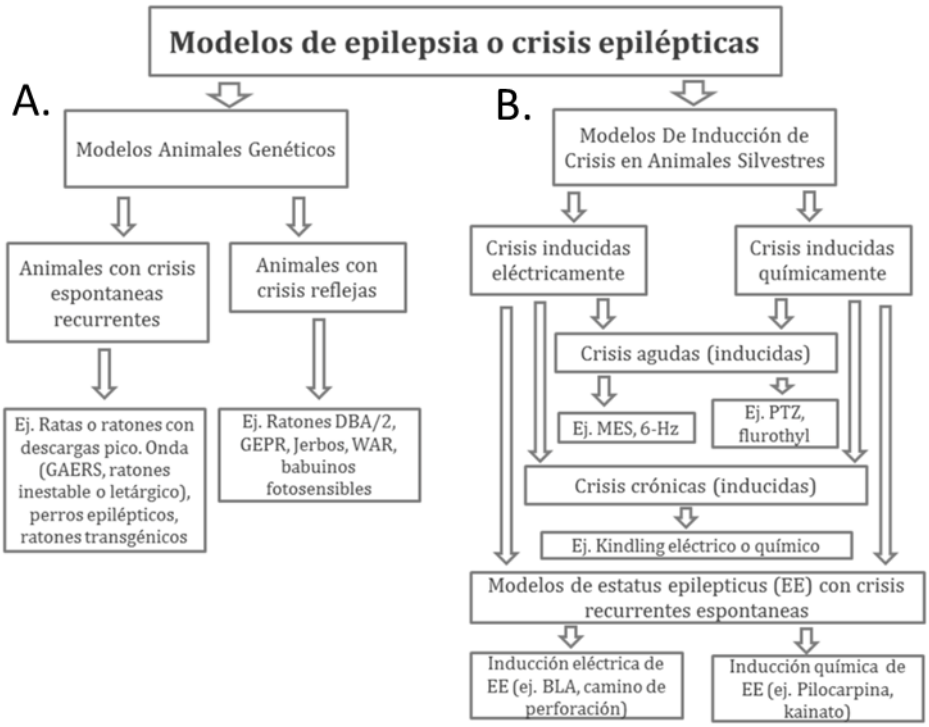

Figura 1. Diagrama de los modelos actuales de experimentación animal en el estudio de la epilepsia. **A**, Modelos animales de epilepsia de origen genético. **B**, Modelos animales de tipo silvestre con inducción de esta patología mediante diferentes fármacos. Modificado de (Barrera-Bailón et al., 2013; Löscher, 2017)

1.3 El Modelo Genético de Crisis Convulsivas Audiogénicas, GASH/Sal

Dentro de la variedad de cepas de roedores genéticamente propensas a sufrir convulsiones, el único hámster científicamente disponible que muestra susceptibilidad a las convulsiones por sonido es el modelo GASH/Sal (por sus siglas en inglés, "*Genetic Audiogenic Seizure Hamster from Salamanca"*) que presenta un patrón de herencia autosómico recesivo (Muñoz et al., 2017). En la cepa GASH/Sal, la estimulación acústica de alta intensidad provoca convulsiones tónico-clónicas generalizadas que pueden reducirse o eliminarse después de la administración de compuestos anticonvulsivos (p. ej. barbitúricos, benzodiazepinas, bromuros, carbamatos e hidantoinatos) (Barrera-Bailón et al., 2013; Cabral-Pereira et al., 2021; Werner & Coveñas, 2017). El grupo de investigación en el que he desarrollado esta tesis doctoral ha contribuido al amplio conocimiento integral que se conoce actualmente sobre los aspectos neuroetológicos (Barrera-Bailón et al., 2013, 2017), electrofisiológicos (Carballosa-Gonzalez et al., 2013), neuroquímicos (Fuerte-Hortigón et al., 2021; Prieto-Martín et al., 2017), moleculares (Díaz-Casado et al., 2020; Díaz-Rodríguez et al., 2020; López-López et al., 2017) y morfológicos (Sánchez-Benito et al., 2017, 2020) que subyacen a las CCA en este modelo GASH/Sal. Las

convulsiones tónico-clónicas generalizadas en este modelo se definen por un breve período de latencia posterior a la estimulación auditiva, seguido de un comportamiento descontrolado, una fase convulsiva y, finalmente, un estado de estupor, con origen en el tronco encefálico (Muñoz et al., 2017). El perfil de convulsiones del GASH/Sal es similar a los exhibidos por otros modelos de susceptibilidad hereditaria (p. ej. las ratas WAR, por sus siglas en inglés "*Wistar Audiogenic Rat*"), ya que también disminuye después de los seis meses de edad, aunque esta propensión a convulsionar se mantiene a través de generaciones (Muñoz et al., 2017). Tanto en los modelos animales como el del GASH/Sal, como en las ratas WAR, GEPRs y GAERS, se ha realizado unos exhaustivos análisis de las crisis convulsivas. Estos estudios abarcan la minuciosa caracterización de las crisis como auténticas crisis epilépticas, la investigación de sus patrones de transmisión, la descripción de sus bases neuroquímicas y neuroanatómicas, la evaluación de respuestas a fármacos antiepilépticos (tanto clásicos, como por ejemplo el valproato, y nuevos, como la lamotrigina, entre otros), así como el análisis de la expresión génica en el colículo inferior (CI), que es considerado el núcleo epileptógeno por excelencia. En definitiva, todos estos análisis han delineado el sustrato anatómico de las crisis convulsivas sensoriales, brindando perspectivas de cómo se generan este tipo de crisis.

1.4 Sustrato Neuroanatómico de las Crisis Convulsivas Audiogénicas

En primer lugar, el sustrato anatómico responsable de la génesis y propagación de la crisis audiogénica se origina en el CI, uno de los principales núcleos del mesencéfalo en la vía auditiva (Muñoz et al., 2017). Este núcleo está dividido en 3 regiones: núcleo central del CI (NCCI), corteza dorsal del CI (CDCI) y corteza externa del CI (CECI). Mientras que la CDCI y la CECI son polimodales desde el punto de vista de la transmisión de la información sensitiva, el NCCI procesa exclusivamente la información auditiva. Diversos estudios genéticos, farmacológicos, electrofisiológicos y morfológicos indican que este núcleo es crítico para la iniciación de las CCA (Raisinghani & Faingold, 2003). Además, como se presenta gráficamente en la Figura 2 (véase más detalles en su pie de figura), investigaciones recientes han señalado que las lesiones en otras estructuras, como el colículo superior (Fuentes-Santamaría et al., 2007; Raisinghani & Faingold, 2003), el sistema olivococlear y el propio receptor auditivo (Sánchez-Benito et al., 2020), también desempeñan un papel fundamental en la generación de las crisis epilépticas. Además, otras áreas mesencefálicas como la sustancia gris periacueductal han sido asociadas con la red neuronal implicada en las crisis auditivas clónicas generalizadas (Raisinghani & Faingold, 2003). Incluso regiones adicionales del telencéfalo, cerebelo y la

corteza han sido relacionadas con las convulsiones provocadas por estímulos auditivos (Raisinghani & Faingold, 2003).

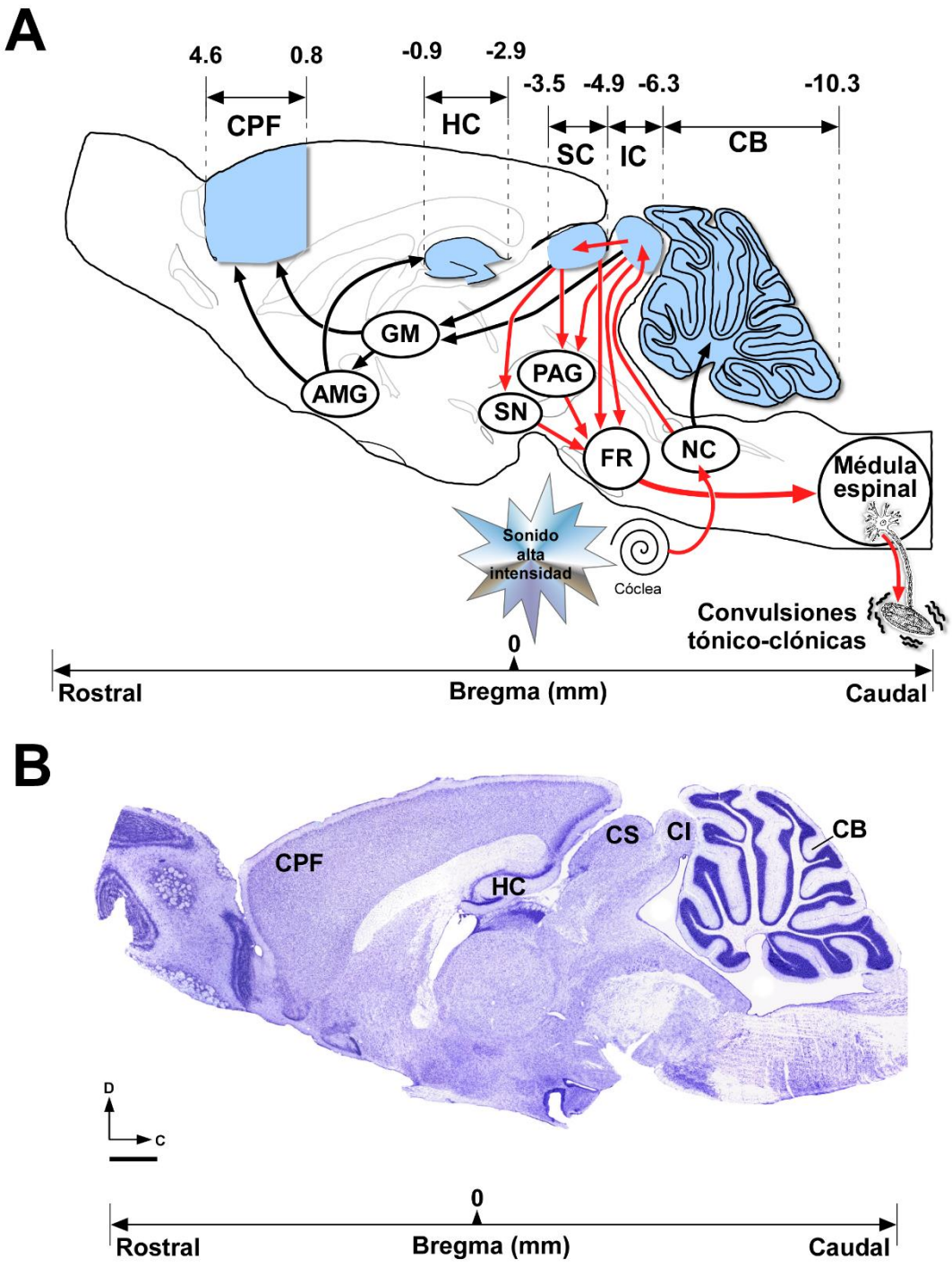

Figura 2. Esquema de los núcleos cerebrales implicados en el desencadenamiento y propagación de las convulsiones audiogénicas (CCA). **A**, Visión general de las estructuras cerebrales involucradas en la red neuronal asociada con CCA agudas y crónicas. La red neuronal que desencadena las convulsiones (representada con flechas rojas) involucra alteraciones en las entradas auditivas ascendentes desde el receptor coclear, a lo largo de la vía auditiva del tronco encefálico (núcleo coclear) hasta el colículo

inferior (CI) (Faingold, 1999; Ribak & Morin, 1995; Sánchez-Benito et al., 2020). La actividad neuronal aberrante en el CI inicia la convulsión audiogénica que se propaga a través de múltiples proyecciones hacia el colículo superior (CS), la sustancia negra (SN), la materia gris periacueductal (PAG) y la formación reticular (FR) del tronco encefálico, que a su vez se proyecta hacia la médula espinal, mediando en última instancia las convulsiones tónico-clónicas (Garcia-Cairasco, 2002). Durante las CCA repetitivas y frecuentes, la red de convulsiones puede extenderse hacia otras regiones cerebrales (proyecciones representadas con flechas negras) como el cuerpo geniculado medial (GM), la amígdala (AMG), el hipocampo (HP) y la corteza prefrontal (CPF) (Faingold, 1999). El cerebelo (CB), que recibe entradas auditivas, podría estar involucrado en la red de CCA (Streng & Krook-Magnuson, 2021; Traynelis et al., 2010). Las regiones cerebrales representadas en azul fueron seleccionadas para los estudios planteados en la presente tesis doctoral. **B**, Sección representativa teñida con Nissl de la sección sagital del cerebro de hámster, en la que se basó el esquema mostrado en la anterior imagen A, muestra las áreas cerebrales incluidas en esta tesis doctoral. Se utilizaron coordenadas de referencia de bregma (en mm) para la selección de esas regiones cerebrales. Barra de escala = 1 mm. (Datos de bregma obtenidos del atlas del cerebro de hámster de (Morin & Wood, 2001).

1.5 Implicación del Sistema Glutamatérgico en los Mecanismos del Proceso Epiléptico

El sistema glutamatérgico desempeña un papel fundamental en los procesos epilépticos, siendo el glutamato el principal neurotransmisor excitatorio en el cerebro de mamíferos. Gran parte de la investigación pasada en epilepsia se ha enfocado en comprender el papel del glutamato en las convulsiones y la epilepsia. De hecho, las crisis epilépticas desencadenan un incremento notable en los niveles de glutamato en el espacio extracelular, promoviendo así la excitotoxicidad. Este fenómeno implica una sobreestimulación de los receptores de glutamato que ha sido asociado con una sobreactivación de las neuronas, desencadenando un daño celular que puede contribuir al proceso patológico de las convulsiones y a la progresión de la epilepsia (Barker-Haliski & White, 2015). De esta forma, las convulsiones crónicas pueden modificar la expresión de receptores y transportadores de glutamato, lo que conlleva a la epileptogenesis. La evidencia también sugiere una relación entre la patología del glutamato en la epilepsia y otros trastornos del sistema nervioso central, como la depresión, comúnmente asociada a la epilepsia (Barker-Haliski & White, 2015). Claramente el sistema glutamatérgico se encuentra fuertemente implicado en gran parte de la señalización aberrante y la patología resultante de la epilepsia, por lo que explorar los diversos mecanismos glutamatérgicos vinculados con esta condición neurológica es crucial. Por consiguiente, una comprensión más profunda de la implicación del sistema glutamatérgico, en particular de los receptores de glutamato (el enfoque principal de esta tesis doctoral), podría brindar claridad sobre la

alteración en la conectividad y sincronización que desempeña un papel significativo en susceptibilidad a sufrir crisis convulsivas y a la evolución de la enfermedad. Este conocimiento avanzado podría, además, allanar el camino hacia estrategias terapéuticas más eficaces y enfoques preventivos para pacientes afectados por la epilepsia.

Los receptores de glutamato se ubican en la superficie celular, permitiendo que este neurotransmisor desempeñe su función en el entorno extracelular. En el SNC, la actividad del glutamato como neurotransmisor se realiza mediante la interacción con dos tipos de receptores: los metabotrópicos, que están acoplados a proteínas G, y los ionotrópicos, que consisten en canales iónicos activados por ligandos y permiten el paso de cationes (Watkins & Jane, 2006). En el caso de los receptores de glutamato ionotrópicos, tomados más en consideración su importancia en esta tesis doctoral, se dividen en cuatro tipos, los receptores de ácido α-amino-3-hidroxi-5-metil-4-isoxazolpropiónico (*AMPA*), los receptores de ácido kaínico o kainato (*KAR*), los receptores de N-metil-D-aspartato (*NMDA*) y los receptores GluD (receptores delta o δ) (Traynelis et al., 2010; Watkins & Jane, 2006) (Figura 3). Estos receptores desempeñan diversas funciones, incluyendo la transmisión sináptica normal, procesos de plasticidad neuronal como la potenciación y depresión sináptica de larga duración, los cuales están asociados con la memoria y el aprendizaje. Asimismo, intervienen en la sinaptogénesis y el desarrollo neuronal (C. V. Hansen et al., 2018). En general, se considera que la desregulación del sistema glutamatérgico puede ser el origen de algunos tipos de epilepsia además de contribuir al desarrollo de distintos tipos de trastornos del SNC como son los casos de la enfermedad de Alzheimer, Corea de Huntington, esclerosis lateral amiotrófica, enfermedad de Parkinson, o isquemia cerebral (Sihra et al., 2014; Traynelis et al., 2010). Así, por ejemplo, es ampliamente aceptado por la comunidad científica que un desequilibrio en la concentración del glutamato presente en el medio extracelular, al depender del balance existente entre su liberación y su retirada (J.-M. Li et al., 2010), puede desencadenar distintos tipos de procesos epilépticos (Fritsch et al., 2014; Rodríguez-Muñoz et al., 2018). Asimismo, también se conoce que, de forma más específica, la inhibición de los receptores NMDA puede inhibir los procesos epileptogénicos en los modelos animales de post-estatus epilépticos (Chou et al., 2020; Gielen et al., 2008; Kim et al., 2013; Rodríguez-Muñoz et al., 2015, 2018).

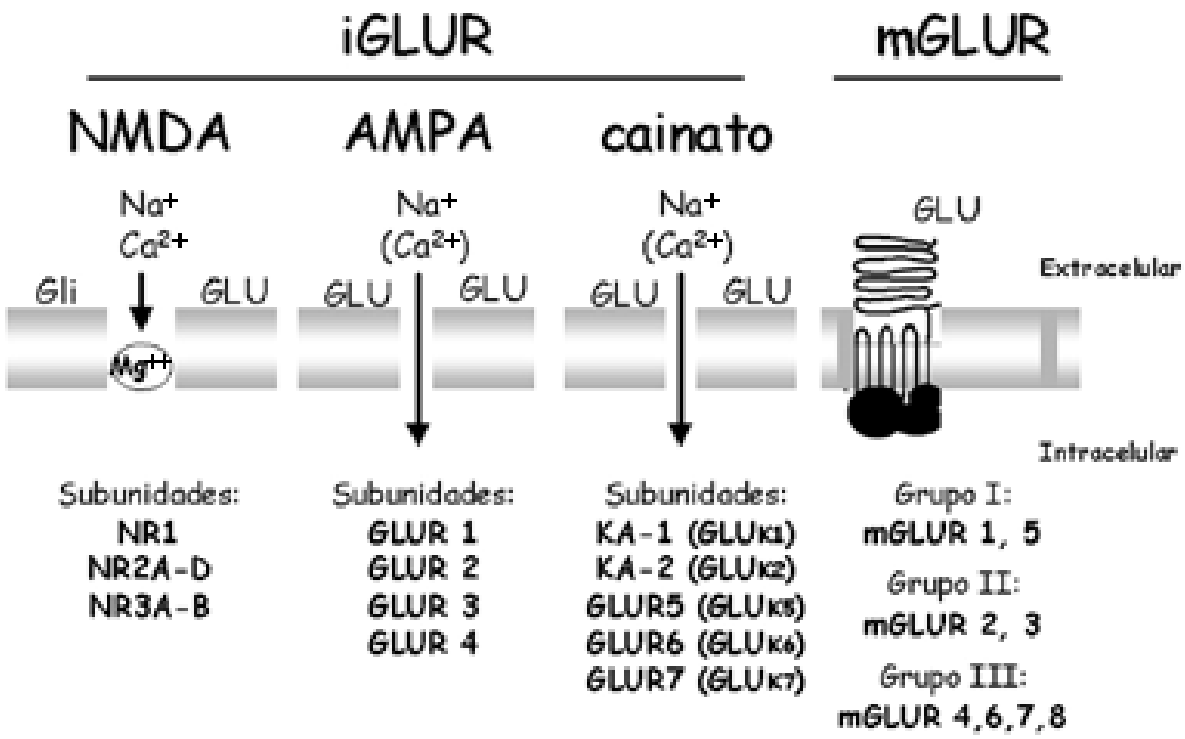

Figura 3. Tipos de Receptores de Glutamato: Ionotrópicos (iGLUR) y Metabotrópicos (mGLUR). Se observan las distintas subunidades que constituyen cada receptor iGLUR y mGLUR, resaltando la complejidad y diversidad de estas importantes estructuras en la señalización neuronal.

En el caso más concreto de los KAR, éstos están ampliamente distribuidos en todo el SNC, tanto en neuronas presinápticas como postsinápticas, modulando la liberación de neurotransmisores tanto excitatorios como inhibitorios que contribuyen al funcionamiento global neuronal (Carta et al., 2014; Lerma y Marques, 2013; Sihra et al., 2014). En ciertas sinapsis glutamatérgicas, la activación de los KAR puede generar una modulación de doble efecto o bifásica. Por un lado, la activación de los KAR ubicados en la parte presináptica de las sinapsis excitadoras puede inducir una disminución en la liberación del neurotransmisor glutamato. Por otro lado, la activación de los KAR situados en la membrana postsináptica, en conjunto con otros receptores de glutamato como los del tipo NMDA o AMPA, puede ocasionar la liberación de glutamato, lo que desencadena la apertura de canales iónicos y, consecuentemente, la despolarización de la membrana postsináptica (Perkinton & Sihra, 1999; Sihra et al., 2014).Por otra parte, cabe mencionar que los KAR se incorporan a las membranas de las neuronas en combinaciones homoméricas o heteroméricas. Como se esquematiza en la Figura 4, los KAR pueden estar conformados hasta por cinco proteínas-subunidades denominadas GluK1-5, codificados por los genes receptor de kainato tipo 1-5 (*Grik1-5*) (Collingridge et al., 2009; Pinheiro & Mulle, 2006). Para constituir un KAR, la presencia de las

subunidades GluK1-3 es obligatoria, siendo capaces de formar canales homoméricos, mientras que cuando un KAR está integrado también por las subunidades GluK4-5 forman receptores heteroméricos (Contractor et al., 2011a; Traynelis et al., 2010). Las subunidades GluK1-5 se han descrito en distintas áreas y/o núcleos del SNC como en las fibras musgosas, en las interneuronas del hipocampo, la amígdala lateral, los ganglios de la raíz dorsal, las células bipolares de la retina y en el núcleo estriado de la corteza cerebral (Artinian et al., 2011; Huettner et al., 1998; Traynelis et al., 2010; Watkins & Jane, 2006). Asimismo, los genes que codificadas las subunidades Gluk1-Gluk5 en la migraña (Swanson et al., 1996), Alzheimer (Aronica et al., 1997), esquizofrenia (Begni et al., 2002; Garey et al., 2006), depresión (Wilson et al., 2006), trastorno bipolar (Begni et al., 2002; Schiffer & Heinemann, 2007), retraso mental (Motazacker et al., 2007), autismo (Jamain et al., 2002) y la propia epilepsia(Boison, 2013; Fritsch et al., 2014; Gariboldi et al., 1996; Wada et al., 1970).

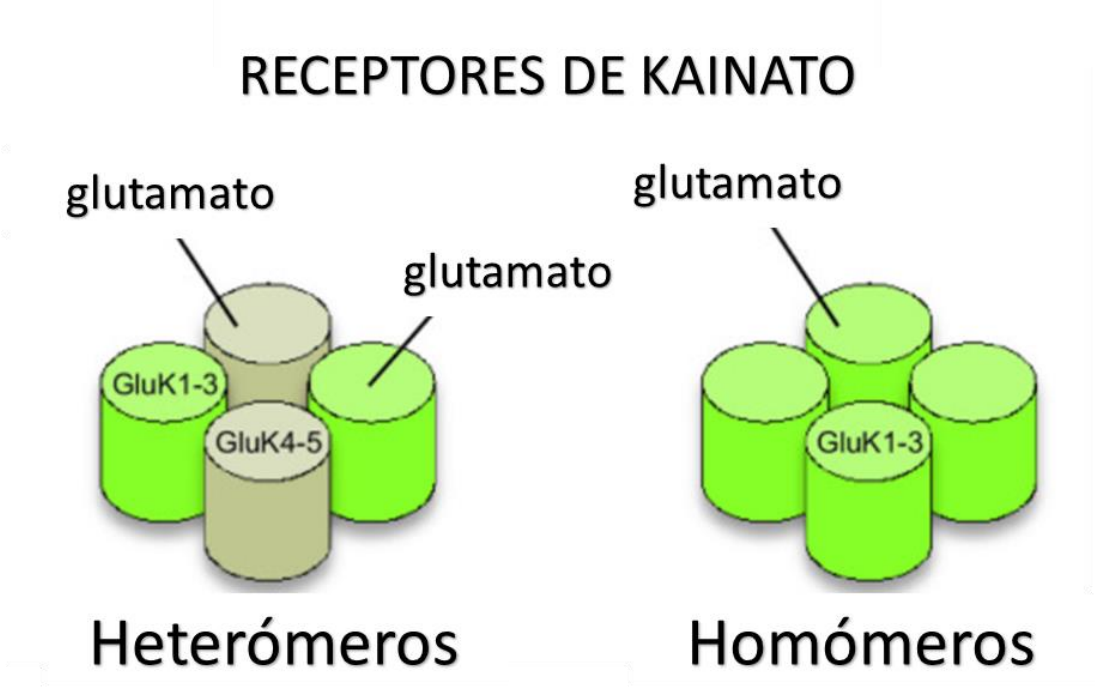

Figure 4. Diversidad estructural de los receptores de kainato (KAR). Las subunidades del receptor de kainato, GluK1-3, tienen la capacidad de ensamblarse como homómeros. Por otro lado, la presencia simultánea de las subunidades GluK4-5 junto con GluK1-3 da lugar a la formación de heterómeros. Destaca la variabilidad y adaptabilidad de los receptores de kainato en la transmisión sináptica. Tomado de (C. V. Hansen et al., 2018).

Como se muestra en la Figura 5 (véase también más detalles en su pie de figura), los KAR comparten una topología de dímeros que se ensamblan conformando un tetrámero.

Asimismo, todas las subunidades GluK1-5 pueden estar sometidas a distintos tipos de modificaciones postraduccionales (glicolisaciones, fosforilaciones, palmitoilaciones y/o acetilaciones) y, a su vez, a éstas se les pueden unir distintos tipos de proteínas auxiliares como las proteínas NETO1 y NETO2 (por sus siglas en inglés, *Neuropilin And Tolloid Like 1 - 2,* respectivamente) (Orav et al., 2017), generando un tipo de estructura del receptor altamente dinámica que, al finalizar su procesamiento y estabilización, se presentan en la membrana plasmática de la neurona conformado en los siguientes dominios (Figura 5):

- Dominio amino-terminal (*ATD*, por sus siglas en inglés, *amino terminal domain*): esencial en el ensamblaje del receptor, su tráfico intracelular y en la regulación funcional del propio KAR (Duan et al., 2018; Karakas et al., 2009; Rossmann et al., 2011; Sheng et al., 2017; Straub et al., 2016).

- Dominio de unión a ligando (*LBD*, por sus siglas en inglés, *ligand binding domain*): en él residen los sitios de unión a agonistas, antagonistas competitivos y algunos moduladores alostéricos como cyclothiazide, aniracetam y CX614 (Galen Wo y Oswald, 1995; Wo y Oswald, 1994).

- Dominio transmembrana (*TMD*, por sus siglas en inglés, *transmembrane domain*): incluye las cuatro regiones de domino transmembrana (*M1-M4*) y están implicadas en el enlace de todos los dominios de la proteína (Karakas et al., 2009b; Rossmann et al., 2011).

- Dominio C-terminal citoplásmico (*CTD*, por sus siglas en inglés, *carboxyl terminal domain*): es en este dominio donde ocurre la mayor cantidad de modificaciones postraduccionales, contribuyendo así a la complejidad y regulación fina de la función de la proteína (Contractor et al., 2011).

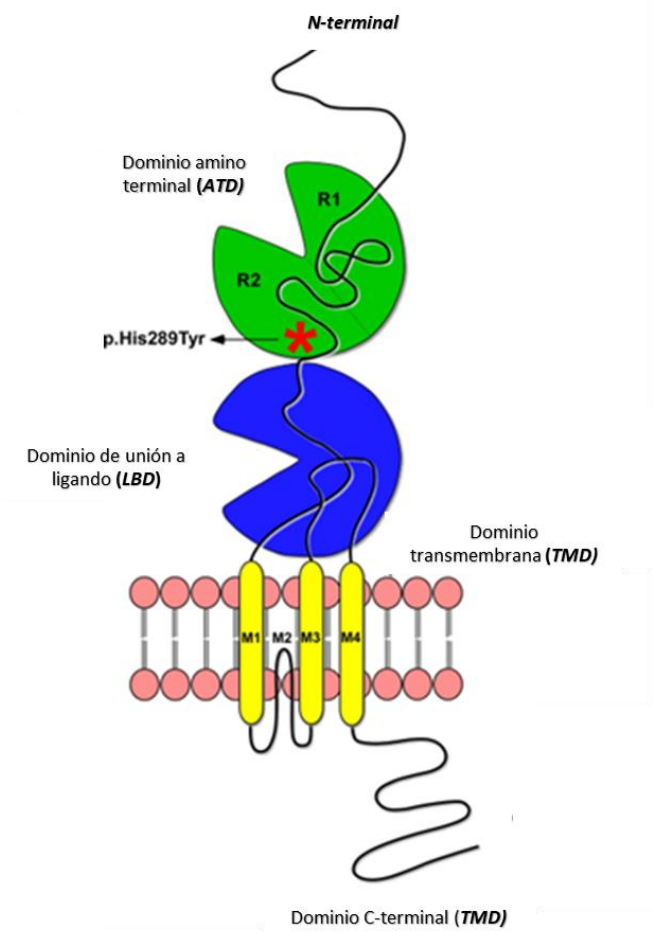

Figura 5. Esquema que muestra la topología de la proteína-subunidad GluK1. Esta subunidad contiene un dominio amino terminal extracelular (*ATD*), seguido de un dominio transmembrana (*M1*), un "*p-loop*" que se sumerge en la bicapa lipídica y forma el poro de la membrana (*M2*) que, a su vez, contiene dos dominios transmembrana sucesivos (*M3 y M4*) que delimitan un bucle extracelular y un bucle intracelular, y, por último, un dominio C-terminal (CTD). El sitio de unión del glutamato se compone de dos segmentos ubicados en el dominio de unión a ligando (LBD, S1 y S2), mientras que el ATD presenta una estructura bilobulada en forma de concha, conformada por dos dominios regulatorios, denominados R1 y R2. La ubicación del polimorfismo p.H289Y en el modelo GASH/Sal está en la región R2 del ATD (representado con un punto rojo asterisco). Esquema de elaboración propia con la información proporcionada en (Furukawa, 2012; Selvakumar et al., 2021).

Dada la importancia del dominio ATD en el caso concreto de la proteína-subunidad GluK1 en el desarrollo de esta tesis doctoral y tal como se muestra en la Figura 5 es de interés destacar que este dominio tiene una estructura bilobulada, con dos lóbulos (*R1 y R2*) altamente conservados (Herguedas et al., 2013). En el procesamiento de la subunidad GluK1, al igual que para otras subunidades similares, el dominio ATD se inserta en la membrana del retículo

endoplásmico siendo sometido a distintos tipos de modificaciones postraduccionales impulsando la dimerización de los dominios LBD y el propio ATD (K. B. Hansen et al., 2021). Posteriormente, la subunidad GluK1 dimerizada se incorpora a la membrana plasmática neuronal y el dominio ATD es esencial en la capacidad de interaccionar con distintos tipos de compuestos alostéricos selectivos influyendo en la dinámica del dominio LBD (Copits et al., 2014; Hansen et al., 2021; Mathers y Usherwood, 1976), permitiendo, en última instancia, cambios en la apertura del canal en respuesta a los ligandos del dominio ATD (Gielen et al., 2008).

En consecuencia, una alteración molecular y/o estructural en el dominio ATD puede contribuir a distintos tipos de cambios funcionales como en la excitación postsináptica, a nivel presináptico, y la propia regulación de la expresión sináptica y superficial de los KAR (Duan et al., 2018a; Fritsch et al., 2014). Hasta la fecha, la mayoría de las variantes genéticas patogénicas descritas en las distintas subunidades que pueden conformar los KAR se localizan en los dominios ATD y TMD (Tabla 1) (K. B. Hansen et al., 2021). Cabe destacar que, en relación con el dominio ATD de la subunidad GluK1, no se ha informado de ninguna variante asociada con epilepsia. Sin embargo, se han documentado mutaciones en el gen codificante de esta subunidad (Grik1) que están vinculadas a la epileptogénesis de tipo juvenil (Izzi et al., 2002a). Además, estas mutaciones se han asociado con epilepsia de lóbulo temporal en estudios de genética poblacional en humanos (Berkovic & Wiebe, 2019). Por otro lado, también han sido asociadas con eventos convulsivos en ratas WAR y en el hámster GASH/Sal (Damasceno et al., 2020; Díaz-Casado et al., 2020; Díaz-Rodríguez et al., 2020; Friedman et al., 2013). De esta forma, un estudio reciente que aplicó secuenciación de exoma completo en hámsteres GASH/Sal y hámsteres silvestres identificó 3 variantes genéticas de alto impacto y 15 de impacto moderado (Díaz-Casado et al., 2020). Entre estas variantes de un solo nucleótido con cambio de sentido, se destaca la sustitución de C por T en la posición 9586732 del gen *Grik1*, que codifica la proteína GluK1, donde el residuo His en la posición 289 es reemplazado por un Tyr (p.H289Y) (Díaz-Casado et al., 2020) (Figura 5). Este hallazgo es relevante, ya que las variantes genéticas de *Grik1* se han asociado con el riesgo genético de epilepsia en humanos (Estudios de Asociación Genómica por el Consorcio de Epilepsias Complejas de la Liga Internacional contra la Epilepsia, 2018). Los polimorfismos en *Grik1* confieren susceptibilidad a la epilepsia de ausencia juvenil (Sander et al., 1997), y variaciones en la región no codificante de este gen, cerca de secuencias reguladoras, podrían modificar la expresión génica sin afectar la estructura del receptor (Izzi et al., 2002). En este contexto, esta tesis doctoral investiga por

primera vez los efectos del polimorfismo de un solo nucleótido con cambio de sentido (C9586732T, p.His289Tyr) en el gen *Grik1* del modelo GASH/Sal.

Como se esquematiza en la Figura 6, al menos las subunidades GluK1, GluK2 y GluK3 presentan distintas isoformas producto de diferentes tipos de *splicing* alternativo. En la subunidad GluK1 han sido identificadas cuatro isoformas, en dos configuraciones moleculares GluK1-1y GluK1-2 diferenciadas por la presencia o ausencia de un fragmento de 15 aminoácidos en el extremo ATD, respectivamente (Bettler et al., 1990; C. V. Hansen et al., 2018), y, consecuentemente como cada una de ellas puede transcribirse en al menos cuatro isoformas, GluK1a, GluK1b, GluK1c y GluK1d, esta último exclusiva en humanos, hacen un total de 8 isoformas distintas (GluK1-1a/d y GluK1-2a/d) de esta subunidad (Barbon & Barlati, 2000; Gregor et al., 1993; Sommer et al., 1991). A este respecto es interesante también destacar que las isoformas GluK1-2b y GluK1-2c contienen en su dominio C-terminal un motivo de retención en el retículo endoplásmico que impide su expresión en las membranas plasmáticas de las neuronas del SNC (Han et al., 2012). La composición de las distintas isoformas de las subunidades en los KAR es determinante en la funcionalidad del receptor al influir en el tráfico de la superficie celular, su localización subcelular y el tipo de interacciones con otros tipos de proteínas intracelulares implicadas en la sintonización de las funciones neuronales [revisado en (Contractor et al., 2011b; Lerma & Marques, 2013; Pahl et al., 2014). Finalmente, aparte de las mencionadas modificaciones postraduccionales, tanto la subunidad GluK1 como la GluK2 pueden ser objeto de edición del RNA, lo que altera sus propiedades funcionales (Figura 6). Así, la edición de un nucleótido en el RNA mensajero transcrito del gen *Grik1* que codifica la subunidad GluK1 puede provocar el cambio de un aminoácido en su estructura proteica, concretamente de una Gln por una Arg (edición del sitio Q/R) modificándose en este caso las propiedades de permeabilidad y la conductancia del canal del KAR al calcio (Sommer et al., 1991).

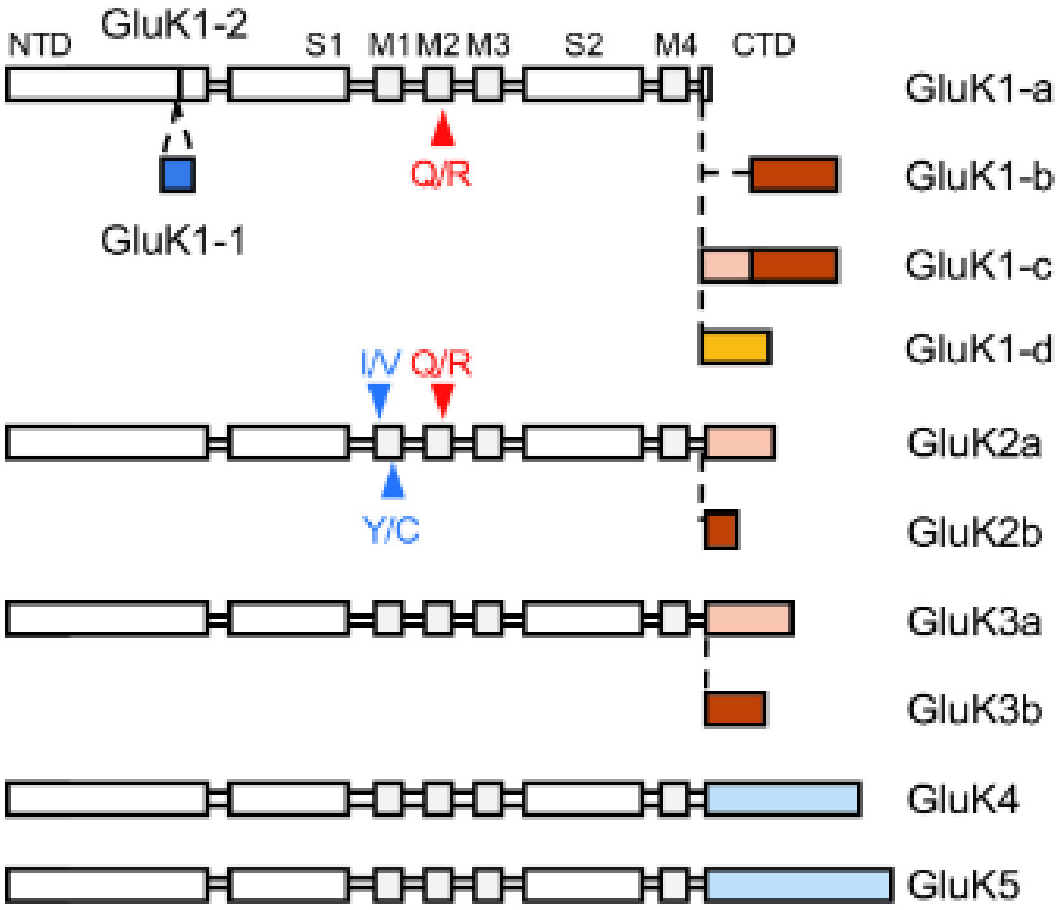

Figura 6. Tipos de subunidades de los KAR e isoformas producto de distintos tipos de *splicing* alternativo. Marcado en rojo se muestra el sitio de edición de RNA Gln/Arg (Q/R) de la región M2 y marcado en azul la edición de RNA Ile/Val (I/V) y Tyr/Cys (Y/C) en la región M1. (Tomado de (C. V. Hansen et al., 2018)

Tabla 1. Resumen del número de variantes genéticas descritas en los distintos genes codificantes de las distintas subunidades de los receptores de kainato (KAR). Algunas variantes genéticas muestran una diversidad de fenotipos, y esta tabla representa únicamente una instantánea de la literatura actual, la cual está influenciada de manera desigual por diversos métodos de diagnóstico. Tabla modificada de (K. B. Hansen et al., 2021)

Gen	**Proteína**	**Tipo de variantes de sentido erróneo**	**Localización estructural**			
			ATD	LBD	TMD	CTD
Gria1	GluA1	12	6	4	5	0
Gria2	GluA2	19	6	2	16	0
Gria3	GluA3	32	7	10	20	0
Gria4	GluA4	6	0	2	4	0
Grik1	GluK1	2	0	0	0	2
Grik2	GluK2	11	5	1	7	1
Grik3	GluK3	2	1	1	0	0
Grik4	GluK4	1	0	0	0	1
Grik5	GluK5	0	0	0	0	0

2. HIPÓTESIS Y OBJETIVOS

Mas no es completa gloria
Vencer en la batalla,
Que al brazo que combate
Lo anima la verdad.
La independencia sola
El gran clamor no acalla;
Si el sol alumbra a todos,
Justicia es libertad.

Rafael Núñez

2. HIPÓTESIS Y OBJETIVOS

2.1 Hipótesis

La investigación preclínica en epilepsia se ha beneficiado de numerosos estudios que utilizan modelos animales para simular crisis convulsivas provocadas por la actividad neuronal anómala. La caracterización de estos modelos requiere una comprensión más profunda de las alteraciones genéticas y moleculares subyacentes a las crisis convulsivas. En este contexto, proponemos que el modelo GASH/Sal, con su susceptibilidad única a las crisis convulsivas audiogénicas, sirve como una herramienta valiosa para explorar los aspectos genéticos y moleculares asociados con este fenómeno. Nuestra hipótesis se enfoca en la posibilidad de que el modelo GASH/Sal exhiba cambios en el perfil de expresión génica en el núcleo epileptogénico, el colículo inferior, junto con mutaciones de alto impacto que podrían estar relacionadas con los procesos de hiperexcitabilidad y desincronización de la actividad sináptica en las áreas cerebrales asociadas a las crisis convulsivas audiogénicas. Específicamente, se postula que la mutación en el gen *Grik1* (C9586732T, p.His289Tyr) tenga un impacto significativo en la funcionalidad de su proteína codificante, la subunidad del receptor de kainato tipo 1 (GluK1) y, por consiguiente, en la actividad del sistema glutamatérgico en el modelo GAHS/Sal.

2.2 Objetivo general

El objetivo general de esta tesis doctoral es ampliar la comprensión de los mecanismos genéticos y moleculares subyacentes a las crisis convulsivas audiogénicas en el modelo GASH/Sal, determinando el efecto del polimorfismo de nucleótido único del gen *Grik1* (C9586732T, p.His289Tyr).

2.2.1 Objetivos específicos

1. Determinar si existe desregulación génica en el colículo inferior del modelo GASH/Sal bajo condiciones basales y tras estimulación sonora intensa desencadénate de crisis convulsivas.
2. Identificar los genes diferencialmente expresados en el colículo inferior del modelo GASH/Sal en relación con el del animal silvestre (control) mediante técnicas de análisis de expresión génica complementarias, incluyendo transcriptoma y RT-qPCR.
3. Determinar los procesos ontológicos asociados a los genes diferencialmente expresados en el núcleo epileptogénico del modelo GASH/Sal y su relación con la susceptibilidad sufrir las crisis convulsivas audiogénicas.

4. Estudiar el impacto potencial del polimorfismo de nucleótido único (C9586732T, p.His289Tyr) del gen *Grik1* en la estructura y estabilidad de su proteína codificante (GluK1).
5. Determinar posibles alteraciones en la expresión del gen *Grik1* y en los niveles de la proteína GluK1 en regiones cerebrales asociadas con crisis convulsivas audiogénicas.
6. Investigar el impacto funcional de la mutación p.His289Tyr en la expresión e incorporación de los receptores GluK1 en la membrana celular, así como en las corrientes inducidas por kainato.

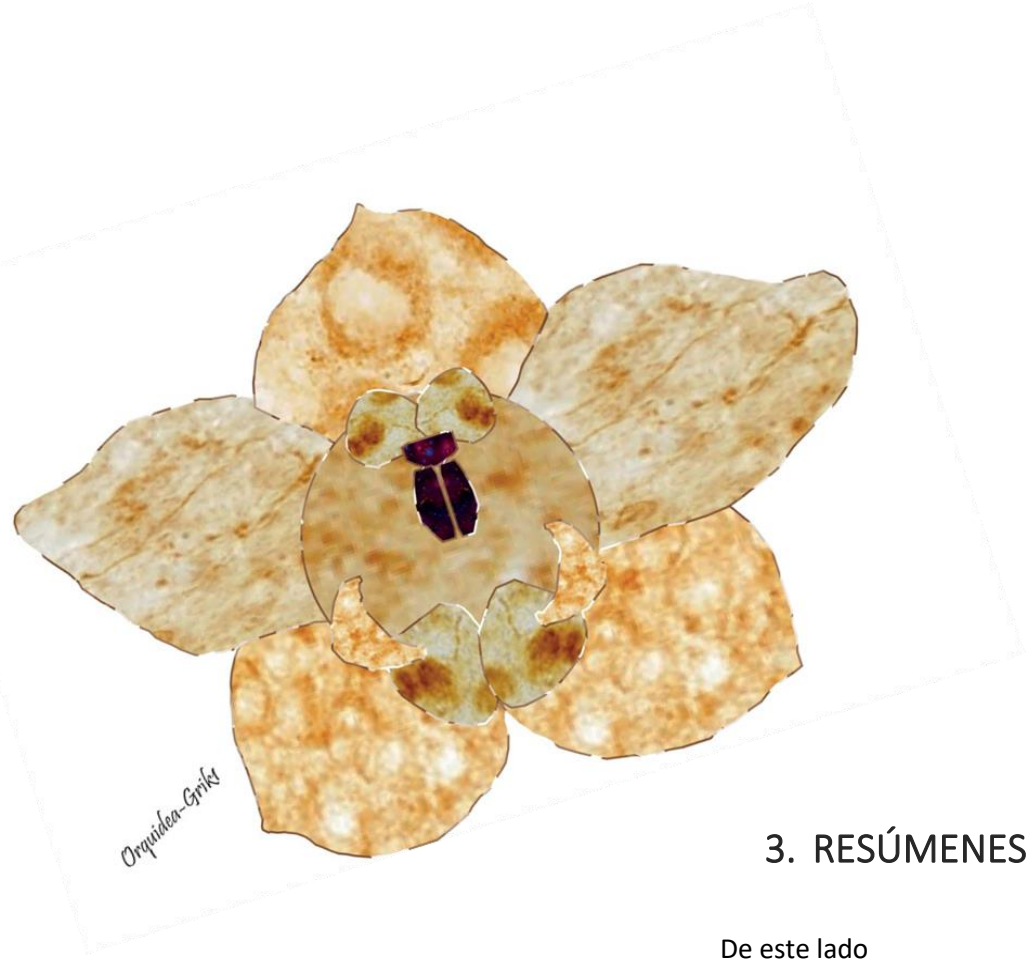

3. RESÚMENES DE LOS ARTÍCULOS

De este lado
no se oyen sollozos
ni pasos en la habitación.
Por la ventana no entran ramas.
En la pared no se estampan siluetas.
A ninguna hora viene un perro a saludar.
En esta cama no duerme un abismo.
La luz no se apaga en mi rostro.
Aquí, como allá, nadie dice mi nombre.

Bibiana Bernal (Calarcá)

3.1 ARTÍCULO 1: *Inferior colliculus transcriptome after status epilepticus in the Genetically Audiogenic Seizure-Prone Hamster GASH/Sal*.

En las siguientes páginas, se proporciona un resumen del artículo científico titulado "*Inferior Colliculus Transcriptome After Status Epilepticus in the Genetically Audiogenic Seizure-Prone Hamster GASH/Sal*", realizado por Díaz-Rodríguez SM, López-López D, Herrero-Turrión MJ, Gómez-Nieto R, Canal-Alonso A y López DE, y publicado en *Frontiers in Neuroscience* en 2020 (Vol. 14, pág. 508; doi: 10.3389/fnins.2020.00508).

3.1.1 Introducción

Es ampliamente reconocido que la etiología de la epilepsia puede manifestarse de diversas maneras. En particular, aproximadamente un tercio de todos los pacientes diagnosticados con epilepsia presenta una predisposición genética (Scheffer et al., 2017). En lo que respecta a este escenario, se ha observado un aumento en la identificación de epilepsias vinculadas a mutaciones específicas en genes. No obstante, es importante destacar que solo alrededor del 1 al 2 % de los casos de epilepsias idiopáticas parecen ser de naturaleza monogénica (Lopes-Cendes & Oliveira Ribeiro, 2013).

Además, numerosas investigaciones acerca de esta patología se llevan a cabo utilizando diversos modelos animales experimentales, en particular, se destacan los modelos audiogénicos de epilepsia. Uno de ellos es el modelo del hámster GASH/Sal, desarrollado en la Universidad de Salamanca, que representa un modelo animal de epilepsia refleja. Este modelo exhibe convulsiones tónico-clónicas generalizadas como respuesta a estímulos sonoros intensos, siendo el colículo inferior (CI) su foco epileptógeno (Muñoz et al., 2017). Estos animales alcanzan su máximo grado de susceptibilidad a padecer las crisis convulsivo-epilépticas, caracterizado como “convulsiones completas reflejas evocadas por sonido”, entre el segundo y cuarto mes de vida, para posteriormente desaparecer paulatinamente este tipo de susceptibilidad (Hernández Noriega, 2017). A lo largo de los últimos años, nuestro grupo de investigación ha ido identificando distintos aspectos que validan a este modelo animal en el estudio de la epilepsia. Así, por ejemplo, hemos identificado desde su tipo de genética con relación a su herencia (Muñoz et al., 2017), los sustratos neuroanatómicos subyacentes a las convulsiones audiogénicas (Sánchez-Benito et al., 2017, 2020), así como los efectos anticonvulsivos después de la administración con un fármaco antiepiléptico (Barrera-Bailón et

al., 2013, 2017). Asimismo, también hemos identificado que GASH/Sal exhibe una desregulación en genes de expresión temprana como *Egr1, Egr2* y *Egr3* (*Early growth response 1-3*) en el CI (López-López et al., 2017), presumiblemente como efecto del estrés asociado a las convulsiones.

Teniendo presente lo expuesto, este artículo estudió el perfil global de expresión génica en el foco epileptogénico (CI) en el modelo GASH/Sal con estimulación sonora para provocar las convulsiones-crisis epileptícas en comparación con animales control que recibieron el mismo tipo de estimulación acústica. Para ello, en primer lugar, se llevó a cabo un análisis comparativo del transcriptoma del CI en GASH/Sal en comparación con hámsteres control después de una estimulación sonora intensa. Posteriormente, un conjunto representativo de los genes diferencialmente expresados en esta comparativa fue utilizado en estudios de RT-qPCR (retrotranscripción y PCR cuantitativa) para validar la desregulación identificada inicialmente.

3.1.2 Material y Métodos

Para la realización de este artículo se utilizaron 12 hámsteres control, todos ellos sometidos a estimulación sonora para provocar las crisis convulsivas, y 18 hámsteres GASH/Sal, 12 de los cuales también les fue provocado las convulsiones epilépticas, mientras que a los otros 6 no fueron sometidos a ningún tipo de estimulación acústica que generará este tipo de patología. Después de la eutanasia de los animales, se procedió a la extracción de los CI izquierdo y derecho. A partir de estos tejidos, se realizaron extracciones y purificaciones de muestras de ARN total para cada individuo, con el propósito de utilizarlas en experimentos subsiguientes. Estos experimentos incluyeron el análisis de los transcriptomas mediante la técnica de RNAseq y la validación de un conjunto de genes con expresión diferencial mediante la técnica de RT-qPCR. En el caso de RNAseq, una avanzada metodología de secuenciación que cuantifica la presencia de ARN mensajero en una muestra biológica, se generaron bibliotecas de cDNAs a partir de las mencionadas muestras de ARN. Específicamente, se utilizaron 6 muestras provenientes de hámsteres GASH/Sal y otras 6 de hámsteres de control. La combinación de ambos tipos de tipos de librerías de cDNA se secuenciaron empleando la plataforma *Genome Analyzer IIx* de Illumina y para la identificación de las secuencias obtenidas se empleó el software STAR (Dobin et al., 2013) utilizando en el alineamiento de estas secuencias el genoma de referencia del hámster sirio (*Mesocricetus auratus*) MesAur1.0 (GCA_000349665.1) (Tchitchek et al., 2014). Seguidamente, se pudo realizar un análisis de expresión génica

diferencial entre los grupos experimentales (GASH/Sal *vs*. control) utilizando el paquete estadístico EdgeR y estableciendo como criterio de expresión diferencial más destacado una tasa de cambio (*log Fold-Change*) en cualesquiera de los genes, superior o inferior a 1,5 (sobreexpresado o infraexpresado, respectivamente). Seguidamente, con la finalidad de validar los resultados obtenidos de genes diferencialmente expresados entre ambos grupos se utilizó el análisis de RT-qPCR. Finalmente, todos los genes diferencialmente expresados se clasificaron funcionalmente utilizando distintas bases de datos biológicas disponibles en plataformas web, como The PANTHER, STRING 10.0, KEGG (Enciclopedia de genes y genomas de Kyoto) y el Consorcio de Ontología Genética. Para completar aún más el análisis de este conjunto de genes, se realizó un análisis metabolómico empleando las bases de datos KEGG y Reactome Pathway Database (Reactome), y utilizando como identificadores el metaboloma de humanos ya que el del hámster sirio aún no se ha descrito. De este modo, se evaluó la sobrerrepresentación de los genes diferencialmente expresados en las vías metabólicas mediante una prueba de distribución hipergeométrica.

3.1.3 Resultados

Inicialmente los resultados obtenidos del análisis comparativo del transcriptoma del CI en GASH/Sal, frente al de sus hámsteres control y ambos grupos de animales tras una estimulación sonora intensa, nos permitieron identificar un total de 23.573 genes en ambos grupos, de estos, 17.587 fueron genes identificados y 5.986 fueron genes no identificados. Del total de los 17.587 genes conocidos, 16.299 fueron genes identificados tanto en los hámsteres control como en los GASH/Sal. Finalmente, el número de genes expresados diferencialmente, seleccionados según los umbrales establecidos (|logFC| ≥ 1.5, valor de expresión génica normalizado superior a 10 cuentas por millón y lecturas superpuestas superiores a 40) fue de 36, de los que 24 estaban sobreexpresados y 12 infraexpresados en la comparativa GASH/Sal *vs*. control. Además, de estos 36 genes diferencialmente expresados, 29 eran conocidos y 7 desconocidos.

Posteriormente, se seleccionó un conjunto representativo de 27 genes con expresión diferencial (todos previamente identificados) para llevar a cabo estudios de RT-qPCR. Estos estudios se realizaron con el propósito de validar los resultados obtenidos a través del análisis de RNA-Seq. Como resultado de este proceso de validación, se confirmó la sobreexpresión de 15 genes (*Egr2, Slc28a1, Fosb, Ttr, Egr3, Kcnj13, Junb, Kcns1, Fos, Egr1, Ogn, Wdr38, Slc13a4, Npas4 y Gadd45g*) en los hámsteres GASH/Sal en comparación con el grupo de control. Asimismo, para 8 genes (*Rfxp2, Slc6a4, Renbp, Grin2c, Gm12695, Rab29, Atp2a3* y *C6*) también

confirmamos su infraexpresión en los animales GASH/Sal (*vs*. control). Por otra parte, en el caso de otros 4 genes (*Sucnr1, Cd163, Atf3 y Mmp3*) no pudimos demostrar diferencias de expresión significativas entre los dos grupos analizados mediante RT-qPCR.

Adicionalmente a este tipo de estudios y con el fin de poder identificar si los cambios en la expresión génica eran inherentes a la línea GASH/Sal o eran inducidos por sonido, analizamos también la expresión génica del mismo conjunto de genes por RT-qPCR entre dos grupos de hámsteres GASH/Sal, en condiciones basales y tras una estimulación acústica intensa. Estos análisis demostraron que 12 genes (*Egr2, Slc28a1, Fosb, Ttr, Egr3, Kcnj13, Kcns1, Fos, Egr1, Ogn, Npas4* y *Gadd45g*) estaban sobreexpresados en el grupo experimental GASH/Sal con convulsiones audiogénicas en comparación al que no recibió el estímulo sonoro, mientras 5 genes (*Junb, Slc13a4, Grin2c, Rab29, Atp2a3* y *C6*) estaban infraexpresados en la misma comparativa. Adicionalmente, en 9 genes (*Wdr38, Sucnr1, Cd163, Atf3, Mmp3, Rfxp2, Slc6a4, Renbp* y *Gm12695*) no se detectaron diferencias estadísticamente significativas entre las dos condiciones experimentales.

Por último, el análisis metabolómico de los 36 genes diferencialmente expresados demostró que 318 vías contenían al menos uno de estos genes y aplicando un filtro estadístico, de las rutas metabólicas más afectadas por su sobreexpresión, se identificaron que las rutas de señalización de las interleucinas-4 y -13 (IL-4 e IL-13) y de las vías de señalización de los transportadores, tanto de nucleósidos como de bases nitrogenadas libres en la membrana plasmática, eran las más destacadas.

3.1.4 Discusión

En este trabajo empleamos la técnica RNAseq para identificar dentro del transcriptoma 36 genes (29 de ellos con secuencia ya identificada y/o conocida) que se expresaban diferencialmente en el CI de la línea de hámster GASH/Sal en comparación al de su control, después de una estimulación sonora de alta intensidad (24 sobreexpresados y 12 infraexpresados). Las discrepancias en los niveles de expresión génica entre ambos grupos experimentos fueron seguidamente validadas mediante RT-qPCR para 23 de los 27 genes seleccionados para este objetivo; 15 genes sobreexpresados (*Egr2, Slc28a1, Fosb, Ttr, Egr3, Kcnj13, Junb, Kcns1, Fos, Egr1, Ogn, Wdr38, Slc13a4, Npas4* y *Gadd45g*) y 8 infraexpresados (*Rfxp2, Slc6a4, Renbp, Grin2c, Gm12695, Rab29, Atp2a3* y *C6*). En el caso de los restantes 4 genes (*Sucnr1, Cd163, Atf3 y Mmp3*) no pudimos demostrar diferencias de expresión significativas entre los dos grupos analizados. Este hecho puede producirse porque en los tipos de técnicas (RNA-seq y RT-qPCR) se emplean diferentes sondas, además de diferentes

métodos para la normalización de los datos de expresión y posibles cambios de expresión de los falsos positivos (Costa et al., 2013).

Varios de los genes identificados, entre ellos *Egr1-3*, cuya expresión se induce de manera rápida y transitoria en respuesta a una amplia gama de estímulos, han sido previamente reportados en la línea GASH/Sal (López-López et al., 2017). Además, estos genes han sido identificados en otros modelos animales de epilepsia, como se evidencia en estudios previos (Grabenstatter et al., 2012; X. Li & Hu, 2005; Lösing et al., 2017), así como en pacientes que presentan epilepsia refractaria (Liu et al., 2016). Este hallazgo respalda la consistencia de la expresión génica observada en la presente investigación con investigaciones previas en distintos contextos epileptogénicos. Otros genes identificados que codifican para factores de transcripción, como *Fosb, Junb, Fos* y *Npas4*, también han sido relacionados con los procesos epileptiformes en modelos animales y muestras de tejido epileptogénico (Beaumont et al., 2012; Elliott & Gall, 2000; Liu et al., 2016; Lösing et al., 2017). En base a la red molecular que conforman estos factores de crecimiento y transcripcionales, identificados también en ratones knockout para el factor de respuesta sérica condicional y en modelos de epilepsia de pilocarpina en ratones (Kuzniewska et al., 2016; Lösing et al., 2017) (Kuzniewska et al., 2016; Lösing et al., 2017), hipotetizamos que la sobreexpresión de estos genes puede ir seguida de una segunda ola de expresión de otros genes efectores relacionados con las vías glutamatérgicas, la transmisión GABAérgica y la transmisión sináptica, explicando así la susceptibilidad a las convulsiones audiogénicas en el modelo GASH/Sal.

Otros genes diferencialmente expresados relacionados con la vía de señalización del calcio, como el gen *Atp2a3*, codificante de la bomba Ca2C ATPasa (SERCA) e involucrado en el mantenimiento de la homeostasis del Ca2C (Contreras-Leal et al., 2016; Feng et al., 2013), y el gen *Grin2c*, codificante de una subunidad del receptor NMDA, también han sido directamente relacionados con procesos epileptogénicos (Kuzniewska et al., 2016; Lösing et al., 2017) o indirectamente asociados, a través de un gen análogo (*Grin2a*) que codifica otra subunidad de los receptores NMDA, con una variedad de trastornos del espectro de la afasia de la epilepsia y la encefalopatía epiléptica (Strehlow et al., 2019). En consecuencia, en el GASH/Sal es posible que el transporte de calcio desde el citosol al retículo sarco/endoplásmico disminuya después de las convulsiones inducidas por sonido debido a cambios en la formación de los canales SERCA, mientras que la baja expresión de *Grin2c* puede contribuir a la desregulación de la excitabilidad neuronal por Ca2C y a su desequilibrio a nivel intracelular como resultado de cambios en la formación del receptor NMDA. Nosotros sugerimos que la expresión de ambos

genes está regulada negativamente en respuesta a mutaciones de genes relacionados con la respuesta del calcio en el CI del GASH/Sal.

Del mismo modo, identificamos los dos genes desregulados que codifican canales de potasio dependientes de voltaje, *Kcns1* y *Kcnj13*, también han sido asociados indirectamente con la epilepsia. El primero de ellos se traduce en la subunidad alfa del canal de potasio Kv9.1 y genera canales funcionales cuando se heterotetrameriza con la subunidad Kv2.1. Interesantemente, mutaciones del gen que codifica esta última proteína (*Kcnb1*) se ha asociado con la epilepsia (Thiffault et al., 2015) y, consecuentemente, sugerimos que la sobreexpresión de *Kcns1* puede ser un mecanismo de compensación de la sobreactivación del canal Kv2.1, ya que una desregulación del gen *Kcnb1*, codificante de Kv2.1, no ha sido detectada en los animales GASH/Sal. Para el segundo de los genes que codifica el canal Kir7.1, un estudio de (Winden et al., 2011) demostró que también este gen estaba sobrexpresado en la epilepsia crónica. Por lo tanto, podemos hipotetizar que la sobreexpresión de *Kcnj13* después de un evento epileptogénico pudiera ser un mecanismo de compensación para la desregulación del canal Kir asociada a este tipo de patología.

La identificación de otros dos genes desregulados en el modelo GASH/Sal, como el codificante del transportador de nucleósido *Slc28* y el *Rfxp2* que codifica un miembro de la familia de receptores acoplados a proteína G, no han sido relacionados hasta el momento con la epilepsia, aunque sí con otros tipos de patologías, como el cáncer y la fibrilación auricular (Lin et al., 2008; Wang et al., 2016), y alteraciones en el sistema reproductivo (Bathgate et al., 2006; Tomiyama et al., 2003), respectivamente. La sobreexpresión de *Slc28a1* puede formar parte de un proceso de compensación fisiológica para aumentar la síntesis de ácido nucleicos hacia la activación de procesos moleculares que atenúen el estrés celular, contribuyendo de este modo a la epileptogénesis en el GASH/Sal, mientras que la infraexpresión de *Rfxp2* puede ser parte de la explicación del porqué este modelo animal presenta dificultades reproductivas.
En contraste, aunque no se ha establecido una relación directa entre el gen codificante de la proteína plasmática del complemento C6, *Gadd45g* (que se sobreexpresa en respuesta a factores estresantes) y el gen responsable de la transtiretina plasmática (TTR) con los procesos epilépticos, es relevante señalar hallazgos conexos. La eliminación de un análogo de C6, la proteína del complemento C5, ha demostrado reducir significativamente el número de convulsiones en ratones con malaria cerebral experimental (Buckingham et al., 2014). En el caso de *Gadd45g*, su sobreexpresión después de eventos convulsivos ha sido documentada tanto en modelos de epilepsia con pilocarpina en ratones como en la epilepsia neocortical

humana (Beaumont et al., 2012; Lösing et al., 2017). Asimismo, las mutaciones en el gen que codifica la TTR se han asociado con la polineuropatía amiloide familiar, una condición que incluye episodios convulsivos (Franco et al., 2016; Suhr et al., 2009). Adicionalmente, nuestro grupo de investigación identificó dos mutaciones en el gen *TTR* en el modelo GASH/Sal (Díaz-Casado et al., 2020), lo que sugiere que la sobreexpresión de este gen en dicho modelo animal podría representar una respuesta compensatoria ante una hipotética deficiencia de proteína TTR funcional.

Por último, nuestro análisis metabolómico detectó una sobrerrepresentación de procesos inflamatorios relacionados con IL-4 e IL-13 en el modelo epiléptico GASH/Sal, coincidiendo así lo reportado por (Musto et al., 2016) cuando afirma que procesos inflamatorios focales o sistémicos no regulados pueden conducir a una conectividad neuronal aberrante y a redes neuronales hiperexcitables, que median la aparición de la epilepsia. Genes que codifican ambos tipos de interleucinas pueden tener el potencial de usarse como biomarcadores moleculares y objetivos para enfoques terapéuticos de la epilepsia.

En conclusión, los resultados obtenidos en este estudio subrayan que la desregulación de genes específicos en el CI del modelo GASH/Sal puede influir de manera directa o indirecta en el delicado equilibrio entre los niveles excitatorios e inhibitorios de las sinapsis neuronales. Esta alteración puede dar lugar a procesos de hiperexcitabilidad y desincronización en la red neuronal, evidenciando así la importancia de estos genes en la modulación de la actividad sináptica en el contexto de generación y propagación de las crisis audiogénicas.

3.2 ARTÍCULO 2: *Delving into the significance of the His289Tyr single-nucleotide polymorphism in the glutamate ionotropic receptor kainate-1 (Grik1) gene of a genetically audiogenic seizure model*.

A continuación, se presenta un resumen detallado del artículo científico titulado "*Delving into the Significance of the His289Tyr Single-Nucleotide Polymorphism in the Glutamate Ionotropic Receptor Kainate-1 (Grik1) Gene of a Genetically Audiogenic Seizure Model*". Este trabajo, elaborado por Díaz-Rodríguez SM, Herrero-Turrión MJ, García-Peral C y Gómez-Nieto R, y se publicó en *Frontiers in Molecular Neuroscience* en 2023 (Volumen 16; Doi: 10.3389/fnmol.2023.1322750).

3.2.4 Introducción

Es conocido que las vías de señalización neuronales se vuelven aberrantes en la epilepsia, caracterizándose ésta por una hiperactividad neuronal elevada, una mayor sincronía y un equilibrio alterado de algunos neurotransmisores en regiones restringidas del cerebro que eventualmente podrían extenderse a muchas otras áreas. El cambio en los mecanismos moleculares y celulares conduce a la ictogénesis y la epileptogénesis en esas regiones del cerebro para finalmente provocar una miríada de síntomas de epilepsia, incluidas las convulsiones como la manifestación conductual más notable de dicha hiperactividad de la red neuronal (Fisher et al., 2005; Pitkänen y Engel, 2014). A este respecto, también se conoce desde hace tiempo que existe una estrecha relación entre el sistema glutamatérgico y la epilepsia y, de forma más específica, existe un gran número de publicaciones científicas centradas en el papel de los receptores de glutamato con la epilepsia (ver revisión de Wang et al., 2022). El glutamato, el neurotransmisor excitador predominante en el SNC de los mamíferos, actúa sobre una variedad de receptores de glutamato ionotrópicos, como los NMDA, AMPA y KAR ver revisión de (Meldrum, 2000). En el caso que nos ocupa en este artículo, los KAR, están formados por combinaciones tetraméricas de cinco subunidades, GluK1-5 (Sihra et al., 2014), pudiendo formar receptores homoméricos, compuestos en exclusiva por las subunidades GluK1-3, o heteroméricos, incluyendo también en este caso las subunidades GluK4-5. A su vez, algunas de las subunidades GluK1-3 presentan diferentes tipos de isoformas producto de distintos tipos de procesos de *splicing* alternativo (Pinheiro y Mulle, 2006). Los KAR están ampliamente distribuidos pre y postsinápticamente en diferentes tipos de células del cerebro, participando en el control de las redes sinápticas, la regulación de la liberación de distintos tipos de neurotransmisores, la modulación de la transmisión excitatoria

e inhibidora y la mejora de la excitabilidad neuronal (Pinheiro y Mulle, 2006; Sihra et al., 2014). Por esta razón, se ha demostrado que estos receptores están involucrados en los desequilibrios excitatorios e inhibidores relacionados con la epilepsia (Lerma y Marques, 2013). De este modo, el kainato se utiliza ampliamente en roedores para inducir convulsiones cerebrales agudas y, después de inyecciones kaínicas repetitivas, como modelo crónico de epilepsia del lóbulo temporal (revisado en (Ben-Ari, 2014)). Las acciones proconvulsivas del ácido kaínico están mediadas en gran medida por la activación de los KAR (revisado en (Falcón-Moya et al., 2018)) y varios estudios han sugerido que, más en concreto, la subunidad GluK1 de estos KAR es clave en favorecer este tipo de desequilibrio en las convulsiones inducidas por kainato (Falcón-Moya et al., 2018; Fritsch et al., 2014; Sihra et al., 2014). El hecho indiscutible es que las investigaciones sobre la epilepsia han avanzado notablemente empleando modelos animales preclínicos de convulsiones y síndromes de epilepsia y, entre éstos, es destacable, el único hámster científicamente disponible que muestra susceptibilidad a las convulsiones al sonido, el de la cepa GASH/Sal (ampliamente detallado en la introducción de esta tesis doctoral). A este respecto, el análisis realizado por nuestro grupo de investigación del exoma del CI en el GASH/Sal, en comparación a la cepa control de la misma especie, identificó 3 variantes genéticas de alto impacto y 15 de impacto moderado (Díaz-Casado et al., 2020). Entre estas variantes de un solo nucleótido, una de las más destacadas era la sustitución de una citosina por una timina en la posición 9586732 (Ensembl versión, ENSMAUG00000000865.1) del gen *Grik1* que modifica la traducción de la subunidad GluK1 que conforma los KAR de una histidina en la posición 289 presente en la cepa control por una tirosina en la línea GASH/Sal (p.H289Y) (Díaz-Casado et al., 2020). Este hallazgo era extremadamente interesante ya que las variantes genéticas de *Grik1* se han relacionado con el riesgo genético de epilepsia en humanos (Consorcio de la Liga Internacional Contra la Epilepsia sobre Epilepsias Complejas, 2018), en concreto, polimorfismos de *Grik1* confieren susceptibilidad a la epilepsia de ausencia juvenil (Sander et al., 1997) y variaciones en la región no codificante de este gen, cerca de las secuencias reguladoras, podrían alterar la expresión génica sin afectar la estructura del KAR conformado por la subunidad GluK1 (Izzi et al., 2002).

En consecuencia, en este artículo se exploró por primera vez los posibles efectos estructurales e incluso funcionales del polimorfismo de nucleótido único (SNP, por sus siglas en inglés, *Single Nucleotide Polymorphism*) en el gen *Grik1* del modelo GASH/Sal (C9586732T, p.His289Tyr) analizando la estructura de su proteína codificada (GluK1) mediante modelado en 3D *in silico*. Este tipo de estudio permitió profundizar el papel que el sistema glutamatérgico tiene en los modelos genéticos de convulsiones audiogénicas (Ross & Coleman, 2000) y, de forma más específica, la de los KAR en la red de convulsiones audiogénicas. Asimismo, se analizaron los

niveles de expresión del gen *Grik1*, así como los de su proteína codificante GluK1 en toda la red de convulsiones epileptogénicas de la línea GASH/Sal. Finalmente, dado que estos análisis se realizaron comparándolos con hámsteres controles, sirios de tipo salvaje de la misma edad, este estudio también proporcionó información valiosa sobre la distribución de la proteína GluK1 en el cerebro del *M. auratus*.

3.2.5 Material y métodos

En primera instancia, para investigar los posibles efectos estructurales del polimorfismo de nucleótido único (SNP) en el gen *Grik1* presente en el modelo GASH/Sal (C9586732T, p.His289Tyr), se llevó a cabo un análisis de la estructura de la proteína codificada (GluK1). Este análisis se basó en estudios *in silico* de modelaje tridimensional de proteínas, utilizando diversas herramientas bioinformáticas. Entre ellas se incluyen el avanzado sistema de predicción basado en inteligencia profunda AlphaFold2 (Jumper et al., 2021), el servidor web Arpeggio (Jubb et al., 2017) y el visor molecular PyMOL. Estas herramientas permitieron calcular las interacciones interatómicas y sus longitudes en los residuos mutados en comparación con los del tipo salvaje, proporcionando así una comprensión detallada de las posibles modificaciones estructurales asociadas al SNP en el gen *Grik1*. Asimismo, para evaluar el efecto del SNP sobre la estabilidad termodinámica de la proteína, se emplearon varios predictores de estabilidad de proteínas: DynaMut2, INPS3D, FoldX y MAESTRO.

A continuación, en este artículo se utilizaron un total de 16 hámsteres dorados sirios (*M. auratus*) de 4 meses de edad [cuando exhiben la máxima susceptibilidad a las convulsiones epilépticas (Muñoz et al., 2017)] y sexo, específicamente 8 hámsteres de tipo salvaje y 8 de la línea GASH/Sal. De todos éstos, un total de 10 animales (5 controles y 5 GASH/Sal) se utilizaron en la realización de los análisis de expresión génica y proteica de *Grik1* y GluK1, mediante las técnicas de RT-qPCR y Western blot, respectivamente. Por otra parte, los restantes animales (6: 3 controles y 3 GASH/Sal) se emplearon en llevar a cabo los estudios de inmunohistoquímica para determinar, utilizando microscopía convencional de campo claro y microscopía láser confocal, la distribución de GluK1 en las áreas cerebrales objeto de estudio (cerebelo, CI, colículo superior, hipocampo y corteza prefrontal).

3.2.6 Resultados

El análisis *in silico* de los posibles efectos estructurales del SNP (C9586732T, p.His289Tyr) del gen *Grik1* en su proteína codificada (GluK1) en el modelo GASH/Sal, en comparación al de su cepa control, indicó que la posición 289 se localizaba en el región regulatoria R2 del ATD. Comparando GluK1 del GASH/Sal con su semejante en el control detectamos que existían unas nuevas interacciones hidrofóbicas proximales e interacciones carbono-π en el caso de la primera de las proteínas, estimando que éstas podrían generar unas condiciones más favorables de estabilización de la proteína GluK1 en el caso del GASH/Sal.

A continuación, la evaluación de los niveles de expresión génica de *Grik1* en GASH/Sal, en comparación a los detectados en la cepa control, fueron significativamente mayores en tres áreas cerebrales, cerebelo, CI y colículo superior; por el contrario, en el hipocampo fue significativamente menor. Por último, en la corteza prefrontal, la expresión de *Grik1* no fue diferente, desde el punto de vista estadístico, al comparar ambos grupos experimentales.
Por otra parte, mediante experimentos de Western blot, el análisis de los niveles de expresión de la proteína GluK1 demostró que, en primer lugar, éstos varían entre las diferentes regiones del cerebro estudiadas en este trabajo. Empleando un anticuerpo policlonal anti-GluK1 detectamos también que en todas las áreas cerebrales analizadas se mostraba la banda esperable de ~104 kDa de peso molecular tanto en los animales GASH/Sal como en los controles, mientras que una segunda banda de ~65 kDa era evidente únicamente en el CI y colículo superior del GASH/Sal en exclusiva. Al contrastar ambos grupos experimentales, se identificó una reducción estadísticamente significativa en los niveles de expresión de GluK1, con un peso molecular aproximado de ~104 kDa, en el cerebelo y el colículo superior del modelo GASH/Sal. Por el contrario, no se detectaron diferencias estadísticamente significativas en el nivel de expresión de GluK1 ~104 kDa en las otras áreas cerebrales estudiadas: CI, hipocampo y corteza prefrontal. Por otra parte, el nivel de expresión de GluK1 de ~65 kDa en las áreas que se detectaron, ambos colículos, era estadísticamente mayor en el caso del GASH/Sal. En este apartado, finalmente se realizó un análisis comparativo de los niveles de expresión relativos de GluK1 entre cada una de las áreas encefálicas analizadas determinando que los mayores niveles de expresión fueron detectados en la corteza prefrontal y el colículo superior, mientras que los menores fueron en el hipocampo y cerebelo.

En lo que respecta al análisis de la distribución de GluK1 en las cinco áreas cerebrales estudiadas tanto en el hámster GASH/Sal como en su control, los resultados obtenidos

determinaron que se obtuvo inmunorreactividad al mismo anticuerpo policlonal frente a GluK1 utilizado en los Western blot en multitud de neuronas de estas áreas cerebrales. En el caso del cerebelo, se detectó inmunomarcado de forma intensa en las regiones cerebelosas que contienen sinapsis de fibras paralelas y células de Purkinje, mientras que, de forma más difusa, también se detectó en el neuropilo en la corteza del cerebelo. Comparando ambos grupos experimentales, en el cerebelo de GASH/Sal se observó en general una menor intensidad de la inmunorreactividad a GluK1, así como en el número de cuerpos celulares y fibras axonales inmunomarcadas, por el contrario, en el neuropilo se observaron intensidades similares. Por lo que respecta al CI, se observó que la distribución de GluK1 era heterogénea en ambos grupos de animales, aunque eran evidentes variaciones de inmunomarcado entre las tres subdivisiones de esta área mesencefálica. Así, la densidad e intensidad del producto inmunorreactivo fue mayor en las cortezas dorsal y externa en comparación con el núcleo central. Asimismo, se observó inmunotinción específica de GluK1 en fibras axonales y en el neuropilo en el exterior regiones del CI. De forma específica, se pudo detectar que en la línea GASH/Sal, en comparación a su control, existía una mayor densidad de inmunorreactividad para GluK1 tanto en los cuerpos celulares como incluso en el número de fibras axonales. En el caso del colículo superior, lo más destacable es que al comparar ambos grupos experimentales, en los animales GASH/Sal se observó una menor cantidad de fibras, incluso con ausencia de terminales axonales inmunopositivos para GluK1, a pesar de que se observó una mayor cantidad de cuerpos celulares inmunomarcados para esta proteína en comparación al grupo de control. En el hipocampo se detectó una fuerte inmunorreactividad de GluK1 en los numerosos cuerpos celulares de sus distintas subregiones (CA1, CA2, CA3 y giro dentado) que componen esta área cerebral en el caso de los hámsteres control, a diferencia de lo detectado en los GASH/Sal, con una significativa reducción, incluso insignificante, de la inmunotinción a esta subunidad de los KAR. Por último, en la corteza prefrontal se observaron diferencias significativas en el inmunomarcado de GluK1 entre ambos grupos experimentales en distintas regiones analizadas de esta corteza (cortezas cinguladas, prelímbica e infralímbica, y áreas vecinas como el indusium griseum y corteza motora); de forma específica y en líneas generales, la inmunorreactividad fue menor en la línea GASH/Sal en comparación a su control. Así, por ejemplo, en la corteza cingulada y en el indusium griseum de los animales control se observó un immunomarcado intenso de fibras GluK1 positivas, así como abundantes pequeños puntos en el neuropilo, en las áreas prelímbicas e infralímbicas se detectaron grupos de neuronas inmunomarcadas nítidamente a esta proteína, al contrario de lo observado en la corteza motora, que lo fue de forma difusa. Por su parte, en la cepa GASH/Sal si se observó una fuerte concentración de cuerpos celulares inmunorreactivos a GluK1 en la corteza motora,

así como en la corteza cingulada, pero en lo que respecta a sus fibras axonales, éstas mostraron poca o ninguna inmunorreactividad en el indusium griseum.

3.2.7 Discusión

El presente trabajo analizó inicialmente los efectos estructurales del SNP del gen *Grik1* en su proteína codificante GluK1 (C9586732T, p.His289Tyr) identificada en el modelo animal GASH/Sal (Díaz-Casado et al., 2020). El abordaje *in silico* de modelado en 3D de la proteína GluK1 nos permitió descubrir que la mutación sin sentido produciría una mayor estabilización de esta proteína por un incremento de sus interacciones intermoleculares, como la aparición de nuevas interacciones hidrofóbicas y, consecuentemente, una prolongación de su vida media y un incremento de su concentración celular. Dada la ubicación de esta mutación, localizaba en la posición 289 en la región regulatoria R2 del ATD, estimamos que ésta podría ejercer un mínimo o insignificante efecto sobre la actividad de la unión del neurotransmisor glutamato sobre la subunidad GluK1. No obstante, como se acaba de mencionar, nuestra hipótesis es que esta mutación puntual puede producir una sobreestabilización en este ATD que afecte al plegamiento, dinámica conformacional, flexibilidad y accesibilidad de la subunidad GluK1. Asimismo, el ensamblaje en tetrámeros del conjunto de los cinco tipos de subunidades del KAR pudiera estar alterado con la presencia de esta variante génica ya que es conocido que las interacciones de alta afinidad en el ATD son necesarias para la biosíntesis de este tipo de receptores (Ayalon & Stern-Bach, 2001; Kumar et al., 2007), y que, más en concreto, el ATD de la subunidad GluK1 puede formar receptores heteroméricos en todas las estequiometrías posibles (Selvakumar et al., 2021). A este respecto, cabe destacar que el ATD contiene interacciones extensas con los dominios de unión del ligando (LBD) que permiten una regulación alostérica compleja, como a través de las proteínas del complemento y el propio péptido señal de los KAR, tal y como se observa en otras subunidades del receptor de glutamato ionotrópico(Krieger et al., 2015). En definitiva, estimamos que la mutación detectada en GluK1 puede afectar la modulación precisa de la función del KAR dentro del cerebro del hámster GASH/Sal.

Los análisis de los niveles de expresión del gen *Grik1*, tanto en la línea GASH/Sal como en la del control (en ambos casos sin ningún tipo de estimulación sonora que provocaran las crisis epilépticas), en las principales áreas cerebrales involucradas en las convulsiones epileptogénicas nos proporcionó una valiosa información sobre los cambios moleculares inherentes que contribuyen al fenotipo epiléptico de GASH/Sal, tal y como se ha realizado en

distintos tipos de publicaciones de nuestro grupo de investigación (Damasceno et al., 2020; Díaz-Casado et al., 2020; Díaz-Rodríguez et al., 2020; Fuerte-Hortigón et al., 2021; López-López et al., 2017; Prieto-Martín et al., 2017; Sánchez-Benito et al., 2020). De este modo, en este artículo se evidenciaron diferencias estadísticamente significativas en el nivel de expresión de *Grik1* entre ambos grupos experimentales. Así, en el cerebelo, CI y colículo superior de los animales GASH/Sal, en comparación a su control, se detectó una sobreexpresión de este gen mientras que en el hipocampo estaba infraexpresado. En particular, la sobreexpresión de *Grik1* en el CI sugiere una contribución potencial a una mayor señalización excitatoria y la posible alteración del equilibrio de la actividad neuronal, incluso en ausencia de convulsiones. Todos estos hechos, junto con los resultados obtenidos por (Sánchez-Benito et al., 2020) en los que también se detectó una desregulación de algunos genes cocleares esenciales, como el de los transportadores vesiculares de glutamato 1 y 2, puede corroborar la hipótesis de una alteración generalizada en la transmisión glutamatérgica propiciando una propagación de la transmisión anormal al CI en la línea hámsteres GASH/Sal a lo largo de la vía acústica primaria (Sánchez-Benito et al., 2020). De este modo, ya se conoce que la señalización del glutamato está desregulada en la epilepsia y se caracteriza por alteraciones transcripcionales en múltiples genes de los receptores de glutamato, varias de sus proteínas auxiliares, como la proteína shisa9/cisteína de 44 kDa (SHISA9/CKAMP44) (Pfisterer et al., 2020), también identificada recientemente en nuestro modelo experimental (García-Peral et al., 2023), e incluso en otro tipo de receptores como los de cannabinoides tipo 1, igualmente identificada su infra- y sobreexpresión en el CI e hipocampo, respectivamente, del GASH/Sal (Fuerte-Hortigón et al., 2021). Todos estos hallazgos apoyan la teoría de la pérdida en el GASH/Sal de esta modulación sináptica intrínseca, que contribuye a la base de la susceptibilidad a las convulsiones audiogénicas.

Por otra parte, dado que la desregulación génica no siempre se correlaciona con la proteica (Vogel & Marcotte, 2012), también realizamos un análisis de los niveles de expresión de la proteína GluK1 en y entre ambos grupos experimentales y en las mismas áreas cerebrales anteriores demostrándose que, al contrario que con su gen codificante, al menos la isoforma esperada de esta subunidad (de ~104 kDa) estaba infraexpresada en el cerebelo y el colículo superior de los animales GASH/Sal (*vs*. control). Por otra parte, la segunda isoforma detectada, de ~65 kDa y producto muy posiblemente de un distinto proceso de *splicing* alternativo y/o modificaciones postraduccionales, estaba presente únicamente en las estructuras coliculares del GASH/Sal y, consecuentemente, en exclusiva en esta línea de animales con epilepsia y al menos está región cerebral. Como conclusión de este apartado, también podemos determinar

que como es conocido que las subunidades de los KAR desempeñan un papel crucial en la oligomerización y expresión superficial de los cotransportadores K^+/Cl^- (Mahadevan et al., 2014), sugerimos que la desregulación de al menos estas dos isoformas proteicas de GluK1 podría provocar también una alteración de la expresión de estos cotransportadores, lo que potencialmente alteraría el delicado equilibrio entre los procesos de inhibición y excitación en las sinapsis neuronales, contribuyendo así a una mayor susceptibilidad del modelo GASH/Sal a las convulsiones audiogénicas.

En lo que respecta al análisis de la distribución de GluK1 en las cinco áreas cerebrales estudiadas, en líneas generales los resultados obtenidos fueron similares a los reportados en otras especies de mamíferos, aunque también identificamos ciertas diferencias. De esta forma, en ambos grupos de hámsteres la inmunoreactividad para GluK1 se localizó en el soma neuronal, tractos de fibras axonales, así como de las terminales, al igual que en el núcleo arqueado, hipotálamo y el núcleo coclear dorsal y cerebelo de rata (Bettler et al., 1990; Diano et al., 2008; Eyigor et al., 2005; Wu & Tang, 2023), neocorteza e hipocampo de perros y monos (Good et al., 1993; Hof et al., 1996; Huntley et al., 1993). Por su parte, la comparación de los dos grupos experimentales utilizados en este artículo demostró una serie de diferencias significativas en la distribución de GluK1 en los cinco núcleos cruciales de la red neuronal convulsiva. De este modo, la identificación de una menor inmunorreactividad a esta subunidad en el cerebelo del GASH/Sal en comparación a su control, podría corresponderse con un desequilibrio en la señalización excitatoria de la línea de hámster epiléptico, lo que conduciría a una hiperexcitabilidad y una mayor probabilidad de activación sincrónica de las neuronas dentro del cerebelo. Estas observaciones respaldan la idea de que el cerebelo participa activamente en las convulsiones, en lugar de reflejar únicamente los aspectos motores de las convulsiones (Streng & Krook-Magnuson, 2021). En el caso del CI, las variaciones detectadas en la distribución de GluK1 entre las regiones central y dorsal/externa en este núcleo, con mayor inmunomarcado en esta última región en comparación a la primera, junto con un incremento de la densidad positiva a GluK1 en el GASH/Sal, podrían perfectamente correlacionarse con las funciones específicas de cada una de estas subdivisiones en los mecanismos de las convulsiones audiogénicas en la cepa GASH/Sal. Asimismo, estas diferencias en la distribución de GluK1 en las distintas regiones del CI, así como en el colículo superior, en este modelo animal sugieren nuevamente potenciales alteraciones subyacentes de la transmisión sináptica del glutamato que pueden estar relacionadas con el papel del CI en la generación de mecanismos epileptogénicos. En cuanto al hipocampo, estructura límbica que indirectamente recibe señales auditivas del tronco del encéfalo y que está estrechamente

asociada con la epileptogenicidad (Ben-Ari, 2014; Reid et al., 1983), los animales GASH/Sal exhibieron una considerable menor inmunorreactividad de GluK1, al igual que con la expresión de gen codificante, hecho que puede ser determinante para comprender el reclutamiento límbico durante convulsiones audiogénicas repetidas en el modelo GASH/Sal. Por último, en general en la corteza prefrontal la inmunorreactividad a GluK1 fue menor en la línea GASH/Sal en comparación a su control y podemos hipotetizar que este hecho podría ser determinante en un aumento en la excitabilidad neuronal alterando, de este modo, la plasticidad sináptica en esta región cerebral en el modelo GASH/Sal.

En definitiva, este estudio evidencia la importancia de la subunidad GluK1, integrante clave en la funcionalidad de los KAR, en los mecanismos subyacentes a las convulsiones, tal y como también lo corroboran los SNPs de *Grik1* identificados en la epilepsia de ausencia juvenil idiopática (Sander et al., 1997), la desregulación de GluK1 detectada en pacientes con epilepsia del lóbulo temporal (J.-M. Li et al., 2010) y en las desregulaciones del gen *Grik1* y su proteína codificante en ratas sometidas a estado epiléptico inducido por ácido kaínico (Ullal et al., 2005).

Asimismo, en el desarrollo de nuevos medicamentos anticonvulsivos cada vez más se tiene en cuenta la importancia de la proteína GluK1 en los KAR, tal y como se demuestra en que los agonistas de esta subunidad pueden inducir convulsiones clónicas (Kaminski et al., 2004; Rogawski et al., 2003) y en que la eficacia del fármaco antiepiléptico topiramato se atribuye en parte al bloqueo que produce a GluK1 (Kaminski et al., 2004). En consecuencia, este trabajo ofreció una información fundamental sobre las alteraciones generalizadas de GluK1 en varias regiones anatómicas del modelo GASH/Sal, pudiendo asentar las bases del desarrollo de futuros experimentos que involucren la administración de agonistas o antagonistas dirigidos a la subunidad GluK1 en los KAR. Estas investigaciones son indispensables para evaluar la posible eficacia anticonvulsiva de GluK1 como objetivo terapéutico en la investigación de la epilepsia. Finalmente, este tipo de estudio permitió profundizar también en el papel que el sistema glutamatérgico tiene en los modelos genéticos de convulsiones audiogénicas (Ross & Coleman, 2000) y, de forma más específica, la de los KAR en la red de convulsiones audiogénicas del hámster GASH/Sal.

3.3 ARTÍCULO 3: *Enhanced Membrane Incorporation of H289Y Mutant GluK1 Receptors from the Audiogenic Seizure-Prone GASH/Sal Model: Functional and Morphological Impacts on Xenopus Oocytes*.

En las páginas subsiguientes de esta tesis doctoral, se detalla un resumen del trabajo titulado "*Enhanced Membrane Incorporation of H289Y Mutant GluK1 Receptors from the Audiogenic Seizure-Prone GASH/Sal Model: Functional and Morphological Impacts on Xenopus Oocytes*". Este estudio, elaborado por Díaz-Rodríguez SM, Ivorra I, Espinosa J, Vegar C, Herrero-Turrión MJ, López DE, Gómez-Nieto R y Alberola-Die A, ha sido publicado en el número especial "*Epilepsy: From Molecular Basis to Therapy*" de la revista International *Journal of Molecular Sciences* en 2023 (Doi: 10.3390/ijms242316852).

3.3.1 Introducción

Como se mencionó en la sección introductoria de esta tesis doctoral, los receptores de glutamato ionotrópicos, clasificados en cuatro tipos (AMPA, KAR, NMDA y GluD), desempeñan un papel crucial en diversas funciones neuronales. La desregulación de estos receptores se ha asociado con ciertos tipos de epilepsia y varias enfermedades neurodegenerativas. En particular, los KAR están conformados por cinco subunidades proteicas (GluK1-5) y en el caso de GluK1 y GluK2 pueden presentarse en varias isoformas producidas por distintos procesamientos de *splicing* alternativo; hasta 8 tipos en el caso de GluK1 y en la elaboración de este trabajo se empleó la isoforma GluK1-2b. Asimismo, para constituir un KAR cada una de estas cinco subunidades proteicas se puede combinar de forma homomérica (compuestos sólo por las subunidades GluK1-3, con baja afinidad al glutamato) o heteromérica (cuando se incluyen GluK4-5, que presentan alta afinidad al mismo neurotransmisor). En el procesamiento de estas subunidades, cada una de ellas con cuatro dominios (ATD, LBD, TMD y CTD), el ATD es esencial en la capacidad de interaccionar con distintos tipos de compuestos alostéricos selectivos para influir en la dinámica del dominio LBD y se inserta en la membrana del retículo endoplásmico, siendo sometido a distintos tipos de modificaciones postraduccionales impulsando la dimerización su dominio y también del LBD, interviniendo de este modo en la funcionalidad de cada subunidad y en última instancia del KAR. En la actualidad, se han descrito un gran número de variantes génicas patogénicas, inclusive en la epilepsia, en los genes codificantes de las distintas subunidades que pueden conformar las distintas subunidades de los KAR, afectando fundamentalmente a los dominios ATD y TMD. El presente trabajo de tesis doctoral aborda por vez primera un análisis exhaustivo de las implicaciones

estructurales y funcionales del SNP identificado en el gen *Grik1* (C9586732T), siendo el enfoque particular en los efectos funcionales los que constituyen el principal objeto de estudio en este tercer artículo. Dicho SNP, designado como C9586732T, presenta la variante p.H289Y situada en la subunidad GluK1, específicamente en el ATD. El análisis se lleva a cabo en la línea de hámster epiléptico GASH/Sal. A este respecto, otras variantes génicas de este gen *Grik1* han sido también relacionadas con la epileptogénesis de tipo juvenil (Izzi et al., 2002b), con eventos convulsivos en ratas WAR y en el hámster GASH/Sal (Friedman et al., 2013; Damasceno et al., 2020; Díaz-Casado et al., 2020; Díaz-Rodríguez et al., 2020), así como en personas en estudios de genética poblacional asociados a epilepsia de lóbulo temporal (Berkovic y Wiebe, 2019).

En este artículo, investigamos el significado funcional del SNP *Grik1* identificado en el hámster GASH/Sal en comparación al de su tipo silvestre [en inglés, *wild-type* (WT)], analizando mediante microscopía láser confocal la expresión y el tráfico de su proteína codificante GluK1, heterólogamente expresada en la superficie celular de ovocitos de *Xenopus laevis*. Asimismo, empleando la técnica de fijación de voltaje de dos electrodos también examinamos los efectos funcionales de la mutación H289Y en GluK1 del GASH/Sal.

3.3.2 Material y Métodos

En primer lugar, para la evaluación del impacto de la mutación H289Y en la función y estabilidad de GluK1 se emplearon dos tipos de herramientas de predicción *in silico* basadas en homología de secuencia: SIFT e iStable.

Por otra parte, para estudiar la expresión y el tráfico de GluK1 con la mutación H289Y (el del GASH/Sal) y el tipo silvestre (su control) en la superficie celular de ovocitos de *X. laevis*, se diseñaron, sintetizaron y clonaron en el vector pcDNA3.1 los dos tipos de fragmentos de cDNAs de *Grik1* de ambos tipos de hámsteres sirios (*M. auratus*). Los dos tipos de vectores de expresión (pcDNA_Grik1_WT y pcDNA_Grik1_H289Y) produjeron mediante PCR cuatro tipos de cDNAs: Grik1_WT y Grik1_H289Y de longitud completa y dos isoformas truncadas (pcDNA_Grik1_WT_nER y pcDNA_Grik1_H289Y_nER) que carecían de la región que codifica el motivo de retención del retículo endoplásmico. Cada uno de estos cuatro amplicones de PCR purificados sirvió de molde para realizar las reacciones bioquímicas de transcripción *in vitro* y poliadenilación y, finalmente, purificación y cuantificación de cada uno de los cuatro mRNAs que se emplearían para comprobar la funcionalidad o no de las correspondientes proteínas codificadas (GluK1-2b) mediante traducción en los ovocitos de *X. laevis*. Para este último

propósito, se utilizaron hembras adultas de *X. laevis* a las que se les extrajo parte de su ovario y se aislaron sus ovocitos en estadios V y VI. Posteriormente, se microinyectaron en estos ovocitos una solución que contenía cada uno de los cuatro tipos de mRNAs mencionados anteriormente.

Para realizar los estudios de expresión y el tráfico de cada proteína GluK1 en la superficie celular de ovocitos de *X. laevis* mediante visualización con microscopía láser confocal se empleó la técnica de inmunohistoquímica. De forma breve, inicialmente los ovocitos microinyectados con cada tipo de mRNA se fijaron con paraformaldehído, se incluyeron en parafina y se seccionaron en muestras de tejido de 10 mm con un microtomo. Seguidamente, se procedió a realizar la técnica de inmunohistoquímica como tal empleando un anticuerpo policlonal anti-GluK1 y las imágenes se visualizaron con el microscopio láser confocal. Finalmente, para estudiar los efectos funcionales de la mutación H289Y en GluK1 del GASH/Sal en ovocitos de *X. laevis* se empleó la técnica de fijación de voltaje de dos electrodos realizando los correspondientes registros de las corrientes de membrana en estas células a las 48-72 h después de la microinyección de los mRNAs.

3.3.3 Resultados

En primer lugar, mediante el análisis del impacto de la mutación H289Y en la función y estabilidad de GluK1 utilizando las herramientas de predicción *in silico* estimamos que esta variante génica era tolerante y no disminuía en modo alguno la estabilidad de esta proteína. Seguidamente, se analizó la expresión y localización de la subunidad proteica GluK1 del tipo silvestre y el mutante H289Y en ovocitos de *X. laevis* utilizando la técnica de inmunohistoquímica y visualizando las imágenes a microscopía láser confocal. Para ello, inicialmente con los dos vectores de expresión microinyectados en los ovocitos que codificaban la proteica completa de GluK1 no pudimos detectar ningún tipo de inmunomarcado frente a esta proteína ya que su secuencia aminoacídica contenía la región de retención en el retículo endoplasmático (Han et al., 2012) impidiendo, de este modo, alcanzar en su transporte intracelular la membrana plasmática del ovocito. Por el contrario, con los otros dos plásmidos que permitían la traducción de la proteína GluK1 truncada (sin la mencionada región de retención), detectamos inmunorreactividad para GluK1 en la membrana plasmática de los ovocitos. La comparación en secciones de estos ovocitos de la inmunorreactividad de GluK1 WT frente a la del GluK1 H289Y demostró que existía un significativo mayor nivel de expresión en esta última proteína (la mutada), fundamentalmente dentro del ovocito en la región más próxima del retículo endoplasmático a la membrana

plasmática y en esta última, tanto en el hemisferio animal como en el vegetal. A este respecto, es también destacable que el nivel de inmunodetección para ambos tipos de proteína GluK1, WT y mutada, fuera significativamente mayor en algunos puntos en el hemisferio animal frente al vegetal.

Empleando la técnica de electrofisiología, los resultados obtenidos de la evaluación de la función de GluK1 H289Y en comparación al de su WT mostraron que el porcentaje promedio del I_{Ka} máximo fue significativamente mayor para los ovocitos que incorporaron GluK1-2a H289Y que para los que expresaban GluK1-2a WT, evidenciando que la proteína mutada mejora las corrientes de kainato en los ovocitos.

No obstante, también demostramos mediante experimentos de "dosis-respuesta" y de corriente-voltaje (I-V) que la incorporación de esta mutación H289Y no modifica significativamente las propiedades funcionales de la proteína GluK1-2a en cuanto a afinidad y/o eficacia frente al kainato y tampoco la permeabilidad del canal del KAR que contiene esta proteína.

3.3.4 Discusión

La investigación del significado funcional del SNP *Grik1* (C9586732T, p.H289Y) identificado en el hámster GASH/Sal (Díaz-Casado et al., 2020) mediante la expresión heteróloga de su proteína codificante GluK1 en ovocitos de *X. laevis* demostró, en primer lugar, que se pudo identificar un mayor nivel de expresión de esta proteína (en comparación a la WT), principalmente en la membrana plasmática y de forma más pronunciada en el hemisferio animal (*vs*. vegetal) de estas células, esto último al igual que lo reportado en otros tipos de receptores muscarínicos de acetilcolina, de GABA, nicotínicos a7 y GluA3 expresados en ovocitos de esta misma especie (Kusano et al., 1982; Martínez-Torres & Miledi, 2001; Palma et al., 2002). Esta distribución diferencial de los receptores entre los hemisferios de los ovocitos podría deberse a una distribución desigual de la maquinaria de traducción y la posterior translocación de las proteínas a la membrana plasmática, o bien a una preexistencia de algunos componentes que facilitan la unión de los receptores a la membrana plasmática (Miledi et al., 1982).

En segundo lugar, la caracterización electrofisiológica por primera vez de la proteína GluK1-2a de *M. auratus* evidenció, también mediante una aproximación *in silico*, que la presencia de esta variante génica en la correspondiente proteína traducida no disminuía su estabilidad al compararse con su WT. Además, también comparando ambos tipos de proteínas GluK1, WT y

mutada, demostramos que esta última mejora significativamente las corrientes de kainato en los ovocitos. Este hecho sugiere que esta ganancia de función de GluK1 H289Y, cuya variante está localizada en el ATD, puede estar relacionada con su mayor nivel de expresión en la superficie de los ovocitos y, consecuentemente, también estar involucrada a través de un mecanismo molecular aún sin determinar en la desregulación del tráfico y expresión sináptica de los KAR que contienen esta subunidad GluK1 y en la que interviene el propio ATD de ésta (Duan et al., 2018). Por otra parte, los experimentos de "dosis-respuesta" y de relación corriente-voltaje (I-V) determinaron que la presencia de esta mutación H289Y en la proteína GluK1-2a no modificaba las propiedades funcionales de afinidad y/o eficacia frente al kainato y tampoco la permeabilidad del canal del KAR que contiene esta proteína. Este resultado parece coherente con que el dominio donde se localiza esta mutación H289Y interviene poco o nada en la regulación de la función de los KAR, principalmente debido a la interacción limitada entre los dominios ATD-LBD (Hansen et al., 2021; Meyerson et al., 2016). Por último, las características electrofisiológicas (valores de EC_{50}, coeficiente de Hill y potencial de inversión) de ambas proteínas GluK1-2a de *M. auratus* objeto de estudio en este trabajo eran similares a las de sus homologas en otras especies, que la unión de una sola molécula de kainato al LBD de estas dos proteínas era suficiente para abrir su canal iónico y que éste también era similar al descrito previamente (Alt et al., 2004; Sommer et al., 1991)

Tanto los resultados obtenidos en este tercer artículo como con los obtenidos en el artículo número dos presentando en esta tesis (Díaz-Rodríguez et al., 2020), respaldan la hipótesis de que la mutación GluK1 H289Y tiene el potencial de desregular el tráfico habitual de GluK1 WT, pero ejerce una influencia relativamente menor sobre sus propiedades funcionales y, en última instancia, la de los KAR. Con la realización de este trabajo se demostró por primera vez la funcionalidad de dos tipos de proteínas GluK1 funcionales de hámster y, en el caso de la subunidad presente en la línea GASH/Sal, su posible implicación a la epileptogénesis que padece ésta. Concluimos que GluK1-2a H289Y parece provocar un mayor tráfico de receptores KAR funcionales a sitios de la membrana neuronal dentro del circuito responsable de las convulsiones, favoreciendo así un desequilibrio excitador de la actividad neuronal en regiones cerebrales críticas dentro del modelo GASH/Sal.

4 CONCLUSIONES

Bendita tierra quindiana
donde la fe patriarcal
y los reflejos del hacha
nos abrieron la heredad.

Jorge Robledo Ortiz

En esta tesis doctoral, se aborda el estudio exhaustivo de las alteraciones genéticas y moleculares presentes en el modelo GASH/Sal, específicamente en relación con el trastorno neurológico de la epilepsia. La investigación se centra en la identificación y caracterización de las asociaciones funcionales de genes vinculados a la susceptibilidad y desencadenamiento de crisis convulsivas en hámsteres GASH/Sal, destacando la mutación que afecta al dominio ATD del receptor GluK1 como un factor clave. El análisis del transcriptoma revela cambios significativos en la expresión génica de diversos elementos relacionados con la señalización sináptica, la homeostasis del calcio y la respuesta neuronal a estímulos ambientales. A través de una evaluación detallada de la expresión del gen *Grik1* en diversas estructuras cerebrales y el análisis de las alteraciones en los niveles de su proteína codificante GluK1, se desentrañan las complejidades de la red neuronal implicada en las convulsiones audiogénicas del modelo GASH/Sal. La distribución anormal de GluK1, evidenciada por técnicas de inmunohistoquímica, revela patrones distintivos en regiones clave del cerebro, proporcionando una comprensión más profunda de la contribución de estos receptores a la hiperexcitabilidad y desincronización neuronal. Además, la caracterización de la mutación H289Y en el dominio ATD de GluK1, mediante estudios en *X. laevis*, destaca su relevancia funcional y su potencial impacto en la expresión y tráfico de los receptores glutamatérgicos que contienen la subunidad GluK1. Estos hallazgos brindan una perspectiva integral sobre las alteraciones moleculares en el modelo GASH/Sal, subrayando la importancia de los receptores de kainato tipo 1 como posibles blancos terapéuticos y resaltando la complejidad de las interacciones genéticas que subyacen a la epilepsia en este contexto específico.

Las conclusiones derivadas de esta tesis doctoral se detallan a continuación:

Primera

Existe una desregulación génica en el colículo inferior, reconocido como el núcleo epileptógeno, del modelo GASH/Sal tanto en condiciones basales como después de una estimulación sonora intensa que desencadena crisis convulsivas.

Segunda

La expresión génica en el colículo inferior de los hámsteres GASH/Sal se revela como un fenómeno extremadamente complejo, corroborado a través de diversos enfoques de análisis. El estudio comparativo del transcriptoma identificó un conjunto de 36 genes con expresión diferencial, de los cuales 24 exhibieron sobreexpresión y 12 infraexpresión en los hámsteres GASH/Sal en relación con el grupo control. Además, la validación mediante RT-qPCR confirmó

la expresión diferencial de 15 genes sobreexpresados y 8 genes infraexpresados en los hámsteres GASH/Sal en comparación con el grupo de control.

Tercera

Se evidencia la alteración en la expresión de genes asociados a diversas rutas celulares, bioquímicas y/o funcionales, incluyendo la regulación de la excitabilidad sináptica, la respuesta al estrés celular, el control transcripcional, el transporte intracelular, así como las vías de señalización de interleucinas-4 y -13, y el transporte de nucleósidos. Esto subraya la complejidad de los procesos afectados en el contexto de las convulsiones audiogénicas en el modelo GASH/Sal.

Cuarta

Las convulsiones audiogénicas en los hámsteres GASH/Sal son desencadenadas por diversos sustratos moleculares, activando múltiples procesos biológicos y rutas metabólicas asociadas a eventos epileptogénicos similares a las convulsiones tónico-clónicas en humanos.

Quinta

El polimorfismo de nucleótido único (p.His289Tyr) en el gen del receptor ionotrópico de kainato tipo 1 (*Grik1*) del modelo GASH/Sal se localiza en el dominio amino-terminal de la proteína correspondiente, afectando a la estabilidad y/o conformación de la subunidad GluK1.

Sexta

El modelo GASH/Sal exhibe modificaciones en el perfil transcripcional del gen *Grik1* en la red neuronal vinculada a las crisis audiogénicas, así como variaciones en los niveles de su proteína codificante (GluK1) en diversas estructuras cerebrales, incluyendo el colículo inferior y superior.

Séptima

La mutación p.His289Tyr en el modelo GASH/Sal posee un impacto funcional al incrementar la expresión y la incorporación de los receptores GluK1 en la membrana celular, mejorando así las corrientes inducidas por kainato.

Octava

La mutación p.His289Tyr induce cambios en el mecanismo de transporte de GluK1, sugiriendo posibles implicaciones en la disfunción de la transmisión sináptica de glutamato en el modelo GASH/Sal.

Novena

El modelo GASH/Sal emerge como un recurso valioso para identificar y caracterizar genes, sustratos moleculares y morfológicos asociados a las crisis convulsivas, proporcionando una base crucial para futuras investigaciones y estrategias terapéuticas dirigidas al sistema glutamatérgico en general y, específicamente, a los receptores de tipo kainato.

5 ANEXOS

5.1 Abreviaturas

Todas las abreviaturas incluidas en esta tesis doctoral están referidas por sus siglas en inglés para facilitar la comprensión del texto y los artículos que lo acompañan.

a.d.u.	Unidades arbitrarias de densidad	Arbitrary density units (a.d.u.).
ABC	Avidina-biotina-peroxidasa	Avidin-biotine-peroxidase
ABD	Dominio de unión al agonista	Agonist binding domain
AMG	Amígdala	Amygdala
AMPA	α -amino-3-hidroxi-5-metil-4-isoxazolpropiónico	α-amino-3-hydroxy-5-methyl-4-isoxazolepropionic
AP-1	Genes de la proteína activadora 1	Activator protein 1 Genes
ATD	Dominio amino terminal	Amino terminal domain
Atf3	Activación del factor de transcripción 3	Activating transcription factor 3
Atp2a3	ATPasa Transporte de Ca2+ en retículo sarcoplásmico/endoplásmico 3	ATPase Sarcoplasmic/endoplasmic reticulum Ca2+ transporting 3
BDNF	Factor neurotrófico derivado del cerebro	Brain-derived neurotrophic factor
bp	Pares de bases	Base pairs
C6	Complemento C6	Complement C6
CCA	Crisis convulsiva auditiva	Auditory seizure
Cd163	Molécula CD163	CD163 molecule
CDCI	Corteza dorsal del colículo inferior	Dorsal cortex of the inferior colliculus
cDNA	Ácido desoxirribonucleico complementario	Complementary deoxyribonucleic acid
CECI	Corteza externa del colículo inferior	External cortex of the inferior colliculus
CGM	Cuerpo geniculado medial	Medial geniculate body
CI	Colículo inferio	Inferior colliculus
Clic2	La proteína 2 del canal intracelular de cloruro	Chloride Intracellular Channel 2
CNS	Sistema nervioso central	Central Nervous System
COS	Complejo olivar superior	Superior olive complex
CPCS	Capas profundas del colículo superior	Deep layers of the superior colliculus
Ct	Ciclo umbral medio	Mean threshold cycle

CTD	Dominio C-terminal citoplásmico	Cytoplasmic C-terminal domain
DAB	diaminobencidina para peroxidasa	Diaminobenzidine for peroxidase
DAPI	4',6-diamidino-2-fenilindol,	4',6-diamidino-2-fenilindol,
DNA	Ácido desoxirribonucleico	Deoxyribonucleic acid
Egr	Genes de respuesta de crecimiento temprano 1, 2, 3 y 4	Early growth response 1, 2, 3 and 4 genes
FC	Tasa de cambio	Fold change
Fos, Fosb	Protooncogén Fos-Fosb	Fos-Fosb proto-oncogene
Gadd45g	Detención del crecimiento y daño al ADN gamma inducible	Growth arrest and DNA damage inducible gamma
GASH/Sal	Epilepsia audiógena de origen genética	Audiogenic epilepsy of genetic origin
GASH/Sal	Convulsiones audiogénicas genéticas en hámster de Salamanca	Genetic audiogenic seizure hamster from Salamanca
GENECARDS	La base de datos de genes humanos.	The human gene database
GEPRs	Ratas genéticamente propensas a la epilepsia	Rats genetically prone to epilepsy
GluK1	Subunidad 1 del receptor de kainato	Kainate receptor subunit 1
GluK2	Subunidad 2 del receptor de kainato	Kainate receptor subunit 2
GluK3	Subunidad 3 del receptor de kainato	Kainate receptor subunit 3
GluK4	Subunidad 2 del receptor de kainato	Kainate receptor subunit 2
GluK5	Subunidad 3 del receptor de kainato	Kainate receptor subunit 3
Gm12695	Cromosoma homólogo C1orf87 desconocido	Chromosome unknown C1orf87 homolog
GO	gen ontológico	Gene ontological
Grik1	Receptor glutamato ionotrópico, tipo 1 de kainato	Ionotropic glutamate receptor, kainate type 1
***Grik1*_WT**	Fragmento completo Grik1 tipo silvestre	The full-length Grik1 Wild type
***Grik1*-H289Y**	Fragmento completo Grik1-H289Y	The full-length Grik1-H289Y
Grik2	Receptor glutamato ionotrópico, tipo 2 de kainato	Ionotropic glutamate receptor, kainate type 2
Grik3	Receptor glutamato ionotrópico, tipo 3 de kainato	Ionotropic glutamate receptor, kainate type 3
Grik4	Receptor glutamato ionotrópico, tipo 2 de kainato	Ionotropic glutamate receptor, kainate type 2

Grik5	Receptor glutamato ionotrópico, tipo 3 de kainato	Ionotropic glutamate receptor, kainate type 3
Grin2c	Subunidad tipo 2C del receptor ionotrópico NMDA de glutamato	Glutamate ionotropic receptor NMDA type subunit 2C
H289Y GluK1-2a	Fragmento truncado WT GluK1-2a	Truncated fragment WT GluK1-2a
H289Y GluK1-2a	Fragmento truncado H289Y GluK1-2a	Truncated fragment H289Y GluK1-2a
Hys	Histidina	Histidine
IC	Colículo inferior	Inferior colliculus
IKas	Corrientes evocadas por el kainato	Currents evoked by the kainate
IL-4, IL-13	Interleucina-4 y -13	Interleukin-4 and -13
ILAE	La Liga Internacional en Contra de la Epilepsia	The International League Against Epilepsy
IntDen	Media de los valores de grises	Mean value of gray
Junb	Protooncogén Junb	Junb proto-oncogene
KAR	Receptores de kainato	Kainate receptors
KCC2	K+/-2Cl− cotrasnportador 2	K+/-2Cl− cotrasnporter 2
Kcnj13	Miembro 13 de la subfamilia J del canal dependiente de voltaje de potasio	Potassium voltage-gated channel subfamily J member 13
Kcns1	Miembro 1 de la subfamilia S del modificador de canal dependiente de voltaje de potasio	Potassium voltage-gated channel modifier subfamily S member 1
KEGG	Enciclopedia de genes y genomas de Kioto	Kyoto encyclopedia of genes and genomes
Kir	Canales de K+ rectificadores hacia el interior	Inwardly rectifying K+ channels
Kv	K+ dependiente de voltaje	Voltage-gated K+
LBD	Dominio de unión a ligando	Ligand binding domain
LGICs	Canales iónicos activados por ligando	Ligand-gated ion channels
logFC	Logaritmo del cambio de pliegue	Logarithm of Fold change
LTD	Depresión de larga duración	Long-term depression
LTP	Potenciación de larga duración	Long lasting enhancement
M1	Hélice transmembrana 1	Transmembrane helix 1

M2	Hélice transmembrana 2	Transmembrane helix 2
M3	Hélice transmembrana 3	Transmembrane helix 3
M4	Hélice transmembrana 4	Transmembrane helix 4
mGluR	Metabotrópicos de glutamato	Glutamate metabotropics
Mmp3	Matriz metalopeptidasa 3	Matrix metallopeptidase 3
mRNA	El ácido ribonucleico mensajero	Messager Ribonucleic acid
NC	Núcleo coclear	Cochlear nucleus
NCCI	Núcleo central del colículo inferior	Central nucleus of the inferior colliculus.
NeuN	Marcador de neuronas	Neuronal Marker
NKCC1	Na-K-2Cl cotransportador 1	Na-K-2Cl cotransporter 1
NLL	Núcleo del lemnisco lateral	Nucleus of lateral lemniscus
NMDA	Receptores de N-metil-d-aspartato	N-methyl-d-aspartate receptors
NMDAR	Receptor de N-metil-D-aspartato	N-methyl -D-aspartate receptor
Npas4	Dominio PAS neuronal 4	Neuronal PAS domain 4
Ogn	osteoglicina	Osteoglycin
PANTHER	Análisis de proteínas a través de relaciones evolutivas.	Protein analysis through evolutionary relationships
PBS	Buffer fosfato salino	Phosphate-buffered saline
PCR	reacción en cadena de la polimerasa	Polymerase chain reaction
Phred	Control de calidad	Control of quality
PRF	Formación reticular pontina	Pontine reticular formation
Q	Glutamina	Glutamine
Rab29	Miembro de la familia de oncogén RAS RAB29	RAB29 Member RAS oncogene family
RawInDent	Suma de los valores de los píxeles.	Sum of the values of the pixels in the image or selection
Renbp	Proteína fijadora de renina	Renin binding protein
Ripa	Radioinmunoprecipitación	Radioimmunoprecipitation
RNA	Ácido ribonucleico	Ribonucleic acid
ROC	Canal receptor-operador	Receptor-operator channel
RT-qPCR	Reacción en cadena de la polimeras cuantitativa en tiempo real	Real-time quantitative polymer chain reaction

Rxfp2	Receptor peptídico 2 de la familia de la relaxina	Relaxin family peptide receptor 2
SC	Colículo Superior	Superior colliculus
SEM	Hemi-estandar desviacion	Hemistandard deviation
SERCA	Ca2+ ATPasa sarco/retículo endoplásmico	Sarco/endoplasmic reticulum Ca2+ ATPase
SHISA9	Miembro de la familia Shisa 9	Shisa Family Member 9
SI	índice de gravedad	severity index
Slc13a4	Familia de portadores de solutos 13 miembros 4	Solute carrier family 13 member 4
Slc28a1	Familia de portadores de solutos 28 miembros 1	Solute carrier family 28 member 1
Slc6a4	Familia de portadores de solutos 6 miembros 4	Solute carrier family 6 member 4
SNR	Reticular de la sustancia negra	Substantia nigra reticular
SPG	Sustancia gris periacueductal	Periaqueductal gray matter
SPN	Polimorfismo de un unico nucleotido	Single-nucleotide polymorphism
Sucnr1	Receptor de succinato 1	Succinate receptor 1
Tbp	La proteína de unión a TATA	TATA-box binding protein
TBS	Solución salina tamponada con Tris	Tris-buffered saline
TBS	Solución salina tamponada con Tris	Tris-buffered saline solution
TBS-T	Solución salina tamponada con Tris - Triton	Tris-buffered saline - triton
TMD	Dominio transmembrana	Transmembrane domain
Ttr	Transtiretina	Transthyretin
Tyr	Tirosina	Tyrosine
WAR	Wistar Audiogénica	Wistar Audiogenic
Wdr38	WD repite el dominio 38.	WD repeat domain 38.

5.2 Comunicaciones a congresos

18 congreso Senc, Santiago de Compostela, 4 al 6 de septiembre de 2019
AUTORES: Zeballos L, Díaz-Casado ME, **Díaz-Rodríguez SM**, Auzmendi J, Lazarowski A, Sancho C, Gómez-Nieto R, López DE.
TITULO: DEFECTS IN THE EXPRESSION OF GENES ASSOCIATED WITH REFRACTORY EPILEPSY IN THE GASH/SAL MODEL.
TIPO DE PARTICIPACIÓN: póster

VI congreso de la sociedad española de epilepsia 2019. málaga 24,25 y 26 octubre 2019.
AUTORES: Sandra M. Díaz-Rodríguez, Daniel López-López, Manuel J. Herrero-Turrión, Samara Damasceno, Elena Díaz-Casado y Dolores E. López.
TITULO: ANÁLISIS DEL TRANSCRIPTOMA DEL FOCO EPILEPTOGÉNICO EN EL MODELO DE EPILEPSIA GASH/Sal. TIPO DE PARTICIPACIÓN: póster

Sesión científica-exhibición de posters. Instituto de Neurociencias de Castilla y León. Salamanca, *21 noviembre de 2019.*
AUTORES: Sandra M. Díaz-Rodríguez, Daniel López-López, Manuel J. Herrero-Turrión, Samara Damasceno, Elena Díaz-Casado y Dolores E. Lopéz
TITULO: ANÁLISIS DEL TRANSCRIPTOMA DEL FOCO EPILEPTOGÉNICO EN EL MODELO DE EPILEPSIA GASH/Sal
TIPO DE PARTICIPACIÓN: póster

Sesión científica-exhibición de posters. Instituto de Neurociencias de Castilla y León. Salamanca, *21 noviembre de 2020.*
AUTORES: **Sandra M. Díaz-Rodríguez**, Daniel López-López, Manuel J. Herrero-Turrión, Samara Damasceno, Elena Díaz-Casado y Dolores E. Lopéz
TITULO: ANÁLISIS DEL TRANSCRIPTOMA DEL FOCO EPILEPTOGÉNICO EN EL MODELO DE EPILEPSIA GASH/Sal
TIPO DE PARTICIPACIÓN: póster

34th International Epilepsy Congress. del 28 agosto al 1 septiembre 2021. Online.
AUTORES: **Sandra Marcela Díaz Rodríguez**, M. Javier Herrero Turrión, Jose M de Pereda, Dolores E. López TITULO: GENE VARIANTS INVOLVED IN THE GLUTAMATE AND CALCIUM PATHWAY IN THE EPILEPTIC MODEL HAMSTER GASH/SAL.
TIPO DE PARTICIPACIÓN: Póster 1035

Sesión científica-exhibición de posters. Instituto de Neurociencias de Castilla y León. Salamanca, *12 noviembre de 2021.*
AUTORES: **Sandra M. Díaz-Rodríguez**, Manuel J. Herrero-Turrión, Ricardo Gómez-Nieto, de Pereda JM, Dolores E. López
TITULO: *GRIK1* AND *CACNA2D3* POLYMORPHISMS AND ITS IMPLICATION IN SEIZURES IN THE GASH/SAL MODEL OF EPILEPSY
TIPO DE PARTICIPACIÓN: póster

VII Congreso de la Sociedad Española de epilepsia. Santander, 21-24 octubre, 2021.
AUTORES: **Sandra M. Díaz-Rodríguez**, Manuel J. Herrero-Turrión, Ricardo Gómez-Nieto, de Pereda JM, Dolores E. López.
TITULO: *GRIK1* AND *CACNA2D3* POLYMORPHISMS AND ITS IMPLICATION IN SEIZURES IN THE GASH/SAL MODEL OF EPILEPSY
TIPO DE PARTICIPACIÓN: Comunicación oral

VII Congreso de la Sociedad Española de epilepsia. Santander, 21-24 octubre, 2021.
AUTORES: Giselda Eunice Cabral Pereira, Laura Zeballos, **Sandra Marcela Diaz Rodríguez**, Jaime Goncalvez Sánchez, Orlando Jorge Castellano Benítez, María Dolores López García
TITULO: LA ADMINISTRACIÓN DE CANNABIDIOL EN EL MODELO ANIMAL DE EPILEPSIA AFECTA EL COMPORTAMIENTO DE LA ACTIVIDAD LOCOMOTORA
TIPO DE PARTICIPACIÓN: CO-21

19th Congreso de la Sociedad Española de Neurociencias. Lleida, 3 al 1 noviembre 2021.
AUTORES: Sandra M. Díaz-Rodríguez, de Pereda JM, Manuel J. Herrero-Turrión, Ricardo Gómez-Nieto, Dolores E. López.
TITULO: *GRIK1* AND *CACNA2D3* POLYMORPHISMS AND ITS IMPLICATION IN SEIZURES IN THE GASH/SAL MODEL OF EPILEPSY
TIPO DE PARTICIPACIÓN: póster

I Jornada de encuentro entre grupos de investigación del Instituto de Investigación Biomédica de Salamanca. Salamanca, 27 de mayo de 2022.
AUTORES: **Sandra M. Díaz-Rodríguez**, de Pereda JM, Manuel J. Herrero-Turrión, Ricardo Gómez-Nieto, Dolores E. Lopéz
TITULO: GRIK1 POLYMORPHISM AND ITS IMPLICATION IN SEIZURES IN THE GASH/SAL MODEL OF EPILEPSY
TIPO DE PARTICIPACIÓN: póster

Congreso Alianza en epilepsia. Salamanca, 22 junio 2022 Asistencia.
International parthership symposium FAPESP/USAL "A holistic approach spanning epilepsa reaserch". Salamanca, 27- 30 junio 2022
Comité Organizador del congreso.
AUTORES: **Sandra M. Díaz-Rodríguez**, de Pereda JM, Manuel J. Herrero-Turrión, Ricardo Gómez-Nieto, Dolores E. Lopéz.
TITULO: GRIK1 POLYMORPHISM AND ITS IMPLICATION IN SEIZURES IN THE GASH/SAL MODEL OF EPILEPSY
TIPO DE PARTICIPACIÓN: póster

Sesión científica-exhibición de posters. Instituto de Neurociencias de Castilla y León. Salamanca, 13 octubre de 2022.
Póster: AUTORES: **Sandra M. Díaz-Rodríguez**, de Pereda JM, Manuel J. Herrero-Turrión, Ricardo Gómez-Nieto, Dolores E. López
TITULO: GRIK1 POLYMORPHISM AND ITS IMPLICATION IN SEIZURES IN THE GASH/SAL MODEL OF EPILEPSY
TIPO DE PARTICIPACIÓN: póster

VIII Congreso de la Sociedad Española de Epilepsia. Santander, 20-22 octubre de 2022.
AUTORES: **Sandra M. Díaz-Rodríguez**, de Pereda JM, Manuel J. Herrero-Turrión, Ricardo Gómez-Nieto, Dolores E. López
TITULO: GRIK1 POLYMORPHISM AND ITS IMPLICATION IN SEIZURES IN THE GASH/SAL MODEL OF EPILEPSY
TIPO DE PARTICIPACIÓN: póster

VIII Congreso de la Sociedad Española de Epilepsia. Santander, 20-22 octubre de 2022.
AUTORES: **Sandra Díaz-Rodríguez**, Laura Zeballos Fernández, David Sánchez-Benito, Rui Milton Patrício Da Silva- Júnior, Giselda Cabral Pereira, Dolores E. López.
TITULO: DIFFERENTIAL PROTEIN PROFILE OF THE EPILEPTOGENIC NUCLEUS OF THE HAMSTER GASH/SAL, A GENETIC MODEL OF AUDIOGENIC SEIZURES.
TIPO DE PARTICIPACIÓN: póster
3er premio

The roots of auditory Neuroscience Spain: from past to future. Salamanca, 8-9 junio de 2023.
TIPO DE PARTICIPACIÓN: Asistente

Congreso Alianza en epilepsia. Salamanca, 29 junio 2023
TIPO DE PARTICIPACIÓN: Asistente.

11th IBRO World Congress of Neuroscience. Granada, 9-13 septiembre 2023
AUTORES: Sandra M. Díaz-Rodríguez, Isabel Ivorra, Javier Espinosa, Armando Alberola-Die, Manuel J. Herrero-Turrión, Ricardo Gómez-Nieto, Dolores E. López.
TITULO: INVESTIGATING THE FUNCTIONAL IMPACT OF THE GENETIC VARIANT P.H289Y IN GRIK1 GENE OF AN ANIMAL MODEL OF AUDIOGENIC SEIZURES: AN ELECTROPHYSIOLOGICAL APPROACH IN XENOPUS OOCYTES.
TIPO DE PARTICIPACIÓN: póster
AUTORES: Sandra M. Díaz-Rodríguez, J. Herrero-Turrión, Carlos Garcia, Dolores E. López, Ricardo Gómez-Nieto,
TITULO: EXPLORING THE SINGLE-NUCLEOTIDE VARIANT EFFECTS OF THE GLUTAMATE RECEPTOR IONOTROPIC KAINATE-1 (GRIK1) GENE IN THE GENETICALLY AUDIOGENIC SEIZURE-PRONE HAMSTER GASH/SAL.
TIPO DE PARTICIPACIÓN: póster

5.3 Premios Recibidos

Categoría: Premio Alumni Internacional "López Martí": Primera edición. (Dotado con 1000€), Destinado: destinado a alumnos extranjeros que han realizado el Máster en Universidad de Salamanca https://alumni.usal.es/entrevistas-premiados-alumni-2019/

Categoría: Poster "TERCER PUESTO"
CONGRESO: SOCIEDAD ESPAÑOLA DE NEUROCIENCIAS, 20-22 octubre de 2022.
Título: Differential protein profile of the epileptogenic nucleus of the hamster GASH/Sal, a genetic model of audiogenic seizures.

5.4 Otros artículos

Cabral-Pereira, G., Sánchez-Benito, D., **Díaz-Rodríguez, S. M**., Gonçalves, J., Sancho, C., Castellano, O., Muñoz, L. J., López, D. E., & Gómez-Nieto, R. (2021). Behavioral and Molecular Effects Induced by Cannabidiol and Valproate Administration in the GASH/Sal Model of Acute Audiogenic Seizures. *Frontiers in Behavioral Neuroscience*, *14* (January), 1–22. https://doi.org/10.3389/fnbeh.2020.612624

6. BIBLIOGRAFÍA

Alt, A., Weiss, B., Ogden, A. M., Knauss, J. L., Oler, J., Ho, K., Large, T. H., & Bleakman, D. (2004). Pharmacological characterization of glutamatergic agonists and antagonists at recombinant human homomeric and heteromeric kainate receptors in vitro. *Neuropharmacology*, *46*(6), 793–806. https://doi.org/10.1016/j.neuropharm.2003.11.026

Aronica, E., Dickson, D. W., Kress, Y., Morrison, J. H., & Zukin, R. S. (1997). Non-plaque dystrophic dendrites in Alzheimer hippocampus: a new pathological structure revealed by glutamate receptor immunocytochemistry. *Neuroscience*, *82*(4), 979–991. https://doi.org/10.1016/S0306-4522(97)00260-1

Artinian, J., Peret, A., Marti, G., Epsztein, J., & Crepel, V. (2011). Synaptic Kainate Receptors in Interplay with INaP Shift the Sparse Firing of Dentate Granule Cells to a Sustained Rhythmic Mode in Temporal Lobe Epilepsy. *Journal of Neuroscience*, *31*(30), 10811–10818. https://doi.org/10.1523/JNEUROSCI.0388-11.2011

Aseervatham, G. S. B., Suryakala, U., Doulethunisha, Sundaram, S., Bose, P. C., & Sivasudha, T. (2016). Expression pattern of NMDA receptors reveals antiepileptic potential of apigenin 8-C-glucoside and chlorogenic acid in pilocarpine induced epileptic mice. *Biomedicine & Pharmacotherapy*, *82*, 54–64. https://doi.org/10.1016/j.biopha.2016.04.066

Ayalon, G., & Stern-Bach, Y. (2001). Functional Assembly of AMPA and Kainate Receptors Is Mediated by Several Discrete Protein-Protein Interactions. *Neuron*, *31*(1), 103–113. https://doi.org/10.1016/S0896-6273(01)00333-6

Barbon, A., & Barlati, S. (2000). Genomic organization, proposed alternative splicing mechanisms, and RNA editing structure of GRIK1. *Cytogenetic and Genome Research*, *88*(3–4), 236–239. https://doi.org/10.1159/000015558

Barker-Haliski, M., & White, H. S. (2015). Glutamatergic Mechanisms Associated with Seizures and Epilepsy. *Cold Spring Harbor Perspectives in Medicine*, *5*(8), a022863. https://doi.org/10.1101/cshperspect.a022863

Barrera-Bailón, B., Oliveira, J. A. C., López, D. E., Muñoz, L. J., Garcia-Cairasco, N., & Sancho, C. (2013). Pharmacological and neuroethological studies of three antiepileptic drugs in the Genetic Audiogenic Seizure Hamster (GASH:Sal). *Epilepsy & Behavior*, *28*(3), 413–425. https://doi.org/10.1016/j.yebeh.2013.05.028

Barrera-Bailón, B., Oliveira, J. A. C., López, D. E., Muñoz, L. J., Garcia-Cairasco, N., & Sancho, C. (2017). Pharmacological and neuroethological study of the acute and chronic effects of lamotrigine in the genetic audiogenic seizure hamster (GASH:Sal). *Epilepsy & Behavior*, *71*, 207–217. https://doi.org/10.1016/j.yebeh.2015.11.005

Bathgate, R. A., Ivell, R., Sanborn, B. M., Sherwood, O. D., & Summers, R. J. (2006). International Union of Pharmacology LVII: Recommendations for the Nomenclature of Receptors for Relaxin Family Peptides. *Pharmacological Reviews*, *58*(1), 7–31. https://doi.org/10.1124/pr.58.1.9

Beaumont, T. L., Yao, B., Shah, A., Kapatos, G., & Loeb, J. A. (2012). Layer-Specific CREB Target Gene Induction in Human Neocortical Epilepsy. *Journal of Neuroscience*, *32*(41), 14389–14401a. https://doi.org/10.1523/JNEUROSCI.3408-12.2012

Begni, S., Popoli, M., Moraschi, S., Bignotti, S., Tura, G. B., & Gennarelli, M. (2002). Association between the ionotropic glutamate receptor kainate 3 (GRIK3) ser310ala polymorphism and schizophrenia. *Molecular Psychiatry*, *7*(4), 416–418. https://doi.org/10.1038/sj.mp.4000987

Ben-Ari, Y. (2014). The GABA excitatory/inhibitory developmental sequence: A personal journey. *Neuroscience*, *279*, 187–219. https://doi.org/10.1016/j.neuroscience.2014.08.001

Berkovic, S. F., & Wiebe, S. (2019). *International League Against Epilepsy's*. https://www.ilae.org/journals/epigraph/epigraph-vol-21-issue-1-winter-2019/ilae-consortium-identifies-novel-epilepsy-genes

Bettler, B., Boulter, J., Hermans-Borgmeyer, I., O'Shea-Greenfield, A., Deneris, E. S., Moll, C., Borgmeyer, U., Hollmann, M., & Heinemann, S. (1990). Cloning of a novel glutamate receptor subunit, GluR5: Expression in the nervous system during development. *Neuron*, *5*(5), 583–595. https://doi.org/10.1016/0896-6273(90)90213-Y

Boison, D. (2013). Adenosine and Seizure Termination: Endogenous Mechanisms. *Epilepsy Currents*, *13*(1), 35–37. https://doi.org/10.5698/1535-7511-13.1.35

Buckingham, S. C., Ramos, T. N., & Barnum, S. R. (2014). Complement C5-deficient mice are protected from seizures in experimental cerebral malaria. *Epilepsia*, *55*(12), e139–e142. https://doi.org/10.1111/epi.12858

Cabral-Pereira, G., Sánchez-Benito, D., Díaz-Rodríguez, S. M., Gonçalves, J., Sancho, C., Castellano, O., Muñoz, L. J., López, D. E., & Gómez-Nieto, R. (2021). Behavioral and Molecular Effects Induced by Cannabidiol and Valproate Administration in the GASH/Sal Model of Acute Audiogenic Seizures. *Frontiers in Behavioral Neuroscience*, *14*(January), 1–22. https://doi.org/10.3389/fnbeh.2020.612624

Carballosa-Gonzalez, M. M., Muñoz, L. J., López-Alburquerque, T., Pardal-Fernández, J. M., Nava, E., de Cabo, C., Sancho, C., & López, D. E. (2013). EEG characterization of audiogenic seizures in the hamster strain GASH:Sal. *Epilepsy Research*, *106*(3), 318–325. https://doi.org/10.1016/j.eplepsyres.2013.07.001

Carta, M., Fièvre, S., Gorlewicz, A., & Mulle, C. (2014). Kainate receptors in the hippocampus. *European Journal of Neuroscience*, *39*(11), 1835–1844. https://doi.org/10.1111/ejn.12590

Chou, T.-H., Tajima, N., Romero-Hernandez, A., & Furukawa, H. (2020). Structural Basis of Functional Transitions in Mammalian NMDA Receptors. *Cell*, *182*(2), 357-371.e13. https://doi.org/10.1016/j.cell.2020.05.052

Collingridge, G. L., Olsen, R. W., Peters, J., & Spedding, M. (2009). A nomenclature for ligand-gated ion channels. *Neuropharmacology*, *56*(1), 2–5. https://doi.org/10.1016/j.neuropharm.2008.06.063

Contractor, A., Mulle, C., & Swanson, G. T. (2011a). Kainate receptors coming of age: milestones of two decades of research. *Trends in Neurosciences*, *34*(3), 154–163. https://doi.org/10.1016/j.tins.2010.12.002

Contractor, A., Mulle, C., & Swanson, G. T. (2011b). Kainate receptors coming of age: milestones of two decades of research. *Trends in Neurosciences*, *34*(3), 154–163. https://doi.org/10.1016/j.tins.2010.12.002

Contreras-Leal, E., Hernández-Oliveras, A., Flores-Peredo, L., Zarain-Herzberg, Á., & Santiago-García, J. (2016). Histone deacetylase inhibitors promote the expression of ATP2A3 gene in breast cancer cell lines. *Molecular Carcinogenesis*, *55*(10), 1477–1485. https://doi.org/10.1002/mc.22402

Copits, B. A., Vernon, C. G., Sakai, R., & Swanson, G. T. (2014). Modulation of ionotropic glutamate receptor function by vertebrate galectins. *The Journal of Physiology*, *592*(10), 2079–2096. https://doi.org/10.1113/jphysiol.2013.269597

Costa, J. J. do N., Passos, M. J., Passos, J. R. de S., Hurk, R. van den, & Silva, J. R. V. (2013). Real time PCR and importance of housekeepings genes for normalization and quantification of mRNA expression in different tissues. *Brazilian Archives of Biology and Technology*, *56*(1), 143–154. https://doi.org/10.1590/S1516-89132013000100019

Damasceno, S., Gómez-Nieto, R., Garcia-Cairasco, N., Herrero-Turrión, M. J., Marín, F., & Lopéz, D. E. (2020). Top Common Differentially Expressed Genes in the Epileptogenic Nucleus of Two Strains of Rodents Susceptible to Audiogenic Seizures: WAR and GASH/Sal. *Frontiers in Neurology*, *11*. https://doi.org/10.3389/fneur.2020.00033

Diano, S., Naftolin, F., & Horvath, T. L. (2008). Kainate Glutamate Receptors (GluR5-7) in the Rat Arcuate Nucleus: Relationship to Tanycytes, Astrocytes, Neurons and Gonadal Steroid Receptors. *Journal of Neuroendocrinology*, *10*(4), 239–247. https://doi.org/10.1046/j.1365-2826.1998.00195.x

Díaz-Casado, E., Gómez-Nieto, R., de Pereda, J. M., Muñoz, L. J., Jara-Acevedo, M., & López, D. E. (2020). Analysis of gene variants in the GASH/Sal model of epilepsy. *PLOS ONE*, *15*(3), e0229953. https://doi.org/10.1371/journal.pone.0229953

Díaz-Rodríguez, S. M., López-López, D., Herrero-Turrión, M. J., Gómez-Nieto, R., Canal-Alonso, A., & Lopéz, D. E. (2020). Inferior Colliculus Transcriptome After Status Epilepticus in the Genetically Audiogenic Seizure-Prone Hamster GASH/Sal. *Frontiers in Neuroscience*, *14*. https://doi.org/10.3389/fnins.2020.00508

Dobin, A., Davis, C. A., Schlesinger, F., Drenkow, J., Zaleski, C., Jha, S., Batut, P., Chaisson, M., & Gingeras, T. R. (2013). STAR: ultrafast universal RNA-seq aligner. *Bioinformatics*, *29*(1), 15–21. https://doi.org/10.1093/bioinformatics/bts635

Duan, G.-F., Ye, Y., Xu, S., Tao, W., Zhao, S., Jin, T., Nicoll, R. A., Shi, Y. S., & Sheng, N. (2018a). Signal peptide represses GluK1 surface and synaptic trafficking through binding to amino-terminal domain. *Nature Communications*, *9*(1), 4879. https://doi.org/10.1038/s41467-018-07403-7

Duan, G.-F., Ye, Y., Xu, S., Tao, W., Zhao, S., Jin, T., Nicoll, R. A., Shi, Y. S., & Sheng, N. (2018b). Signal peptide represses GluK1 surface and synaptic trafficking through binding to amino-

terminal domain. *Nature Communications*, *9*(1), 4879. https://doi.org/10.1038/s41467-018-07403-7

Elliott, R. C., & Gall, C. M. (2000). Changes in Activating Protein 1 (AP-1) Composition Correspond with the Biphasic Profile of Nerve Growth Factor mRNA Expression in Rat Hippocampus after Hilus Lesion-Induced Seizures. *The Journal of Neuroscience*, *20*(6), 2142–2149. https://doi.org/10.1523/JNEUROSCI.20-06-02142.2000

Eyigor, O., Minbay, Z., Cavusoglu, I., & Jennes, L. (2005). Localization of kainate receptor subunit GluR5-immunoreactive cells in the rat hypothalamus. *Molecular Brain Research*, *136*(1–2), 38–44. https://doi.org/10.1016/j.molbrainres.2005.01.015

Faingold, C. L. (1999). Neuronal networks in the genetically epilepsy-prone rat. *Adv Neurol*, *79*, 311-21.

Falcón-Moya, R., Losada-Ruiz, P., Sihra, T. S., & Rodríguez-Moreno, A. (2018). Cerebellar Kainate Receptor-Mediated Facilitation of Glutamate Release Requires Ca2+-Calmodulin and PKA. *Frontiers in Molecular Neuroscience*, *11*. https://doi.org/10.3389/fnmol.2018.00195

Feng, M., Wang, Q., Wang, H., & Guan, W. (2013). Tumor necrosis factor-alpha preconditioning attenuates liver ischemia/reperfusion injury through preserving sarco/endoplasmic reticulum calcium-ATPase function. *Journal of Surgical Research*, *184*(2), 1109–1113. https://doi.org/10.1016/j.jss.2013.04.019

Fisher, R. S., Boas, W. van E., Blume, W., Elger, C., Genton, P., Lee, P., & Engel, J. (2005). Epileptic Seizures and Epilepsy: Definitions Proposed by the International League Against Epilepsy (ILAE) and the International Bureau for Epilepsy (IBE). *Epilepsia*, *46*(4), 470–472. https://doi.org/10.1111/j.0013-9580.2005.66104.x

Franco, A., Bentes, C., de Carvalho, M., Pereira, P., Pimentel, J., & Conceição, I. (2016). Epileptic seizures as a presentation of central nervous system involvement in TTR Val30Met-FAP. *Journal of Neurology*, *263*(11), 2336–2338. https://doi.org/10.1007/s00415-016-8299-5

Franois, J., Boehrer, A., & Nehlig, A. (2008). Effects of Carisbamate (RWJ-333369) in Two Models of Genetically Determined Generalized Epilepsy, the GAERS and the Audiogenic Wistar AS. *Epilepsia*, *49*(3), 393–399. https://doi.org/10.1111/j.1528-1167.2007.01278.x

Friedman, L. K., Mancuso, J., Patel, A., Kudur, V., Leheste, J. R., Iacobas, S., Botta, J., Iacobas, D. A., & Spray, D. C. (2013). Transcriptome profiling of hippocampal CA1 after early-life seizure-induced preconditioning may elucidate new genetic therapies for epilepsy. *European Journal of Neuroscience*, *38*(1), 2139–2152. https://doi.org/10.1111/ejn.12168

Fritsch, B., Reis, J., Gasior, M., Kaminski, R. M., & Rogawski, M. A. (2014). Role of GluK1 Kainate Receptors in Seizures, Epileptic Discharges, and Epileptogenesis. *Journal of Neuroscience*, *34*(17), 5765–5775. https://doi.org/10.1523/JNEUROSCI.5307-13.2014

Fuentes-Santamaría, V., Alvarado, J. C., Herranz, A. S., García-Atarés, N., & López, D. E. (2007). Morphologic and neurochemical alterations in the superior colliculus of the genetically epilepsy-prone hamster (GPG/Vall). *Epilepsy Research*, *75*(2–3), 206–219. https://doi.org/10.1016/j.eplepsyres.2007.06.005

Fuerte-Hortigón, A., Gonçalves, J., Zeballos, L., Masa, R., Gómez-Nieto, R., & López, D. E. (2021). Distribution of the Cannabinoid Receptor Type 1 in the Brain of the Genetically Audiogenic Seizure-Prone Hamster GASH/Sal. *Frontiers in Behavioral Neuroscience*, *15*. https://doi.org/10.3389/fnbeh.2021.613798

Furukawa, H. (2012). Structure and function of glutamate receptor amino terminal domains. *The Journal of Physiology*, *590*(1), 63–72. https://doi.org/10.1113/jphysiol.2011.213850

Galen Wo, Z., & Oswald, R. E. (1995). Unraveling the modular design of glutamate-gated ion channels. *Trends in Neurosciences*, *18*(4), 161–168. https://doi.org/10.1016/0166-2236(95)93895-5

Garcia-Cairasco, N. (2002). A critical review on the participation of inferior colliculus in acoustic-motor and acoustic-limbic networks involved in the expression of acute and kindled audiogenic seizures. *Hearing Research*, *168*(1–2), 208–222. https://doi.org/10.1016/S0378-5955(02)00371-4

Garcia-Cairasco, N., Umeoka, E. H. L., & Cortes de Oliveira, J. A. (2017). The Wistar Audiogenic Rat (WAR) strain and its contributions to epileptology and related comorbidities: History and perspectives. *Epilepsy & Behavior*, *71*, 250–273. https://doi.org/10.1016/j.yebeh.2017.04.001

Garcia-Cairasco, N., Wakamatsu, H., Oliveira, J. A. C., Gomes, E. L. T., Del Bel, E. A., & Mello, L. E. A. M. (1996). Neuroethological and morphological (Neo-Timm staining) correlates of limbic recruitment during the development of audiogenic kindling in seizure susceptible Wistar rats. *Epilepsy Research*, *26*(1), 177–192. https://doi.org/10.1016/S0920-1211(96)00050-2

García-Peral, C., Ledesma, M. M., Herrero-Turrión, M. J., Gómez-Nieto, R., Castellano, O., & López, D. E. (2023). Proteomic and Bioinformatic Tools to Identify Potential Hub Proteins in the Audiogenic Seizure-Prone Hamster GASH/Sal. *Diagnostics*, *13*(6), 1048. https://doi.org/10.3390/diagnostics13061048

Garey, L. J., Von Bussmann, K. A., & Hirsch, S. R. (2006). Decreased numerical density of kainate receptor-positive neurons in the orbitofrontal cortex of chronic schizophrenics. *Experimental Brain Research*, *173*(2), 234–242. https://doi.org/10.1007/s00221-006-0396-8

Gariboldi, M., Tutka, P., Samanin, R., & Vezzani, A. (1996). Stimulation of 5-HT1A receptors in the dorsal hippocampus and inhibition of limbic seizures induced by kainic acid in rats. *British Journal of Pharmacology*, *119*(5), 813–818. https://doi.org/10.1111/j.1476-5381.1996.tb15745.x

Gielen, M., Le Goff, A., Stroebel, D., Johnson, J. W., Neyton, J., & Paoletti, P. (2008). Structural Rearrangements of NR1/NR2A NMDA Receptors during Allosteric Inhibition. *Neuron*, *57*(1), 80–93. https://doi.org/10.1016/j.neuron.2007.11.021

Gómez-Nieto, R., López, D. E., & Garcia-Cairasco, N. (2021). Editorial: Challenges and Conundrums in Cannabinoid-Based Treatments for Epilepsy Syndromes and Associated Neurobehavioral Comorbidities. *Frontiers in Behavioral Neuroscience*, *15*. https://doi.org/10.3389/fnbeh.2021.781852

Good, P. F., Huntley, G. W., Rogers, S. W., Heinemann, S. F., & Morrison, J. H. (1993). Organization and quantitative analysis of kainate receptor subunit GluR5-7 immunoreactivity in monkey hippocampus. *Brain Research*, *624*(1–2), 347–353. https://doi.org/10.1016/0006-8993(93)90102-S

Grabenstatter, H. L., Russek, S. J., & Brooks-Kayal, A. R. (2012). Molecular pathways controlling inhibitory receptor expression. *Epilepsia*, *53*, 71–78. https://doi.org/10.1111/epi.12036

Gregor, P., O'Hara, B. F., Yang, X., & Uhl, G. R. (1993). Expression and novel subunit isoforms of glutamate receptor genes GluR5 and GluR6. *NeuroReport*, *4*(12), 1343–1346. https://doi.org/10.1097/00001756-199309150-00014

Han, Y., Wang, C., Park, J. S., & Niu, L. (2012). Channel-Opening Kinetic Mechanism of Wild-Type GluK1 Kainate Receptors and a C-Terminal Mutant. *Biochemistry*, *51*(3), 761–768. https://doi.org/10.1021/bi201446z

Hansen, K. B., Wollmuth, L. P., Bowie, D., Furukawa, H., Menniti, F. S., Sobolevsky, A. I., Swanson, G. T., Swanger, S. A., Greger, I. H., Nakagawa, T., McBain, C. J., Jayaraman, V., Low, C.-M., Dell'Acqua, M. L., Diamond, J. S., Camp, C. R., Perszyk, R. E., Yuan, H., & Traynelis, S. F. (2021). Structure, Function, and Pharmacology of Glutamate Receptor Ion Channels. *Pharmacological Reviews*, *73*(4), 1469–1658. https://doi.org/10.1124/pharmrev.120.000131

Hansen, C. V., Schroll, H. J., & Wüstner, D. (2018). A Discontinuous Galerkin Model for Fluorescence Loss in Photobleaching. *Scientific Reports*, *8*(1), 1387. https://doi.org/10.1038/s41598-018-19159-7

Herguedas, B., Krieger, J., & Greger, I. H. (2013). *Receptor Heteromeric Assembly—How It Works and Why It Matters* (pp. 361–386). https://doi.org/10.1016/B978-0-12-386931-9.00013-1

Hernández Noriega, S. (2017). *Efecto de las crisis repetitivas en el modelo experimental de epilepsia GASH: Sal* [Universidad de Salamanca]. https://doi.org/10.14201/gredos.136900

Hirvonen, J., Goodwin, R. S., Li, C.-T., Terry, G. E., Zoghbi, S. S., Morse, C., Pike, V. W., Volkow, N. D., Huestis, M. A., & Innis, R. B. (2012). Reversible and regionally selective downregulation of brain cannabinoid CB1 receptors in chronic daily cannabis smokers. *Molecular Psychiatry*, *17*(6), 642–649. https://doi.org/10.1038/mp.2011.82

Hof, P. R., Vissavajjhala, P., Rosenthal, R. E., Fiskum, G., & Morrison, J. H. (1996). Distribution of glutamate receptor subunit proteins G1uR2(4), GluR5/6/7, and NMDAR1 in the canine and primate cerebral cortex: a comparative immunohistochemical analysis. *Brain Research*, *723*(1–2), 77–89. https://doi.org/10.1016/0006-8993(96)00218-1

Huettner, J. E., Stack, E., & Wilding, T. J. (1998). Antagonism of neuronal kainate receptors by lanthanum and gadolinium. *Neuropharmacology*, *37*(10–11), 1239–1247. https://doi.org/10.1016/S0028-3908(98)00082-3

Huntley, G., Rogers, S., Moran, T., Janssen, W., Archin, N., Vickers, J., Cauley, K., Heinemann, S., & Morrison, J. (1993). Selective distribution of kainate receptor subunit immunoreactivity in monkey neocortex revealed by a monoclonal antibody that recognizes glutamate receptor subunits GluR5/6/7. *The Journal of Neuroscience*, *13*(7), 2965–2981. https://doi.org/10.1523/JNEUROSCI.13-07-02965.1993

Ilie, A., Raimondo, J. V., & Akerman, C. J. (2012). Adenosine Release during Seizures Attenuates GABAA Receptor-Mediated Depolarization. *Journal of Neuroscience*, *32*(15), 5321–5332. https://doi.org/10.1523/JNEUROSCI.5412-11.2012

Izzi, C., Barbon, A., Kretz, R., Sander, T., & Barlati, S. (2002a). Sequencing of theGRIK1 gene in patients with juvenile absence epilepsy does not reveal mutations affecting receptor structure. *American Journal of Medical Genetics*, *114*(3), 354–359. https://doi.org/10.1002/ajmg.10254

Izzi, C., Barbon, A., Kretz, R., Sander, T., & Barlati, S. (2002b). Sequencing of theGRIK1 gene in patients with juvenile absence epilepsy does not reveal mutations affecting receptor structure. *American Journal of Medical Genetics*, *114*(3), 354–359. https://doi.org/10.1002/ajmg.10254

Jamain, S., Betancur, C., Quach, H., Philippe, A., Fellous, M., Giros, B., Gillberg, C., Leboyer, M., & Bourgeron, T. (2002). Linkage and association of the glutamate receptor 6 gene with autism. *Molecular Psychiatry*, *7*(3), 302–310. https://doi.org/10.1038/sj.mp.4000979

Jobe, P. C., & Dailey, J. W. (2006). Genetically Epilepsy-Prone Rats (GEPRs) in Drug Research. *CNS Drug Reviews*, *6*(3), 241–260. https://doi.org/10.1111/j.1527-3458.2000.tb00150.x

Jubb, H. C., Higueruelo, A. P., Ochoa-Montaño, B., Pitt, W. R., Ascher, D. B., & Blundell, T. L. (2017). Arpeggio: A Web Server for Calculating and Visualising Interatomic Interactions in Protein Structures. *Journal of Molecular Biology*, *429*(3), 365–371. https://doi.org/10.1016/j.jmb.2016.12.004

Jumper, J., Evans, R., Pritzel, A., Green, T., Figurnov, M., Ronneberger, O., Tunyasuvunakool, K., Bates, R., Žídek, A., Potapenko, A., Bridgland, A., Meyer, C., Kohl, S. A. A., Ballard, A. J., Cowie, A., Romera-Paredes, B., Nikolov, S., Jain, R., Adler, J., … Hassabis, D. (2021). Highly accurate protein structure prediction with AlphaFold. *Nature*, *596*(7873), 583–589. https://doi.org/10.1038/s41586-021-03819-2

Kaminski, R. M., Banerjee, M., & Rogawski, M. A. (2004). Topiramate selectively protects against seizures induced by ATPA, a GluR5 kainate receptor agonist. *Neuropharmacology*, *46*(8), 1097–1104. https://doi.org/10.1016/j.neuropharm.2004.02.010

Kandratavicius, L., Balista, P., Lopes-Aguiar, C., Ruggiero, R., Umeoka, E., Garcia-Cairasco, N., Bueno-Junior, L., & Leite, J. (2014). Animal models of epilepsy: use and limitations. *Neuropsychiatric Disease and Treatment*, *10*, 1693. https://doi.org/10.2147/NDT.S50371

Karakas, E., Simorowski, N., & Furukawa, H. (2009a). Structure of the zinc-bound amino-terminal domain of the NMDA receptor NR2B subunit. *The EMBO Journal*, *28*(24), 3910–3920. https://doi.org/10.1038/emboj.2009.338

Karakas, E., Simorowski, N., & Furukawa, H. (2009b). Structure of the zinc-bound amino-terminal domain of the NMDA receptor NR2B subunit. *The EMBO Journal*, *28*(24), 3910–3920. https://doi.org/10.1038/emboj.2009.338

KIM, K.-T., KIM, J., HAN, Y. J., KIM, J. H., LEE, J. S., & CHUNG, J.-H. (2013). Assessment of NMDA receptor genes (GRIN2A, GRIN2B and GRIN2C) as candidate genes in the development of degenerative lumbar scoliosis. *Experimental and Therapeutic Medicine*, *5*(3), 977–981. https://doi.org/10.3892/etm.2013.910

Krieger, J., Bahar, I., & Greger, I. H. (2015). Structure, Dynamics, and Allosteric Potential of Ionotropic Glutamate Receptor N-Terminal Domains. *Biophysical Journal*, *109*(6), 1136–1148. https://doi.org/10.1016/j.bpj.2015.06.061

Kumar, S., Dunsby, C., Beule, P. A. A. De, Owen, D. M., Anand, U., Lanigan, P. M. P., Benninger, R. K. P., Davis, D. M., Neil, M. A. A., Anand, P., Benham, C., Naylor, A., & French, P. M. W. (2007). Multifocal multiphoton excitation and time correlated single photon counting detection for 3-D fluorescence lifetime imaging. *Optics Express*, *15*(20), 12548. https://doi.org/10.1364/OE.15.012548

Kusano, K., Miledi, R., & Stinnakre, J. (1982). Cholinergic and catecholaminergic receptors in the *Xenopus* oocyte membrane. *The Journal of Physiology*, *328*(1), 143–170. https://doi.org/10.1113/jphysiol.1982.sp014257

Kuzniewska, B., Nader, K., Dabrowski, M., Kaczmarek, L., & Kalita, K. (2016). Adult Deletion of SRF Increases Epileptogenesis and Decreases Activity-Induced Gene Expression. *Molecular Neurobiology*, *53*(3), 1478–1493. https://doi.org/10.1007/s12035-014-9089-7

Kwan, P., Arzimanoglou, A., Berg, A. T., Brodie, M. J., Allen Hauser, W., Mathern, G., Moshé, S. L., Perucca, E., Wiebe, S., & French, J. (2009). Definition of drug resistant epilepsy: Consensus proposal by the ad hoc Task Force of the ILAE Commission on Therapeutic Strategies. *Epilepsia*, *51*(6), 1069–1077. https://doi.org/10.1111/j.1528-1167.2009.02397.x

Lerma, J., & Marques, J. M. (2013). Kainate Receptors in Health and Disease. *Neuron*, *80*(2), 292–311. https://doi.org/10.1016/j.neuron.2013.09.045

Li, J.-M., Zeng, Y.-J., Peng, F., Li, L., Yang, T.-H., Hong, Z., Lei, D., Chen, Z., & Zhou, D. (2010). Aberrant glutamate receptor 5 expression in temporal lobe epilepsy lesions. *Brain Research*, *1311*, 166–174. https://doi.org/10.1016/j.brainres.2009.11.024

Li, X., & Hu, Y. (2005). Gene expression profiling reveals the mechanism of action of anticonvulsant drug QYS. *Brain Research Bulletin*, *66*(2), 99–105. https://doi.org/10.1016/j.brainresbull.2005.03.017

Lin, Y., Bloodgood, B. L., Hauser, J. L., Lapan, A. D., Koon, A. C., Kim, T.-K., Hu, L. S., Malik, A. N., & Greenberg, M. E. (2008). Activity-dependent regulation of inhibitory synapse development by Npas4. *Nature*, *455*(7217), 1198–1204. https://doi.org/10.1038/nature07319

Liu, X., Ou, S., Xu, T., Liu, S., Yuan, J., Huang, H., Qin, L., Yang, H., Chen, L., Tan, X., & Chen, Y. (2016). New differentially expressed genes and differential DNA methylation underlying refractory epilepsy. *Oncotarget*, *7*(52), 87402–87416. https://doi.org/10.18632/oncotarget.13642

Lopes-Cendes, I., & Oliveira Ribeiro, P. A. (2013). Aspectos genéticos de las epilepsias: una visión actualizada. *Revista Médica Clínica Las Condes*, *24*(6), 909–914. https://doi.org/10.1016/S0716-8640(13)70244-X

López-López, D., Gómez-Nieto, R., Herrero-Turrión, M. J., García-Cairasco, N., Sánchez-Benito, D., Ludeña, M. D., & López, D. E. (2017). Overexpression of the immediate-early genes Egr1, Egr2, and Egr3 in two strains of rodents susceptible to audiogenic seizures. *Epilepsy & Behavior*, *71*, 226–237. https://doi.org/10.1016/j.yebeh.2015.12.020

Löscher, W. (2017). Animal Models of Seizures and Epilepsy: Past, Present, and Future Role for the Discovery of Antiseizure Drugs. *Neurochemical Research*, *42*(7), 1873–1888. https://doi.org/10.1007/s11064-017-2222-z

Lösing, P., Niturad, C. E., Harrer, M., Reckendorf, C. M. Z., Schatz, T., Sinske, D., Lerche, H., Maljevic, S., & Knöll, B. (2017). SRF modulates seizure occurrence, activity induced gene transcription and hippocampal circuit reorganization in the mouse pilocarpine epilepsy model. *Molecular Brain*, *10*(1), 30. https://doi.org/10.1186/s13041-017-0310-2

Mahadevan, V., Pressey, J. C., Acton, B. A., Uvarov, P., Huang, M. Y., Chevrier, J., Puchalski, A., Li, C. M., Ivakine, E. A., Airaksinen, M. S., Delpire, E., McInnes, R. R., & Woodin, M. A. (2014). Kainate Receptors Coexist in a Functional Complex with KCC2 and Regulate Chloride Homeostasis in Hippocampal Neurons. *Cell Reports*, *7*(6), 1762–1770. https://doi.org/10.1016/j.celrep.2014.05.022

Martínez-Torres, A., & Miledi, R. (2001). Expression of γ-aminobutyric acid ρ1 and ρ1Δ450 as gene fusions with the green fluorescent protein. *Proceedings of the National Academy of Sciences*, *98*(4), 1947–1951. https://doi.org/10.1073/pnas.98.4.1947

Mathers, D. A., & Usherwood, P. N. R. (1976). Concanavalin A blocks desensitisation of glutamate receptors on insect muscle fibres. *Nature*, *259*(5542), 409–411. https://doi.org/10.1038/259409a0

McCandless, D. W., & Schwartzenburg, F. C. (1982). Audiogenic Seizure-Induced Changes in Energy Metabolites in Cerebral Cortical and Cerebellar Layers. *Epilepsia*, *23*(5), 481–489. https://doi.org/10.1111/j.1528-1157.1982.tb05436.x

Meyerson, J. R., Chittori, S., Merk, A., Rao, P., Han, T. H., Serpe, M., Mayer, M. L., & Subramaniam, S. (2016). Structural basis of kainate subtype glutamate receptor desensitization. *Nature*, *537*(7621), 567–571. https://doi.org/10.1038/nature19352

Miledi, R., Parker, I., & Sumikawa, K. (1982). Properties of acetylcholine receptors translated by cat muscle mRNA in Xenopus oocytes. *The EMBO Journal*, *1*(11), 1307–1312. https://doi.org/10.1002/j.1460-2075.1982.tb01315.x

Morin, L. P., & Wood, R. I. (2001). *A stereotaxic atlas of the golden hamster brain* (Academic Press, Ed.).

Motazacker, M. M., Rost, B. R., Hucho, T., Garshasbi, M., Kahrizi, K., Ullmann, R., Abedini, S. S., Nieh, S. E., Amini, S. H., Goswami, C., Tzschach, A., Jensen, L. R., Schmitz, D., Ropers, H. H., Najmabadi, H., & Kuss, A. W. (2007). A Defect in the Ionotropic Glutamate Receptor 6 Gene (GRIK2) Is Associated with Autosomal Recessive Mental Retardation. *The American Journal of Human Genetics*, *81*(4), 792–798. https://doi.org/10.1086/521275

Muñoz, L. J., Carballosa-Gautam, M. M., Yanowsky, K., García-Atarés, N., & López, D. E. (2017). The genetic audiogenic seizure hamster from Salamanca: The GASH:Sal. *Epilepsy and Behavior*, *71*, 181–192. https://doi.org/10.1016/j.yebeh.2016.03.002

Musto, A. E., Rosencrans, R. F., Walker, C. P., Bhattacharjee, S., Raulji, C. M., Belayev, L., Fang, Z., Gordon, W. C., & Bazan, N. G. (2016). Dysfunctional epileptic neuronal circuits and dysmorphic dendritic spines are mitigated by platelet-activating factor receptor antagonism. *Scientific Reports*, *6*(1), 30298. https://doi.org/10.1038/srep30298

Orav, E., Atanasova, T., Shintyapina, A., Kesaf, S., Kokko, M., Partanen, J., Taira, T., & Lauri, S. E. (2017). NETO1 Guides Development of Glutamatergic Connectivity in the Hippocampus by Regulating Axonal Kainate Receptors. *Eneuro*, *4*(3), ENEURO.0048-17.2017. https://doi.org/10.1523/ENEURO.0048-17.2017

Ottman, R. (2005). Analysis of Genetically Complex Epilepsies Ruth. *Epilepsia*, *46*(10), 7–14. https://doi.org/10.1038/mp.2011.182.doi

Pahl, S., Tapken, D., Haering, S., & Hollmann, M. (2014). Trafficking of Kainate Receptors. *Membranes*, *4*(3), 565–595. https://doi.org/10.3390/membranes4030565

Palma, E., Mileo, A. M., Martínez-Torres, A., Eusebi, F., & Miledi, R. (2002). Some properties of human neuronal α7 nicotinic acetylcholine receptors fused to the green fluorescent protein. *Proceedings of the National Academy of Sciences*, *99*(6), 3950–3955. https://doi.org/10.1073/pnas.052699299

Perkinton, M. S., & Sihra, T. S. (1999). A high-affinity presynaptic kainate-type glutamate receptor facilitates glutamate exocytosis from cerebral cortex nerve terminals (synaptosomes). *Neuroscience*, *90*(4), 1281–1292. https://doi.org/10.1016/S0306-4522(98)00573-9

Perucca, E. (2017). Cannabinoids in the Treatment of Epilepsy: Hard Evidence at Last? *Journal of Epilepsy Research*, *7*(2), 61–76. https://doi.org/10.14581/jer.17012

Pfisterer, U., Petukhov, V., Demharter, S., Meichsner, J., Thompson, J. J., Batiuk, M. Y., Asenjo-Martinez, A., Vasistha, N. A., Thakur, A., Mikkelsen, J., Adorjan, I., Pinborg, L. H., Pers, T. H., von Engelhardt, J., Kharchenko, P. V., & Khodosevich, K. (2020). Identification of epilepsy-associated neuronal subtypes and gene expression underlying epileptogenesis. *Nature Communications*, *11*(1), 5038. https://doi.org/10.1038/s41467-020-18752-7

Pinheiro, P., & Mulle, C. (2006). Kainate receptors. *Cell and Tissue Research*, *326*(2), 457–482. https://doi.org/10.1007/s00441-006-0265-6

Poletaeva, I. I., Surina, N. M., Kostina, Z. A., Perepelkina, O. V., & Fedotova, I. B. (2017). The Krushinsky-Molodkina rat strain: The study of audiogenic epilepsy for 65 years. *Epilepsy & Behavior*, *71*, 130–141. https://doi.org/10.1016/j.yebeh.2015.04.072

Prieto-Martín, A. I., Aroca-Aguilar, J. D., Sánchez-Sánchez, F., Muñoz, L. J., López, D. E., Escribano, J., & de Cabo, C. (2017). Molecular and neurochemical substrates of the audiogenic seizure strains: The GASH:Sal model. *Epilepsy & Behavior*, *71*, 218–225. https://doi.org/10.1016/j.yebeh.2015.05.025

Raisinghani, M., & Faingold, C. L. (2003). Identification of the requisite brain sites in the neuronal network subserving generalized clonic audiogenic seizures. *Brain Research*, *967*(1–2), 113–122. https://doi.org/10.1016/S0006-8993(02)04232-4

Reid, H. M., Bowler, K. J., & Weiss, C. (1983). Hippocampal lesions increase the severity of unilaterally induced audiogenic seizures and decrease their latency. *Experimental Neurology*, *81*(1), 240–244. https://doi.org/10.1016/0014-4886(83)90171-1

Ribak, C. E., & Morin, C. L. (1995). The role of the inferior colliculus in a genetic model of audiogenic seizures. *Anatomy and Embryology*, *191*(4), 279–295. https://doi.org/10.1007/BF00534681

Rodríguez-Muñoz, M., Onetti, Y., Cortés-Montero, E., Garzón, J., & Sánchez-Blázquez, P. (2018). Cannabidiol enhances morphine antinociception, diminishes NMDA-mediated seizures and reduces stroke damage via the sigma 1 receptor. *Molecular Brain*, *11*(1), 51. https://doi.org/10.1186/s13041-018-0395-2

Rodríguez-Muñoz, M., Sánchez-Blázquez, P., Herrero-Labrador, R., Martínez-Murillo, R., Merlos, M., Vela, J. M., & Garzón, J. (2015). The σ1 Receptor Engages the Redox-Regulated HINT1 Protein to Bring Opioid Analgesia Under NMDA Receptor Negative Control. *Antioxidants & Redox Signaling*, *22*(10), 799–818. https://doi.org/10.1089/ars.2014.5993

ROGAWSKI, M. A., GRYDER, D., CASTANEDA, D., YONEKAWA, W., BANKS, M. K., & LI, H. E. (2003). GluR5 Kainate Receptors, Seizures, and the Amygdala. *Annals of the New York Academy of Sciences*, *985*(1), 150–162. https://doi.org/10.1111/j.1749-6632.2003.tb07079.x

Ross, K. C., & Coleman, J. R. (2000). Developmental and genetic audiogenic seizure models: behavior and biological substrates. *Neuroscience & Biobehavioral Reviews*, *24*(6), 639–653. https://doi.org/10.1016/S0149-7634(00)00029-4

Rossmann, M., Sukumaran, M., Penn, A. C., Veprintsev, D. B., Babu, M. M., & Greger, I. H. (2011). Subunit-selective N-terminal domain associations organize the formation of AMPA receptor heteromers. *The EMBO Journal*, *30*(5), 959–971. https://doi.org/10.1038/emboj.2011.16

Sánchez-Benito, D., Gómez-Nieto, R., Hernández-Noriega, S., Murashima, A. A. B., de Oliveira, J. A. C., Garcia-Cairasco, N., López, D. E., & Hyppolito, M. A. (2017). Morphofunctional alterations in the olivocochlear efferent system of the genetic audiogenic seizure-prone hamster GASH:Sal. *Epilepsy & Behavior*, *71*, 193–206. https://doi.org/10.1016/j.yebeh.2016.05.040

Sánchez-Benito, D., Hyppolito, M. A., Alvarez-Morujo, A. J., López, D. E., & Gómez-Nieto, R. (2020). Morphological and molecular correlates of altered hearing sensitivity in the genetically audiogenic seizure-prone hamster GASH/Sal. *Hearing Research*, *392*, 107973. https://doi.org/10.1016/j.heares.2020.107973

Sander, M., Neubüser, A., Kalamaras, J., Ee, H. C., Martin, G. R., & German, M. S. (1997). Genetic analysis reveals that PAX6 is required for normal transcription of pancreatic hormone genes and islet development. *Genes & Development*, *11*(13), 1662–1673. https://doi.org/10.1101/gad.11.13.1662

Scheffer, I. E., Berkovic, S., Capovilla, G., Connolly, M. B., French, J., Guilhoto, L., Hirsch, E., Jain, S., Mathern, G. W., Moshé, S. L., Nordli, D. R., Perucca, E., Tomson, T., Wiebe, S., Zhang, Y.-H., & Zuberi, S. M. (2017). ILAE classification of the epilepsies: Position paper of the ILAE Commission for Classification and Terminology. *Epilepsia*, *58*(4), 512–521. https://doi.org/10.1111/epi.13709

Schiffer, H. H., & Heinemann, S. F. (2007). Association of the human kainate receptorGluR7 gene (GRIK3) with recurrent major depressive disorder. *American Journal of Medical Genetics Part B: Neuropsychiatric Genetics*, *144B*(1), 20–26. https://doi.org/10.1002/ajmg.b.30374

Selvakumar, P., Lee, J., Khanra, N., He, C., Munguba, H., Kiese, L., Broichhagen, J., Reiner, A., Levitz, J., & Meyerson, J. R. (2021). Structural and compositional diversity in the kainate receptor family. *Cell Reports*, *37*(4), 109891. https://doi.org/10.1016/j.celrep.2021.109891

Serikawa, T., Mashimo, T., Kuramoto, T., Voigt, B., Yukihiro, O., & Sasa, M. (2015). Advances on genetic rat models of epilepsy. *Experimental Animals*, *64*(1), 1–7. https://doi.org/10.1538/expanim.14-0066

Sheng, N., Shi, Y. S., & Nicoll, R. A. (2017). Amino-terminal domains of kainate receptors determine the differential dependence on Neto auxiliary subunits for trafficking. *Proceedings of the National Academy of Sciences*, *114*(5), 1159–1164. https://doi.org/10.1073/pnas.1619253114

Sihra, T. S., Flores, G., & Rodríguez-Moreno, A. (2014). Kainate Receptors. *The Neuroscientist*, *20*(1), 29–43. https://doi.org/10.1177/1073858413478196

Sommer, B., Köhler, M., Sprengel, R., & Seeburg, P. H. (1991). RNA editing in brain controls a determinant of ion flow in glutamate-gated channels. *Cell*, *67*(1), 11–19. https://doi.org/10.1016/0092-8674(91)90568-J

Straub, C., Noam, Y., Nomura, T., Yamasaki, M., Yan, D., Fernandes, H. B., Zhang, P., Howe, J. R., Watanabe, M., Contractor, A., & Tomita, S. (2016). Distinct Subunit Domains Govern Synaptic Stability and Specificity of the Kainate Receptor. *Cell Reports*, *16*(2), 531–544. https://doi.org/10.1016/j.celrep.2016.05.093

Strehlow, V., Heyne, H. O., Vlaskamp, D. R. M., Marwick, K. F. M., Rudolf, G., de Bellescize, J., Biskup, S., Brilstra, E. H., Brouwer, O. F., Callenbach, P. M. C., Hentschel, J., Hirsch, E., Kind, P. C., Mignot, C., Platzer, K., Rump, P., Skehel, P. A., Wyllie, D. J. A., Hardingham, G. E., … Willemsen, M. H. (2019). GRIN2A -related disorders: genotype and functional consequence predict phenotype. *Brain*, *142*(1), 80–92. https://doi.org/10.1093/brain/awy304

Streng, M. L., & Krook-Magnuson, E. (2021). The cerebellum and epilepsy. *Epilepsy & Behavior*, *121*, 106909. https://doi.org/10.1016/j.yebeh.2020.106909

Suhr, O. B., Andersen, O., Aronsson, T., Jonasson, J., Kalimo, H., Lundahl, C., Lundgren, H.-E., Melberg, A., Nyberg, J., Olsson, M., Sandberg, A., & Westermark, P. (2009). Report of five rare or previously unknown amyloidogenic transthyretin mutations disclosed in Sweden. *Amyloid*, *16*(4), 208–214. https://doi.org/10.3109/13506120903421587

Swanson, G. T., Feldmeyer, D., Kaneda, M., & Cull-Candy, S. G. (1996). Effect of RNA editing and subunit co-assembly single-channel properties of recombinant kainate receptors. *The Journal of Physiology*, *492*(1), 129–142. https://doi.org/10.1113/jphysiol.1996.sp021295

Tchitchek, N., Safronetz, D., Rasmussen, A. L., Martens, C., Virtaneva, K., Porcella, S. F., Feldmann, H., Ebihara, H., & Katze, M. G. (2014). Sequencing, Annotation and Analysis of the Syrian Hamster (Mesocricetus auratus) Transcriptome. *PLoS ONE*, *9*(11), e112617. https://doi.org/10.1371/journal.pone.0112617

Thiffault, I., Speca, D. J., Austin, D. C., Cobb, M. M., Eum, K. S., Safina, N. P., Grote, L., Farrow, E. G., Miller, N., Soden, S., Kingsmore, S. F., Trimmer, J. S., Saunders, C. J., & Sack, J. T. (2015). A novel epileptic encephalopathy mutation in KCNB1 disrupts Kv2.1 ion

selectivity, expression, and localization. *The Journal of General Physiology*, *146*(5), 399–410. https://doi.org/10.1085/jgp.201511444

Tomiyama, H., Hutson, J. M., Truong, A., & Agoulnik, A. I. (2003). Transabdominal Testicular Descent is Disrupted in Mice with Deletion of Insulinlike Factor 3 Receptor. *Journal of Pediatric Surgery*, *38*(12), 1793–1798. https://doi.org/10.1016/j.jpedsurg.2003.08.047

Traynelis, S. F., Wollmuth, L. P., McBain, C. J., Menniti, F. S., Vance, K. M., Ogden, K. K., Hansen, K. B., Yuan, H., Myers, S. J., & Dingledine, R. (2010). Glutamate Receptor Ion Channels: Structure, Regulation, and Function. *Pharmacological Reviews*, *62*(3), 405–496. https://doi.org/10.1124/pr.109.002451

Ullal, G., Fahnestock, M., & Racine, R. (2005). Time-dependent Effect of Kainate-induced Seizures on Glutamate Receptor GluR5, GluR6, and GluR7 mRNA and Protein Expression in Rat Hippocampus. *Epilepsia*, *46*(5), 616–623. https://doi.org/10.1111/j.1528-1167.2005.49604.x

Vogel, C., & Marcotte, E. M. (2012). Insights into the regulation of protein abundance from proteomic and transcriptomic analyses. *Nature Reviews Genetics*, *13*(4), 227–232. https://doi.org/10.1038/nrg3185

Wada, J. A., Terao, A., White, B., & Jung, E. (1970). Inferior colliculus lesion and audiogenic seizure susceptibility. *Experimental Neurology*, *28*(2), 326–332. https://doi.org/10.1016/0014-4886(70)90240-2

Wang, G.-X., Wang, D.-W., Liu, Y., & Ma, Y.-H. (2016). Intractable epilepsy and the P-glycoprotein hypothesis. *International Journal of Neuroscience*, *126*(5), 385–392. https://doi.org/10.3109/00207454.2015.1038710

Watkins, J. C., & Jane, D. E. (2006). The glutamate story. *British Journal of Pharmacology*, *147*(S1), S100–S108. https://doi.org/10.1038/sj.bjp.0706444

Werner, F.-M., & Coveñas, R. (2017). Classical neurotransmitters and neuropeptides involved in generalized epilepsy in a multi-neurotransmitter system: How to improve the antiepileptic effect? *Epilepsy & Behavior*, *71*, 124–129. https://doi.org/10.1016/j.yebeh.2015.01.038

WHO. (2006). Neurological disorders: a public health approach. *Neurological Disorders: Public Health Challenges*, 40–110. https://doi.org/10.1037/e521482010-002

Wilson, G. M., Flibotte, S., Chopra, V., Melnyk, B. L., Honer, W. G., & Holt, R. A. (2006). DNA copy-number analysis in bipolar disorder and schizophrenia reveals aberrations in genes involved in glutamate signaling. *Human Molecular Genetics*, *15*(5), 743–749. https://doi.org/10.1093/hmg/ddi489

Winden, K. D., Karsten, S. L., Bragin, A., Kudo, L. C., Gehman, L., Ruidera, J., Geschwind, D. H., & Engel, J. (2011). A Systems Level, Functional Genomics Analysis of Chronic Epilepsy. *PLoS ONE*, *6*(6), e20763. https://doi.org/10.1371/journal.pone.0020763

Wo, Z. G., & Oswald, R. E. (1994). Transmembrane topology of two kainate receptor subunits revealed by N-glycosylation. *Proceedings of the National Academy of Sciences*, *91*(15), 7154–7158. https://doi.org/10.1073/pnas.91.15.7154

Wu, Q.-W., & Tang, Z.-Q. (2023). Focusing on the Emerging Role of Kainate Receptors in the Dorsal Cochlear Nucleus (DCN) and Cerebellum. *International Journal of Molecular Sciences*, *24*(2), 1718. https://doi.org/10.3390/ijms24021718

7. COMPENDIO DE ARTÍCULOS

frontiers in Neuroscience

ORIGINAL RESEARCH
published: 26 May 2020
doi: 10.3389/fnins.2020.00508

Inferior Colliculus Transcriptome After Status Epilepticus in the Genetically Audiogenic Seizure-Prone Hamster GASH/Sal

*Sandra M. Díaz-Rodríguez[1,2,3], Daniel López-López[1], Manuel J. Herrero-Turrión[1,2,4], Ricardo Gómez-Nieto[1,2,3], Angel Canal-Alonso[2,5] and Dolores E. Lopéz[1,2,3]**

[1] Institute of Neurosciences of Castilla y León, University of Salamanca, Salamanca, Spain, [2] Institute of Biomedical Research of Salamanca, University of Salamanca, Salamanca, Spain, [3] Department of Cellular Biology and Pathology, University of Salamanca, Salamanca, Spain, [4] Neurological Tissue Bank INCYL (BTN-INCYL), Salamanca, Spain, [5] BISITE Research Group, University of Salamanca, Salamanca, Spain

OPEN ACCESS

Edited by:
David F. Clayton,
Queen Mary University of London,
United Kingdom

Reviewed by:
Kazuhiro Wada,
Hokkaido University, Japan
Claudia Vianna Maurer-Morelli,
State University of Campinas, Brazil

***Correspondence:**
Dolores E. Lopéz
lopezde@usal.es

Specialty section:
This article was submitted to Neurogenomics, a section of the journal Frontiers in Neuroscience

Received: 07 January 2020
Accepted: 22 April 2020
Published: 26 May 2020

Citation:
Díaz-Rodríguez SM, López-López D, Herrero-Turrión MJ, Gómez-Nieto R, Canal-Alonso A and Lopéz DE (2020) Inferior Colliculus Transcriptome After Status Epilepticus in the Genetically Audiogenic Seizure-Prone Hamster GASH/Sal. Front. Neurosci. 14:508. doi: 10.3389/fnins.2020.00508

The Genetic Audiogenic Seizure Hamster from Salamanca (GASH/Sal), an animal model of reflex epilepsy, exhibits generalized tonic–clonic seizures in response to loud sound with the epileptogenic focus localized in the inferior colliculus (IC). Ictal events in seizure-prone strains cause gene deregulation in the epileptogenic focus, which can provide insights into the epileptogenic mechanisms. Thus, the present study aimed to determine the expression profile of key genes in the IC of the GASH/Sal after the status epilepticus. For such purpose, we used RNA-Seq to perform a comparative study between the IC transcriptome of GASH/Sal and that of control hamsters both subjected to loud sound stimulation. After filtering for normalization and gene selection, a total of 36 genes were declared differentially expressed from the RNA-seq analysis in the IC. A set of differentially expressed genes were validated by RT-qPCR showing significant differentially expression between GASH/Sal hamsters and Syrian control hamsters. The confirmed differentially expressed genes were classified on ontological categories associated with epileptogenic events similar to those produced by generalized tonic seizures in humans. Subsequently, based on the result of metabolomics, we found the interleukin-4 and 13-signaling, and nucleoside transport as presumably altered routes in the GASH/Sal model. This research suggests that seizures in GASH/Sal hamsters are generated by multiple molecular substrates, which activate biological processes, molecular processes, cellular components and metabolic pathways associated with epileptogenic events similar to those produced by tonic seizures in humans. Therefore, our study supports the use of the GASH/Sal as a valuable animal model for epilepsy research, toward establishing correlations with human epilepsy and searching new biomarkers of epileptogenesis.

Keywords: audiogenic seizure, GASH/Sal, metabolomic, RNA-seq, RT-qPCR

INTRODUCTION

Epilepsy is one of the most common neurological disorders, affecting approximately one percent of the population. Although the etiology of epilepsy can be structural, genetic, infectious, metabolic, immune or unknown (last ILAE definition, Scheffer et al., 2017), genetic epilepsy accounts for one-third of all patients with epilepsy (Scheffer et al., 2017). In recent decades, an increasing number of epilepsy associated mutations have been identified, mainly in rare monogenic epileptic syndromes; however, only 1 to 2 % of idiopathic epilepsies appear to be monogenic (Lopes-Cendes and Oliveira Ribeiro, 2013). Examples of monogenic epileptic syndromes are autosomal dominant nocturnal frontal lobe epilepsy and progressive myoclonic epilepsy, in which, mutations of a single gene are sufficient to produce epileptic seizures (Lopes-Cendes and Oliveira Ribeiro, 2013).

Among the most commonly used and well characterized *in vivo* genetic models of epilepsy are the so-called genetically audiogenic seizure models, those with reflex epilepsy induced by high-intensity acoustic stimulation (Ross and Coleman, 2000; Kandratavicius et al., 2014; Garcia-Cairasco et al., 2017; Muñoz et al., 2017). This predisposition to seizures has enabled researchers to use audiogenic models of epilepsy in a wide range of studies on cellular and molecular activity, behavior, epilepsy comorbidities, development of new drugs, and ictogenic processes (Kandratavicius et al., 2014).

Among these models, the Genetic Audiogenic Seizure Hamster from Salamanca (GASH/Sal), developed and maintained at the Animal Experimentation Service of the University of Salamanca, exhibits an autosomal recessive pattern of heredity with audiogenic susceptibility (Muñoz et al., 2017). As occurs in other animal models of audiogenic epilepsy, the inferior colliculus (IC) is crucial for the initiation and propagation of audiogenic seizures in the GASH/Sal (Kesner, 1966; Wada et al., 1970; Faingold, 2004; Muñoz et al., 2017). These animals reach their maximum degree of seizure susceptibility between the second and fourth month of life, which then gradually disappears (Muñoz et al., 2017), and their seizures have been characterized as complete sound-evoked reflex seizures (Carballosa-Gonzalez et al., 2013). Furthermore, several studies have reported the inheritance pattern (Muñoz et al., 2017), and the neuroanatomical substrates underlying audiogenic seizure susceptibility (Sánchez-Benito et al., 2017, 2020) as well as the anticonvulsant effects after antiepileptic drug administration (Barrera-Bailón et al., 2013, 2017). It has also been found that the GASH/Sal exhibits altered gene expression of early growth response genes 1 to 3 (*Egr1, Egr2,* and *Egr3*) in the IC, presumably as an effect of stress associated to seizures (López-López et al., 2017).

The present study evaluates the global gene expression profiling of the IC in the GASH/Sal with sound-induced seizures when compared to control animals that received the same acoustic stimulation. To do so, we carried out a comparative transcriptome analysis of the IC in the GASH/Sal and matched control hamsters after loud sound stimulation. Our RNA-Seq findings showed that audiogenic seizures disrupted the gene expression in the IC of GASH/Sal hamsters, as validated by quantitative reverse transcription real-time PCR (RT-qPCR) for a specific set of genes. These results are of importance for searching common link to this heterogeneous disease in humans, with potential applications for diagnostic and therapeutic approaches in the clinical context.

METHODOLOGY

Animals

A total of 30, 3-month-old male Syrian hamsters (*Mesocricetus auratus*) were used in this study, namely 18 GASH/Sal hamsters from the inbred strain maintained at the animal's facility of the University of Salamanca (Salamanca, Spain), and 12 controls, that is, RjHan:AURA Syrian hamsters, from Janvier Labs (Le Genest-Saint-Isle, France). The animals were subdivided into three groups: (1) The acoustically stimulated control group (Syrian control hamster stimulated, $n = 12$). All control hamsters exhibited absence of seizures after loud acoustic stimulation. (2) The acoustically stimulated GASH/Sal (GASH/Sal Stim; $n = 12$), corresponding to seizure-prone animals that were subjected to loud acoustic stimulation and presented generalized tonic–clonic seizures and clonic spasms. (3) The naïve GASH/Sal group ($n = 6$), corresponding to seizure-prone animals that did not receive any loud acoustic stimulation, and hence showed absence of audiogenic seizures.

The control and GASH/Sal animals that were exposed to loud sound stimulation were individually placed within an acrylic cylinder to receive a single high-intensity acoustic stimulus for 10 s. The stimulus used in the high-intensity acoustic stimulation protocol was recorded using a high-pass filter (N500 Hz; microphone Bruel and Kjaer #4134 and preamplifier Bruel and Kjaer #2619), digitized above 4 kHz, and reproduced by a computer coupled to an amplifier (Fonestar MA-25T, Revilla de Camargo, Spain) and a tweeter (Beyma T2010,

Abbreviations: Actb, beta-actin; AP-1, Activator protein 1 Genes; *Atf3*, Activating transcription factor 3; *Atp2a3*, ATPase Sarcoplasmic/endoplasmic reticulum Ca^{2+} transporting 3; BDNF, Brain-derived neurotrophic factor; bp, Base pairs; C6, Complement C6; *Cd163*, CD163 molecule; cDNA, Complementary deoxyribonucleic acid; Ct, Mean threshold cycle; DNA, Deoxyribonucleic acid; *Egr1,2,3,4*, Early growth response 1, 2, 3 and 4 genes; FC, Fold change; *Fos, Fosb*, Fos-Fosb proto-oncogene; *Gadd45g*, Growth arrest and DNA damage inducible gamma; GASH/Sal, Genetic audiogenic seizure hamster from Salamanca; GENECARDS, The human gene database; *Gm12695*, Chromosome unknown C1orf87 homolog; GO, Gene ontological; *Grin2c*, Glutamate ionotropic receptor NMDA type subunit 2C; IC, inferior colliculus; IL-4, IL-13, Interleukin-4 and -13; *Junb*, Junb proto-oncogene; *Kcnj13,* Potassium voltage-gated channel subfamily J member 13; *Kcns1*, Potassium voltage-gated channel modifier subfamily S member 1; KEGG, Kyoto encyclopedia of genes and genomes; *Kir*, Inwardly rectifying K^+ channels; *Kv*, Voltage-gated K^+; logFC, Logarithm of Fold change; *Mmp3*, Matrix metallopeptidase 3; NMDAR, N-methyl-D-aspartate receptor; *Npas4*, Neuronal PAS domain 4; *Ogn*, Osteoglycin; PANTHER, Protein analysis through evolutionary relationships; Phred, Control of quality; *Rab29,* RAB29 Member RAS oncogene family; *Renbp*, Renin binding protein; ROC, receptor-operator channel; RNA, Ribonucleic acid; RT-qPCR, Quantitative reverse transcription real-time PCR; *Rxfp2*, Relaxin family peptide receptor 2; SERCA, Sarco/endoplasmic reticulum Ca^{2+} ATPase; SI, severity index; *Slc13a4*, Solute carrier family 13 member 4; *Slc28a1*, Solute carrier family 28 member 1; *Slc6a4*, Solute carrier family 6 member 4; *Sucnr1*, Succinate receptor 1; *Ttr*, Transthyretin; *Wdr38*, WD repeat domain 38.

Valencia, Spain) in the upper portion of the arena. The delivered sound was a semirandom acoustic stimulus of 0–18 kHz with an intensity of 115 to 120 dB (Barrera-Bailón et al., 2013; López-López et al., 2017).

All animals submitted to the high-intensity acoustic stimulation protocol were evaluated according to the severity index (SI) described by Garcia-Cairasco et al. (1996). The hamsters corresponding to the control group exhibited normal hearing with positive Preyer's reflex and absence of seizures with a SI score of 0. The GASH/Sal animals corresponding to the high-intensity acoustic stimulation group (GASH/Sal Stim) exhibited all the consecutive phases of the audiogenic seizures with generalized tonic–clonic seizures and clonic spasms, and hence reached the maximum SI (scores of 8). These GASH/Sal animals underwent audiogenic seizures that are very stable and specifically dependent upon the high intensity acoustic stimulation with a duration as short as 10 s (Sánchez-Benito et al., 2017). After acoustic stimulation, the seizure appeared within seconds and lasted for approximately 5 min (Sánchez-Benito et al., 2017).

All experimental procedures and protocols were performed in accordance with the guidelines of EU (Directive 2010/63/UE) for the care and use of laboratory animals and approved by the Bioethics Committee of the USAL (approval number 300). All efforts were made to minimize the number of animals and their suffering. After weaning, the animals were separated from the colony and maintained in Eurostandard Type III cages (Tecniplast, Italy), containing up to 4 individuals, with Lignocel bedding (Rettenmaier Iberica). The animals were maintained in an acoustically controlled environment under 14/10 light/dark cycles at constant room temperature (22–24°C) and *ad libitum* access to food (Teckad Global 2918 irradiated diet) and water. The absence of seizures before starting the experiments was ensured by the strict control of housing conditions and handling.

RNA Isolation

Tissue samples for each set of experiments were obtained and processed in parallel for both animal groups, and were performed at the same time of the day (early in the morning). The euthanasia and tissue collection for gene expression analysis were set 60 min after the high acoustic stimulation as established previously by López-López et al. (2017). For tissue sampling, all animals were deeply anesthetized under gas anesthesia (2.5% isoflurane), the brains were removed quickly after decapitation and the IC was isolated, surgically removed, and placed in QIAzol Lysis Reagent (#79306, QIAgen). Then, the samples containing the IC tissue were homogenized using TissueLyser II instrument (#85300, QIAgen), according to the manufacturer's instructions. After separating the different phases, the aqueous phase was used to extract RNA following the instructions of the RNeasy Mini Kit (#74104, QIAgen). RNA concentrations and quality were assessed using an Agilent 2100 Bioanalyzer to assess the integrity of the 18S and 28S rRNA bands, as well as an RNA integrity number (RIN) $>$ 8.0, with 0 corresponding to fully degraded RNA and 10 corresponding to intact RNA, were used for data analysis (López-López et al., 2017).

RNA-Seq and Data Analysis

To generate cDNA libraries of the IC of GASH/Sal and control hamsters, RNA samples were pooled from 6 GASH/Sal and 6 control hamsters after loud sound stimulation, mixing 1 μg of each sample. The two-cDNA libraries were prepared using 3 μg of total RNA of each animal group, and the TruSeq RNA Sample prep kit v2 (Illumina), adding a capture step of RNA polyA to eliminate rRNA. Subsequently, both cDNA libraries were sequenced on a Genome Analyzer IIx (Genome Analyzer IIx, Illumina) in the single read format (1 × 75 bp) at the Cenit Support Systems laboratory (Salamanca, Spain).

The purity criteria of samples for cDNA library construction were determined using the Illumina sequencer software FASTQC (Andrews, 2010) to test the quality of the samples and to select the most suitable parameters for alignment. All our samples successfully passed this quality control step (Phred, 0–40). Then, the reads were aligned and counted on the reference genome of Syrian hamster MesAur1.0 (GCA_000349665.1) (Tchitchek et al., 2014) using the STAR software (Dobin et al., 2013). Lastly, a differential expression analysis between the groups of samples (GASH/Sal *vs.* control) was performed using the EdgeR statistical package (Robinson et al., 2010). Genes with a rate of change (log Fold-Change) higher than 1.5 (over-expressed) or lower than 1.5 (under-expressed) [$|\log FC| \geq 1.5$] and with a count higher than 40 reads were selected for further analysis in this study.

Quantitative Reverse Transcription Real-Time PCR (RT-qPCR)

RT-qPCR analysis was used to confirm a set of 27 gene expression changes observed in the RNA-seq. For our RT-qPCR analysis, we used an aliquot of the same RNA samples as those used for the RNA-seq experiment, and additionally, new RNA samples from 6 GASH/Sal with sound-induced seizures and 6 sound-stimulated controls were also used. We also used RNA samples from the naïve GASH/Sal group (n = 6), corresponding to seizure-prone animals that did not develop any audiogenic seizure.

For reverse-transcription, we followed the protocol routinely used in our laboratory (López-López et al., 2017). Briefly, total RNA (2 μg) was mixed with oligo-dT and random hexamer primers for reverse-transcription into cDNA using the First Strand cDNA Synthesis Kit (K1621, Promega Corporation, Madison, WI, United States). In all cases, a reverse transcriptase negative control was used to test genomic DNA contamination.

Subsequently, quantitative qPCR was performed using the SYBR Green method with a 2 × Master Mix (#4367659, Applied Biosystems). Each reaction contained 10 μL of Master Mix, 0.4 μL of each pair of primers, 3 μL of each cDNA sample in a different serial cDNA quantity for each gene, and MilliQ water (RNA free) up to 20 μL. The amplification reaction was performed in the QuantStudio 7 Flex Real-Time PCR System (Applied Biosystems) under the following conditions: 10 min at 95°C followed by 40 cycles of 15 s at 95°C and 30 s at 60°C depending on each pair of primers. RT-qPCR experiments were performed in replicates of 6 to 7 samples and conducted in triplicate for each gene product examined. The list of primers used is provided in **Table 1**.

TABLE 1 | Oligonucleotide primers used for RT-qPCR, indicating the location of each primer in the corresponding Ensembl sequences of the Syrian hamster[(a)].

Gen target	ID transcript ensembl *Mesocricetus auratus*[a]	Primer forward	Primer reverse	Size of products	E[b]
Egr1	*ENSMAUG00000007358*	CAGC(A/G)GCGC(T/C)TTCAATCCTC	GTGGTCAGGTGCTCGTAGGG	60	2.04
Egr2	*ENSMAUG00000021143*	AGGCCCTTGGATCTCCCATA	CAGCTGGCACCAGGGTACTG	162	2.00
Egr3	*ENSMAUG00000000747*	CCACAAGCCCTTCCAGTGTC	GTGCGGATGTGAGTGGTGAG	75	1.98
Ttr	*ENSMAUG00000011770*	GCCTCGCTGGACTG(G/A)(C/T)ATTT(A/G)	TCGGACAGCATCCAGGACTT	85	2.00
Rxfp2	*ENSMAUG00000017558*	AAGCTGTGCCAAAGGTTTCTA	TTGCTGAAAACTTTGACTGGAA	88	1.99
C6	*ENSMAUG00000007780*	CTGTGTCCTTGGAGACTACGG	GTCACCAGAGGTTCTGTGCAT	126	1.98
Atp2a3	*ENSMAUG00000005976*	TGTGTGGCTGTATGGGTCAT	GCCACGGCAATCTTGAAGTA	92	1.98
Rab29	*ENSMAUG00000017388*	TTGCTCTGAAGGTTCTCCAGT	GGCTGTTGCTGAAAGTAGTGG	168	2.06
Gm12695	*ENSMAUG00000020018*	GGTCTCCCCAGAAGAAAGTCT	AGGCTGGAGTTCAATGGGTA	162	1.94
Grin2c	*ENSMAUG00000019504*	GTTCAGCCGTTGGCCTCTAT	ACCCAGATCACACCAGACCT	90	1.90
Renbp	*ENSMAUG00000019504*	CGAGCACAAGTCATTGACAAA	ATCATGGCTTCACTGTGTGG	158	2.09
Slc6a4	*ENSMAUG00000012677*	GCGGTACTGGATGAGTTTCC	TCTATGAGTGCCACCGTGAG	176	1.98
Mmp3	*ENSMAUG00000011335*	CCGTGATACCCACCAAATCT	GGGCCAAAATGAAGAGATCA	92	1.93
Atf3	*ENSMAUG00000011335*	GGCAACTGGGGAGTCCTTAT	GAGACGAAGGATGCTCTTGC	120	1.98
Gadd45g	*ENSMAUG00000011335*	TTGCTGTTCTTGGATCGTACA	GACTTTGGCGGACTCGTAGA	168	1.89
Slc13a4	*ENSMAUG00000018591*	AGGGGATAGAGCCCATCATC	GCTGACAAACTCCGTGACAA	165	2.07
Npas4	*ENSMAUG00000016391*	GGCTACATTCCTTTCCGATG	CTACAAAGTCACCGCAGCAC	149	2.01
Wdr38	*ENSMAUG00000005054*	AGCTTCAGCCCTGACTCAAA	GAGGCTGAGTAGCACAAGCA	65	2.07
Ogn	*ENSMAUG00000011988*	ACCATTGCCAAAGGAATCAG	GTTCTTCTAACAGAGACAGTTTTGAA	170	2.08
Sucnr1	*ENSMAUG00000019748*	CAGTCTGTGCCTGACTTTGC	ACAGAGAAGATCGCCACCAC	164	1.95
Fos	*ENSMAUG00000019419*	CAGCTCGCACCAGTGTCTAC	ACTTCCGGAAAACATCATGG	76	2.00
Kcns1	*ENSMAUG00000000788*	CGCTTGTGCGATGATTATGA	ACTCGCCGCTCCAGATAG	100	2.02
Junb	*ENSMAUG00000004233*	GCAGCTACTTTTCGGGTCAG	TTCATCTTGTGCAGGTCGTC	200	1.97
Kcnj13	*ENSMAUG00000010435*	TCAAAGATACCGGAGGATGG	CAAAGACAAGCCAGTGGACA	178	2.07
Cd163	*ENSMAUG00000000759*	AGAAGAGAAGCGGAGGGTTC	ACCAGGACAAACTCCAGACG	163	2.03
Fosb	*ENSMAUG00000000999*	AGAAGAGAAGCGGAGGGTTC	ACCAGGACAAACTCCAGACG	182	2.09
Slc28a1	*ENSMAUG00000015388*	TTAATTGCTGCCTCCGTAATG	GAACTTGGACTCCTCCACCTC	84	1.94
Actb	*ENSMAUG00000008763*	AGCCATGTACGTAGCCATCC	ACCCTCATAGATGGGCACAG	105	2.03

qPCR primer efficiency (E^b) was calculated according to the following equation: $E = 10^{(-1/slope)}$.

A standard curve was made to verify the efficiency (E) of the primers of the target and reference genes and it was constructed by serial dilutions of cDNA isolated: 80, 40, 20, 10, 5, 2.5 and 1.25 ng/μl. Data showed that all genes used in this work were expressed at a high level and investigated transcripts showed high linearity ($R^2 > 0.95$). Real-time PCR efficiencies of one cycle in the exponential phase were calculated according to the equation $E = 10^{[-1/slope]}$. High PCR efficiency rates were shown to occur in the investigated range of nanogram cDNA input, and all genes produced approximately identical slopes (**Table 1**).

To decide which was the most stable gene as an endogenous reference for RT-qPCR data normalization two candidates [β-actin (*Actb*) and glyceraldehyde 3-phosphate dehydrogenase (*Gapdh*)] were selected and their expression was measured by NormFinder software (Andersen et al., 2004) that calculate intra- and intergroup variations in gene expression. Thus, the mean threshold cycle (Ct) value and primer efficiency value of *Actb* were used for data normalization.

The comparative Ct method was used for quantitative data analysis (Schmittgen and Livak, 2008). After removing outliers (Burns et al., 2005), the relative gene expression value (FC) of each transcript was calculated according to the formula $2^{-(\Delta Ct\text{“}condition\ 1\text{”} - \Delta Ct\ \text{“}condition\ 2\text{”})}$, where in "condition 1" corresponds to the experimental sample, "condition 2" to the sample from the control animal, and the ΔCt of each "condition" is $Ct_{\text{“experimental gene”}} - Ct_{\text{“endogenous gene”}}$ (Schmittgen and Livak, 2008). The standard error of each relative gene expression value was calculated as a measure of data variation. Significant differences in qPCR results were determined using the Student's *t*-test, and the results were considered significant when $^*p < 0.05$, $^{**}p < 0.01$, and $^{***}p < 0.001$. The data were plotted using GraphPad Prism (version 6.05).

The confirmed differentially expressed genes by RT-qPCR were functionally classified using biological databases available on web platforms such as The PANTHER (Protein Analysis Through Evolutionary Relationships) Classification System,[1] STRING 10.0,[2] KEGG (Kyoto Encyclopedia of Genes and Genomes)[3] and the Consortium of Genetic Ontology.[4] Both Fisher's exact test and the hyper-geometric test were used to identify significantly

[1]www.pantherdb.org
[2]https://string-db.org
[3]https://www.genome.jp/kegg
[4]www.geneontology.org

overrepresented functional categories, with at least 3 annotated genes, at p-value < 0.05.

Metabolomic Studies

For metabolomics analysis, we evaluated overrepresentation in metabolic pathways using a hypergeometric distribution test. Since the metabolome of the Syrian hamster has not been described yet, the identifiers were converted into their human equivalent using the databases KEGG, Reactome Pathway Database (Reactome)[5] and the Human Gene Database (GeneCards).[6]

To correct false positives in this analysis, a False Discovery Rate was applied using the Benjamini-Hochberg's method (Benjamini and Hochberg, 1995). Interactions between unrelated metabolic pathways have been considered to maximize the scope of analysis. An enrichment network representing gene sets in grouped nodes was performed in the study set (Reimand et al., 2019). In addition, an overrepresentation analysis of the total data was performed to identify any priority pathway in the epileptogenic focus. To determine the gene expression level groups, k-means clustering was performed (MacQueen, 1967). This clustering makes it possible to establish relationships between distant genes based on the assumption that related genes will be expressed similarly. Both metabolomic analyses were exclusively performed in the differentially expressed genes of interest that were confirmed using the RT-qPCR approach.

RESULTS

Analysis and Comparison of the IC Transcriptomes

After the high-intensity acoustic stimulation, the transcriptomes of the IC in the GASH/Sal and Syrian control hamsters were obtained and analyzed using the Syrian hamster as reference genome (Tchitchek et al., 2014). A total of 23573 genes were detected in both transcriptomes; out of which 17587 genes were identified as known groups of genes, and the other 5986 genes matched with transcripts from unidentified genes (**Figure 1A**). Out of the total 17587 transcripts from known genes, 16299 were common genes identified in both control and GASH/Sal hamsters (**Figure 1B**). Bioinformatics analysis of the IC transcriptomes in both animal groups showed 23–25 million short-insert Illumina reads, with 93% average mappings in a length of 75 bp, 7–8% splice sites and a 45–55% GC content (**Table 2**). No anomaly or deviation was detected in any quality control for all samples. The sequences corresponding to the IC transcriptomes of GASH/Sal and control hamsters after high-intensity acoustic stimulation were made available to the scientific community by depositing them in NCBI (**Supplementary Figure S1**).

On the other hand, the gene expression analysis of the IC transcriptomes in the GASH/Sal and control hamsters after loud sound stimulation provided a list of 16299 commonly expressed genes (**Figure 1**).

[5]https://reactome.org/

[6]https://genecards.org/

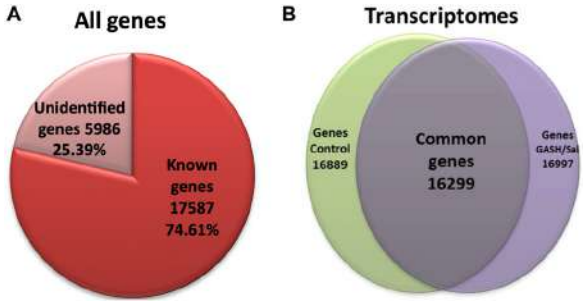

FIGURE 1 | Number of genes detected and expressed in the IC transcriptomes of GASH/Sal and control hamsters after high acoustic stimulation. **(A)** Total number of detected genes in the RNA-Seq experiment. **(B)** Total known genes that were expressed in both transcriptomes. Notice that 16299 correspond to genes that were expressed in both experimental groups. 16889 were those genes expressed in the control IC, out of which 590 genes did not meet the selection criteria, and hence were not considered in this study. 16997 correspond to the genes expressed in the IC of the GASH/Sal, out of which 698 genes did not meet the selection criteria and were excluded.

Top Differentially Expressed Genes Selected With Specific Criteria

Of the total 16299 commonly expressed genes, 36 genes were specifically selected using a cut off threshold of ($|\log FC| \geq 1.5$), normalized gene expression value above 10 counts per million (CPM) and a reads overlapping (COUNTS) greater than 40.

Of these 36 genes, 24 genes were found to have significantly increased mRNA expression levels (at least 1.5-fold), whereas the mRNA expression levels of 12 genes was significantly decreased (at least 1.5-fold) when comparing the IC of the GASH/Sal and the control hamsters. Moreover, of 36 differentially expressed genes, 29 genes were known and 7 were unknown genes, with undefined sequences (**Figure 2** and **Table 3**).

Validation by Quantitative Reverse Transcription Real-Time PCR (RT-qPCR)

We performed RT-qPCRs to validate a set of differentially expressed genes (27) found in the comparative RNA transcriptome analysis of the GASH/Sal and control inferior colliculi. The genes tested for RT-qPCR confirmation were selected based on the two specific criteria ($|\log FC| \geq 1.5$, CPM > 10 and COUNTS > 40), the ontological categories and/or their potential roles in epileptogenic events. As shown in **Figure 3**, these analyses confirmed that *Egr2, Slc28a1, Fosb, Ttr* (Transthyretin), *Egr3, Kcnj13, Junb, Kcns1, Fos, Egr1*, *Ogn* (Osteoglycin), *Wdr38 (WD Repeat* domain 38), *Slc13a4, Npas4* and *Gadd45g* (Growth arrest and DNA damage inducible gamma) were overexpressed in the GASH/Sal *vs.* control hamsters after high acoustic stimulation. In addition, the genes *Rfxp2* (Relaxin family peptide receptor 2), *Slc6a4, Renbp* (Renin binding protein), *Grin2c* (Glutamate ionotropic receptor NMDA type subunit 2C), *Gm12695* (Chromosome unknown C1orf87 homolog), *Rab29* (RAB29, member RAS oncogene family), *Atp2a3* (ATPase sarcoplasmic/endoplasmic reticulum Ca^{2+} transporting 3) and *C6* (Complement C6) were significantly

TABLE 2 | Data from the alignments of RNA-Seq reads of the epileptogenic focus in GASH/Sal and control hamsters after loud sound stimulation.

Sample	Uniquely mapped reads number	Uniquely mapped reads (%)	Average mapped length	Mismatch rate per base (%)	Deletion rate per base (%)	Deletion average length	Insertion rate per base	Insertion average length	Splice site (%)	CG content (%)
GASH/Sal	25955861	93.20	75.64	0.31	0.01	1.58	0.00%	1.38	7.91	45
Control	23412284	93.40	75.65	0.31	0.01	1.58	0.00%	1.4	8.01	55

down regulated in GASH/Sal animals, when compared with control hamsters. The genes *Sucnr1* (Succinate receptor 1), *Cd163* (CD163 Molecule), *Atf3* (Activating transcription factor 3) and *Mmp3* (Matrix metallopeptidase 3) showed no significant difference between the two transcriptomes, and the *Egr4* gene could not be analyzed because this transcript is associated with several mRNA products.

Using the RT-qPCR approach, we further analyzed the differential gene expression between the GASH/Sal under free-seizure conditions and the GASH/Sal with sound-induced seizures to determine the gene expression changes due to the effects of having an audiogenic seizure. As shown in **Figure 4**, these analyses confirmed that *Egr2, Slc28a1, Fosb, Ttr*, *Egr3, Kcnj13, Kcns1, Fos, Egr1*, *Ogn, Npas4* and *Gadd45g* were overexpressed in the GASH/Sal with audiogenic seizures. In addition, the genes *Junb, Slc13a4, Grin2c, Rab29*, *Atp2a3* and *C6* were significantly down regulated in GASH/Sal under free-seizure conditions, when compared to GASH/Sal with sound induced-seizures. On the other hand, the genes *Wdr38, Sucnr1, Cd163, Atf3, Mmp3, Rfxp2, Slc6a4, Renbp and Gm12695*, showed no significant difference between the two experimental conditions.

Finally, we did not evaluate some genes such as ENSMAUG00000010962, ENSMAUG00000016501, ENSMAUG00000016095, ENSMAUG00000008202, ENSMAUG00000011099, ENSMAUG00000013227 and ENSMAUG00000013872 because they had no products or defined sequences.

Functional Association Networks and Gene Ontology Analysis of the Top Differentially Expressed Genes

To better understand the possible functional association networks resulting from the altered mRNA expression in the epileptogenic nucleus of the GASH/Sal, we searched for the available protein-protein interactions of the 24 confirmed differentially expressed genes using the software STRING. The STRING database contains information on known and predicted, direct physical, and indirect functional protein-protein interactions. This analysis showed interactions of early growth response genes (***Egr1-4***), the genes encoding proto-oncogene AP-1 transcription factor subunit (***Fos, FosB, Junb***) and the gene encoding for the neuronal PAS domain protein 4 (***Npas4***) (**Figure 5**). The level of trust of the associations is represented by the thickness and number of lines with a p-value < 0.05 (interaction score in STRING database > 0.95). Based on this network analysis, we generated the following interaction networks: 13.7% of the genes were related to early growth response; 10.3% were transcriptional factors such as ***Fos, FosB*** and ***Junb***; 10.3% encoded solute carrier proteins (***Slc28a1***, ***Slc13a4*** and ***Slc6a4***); and 6.8% encoded potassium voltage-gated channels (***Kcnj13***, ***Knsc1***), among others (**Table 3**).

To further analyze the functionality of the networks, we carried out a PANTHER analysis of the 24 differentially expressed genes to determine which functional Gene Ontology (GO) categories (molecular process, biological process and cellular component) were highly represented (**Figure 6**).

Metabolomics Analysis

Metabolomics analysis using the 16299 differentially expressed genes in the epileptogenic focus, showed no significant difference, which implies an overall expression balance between metabolic pathways. On the other hand, the 36 differentially expressed genes were studied, and when performing their metabolomic analysis, 318 pathways contained at least one of those genes. Applying the criterion to confer a metabolic pathway with a $p < 0.01$ as significant, we found that the most affected routes by the overexpression of these genes were the interleukins- 4 and -13 (IL-4 and IL-13) signaling (10.3180/R-HSA-6785807.1), and the transporters of both nucleosides and free bases in the plasma membrane (10.3180/REACT_1206.3) (**Table 4**).

Of the top differentially expressed genes, 21 of them have a human homolog described in the metabolome. These 21 genes were clustered according to their gene expression levels by k-means clustering (MacQueen, 1967), which resulted in 3 clusters (**Figure 7**). In cluster 1, the *Rxfp2* gene stands out from the other study genes as a single-member cluster (red circle, **Figure 7**). Cluster 2 includes all study genes with no significant differences between them and expressed at standard levels (*Atp2a3, Egr1, Egr3, Fos, Gadd45g, Grin2c, Junb, Kcnj13, Kcns1, Npas4, Ogn, Rab29, Renbp, Slc13a4, Slc6a4, Wdr38*; as shown in blue circles in the **Figure 7**). Lastly, cluster 3 groups five genes (*C6, Egr2, Fosb, Slc28a1* and *Ttr*) with significant differences from the two previous groups (green circles, **Figure 7**). Overrepresentation analysis of cluster 3 (which is of greater interest in our study) showed that the route with the lowest p-value corresponds to the transport of nucleosides and free bases in the plasmatic membrane (*Slc28a1*). Furthermore, cluster 3 has genes corresponding to metabolic pathways, a finding that reinforces the results from our metabolomics analyses and highlights interleukins IL-4 and IL-13 signaling and nucleoside transport as possible damaged or altered routes in our model.

DISCUSSION

Epilepsy is a neurological disorder with a high epidemiological impact worldwide. In this context, epilepsy research

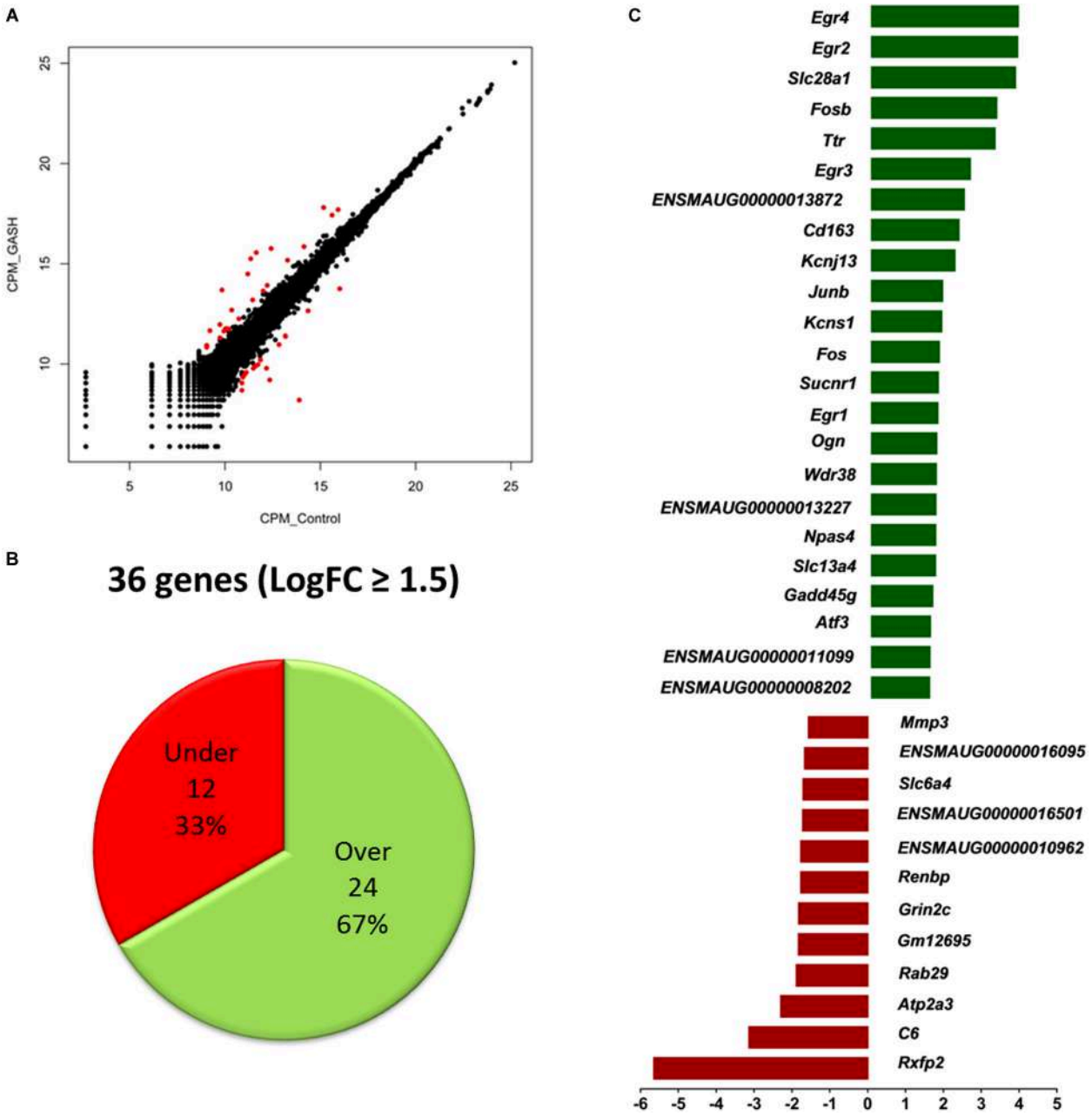

FIGURE 2 | Top differentially expressed genes selected by the criteria of |LogFC| ≥ 1.5, CPM > 10 and COUNTS > 40 when comparing the IC transcriptomes of the GASH/Sal hamster and the Syrian control hamster after high-intensity acoustic stimulation. **(A)** Scatterplot matrix of the expression value (measured as counts per million mapped reads, CPM) of each gene in GASH/Sal *vs*. control samples. Genes with significant differential expression are represented in red. **(B)** Number of differentially expressed genes. **(C)** Identification of differentially expressed genes over- (in green) and underexpressed (in red).

on experimental animal models plays a critical role in determining the cellular and molecular factors underlying ictogenesis and epileptogenesis, searching for parallel factors with human epilepsies. In the present study, RNA-seq was used to identify changes in gene expression in the epileptogenic focus (namely the IC) between GASH/Sal and control hamsters after high-intensity sound stimulation.

The RNA-Seq approach is a sensitive and accurate method for the quantification of gene expression levels. Despite its reliability, the RNA-Seq data exhibits some variations due to normalization and differences in probes which make necessary to be validated by RT-qPCR (Wang et al., 2009). Accordingly, our RNA-Seq results were confirmed by RT-qPCR, showing 24 differentially expressed (known) genes between the IC of GASH/Sal and control animals. Moreover, to understand the possible functional

TABLE 3 | Analysis of RNA-seq data of the differentially expressed genes with |logFC| ≥ 1.5, CPM > 10 and COUNTS > 40 in the IC transcriptome of GASH/Sal in comparison with the IC transcriptome of the Syrian control, both after acoustic stimulation.

Symbol	CPM_Control	CPM_GASH	FC	LogFC_CPM	Full name
Egr4	3197.37	48350.78	15.15	3.92	Early Growth Response 4
Egr2	2611.30	39070.74	15.00	3.91	Early Growth Response 2
Slc28a1	918.19	13240.31	14.52	3.86	Solute Carrier Family 28 Member 1
Fosb	5476.56	55621.13	10.17	3.35	FosB Proto-Oncogene, AP-1 Transcription Factor Subunit
Ttr	2350.82	23111.44	9.86	3.30	Transthyretin
Egr3	36994.47	229400.22	6.20	2.63	Early Growth Response 3
ENSMAUG00000013872	592.59	3250.97	5.55	2.47	
Cd163	1308.90	6620.16	5.08	2.35	CD163 Molecule
Kcnj13	853.07	4019.38	4.75	2.25	Potassium Voltage-Gated Channel Subfamily J Member 13
Kcns1	527.47	1950.58	3.74	1.90	Potassium Voltage-Gated Channel Modifier Subfamily S Member 1
Junb	9969.82	37120.16	3.73	1.90	Junb Proto-Oncogene, AP-1 Transcription Factor Subunit
Fos	50278.88	176025.21	3.50	1.81	Fos Proto-Oncogene, AP-1 Transcription Factor Subunit
Egr1	62586.49	213145.37	3.41	1.77	Early Growth Response 1
Ogn	2806.66	9398.26	3.36	1.75	Osteoglycin
Wdr38	1048.43	3487.40	3.35	1.74	WD Repeat Domain 38
Npas4	18109.77	59285.86	3.27	1.71	Neuronal PAS Domain 4
Slc13a4	4760.25	15545.54	3.27	1.71	Solute Carrier Family 13 Member 4
ENSMAUG00000013227	983.31	3191.86	3.27	1.71	
Sucnr1	527.47	1832.36	3.13	1.64	Succinate Receptor 1
Gadd45g	4109.05	12767.44	3.11	1.64	Growth Arrest And DNA Damage Inducible Gamma
Atf3	853.07	2541.67	3.00	1.59	Activating Transcription Factor 3
ENSMAUG00000011099	1178.67	3428.29	2.92	1.55	
ENSMAUG00000008202	1699.62	4906.01	2.90	1.53	
Mmp3	2090.34	709.30	0.34	−1.56	Matrix Metallopeptidase 3
ENSMAUG00000016095	3718.33	1182.17	0.32	−1.65	
Slc6a4	3067.14	945.74	0.31	−1.70	Solute Carrier Family 6 Member 4
ENSMAUG00000016501	21040.16	6442.83	0.31	−1.71	
Renbp	3392.73	1004.85	0.30	−1.76	Renin Binding Protein
ENSMAUG00000010962	9188.38	2718.99	0.30	−1.77	
Grin2c	9253.50	2659.88	0.29	−1.81	Glutamate Ionotropic Receptor NMDA Type Subunit 2C
Rab29	7299.91	2009.69	0.28	−1.87	RAB29, Member RAS Oncogene Family
Atp2a3	66493.67	13831.40	0.21	−2.28	ATPase Sarcoplasmic/Endoplasmic Reticulum Ca2+ Transporting 3
C6	5216.08	591.09	0.11	−3.13	Complement C6
Rxfp2	15244.51	295.54	0.02	−5.69	Relaxin Family Peptide Receptor 2

associations and the biological relevance of these genes, we searched for significantly overrepresented biological processes or molecular functions in several ontological processes such as positive regulation of transcription through RNA polymerase II promoter, transport, voltage-gated ion channel activity and transcription factor complex.

Methodological Discussion

In the present study, the altered gene expression in the IC of the GASH/Sal with sound-induced seizures was determined by a comparative transcriptome analysis using RNA-seq. This allowed us to interpret in a global and comprehensive manner the functional elements of the genome and reveal differences in gene expression between cells and tissue from different sources. The key objectives of the transcriptome are: to catalog the transcripts, including mRNA, non-coding RNA and small RNA and to determine transcriptional structures and quantify expression levels (Wang et al., 2009).

In our study, we assessed the gene expression levels of the IC in GASH/Sal with sound-induced seizures and control hamsters that were subjected to the same acoustic stimulation protocol. For such purpose, we used an interval of 60 min between the high-intensity acoustic stimulation and the animal euthanasia for the extraction of the IC tissue samples. Subsequently, we identified the immediate-early genes that activate metabolic processes induced by response to a stimulus (Vaudry, 2002; Fowler et al., 2011), as suggested in studies with early growth response genes (López-López et al., 2017). In addition, our bioinformatics evaluation of the RNA-seq pool of IC transcripts in GASH/Sal with audiogenic seizures *vs.* sound-stimulated control hamsters followed a restrictive criteria that included the |logFC| ≥ 1.5 ranges and a normalized expression value higher than 10 counts

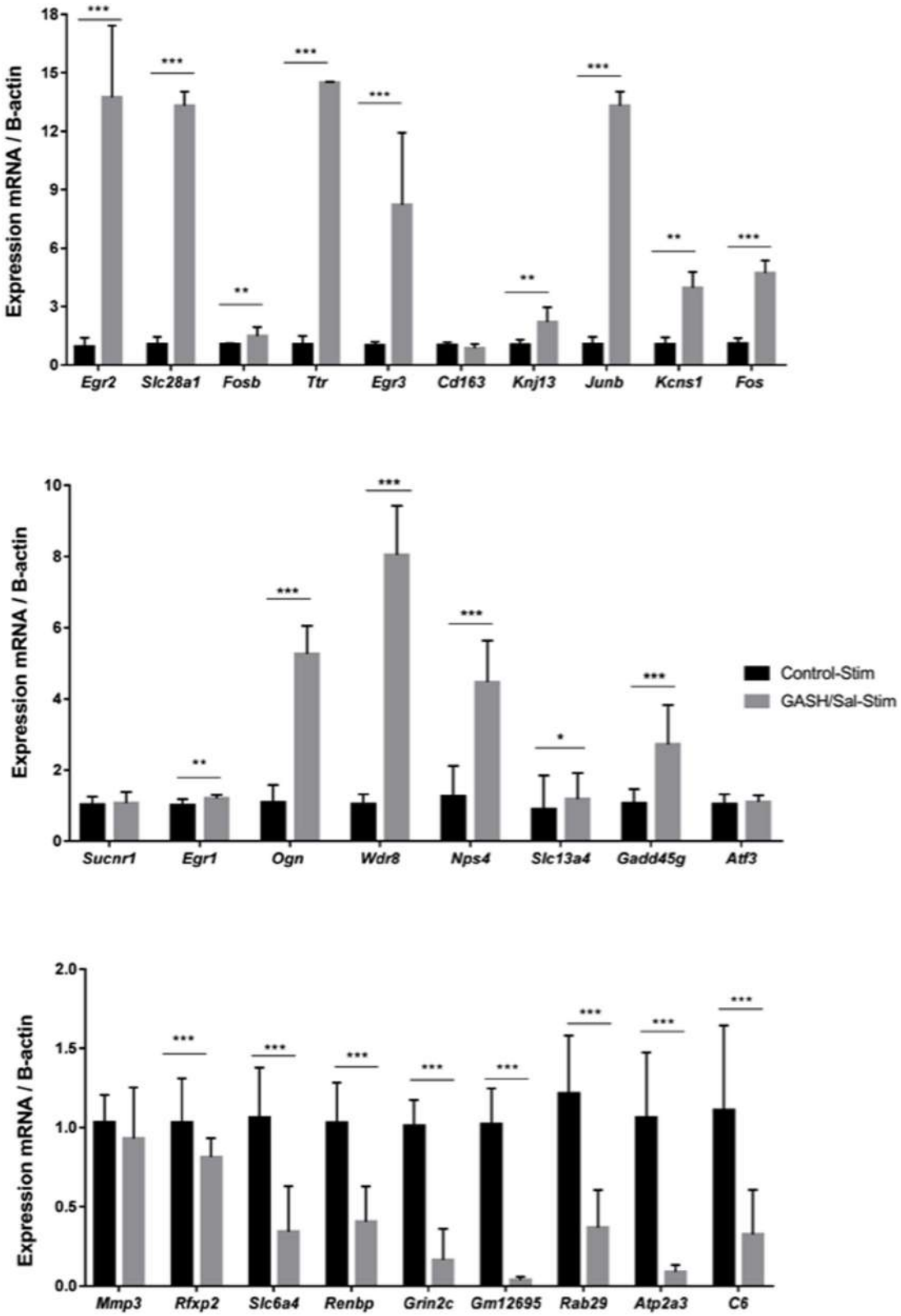

FIGURE 3 | mRNA expression levels of IC genes in GASH/Sal and control animals after high-intensity acoustic stimulation. Histograms show mRNA expression levels of 27 genes selected from the comparative transcriptome analysis shown in **Figure 2**. Asterisks indicate statistically significant differences in expression of each gene in the IC of GASH/Sal animals as compared to controls. Significance was set at $*p < 0.05$, $**p < 0.01$, $***p < 0.001$. Error bars indicate hemi-standard deviation (SD).

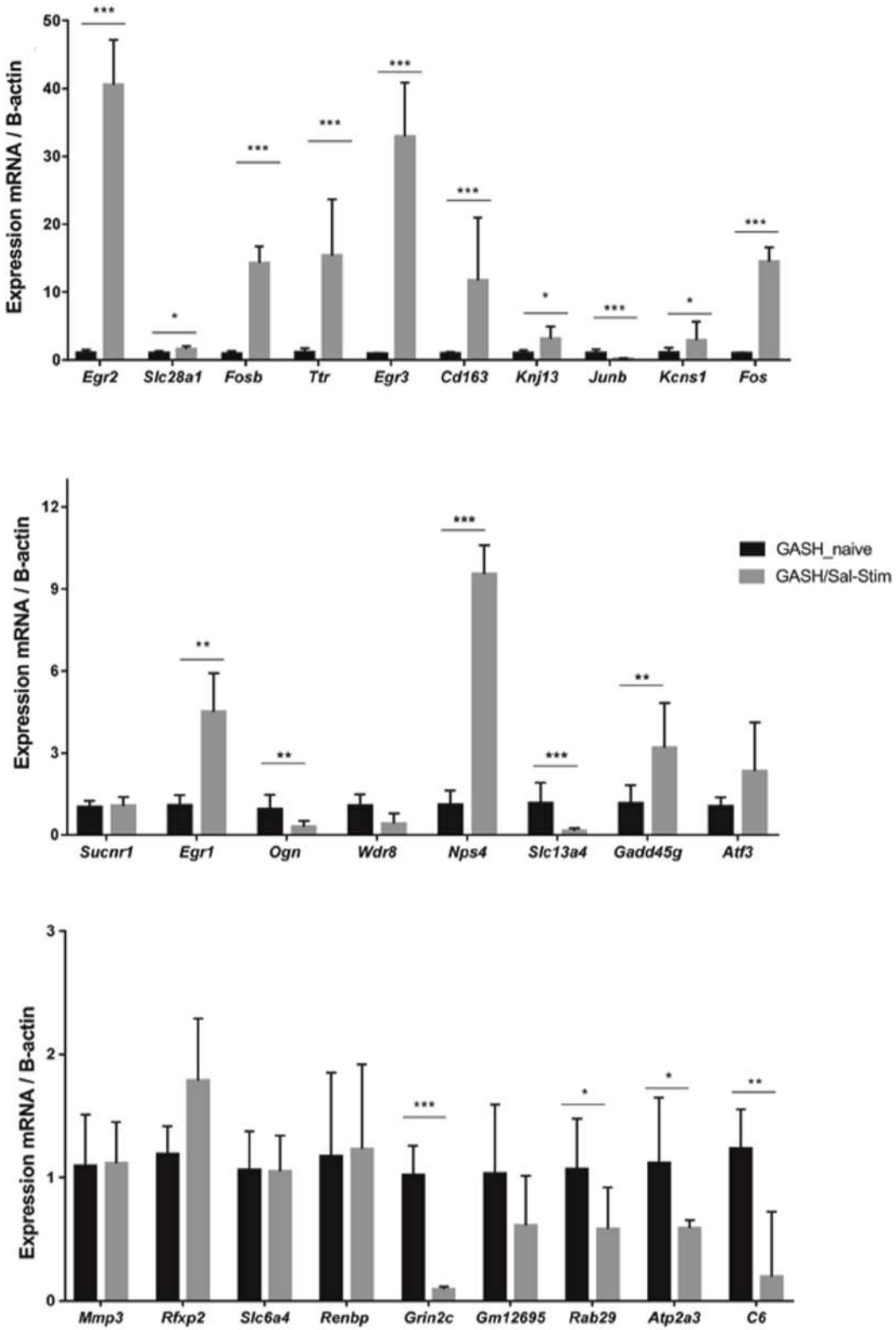

FIGURE 4 | mRNA expression levels of IC genes in GASH/Sal under-free seizure conditions (GASH/Sal naïve) and GASH/Sal animals with seizures after high-intensity acoustic stimulation (GASH/Sal-Stim). Histograms show mRNA expression levels of 27 genes selected from the comparative transcriptome analysis shown in **Figure 2**. Asterisks indicate statistically significant differences in expression of each gene in the IC of GASH/Sal animals with audiogenic seizure as compared to GASH/Sal naïve. Significance was set at $^{*}p < 0.05$, $^{**}p < 0.01$, $^{***}p < 0.001$. Error bars indicate hemi-standard deviation (SD).

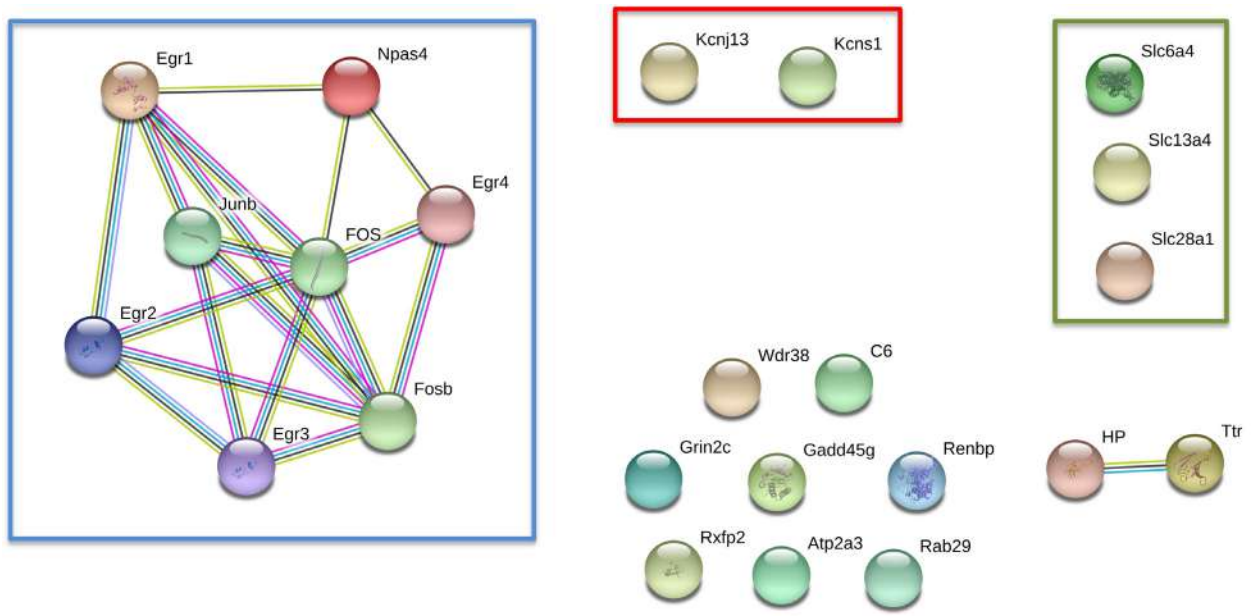

FIGURE 5 | Network-Based Integration of 24 differentially expressed genes in the IC of GASH/Sal *vs.* control hamsters after high-intensity acoustic stimulation. In red box: genes encoding potassium voltage-gated channels; green box: genes encoding solute carrier proteins, and blue box: molecular network.

to select differentially expressed immediate-early genes. Lastly, a set of transcripts selected as differentially expressed were confirmed by RT-qPCR in order to validate the differentially expressed genes that were previously identified in the IC transcriptomes of GASH/Sal and control hamsters after high-intensity acoustic stimulation.

The RT-qPCR approach quantifies the expression levels of a given gene by fluorescence, which is directly proportional to the amplification of the target cDNA. The analysis of these results requires determining the value of baseline fluorescence or background noise, which does not correspond to the amplification of the sample. This value is calculated by automated analysis of the amplification graph. The qPCR machine provides the threshold value, which refers to the increase in fluorescence that is considered significant with respect to the baseline value. Ultimately, Ct is defined as the cycle at which the fluorescence exceeds the threshold value. The results are normalized and analyzed based on the values of Ct of the different samples for each gene of interest. Data normalization in quantitative experiments, such as qPCR, requires using constitutive genes as calibrators. These constitutive or reference genes show stable expression, regardless of cell type or treatment applied (Chapman and Waldenström, 2015). In this study, *Actb* was used as the reference gene because it was the most stable gene according to the expression level measured by NormFinder software in the intra- and intergroup analyses (Andersen et al., 2004),. Moreover, it has been previously reported that the *Gapdh* gene is overexpressed in the Syrian hamster (McCann et al., 2017). Reference genes make it possible to normalize the amount of cDNA used in each reaction. The results were analyzed using the $2^{-\Delta\Delta CT}$ method, which quantifies relative changes in gene expression. These changes were expressed as FC values, which have been normalized using the reference gene and in relation to the control condition (Schmittgen and Livak, 2008).

Differences between RT-qPCR and RNA-seq experiments used for selecting the commonly expression genes in the comparative analysis of both transcriptomes occur for several reasons, including the fact that different probes are used for the RT-qPCR and RNA-seq experiments, differences in the methods for normalization of expression data and possible false-positive expression changes (Costa et al., 2013).

Molecular Networks of Differentially Expressed Genes

In the molecular network analysis, the EGR gene family was identified as the main axis of gene interactions. These genes encode a family of zinc-finger proteins, which bind to DNA, RNA, or proteins (Crosby et al., 1991; O'Donovan et al., 1999). *Egr1, Egr2*, and *Egr3* are immediate-early genes whose transcription can be rapidly and transiently induced by a broad range of cellular stimuli, including environmental, physiological, and pathological stimuli (Beckmann and Wilce, 1997; López-López et al., 2017). In this network, we also identified *Fosb*, *Junb* and *Fos* genes that were overexpressed in the GASH/Sal model in relation to the respective controls. This is a key alteration because these genes encode transcription factors involved in several biological processes, including cell proliferation, differentiation, apoptosis, and inflammation (Hess, 2004). Another overexpressed gene that belongs to this network is *Npas4*, a neuron-specific transcriptional factor critical for activity-dependent regulation of GABAergic synapse

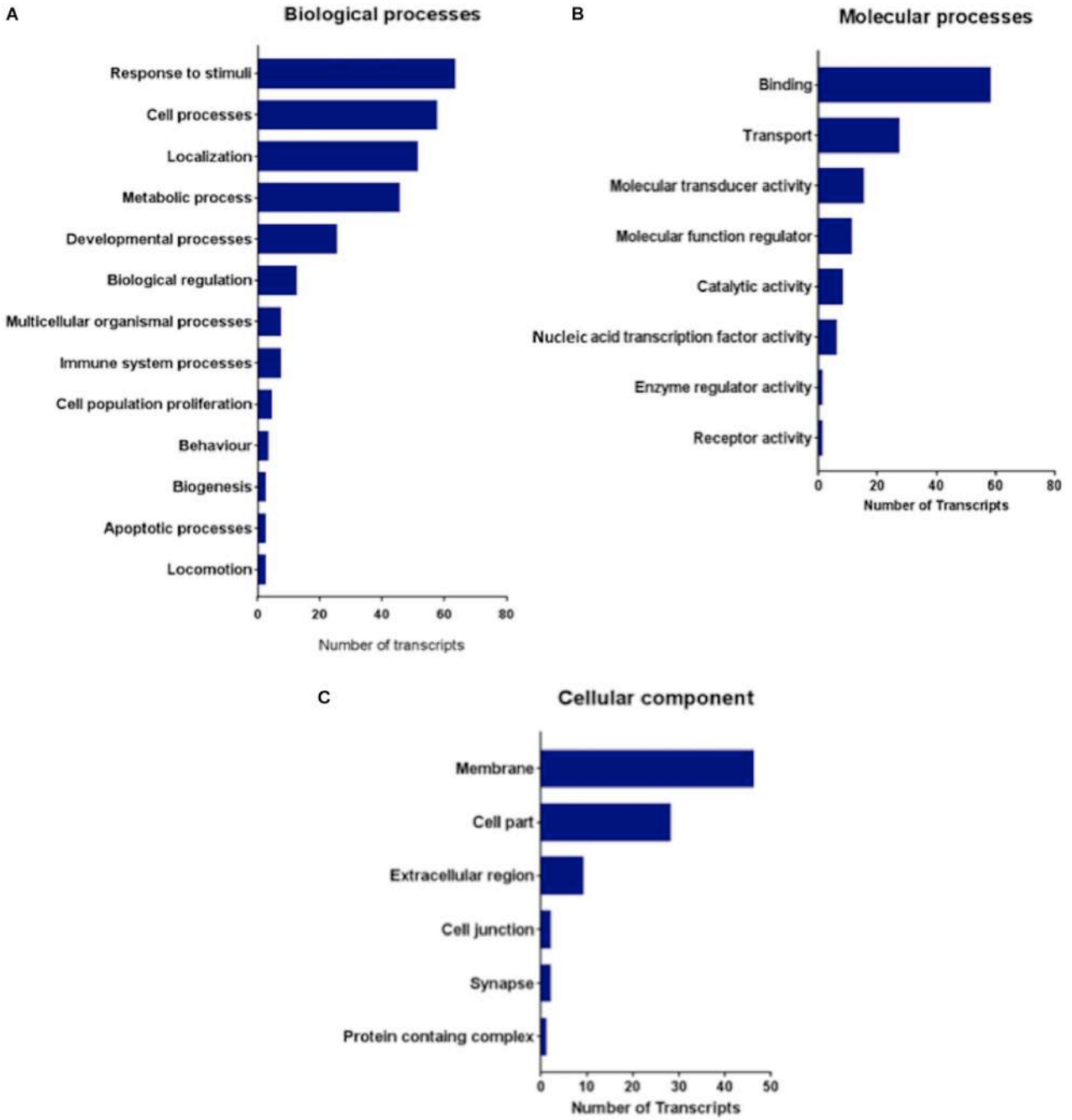

FIGURE 6 | Represented gene ontology terms of 24 differentially expressed genes in the IC comparative transcriptomes of GASH/Sal *vs.* control hamsters after high-intensity acoustic stimulation. **(A)** Biological processes, **(B)** molecular processes, and **(C)** cellular components.

TABLE 4 | Metabolic pathways analyzed using the KEEG, REACTOME and GeneCards databases.

Pathway	Entities found	Entities total	Interactions found	Interactions	*p*-valor	Reactions	Reactions total
Transport of nucleosides and free bases in the plasma membrane	21	3	0	7	1.88E–03	2	16
Signaling IL-4 Il-13	7	211	0	138	1.66E–05	2	46

This analysis identifies significantly overrepresented functional annotations.

development *in vitro* through BDNF expression (Lin et al., 2008). *Npas4* gene is directly involved in activity-dependent gene expression control and regulation of long-lasting brain functions, such as memory formation, adaptation, and synaptic plasticity (Lin et al., 2008; Ye et al., 2016). Lastly, *Egr* genes have been also reported in previous studies on epilepsy in the GASH/Sal hamster (López-López et al., 2017), in polycarpic-induced rat models (Lösing et al., 2017), in patients with refractory epilepsy (Liu et al., 2016), in the IC of the DBA/2J mice after induced audiogenic seizures (Li and Hu, 2005) and in an animal model of temporal lobe Epilepsy (Grabenstatter et al., 2014). Similarly, the genes *Npas4, Junb, Fos* and *Fosb* have also been related to epileptiform processes in animal models and epileptogenic tissue samples (Elliott and Gall, 2000; Beaumont et al., 2012; Liu et al., 2016; Lösing et al., 2017).

Overall, the GO analysis of this molecular network demonstrated that several GO terms identified in this study have been related to epilepsy in previous studies on refractory epilepsy of the mesial temporal lobe (Bando et al., 2011) and in rat models of febrile seizures (Wang et al., 2014). In addition, this molecular network was also identified in conditional serum response factor (SRF) knockout mice and mouse pilocarpine epilepsy models (Kuzniewska et al., 2016; Lösing et al., 2017). Thus, overexpression of transcriptional factors, growth factors and *Npas4* may be followed by a second wave of expression of further effector genes related to glutamatergic pathways, GABAergic transmission and synaptic transmission, thereby accounting for the audiogenic seizure susceptibility in the GASH/Sal model.

Deregulated Genes Involved in Calcium Channels

We observed underexpression of *Atp2a3* and *Grin2c* genes related to the calcium-signaling pathway in our comparative study of the IC transcriptomes in GASH/Sal *vs.* control hamsters after loud sound stimulation. The gene *Atp2a3* encodes a Ca^{2+} ATPase pump (SERCA), which actively re-accumulates released Ca^{2+} back into the sarco/endoplasmic reticulum, participating in the maintenance of Ca^{2+} homeostasis (Feng et al., 2013; Contreras-Leal et al., 2016). Moreover, this gene has been related to carcinogenic processes (Korošec et al., 2009), diabetes (Liang et al., 2011; Estrada et al., 2012) and epileptogenic processes (Kuzniewska et al., 2016; Lösing et al., 2017). On the other hand, the *Grin2c* encodes a subunit of the N-methyl-D-aspartate (NMDA) receptor. The receptor is a tetramer of different subunits (typically heterodimer of subunit 1 with one or more of subunits 2A-D, also named GRIN2A-D), forming a channel that have been related to receptor operated calcium channels (Ishi et al., 1993) and whose properties are determined by subunit composition (**Figure 8**).

Although *Grin2c* gene has not been related to epileptogenic processes, the subunit GRIN2A appears to be associated with the broadest and best characterized phenotypic spectrum, including a variety of disorders of the epilepsy aphasia spectrum and developmental and epileptic encephalopathy (Strehlow et al., 2019). In relation to these channels, it is known that the elevated intracellular calcium ion concentration activates processes such as hormone secretion, neurotransmitter release and calcium-dependent transcription of several genes, in addition to promoting spontaneous pacemaker activity in some neurons, muscles and secretory cells (Dolphin, 2016). Thus, the low expression of *Grin2c* observed in GASH/Sal animals after sound-induced seizures may contribute to Ca^{2+} deregulation of neuronal excitability and to the imbalance in intracellular Ca^{2+} as a result of changes in the formation of a receptor operated channel. Finally, with respect to the function of *Atp2a3*, calcium transport from the cytosol into the sarco/endoplasmic reticulum is decreased in the GASH/Sal after sound-induced seizures due to changes in the formation of SERCA channels. Most likely, both *Grin2c* and *Atp2a3* expression is downregulated in response to mutations of genes related to calcium response in the IC of the GASH/Sal.

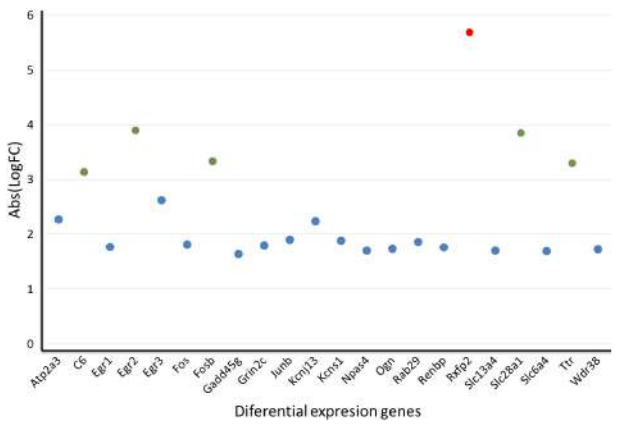

FIGURE 7 | Gene distribution in each metabolic cluster of 24 differentially expressed genes in the IC of sound-stimulated GASH/Sal hamsters in relation to their controls. Red circle: In cluster 1, the *Rxfp2* stands out from the other genes as an outlier; Blue circle: cluster 2 includes all genes studied with no significant differences; Green circle: cluster 3 groups five genes with significant differences.

Deregulated Genes Involved in Potassium Channels

Kcns1 and *Kcnj13* were overexpressed in the transcriptome of GASH/Sal animals when compared with the respective controls. *Kcns1* and *Kcnj13* genes encode voltage-dependent potassium channels and have been related to nociceptive signaling and retinal disturbance (Hao et al., 2013; Coussa et al., 2017). In particular, *Kcns1* encodes a potassium channel alpha subunit (Kv9.1) of the subfamily of electrically silent Kv (KvS) channel subunits (Kv5, Kv6, Kv8 and Kv9), which nevertheless generate functional channels at the plasma membrane when they heterotetramerize with Kv2 subunits. Interestingly, Kv9.1 was detected in the anterior and posterior ventral cochlear nucleus, and in the dorsal cochlear nucleus (Bocksteins, 2016). In addition, it has been suggested that the hyperpolarizing shift in voltage-dependent of Kv2.1 activation observed in rat neocortical pyramidal neurons could be caused by heterotetramerization

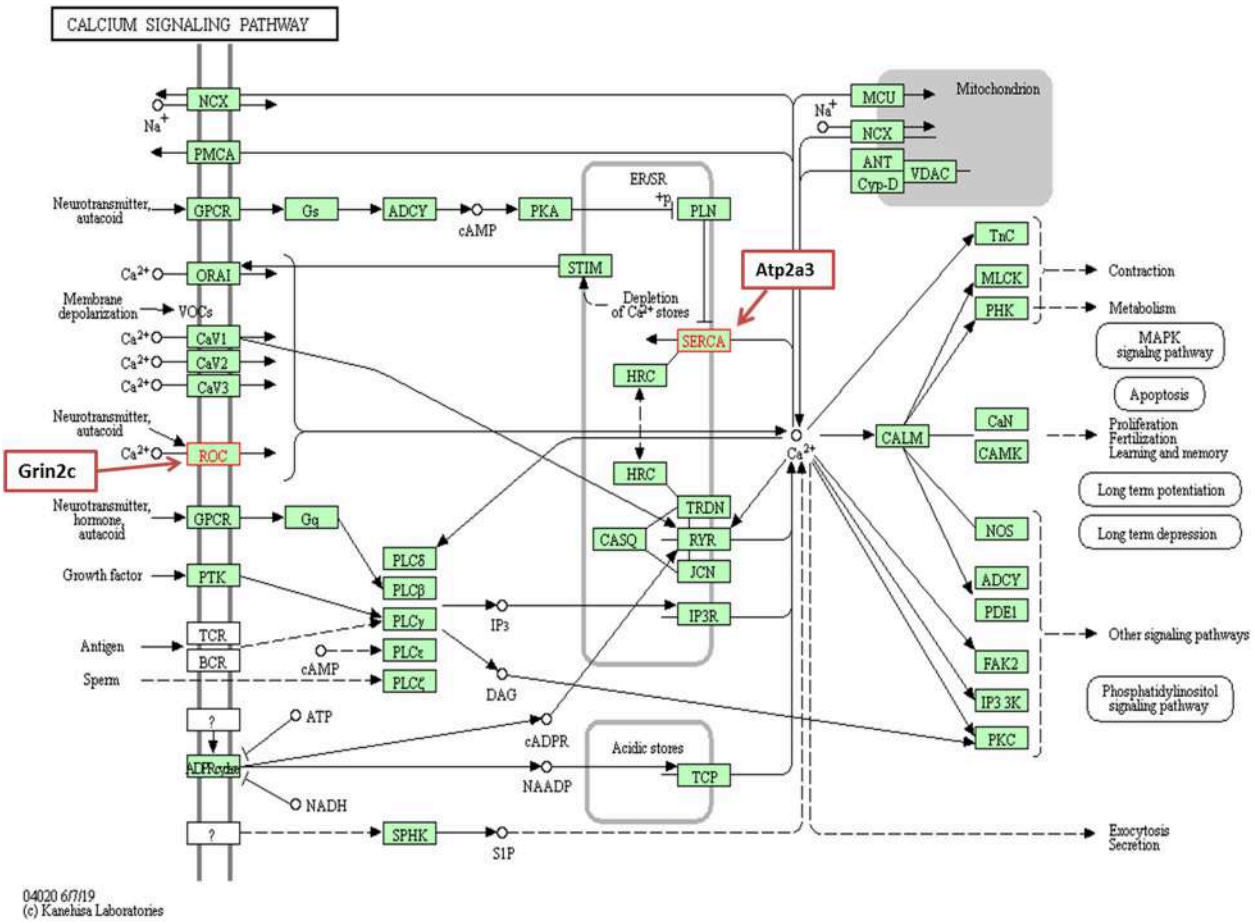

FIGURE 8 | Calcium signaling pathway. *Grin2c* encodes an NMDAR channel that is associated with a ROC channel, and *Atp2a3* encodes a SERCA channel.

with the KvS subunit Kv9.1 (Bocksteins, 2016). Moreover, Kv2.1 is associated with epilepsy-related mutations, thus raising the possibility that the epileptogenic effects on Kv2.1 may arise from an electrophysiological defect (Thiffault et al., 2015). In this context, *Knsc1* overexpression may be a mechanism of compensation for Kv2.1 channel over activation, thus explaining why the transcription of *Kcnb1*, which encodes Kv2.1, is not altered in GASH/Sal animals. Instead, Kcns1 expression is likely a target of gene expression modulation in response to *Kcnb1* mutations that cause epilepsy.

On the other hand, *Kcnj13* encodes channel Kir7.1, which is one of the most recently described members of the Kir channel super family expressed in brain, nephron, small intestine, and stomach (Pattnaik et al., 2012). A recent evidence indicates that mutant Kir7.1 channels are associated with inherited eye pathologies such as vitreo retinal degeneration and leber congenital amaurosis. Based on such finding, mutations implicated in channelopathies may result from the loss of function Kir7.1 channels (Coussa et al., 2017). Although Kir7.1 channels have not been directly associated with epilepsy, Winden et al. (2011) showed that *Kcnj13* was overregulated in chronic epilepsy. Consistent with this, our comparative transcriptome and RT-qPCR analyses of the IC in GASH/Sal and control hamsters suggest that *Kcnj13* overexpression following an epileptogenic event is a mechanism of compensation for Kir channel deregulation associated with epileptogenicity.

Metabolomics Analysis

Our study showed that the gene expression of the nucleoside transporters SLC28 was overregulated in the GASH/Sal model, SLC28 and SLC29 are integral membrane proteins involved in the transport of nucleobases and nucleosides for the synthesis of nucleic acids (Pérez-Torras et al., 2013). The two families of nucleoside transporters SLC28 and SLC29 have several members that participates in modulating neurotransmission, vascular tone, immune responses and other physiological processes (Mulinta et al., 2017). The *Slc28a1* gene stands out as the protein-coding gene for Solute Carrier Family 28 Member 1 (Pastor-Anglada et al., 2005), and has been related to some pathologies such as cancer (Wang and Buolamwini, 2019), atrial fibrillation (Lin et al., 2016), and antiretroviral therapy absorption (Moketla et al., 2018), but not to epilepsy. Thus, *Slc28a1* overexpression in the IC of GASH/Sal animals in comparison with their controls may result from a process of physiological

compensation whereby *Slc28a1* overexpression increases nucleic acid synthesis toward activating molecular processes to attenuate cellular stress, and consequently, contributing to epileptogenesis in the GASH/Sal.

On the other hand, it is known that epileptogenesis is associated with an increased, strong and persistent inflammatory state in the microenvironment of neural tissues, as is the case in subtle neuronal damage, gliosis and microgliosis (Alyu and Dikmen, 2017). Although the cellular and molecular mechanisms of epileptogenesis remain unclear, non-regulated focal or systemic inflammatory processes may lead to aberrant neuronal connectivity and hyperexcitable neural networks, which mediate the onset of epilepsy (Musto et al., 2016). In relation with this, our metabolomics analysis showed overrepresentation of inflammatory processes related to IL-4 and IL-13. These interleukins are well-known anti-inflammatory cytokines involved in cell repair and regeneration in inflammatory conditions (Kasaian et al., 2014). Therefore, the overrepresentation of this pathway may be associated with the aberrant onset of neuronal interactions underlying epilepsy, and the genes encoding of both interleukins can have the potential to be used as molecular biomarkers and targets for therapeutic approaches to epilepsy.

Rxfp2 is another key gene that showed disrupted expression in our metabolomics analysis. In this case, *Rxfp2* was found underexpressed in GASH/Sal animals after sound-induced seizure when compared to their controls. The *Rxfp2* gene encodes a member of the G-protein-coupled receptor family and is expressed in sexual organs, kidney and brain; unsurprisingly, this gene has been related to alterations in the female and male reproductive system (Bathgate et al., 2006). According to Tomiyama et al. (2003), *Rxfp2* receptor downregulation and deactivation causes cryptorchidism, decreased spermatogenesis and male sterility. Our findings of *Rxfp2* downregulation are consistent with the results reported by Tomiyama et al. (2003), because GASH/Sal animals exhibit breeding difficulties, which may be influencing lineage of the species (unpublished data). However, to date, no direct relationship has been found between the *Rxfp2* gene and seizures.

Genes Related to Epilepsy

The *C6* gene was overexpressed in the transcriptome analysis of GASH/Sal animals after audiogenic seizure. The C6 complement is one of the five plasma proteins incorporated into the potentially lytic terminal complement complex (Discipio and Gagnon, 1982; Walport, 2001). Since C6 is part of the membrane attack complex, this protein together with other complement components is involved in the destruction of susceptible cells and transmission of apoptosis signals (Muller-Eberhard, 1986). Furthermore, C6 deficiency has been implicated in decreased hemolytic activity (Dragon-Durey et al., 2003) and susceptibility to collagen antibody-induced lesions in arthritis (Banda et al., 2012). Interestingly, a study conducted by Buckingham et al. (2014) showed that deletion of the complement protein C5 significantly reduces the number of seizures in mice with the experimental cerebral malaria. Although no direct relationship has been found between C6 and epilepsy, our results indicated that it is worthwhile to explore whether the C6 contributes to seizure development as occurred with the C5 component. Based on the above, *C6* downregulation in the IC of GASH/Sal hamsters is likely related to membrane attack complex inhibition, which may act as a modulator after a seizure in this animal model.

Conversely, *Gadd45g* was found overexpressed in GASH/Sal with audiogenic seizures compared to control hamsters. *Gadd45g* is a member of a group of genes whose transcript levels increase in response to environmental stressors such as radiation or chemicals and which have been linked to cell cycle arrest, senescence, apoptosis, repair and demethylation of DNA, as well as functional maturation in various cellular systems, including the hematopoietic system. Although this gene in particular has not been implicated in epilepsy, studies focused on the serum response factor have shown *Gadd45g* overexpression after seizures in mouse pilocarpine epilepsy models (Lösing et al., 2017) and in human neocortical epilepsy (Beaumont et al., 2012). Therefore, *Gadd45g* overexpression may result from increased susceptibility to environmental stressors related to deregulated methylation processes passed along the GASH/Sal lineage.

Finally, *Ttr* was also overexpressed in GASH/Sal animals after audiogenic seizures. Plasma transthyretin (*Ttr*, previously termed prealbumin) is a 55k Da protein that participates in the transport of thyroxine and retinol plasma (vitamin A) (Herbert et al., 1986), and is usually located in the liver, central nervous system, and retinal pigmented epithelium (Soprano et al., 1985). In clinical studies, *Ttr* has been associated with familial amyloid polyneuropathy, an autosomal dominant multisystem neurological disease (Planté-Bordeneuve and Said, 2011), resulting from mutations that can cause seizures (Suhr et al., 2009; Franco et al., 2016). Thus, the overregulation of *Ttr* in the GASH/Sal model might affect the central nervous system, by producing seizures after loud sound stimulation. Nevertheless, *Ttr* gene was found overexpressed in the GASH/Sal also under free-seizure. Since a recent study reported that the GASH/Sal model carries two mutations in the *Ttr* gene that affect its structure and function (Díaz-Casado et al., 2020), our study indicated that the *Ttr* overexpression in the GASH/Sal might be compensatory mechanism to solve lack of functional TTR protein.

Molecular Impacts of the Genes Deregulation in the IC

Audiogenic seizure rodent strains have been investigated worldwide to elucidate the neuronal and molecular mechanisms underlying seizure generation and propagation (Simler et al., 1999; Yechikhov et al., 2001; Garcia-Cairasco, 2002). Many similarities exist in the audiogenic seizure networks of various rodent models of audiogenic seizure, particularly regarding the critical role of the IC in seizure initiation, but how the audiogenic seizure susceptibility occurs and seizure arises is unknown (Faingold, 2004). Electrical stimulation of the lateral lemniscal pathways projecting to the IC evokes excitatory and inhibitory postsynaptic responses converging on a common neural population (Wagner, 1996; Moore et al., 1998; Ma et al., 2002). Most

IC neurons receive both excitatory and inhibitory input from ascending fibers.

Glutamate is the primary excitatory transmitter throughout the IC (Adams and Wenthold, 1979; Bergman et al., 1989; Saint Marie, 1996). In addition, high levels of GABA exist in the IC (Tachibana and Kuriyama, 1974; Banay-Schwartz et al., 1989; Faingold et al., 1989) and many GABAergic neurons are likely to affect neuronal responses through intrinsic or commissural projections (Mugnaini and Oertel, 1985; Oliver et al., 1994). Based on this, our findings show deregulated gene expressions in the IC that might affect directly or indirectly the normal balance of excitatory and inhibitory conductance, resulting in neuronal network hyperexcitability and desynchronization.

In our experiments, the mRNA expression levels of *Egr3* was increased in the IC of the GASH/Sal, a result that was consistent with those obtained in previous studies (López-López et al., 2017). *Egr3* gene encodes a transcriptional factor that induce changes in $GABA_AR$ expression. This last gen encode a subunit of the $GABA_A$ receptor ($GABA_AR$), an ion channel that mediates the majority of inhibition in the central nervous system, and it has been associated with changes in $GABA_AR$ expression after the status epilepticus (Grabenstatter et al., 2012). Seizure induced transcriptional upregulation of the α4 subunit gene of the $GABA_AR$ (Roberts et al., 2005), which diminishes the effectiveness of GABA-mediated inhibition, and particularly, has been involved in the etiology of temporal lobe epilepsy (Grabenstatter et al., 2012). Moreover, within auditory pathways, the intrinsic electrical properties of neurons, and in particular their complement of potassium channels, play a key role in shaping the timing and pattern of action potentials produced by sound stimuli (Wu, 2005). The *Kcns1* gene (also known as Kv9.1) encodes a potassium channel alpha subunit that is expressed in a variety of neurons, including those of the IC, and is overexpressed in the GASH/Sal after the seizures. KCNS1 alters the kinetics and the voltage-dependence of activation and inactivation of KV2.1, a channel subunit that generates slowly inactivating delayed rectifier potassium currents. Because KV2.1 is expressed in IC (Hwang et al., 1992), this channel may be modulated by KCNS1, which might affect firing patterns significantly (Richardson and Kaczmarek, 2000).

In model neurons with rapidly inactivating inward current, the change in the voltage-dependence of activation produced by KCNS1 may allow the cells to follow high frequency stimulation more effectively (Richardson and Kaczmarek, 2000), which in turn might contribute to hyperexcitability through gene overexpression.

The disruption in gene expression of calcium and potassium channels, together with epileptogenesis-related genes that were found in our study, led us to infer that the altered gene expressions reported in the IC of the GASH/Sal might cause defects in biological process that contribute to its epileptogenic brain alterations. Future experiments that block the expression of these candidate genes and their correlations with changes in seizure severity will shed light on their role in epileptogenic mechanisms in the IC.

CONCLUSION

Our data show gene deregulation in the IC of GASH/Sal animals compared to control hamsters. This genetic dysregulation involves 24 confirmed differentially expressed (know) genes and 7 unknown genes with undescribed sequences. Our findings suggest that audiogenic seizures are triggered in GASH/Sal hamsters through multiple molecular substrates, which activate several biological processes and metabolic pathways associated with epileptogenic events similar to those produced by tonic clonic seizures in humans. Therefore, we conclude that the GASH/Sal model could help to identify and characterize genes and pathways that were associated with seizures, whose could represent plausible antiepileptic drug targets.

DATA AVAILABILITY STATEMENT

Publicly available datasets were analyzed in this study. This data can be found here: https://www.ncbi.nlm.nih.gov/bioproject/230618.

ETHICS STATEMENT

The animal study was reviewed and approved by Bioethics Committee of the University of Salamanca (approval number 300).

AUTHOR CONTRIBUTIONS

SD-R: validation, formal analysis, investigation, writing – original draft, visualization, conceptualization, software and data curation. DL-L, MH-T, and RG-N: writing – review and editing. AC-A: metabolomic analysis. DL: conceptualization, writing – review and editing, supervision, project administration and funding acquisition. All authors contributed to the revision of the manuscript and agreed with review the article.

FUNDING

This study was supported by the Spanish JCyL cofinanced with the European Union FEDER funds 2017 #SA070P17 (IP-López DE) and the JCyL predoctoral research fellowship 2019 (BOCYL, EDU/556/2019). The University of Salamanca pay part of the open access publication fees.

SUPPLEMENTARY MATERIAL

The Supplementary Material for this article can be found online at: https://www.frontiersin.org/articles/10.3389/fnins.2020.00508/full#supplementary-material

FIGURE S1 | Detail of the NCBI GenBank database [https://submit.ncbi.nlm.nih.gov/subs/] showing the corresponding "project," "sample," and "experiment" inputs.

REFERENCES

Adams, J. C., and Wenthold, R. J. (1979). Distribution of putative amino acid transmitters, choline acetyltransferase and glutamate decarboxylase in the inferior colliculus. *Neuroscience* 4, 1947–1951. doi: 10.1016/0306-4522(79)90067-8

Alyu, F., and Dikmen, M. (2017). Inflammatory aspects of epileptogenesis: contribution of molecular inflammatory mechanisms. *Acta Neuropsychiatr.* 29, 1–16. doi: 10.1017/neu.2016.47

Andersen, C. L., Jensen, J. L., and Ørntoft, T. F. (2004). Normalization of real-time quantitative reverse transcription-PCR data: a model-based variance estimation approach to identify genes suited for normalization, applied to bladder and colon cancer data sets. *Cancer Res.* 64, 5245–5250. doi: 10.1158/0008-5472.CAN-04-0496

Andrews, S. (2010). FastQC: a quality control tool for high throughput sequence data. Available online at: http://www.bioinformatics.babraham.ac.uk/projects/fastqc

Banay-Schwartz, M., Lajtha, A., and Palkovits, M. (1989). Changes with aging in the levels of amino acids in rat CNS structural elements II. Taurine and small neutral amino acids. *Neurochem. Res.* 14, 563–570. doi: 10.1007/BF00964919

Banda, N. K., Hyatt, S., Antonioli, A. H., White, J. T., Glogowska, M., Takahashi, K., et al. (2012). Role of C3a receptors, C5a receptors, and complement protein C6 deficiency in collagen antibody-induced arthritis in mice. *J. Immunol.* 188, 1469–1478. doi: 10.4049/jimmunol.1102310

Bando, S. Y., Alegro, M. C., Amaro, E., Silva, A. V., Castro, L. H. M., Wen, H.-T., et al. (2011). Hippocampal CA3 transcriptome signature correlates with initial precipitating injury in refractory mesial temporal lobe epilepsy. *PLoS One* 6:e26268. doi: 10.1371/journal.pone.0026268

Barrera-Bailón, B., Oliveira, J. A. C., López, D. E., Muñoz, L. J., Garcia-Cairasco, N., and Sancho, C. (2013). Pharmacological and neuroethological studies of three antiepileptic drugs in the genetic audiogenic seizure hamster (GASH:Sal). *Epilepsy Behav.* 28, 413–425. doi: 10.1016/j.yebeh.2013.05.028

Barrera-Bailón, B., Oliveira, J. A. C., López, D. E., Muñoz, L. J., Garcia-Cairasco, N., and Sancho, C. (2017). Pharmacological and neuroethological study of the acute and chronic effects of lamotrigine in the genetic audiogenic seizure hamster (GASH:Sal). *Epilepsy Behav.* 71, 207–217. doi: 10.1016/j.yebeh.2015.11.005

Bathgate, R. A., Ivell, R., Sanborn, B. M., Sherwood, O. D., and Summers, R. J. (2006). International union of pharmacology LVII: recommendations for the nomenclature of receptors for relaxin family peptides. *Pharmacol. Rev.* 58, 7–31. doi: 10.1124/pr.58.1.9

Beaumont, T. L., Yao, B., Shah, A., Kapatos, G., and Loeb, J. A. (2012). Layer-specific CREB target gene induction in human neocortical epilepsy. *J. Neurosci.* 32, 14389–14401. doi: 10.1523/JNEUROSCI.3408-12.2012

Beckmann, A. M., and Wilce, P. A. (1997). Egr transcription factors in the nervous system. *Neurochem. Int.* 31, 477–510. doi: 10.1016/s0197-0186(96)00136-2

Benjamini, Y., and Hochberg, Y. (1995). Controlling the false discovery rate: a practical and powerful approach to multiple testing. *J. R. Stat. Soc.* 57, 289–300.

Bergman, M., Staatz-Benson, C., and Potashner, S. J. (1989). Amino acid uptake and release in the guinea pig cochlear nucleus after inferior colliculus ablation. *J. Neurophysiol.* 42, 283–291. doi: 10.1016/0378-5955(89)90152-4

Bocksteins, E. (2016). Kv5, Kv6, Kv8, and Kv9 subunits: no simple silent bystanders. *J. Gen. Physiol.* 147, 105–125. doi: 10.1085/jgp.201511507

Buckingham, S. C., Ramos, T. N., and Barnum, S. R. (2014). Complement C5-deficient mice are protected from seizures in experimental cerebral malaria. *Epilepsia* 55, e139–e142. doi: 10.1111/epi.12858

Burns, M. J., Nixon, G. J., Foy, C. A., and Harris, N. (2005). Standardisation of data from real-time quantitative PCR methods - evaluation of outliers and comparison of calibration curves. *BMC Biotechnol.* 5:31. doi: 10.1186/1472-6750-5-31

Carballosa-Gonzalez, M. M., Muñoz, L. J., López-Alburquerque, T., Pardal-Fernández, J. M., Nava, E., de Cabo, C., et al. (2013). EEG characterization of audiogenic seizures in the hamster strain GASH:Sal. *Epilepsy Res.* 106, 318–325. doi: 10.1016/j.eplepsyres.2013.07.001

Chapman, J. R., and Waldenström, J. (2015). With reference to reference genes: a systematic review of endogenous controls in gene expression studies. *PLoS One* 10:e0141853. doi: 10.1371/journal.pone.0141853

Contreras-Leal, E., Hernández-Oliveras, A., Flores-Peredo, L., Zarain-Herzberg, Á., and Santiago-García, J. (2016). Histone deacetylase inhibitors promote the expression of ATP2A3 gene in breast cancer cell lines. *Mol. Carcinog.* 55, 1477–1485. doi: 10.1002/mc.22402

Costa, C., Giménez-Capitán, A., Karachaliou, N., and Rosell, R. (2013). Comprehensive molecular screening: from the RT-PCR to the RNA-seq. *Transl. Lung Cancer Res.* 2, 87–91. doi: 10.3978/j.issn.2218-6751.2013.02.05

Coussa, R. G., Lopez Solache, I., and Koenekoop, R. K. (2017). Leber congenital amaurosis, from darkness to light: an ode to Irene Maumenee. *Ophthalmic Genet.* 38, 7–15. doi: 10.1080/13816810.2016.1275021

Crosby, S. D., Puetz, J. J., Simburger, K. S., Fahrner, T. J., and Milbrandt, J. (1991). The early response gene NGFI-C encodes a zinc finger transcriptional activator and is a member of the GCGGGGGCG (GSG) element-binding protein family. *Mol. Cell. Biol.* 11, 3835–3841. doi: 10.1128/MCB.11.8.3835

Díaz-Casado, E., Gómez-Nieto, R., de Pereda, J. M., Muñoz, L. J., Jara-Acevedo, M., and López, D. E. (2020). Analysis of gene variants in the GASH/Sal model of epilepsy. *PLoS One* 15:e0229953. doi: 10.1371/journal.pone.0229953

Discipio, R. G., and Gagnon, J. (1982). Characterization of human complement components C6 and C7. *Mol. Immunol.* 19, 1425–1431. doi: 10.1016/0161-5890(82)90189-4

Dobin, A., Davis, C. A., Schlesinger, F., Drenkow, J., Zaleski, C., Jha, S., et al. (2013). STAR: ultrafast universal RNA-seq aligner. *Bioinformatics* 29, 15–21. doi: 10.1093/bioinformatics/bts635

Dolphin, A. C. (2016). Voltage-gated calcium channels and their auxiliary subunits: physiology and pathophysiology and pharmacology. *J. Physiol.* 594, 5369–5390. doi: 10.1113/JP272262

Dragon-Durey, M. A., Fremeaux-Bacchi, V., Blouin, J., Barraud, D., Fridman, W. H., and Kazatchkine, M. D. (2003). Restricted genetic defects underlie human complement C6 deficiency. *Clin. Exp. Immunol.* 132, 87–91. doi: 10.1046/j.1365-2249.2003.02099.x

Elliott, R. C., and Gall, C. M. (2000). Changes in activating protein 1 (AP-1) composition correspond with the biphasic profile of nerve growth factor mRNA expression in rat hippocampus after hilus lesion-induced seizures. *J. Neurosci.* 20, 2142–2149. doi: 10.1523/JNEUROSCI.20-06-02142.2000

Estrada, I. A., Donthamsetty, R., Debski, P., Zhou, M.-H., Zhang, S. L., Yuan, J. X.-J., et al. (2012). STIM1 restores coronary endothelial function in type 1 diabetic mice. *Circ. Res.* 111, 1166–1175. doi: 10.1161/CIRCRESAHA.112.275743

Faingold, C. L. (2004). Emergent properties of CNS neuronal networks as targets for pharmacology: application to anticonvulsant drug action. *Prog. Neurobiol.* 72, 55–85. doi: 10.1016/j.pneurobio.2003.11.003

Faingold, C. L., Gehlbach, G., and Caspary, D. M. (1989). On the role of GABA as an inhibitory neurotransmitter in inferior colliculus neurons: iontophoretic studies. *Brain Res.* 500, 302–312. doi: 10.1016/0006-8993(89)90326-0

Feng, M., Wang, Q., Wang, H., and Guan, W. (2013). Tumor necrosis factor-alpha preconditioning attenuates liver ischemia/reperfusion injury through preserving sarco/endoplasmic reticulum calcium-ATPase function. *J. Surg. Res.* 184, 1109–1113. doi: 10.1016/j.jss.2013.04.019

Fowler, T., Sen, R., and Roy, A. L. (2011). Regulation of primary response genes. *Mol. Cell* 44, 348–360. doi: 10.1016/j.molcel.2011.09.014

Franco, A., Bentes, C., de Carvalho, M., Pereira, P., Pimentel, J., and Conceição, I. (2016). Epileptic seizures as a presentation of central nervous system involvement in TTR Val30Met-FAP. *J. Neurol.* 263, 2336–2338. doi: 10.1007/s00415-016-8299-5

Garcia-Cairasco, N. (2002). A critical review on the participation of inferior colliculus in acoustic-motor and acoustic-limbic networks involved in the expression of acute and kindled audiogenic seizures. *Hear. Res.* 168, 208–222. doi: 10.1016/s0378-5955(02)00371-4

Garcia-Cairasco, N., Doretto, M. C., Ramalho, M. J., Antunes-Rodrigues, J., and Nonaka, K. O. (1996). Audiogenic and audiogenic-like seizures: locus of induction and seizure severity determine postictal prolactin patterns. *Pharmacol. Biochem. Behav.* 53, 503–510. doi: 10.1016/0091-3057(95)02040-3

Garcia-Cairasco, N., Umeoka, E. H. L., and Cortes de Oliveira, J. A. (2017). The Wistar Audiogenic Rat (WAR) strain and its contributions to epileptology and related comorbidities: history and perspectives. *Epilepsy Behav.* 71, 250–273. doi: 10.1016/j.yebeh.2017.04.001

Grabenstatter, H. L., Cogswell, M., Cruz Del Angel, Y., Carlsen, J., Gonzalez, M. I., Raol, Y. H., et al. (2014). Effect of spontaneous seizures on GABA A receptor α4 subunit expression in an animal model of temporal lobe epilepsy. *Epilepsia* 55, 1826–1833. doi: 10.1111/epi.12771

Grabenstatter, H. L., Russek, S. J., and Brooks-Kayal, A. R. (2012). Molecular pathways controlling inhibitory receptor expression. *Epilepsia* 53, 71–78. doi: 10.1111/epi.12036

Hao, J., Padilla, F., Dandonneau, M., Lavebratt, C., Lesage, F., Noël, J., et al. (2013). Kv1.1 channels act as mechanical brake in the senses of touch and pain. *Neuron* 77, 899–914. doi: 10.1016/j.neuron.2012.12.035

Herbert, J., Wilcox, J. N., Pham, K.-T. C., Fremeau, R. T., Zeviani, M., Dwork, A., et al. (1986). Transthyretin: a choroid plexus-specific transport protein in human brain: the 1986 S. Weir Mitchell Award. *Neurology* 36, 900–900. doi: 10.1212/WNL.36.7.900

Hess, J. (2004). AP-1 subunits: quarrel and harmony among siblings. *J. Cell Sci.* 117, 5965–5973. doi: 10.1242/jcs.01589

Hwang, P. M., Glatt, C. E., Bredt, D. S., Yellen, G., and Snyder, S. H. (1992). A novel K+ channel with unique localizations in mammalian brain: molecular cloning and characterization. *Neuron* 8, 473–481. doi: 10.1016/0896-6273(92)90275-I

Ishi, T., Moriyoshi, K., Sugihara, H., Sakurada, K., Kadotani, H., Yokoi, M., et al. (1993). Molecular characterization of the family of the N-Methyl-D-aspartate receptor subunits. *J. Biol. Chem.* 268, 2836–2843. doi: 10.1016/s0169-328x(99)00100-x

Kandratavicius, L., Balista, P., Lopes-Aguiar, C., Ruggiero, R., Umeoka, E., Garcia-Cairasco, N., et al. (2014). Animal models of epilepsy: use and limitations. *Neuropsychiatr. Dis. Treat.* 10, 1693–1705. doi: 10.2147/NDT.S50371

Kasaian, M. T., Page, K. M., Fish, S., Brennan, A., Cook, T. A., Moreira, K., et al. (2014). Therapeutic activity of an interleukin-4/interleukin-13 dual antagonist on oxazolone-induced colitis in mice. *Immunology* 143, 416–427. doi: 10.1111/imm.12319

Kesner, R. P. (1966). Subcortical mechanisms of audiogenic seizures. *Exp. Neurol.* 15, 192–205.

Korošec, B., Glavaè, D., Volavšek, M., and Ravnik-Glavaè, M. (2009). ATP2A3 gene is involved in cancer susceptibility. *Cancer Genet. Cytogenet.* 188, 88–94. doi: 10.1016/j.cancergencyto.2008.10.007

Kuzniewska, B., Nader, K., Dabrowski, M., Kaczmarek, L., and Kalita, K. (2016). Adult deletion of SRF increases epileptogenesis and decreases activity-induced gene expression. *Mol. Neurobiol.* 53, 1478–1493. doi: 10.1007/s12035-014-9089-7

Li, X., and Hu, Y. (2005). Gene expression profiling reveals the mechanism of action of anticonvulsant drug QYS. *Brain Res. Bull.* 66, 99–105. doi: 10.1016/j.brainresbull.2005.03.017

Liang, K., Du, W., Zhu, W., Liu, S., Cui, Y., Sun, H., et al. (2011). Contribution of different mechanisms to pancreatic beta-cell hyper-secretion in non-obese diabetic (n.d.) mice during pre-diabetes. *J. Biol. Chem.* 286, 39537–39545. doi: 10.1074/jbc.M111.295931

Lin, H., Mueller-Nurasyid, M., Smith, A. V., Arking, D. E., Barnard, J., Bartz, T. M., et al. (2016). Gene-gene interaction analyses for atrial fibrillation. *Sci. Rep.* 6:35371. doi: 10.1038/srep35371

Lin, Y., Bloodgood, B. L., Hauser, J. L., Lapan, A. D., Koon, A. C., Kim, T.-K., et al. (2008). Activity-dependent regulation of inhibitory synapse development by Npas4. *Nature* 455, 1198–1204. doi: 10.1038/nature07319

Liu, X., Ou, S., Xu, T., Liu, S., Yuan, J., Huang, H., et al. (2016). New differentially expressed genes and differential DNA methylation underlying refractory epilepsy. *Oncotarget* 7, 87402–87416. doi: 10.18632/oncotarget.13642

Lopes-Cendes, I., and Oliveira Ribeiro, P. A. (2013). Aspectos genéticos de las epilepsias: una visión actualizada. *Rev. Méd. Clín. Condes* 24, 909–914. doi: 10.1016/S0716-8640(13)70244-X

López-López, D., Gómez-Nieto, R., Herrero-Turrión, M. J., García-Cairasco, N., Sánchez-Benito, D., Ludeña, M. D., et al. (2017). Overexpression of the immediate-early genes Egr1, Egr2, and Egr3 in two strains of rodents susceptible to audiogenic seizures. *Epilepsy Behav.* 71, 226–237. doi: 10.1016/j.yebeh.2015.12.020

Lösing, P., Niturad, C. E., Harrer, M., Reckendorf, C. M. Z., Schatz, T., Sinske, D., et al. (2017). SRF modulates seizure occurrence, activity induced gene transcription and hippocampal circuit reorganization in the mouse pilocarpine epilepsy model. *Mol. Brain* 10:30. doi: 10.1186/s13041-017-0310-2

Ma, C., Kelly, J., and Wu, S. (2002). AMPA and NMDA receptors mediate synaptic excitation in the rat's inferior colliculus. *Hear. Res.* 168, 25–34. doi: 10.1016/s0378-5955(02)00370-2

MacQueen, J. (1967). "Some methods for classification and analysis of multivariate observations," in *Proceedings of the Fifth Berkeley Symposium on Mathematical Statistics and Probability*, Vol. 1 (Berkeley, CA), 281–297. doi: 10.1504/ijdmb.2015.067955

McCann, K. E., Sinkiewicz, D. M., Norvelle, A., and Huhman, K. L. (2017). De novo assembly, annotation, and characterization of the whole brain transcriptome of male and female Syrian hamsters. *Sci. Rep.* 7:40472. doi: 10.1038/srep40472

Moketla, M. B., Wadley, A. L., Kamerman, P., and de Assis Rosa, D. (2018). Pharmacogenetic variation influences sensory neuropathy occurrence in Southern Africans treated with stavudine-containing antiretroviral therapy. *PLoS One* 13:e0204111. doi: 10.1371/journal.pone.0204111

Moore, D., Kotak, V., and Sanes, D. (1998). Commissural and lemniscal synaptic input to the gerbil inferior colliculus. *J. Neurophysiol.* 80, 2229–2236. doi: 10.1152/jn.1998.80.5.2229

Mugnaini, E., and Oertel, W. H. (1985). "An atlas of the distribution of GABAergic neurons and terminals in the rat CNS as revealed by GAD immunohistochemistry," in *Handbook of Chemical Neuroanatomy, GABA and Neuropeptides in the CNS, Part I*, Vol. 4, eds A. Björklund, and T. Hökfelt (Amsterdam: Elsevier), 436–608.

Mulinta, R., Yao, S. Y. M., Ng, A. M. L., Cass, C. E., and Young, J. D. (2017). Substituted cysteine accessibility method (SCAM) analysis of the transport domain of human concentrative nucleoside transporter 3 (hCNT3) and other family members reveals features of structural and functional importance. *J. Biol. Chem.* 292, 9505–9522. doi: 10.1074/jbc.M116.743997

Muller-Eberhard, H. J. (1986). The membrane attack complex of complement. *Annu. Rev. Immunol.* 4, 503–528. doi: 10.1146/annurev.iy.04.040186.002443

Muñoz, L. J., Carballosa-Gautam, M. M., Yanowsky, K., García-Atarés, N., and López, D. E. (2017). The genetic audiogenic seizure hamster from Salamanca: the GASH:Sal. *Epilepsy Behav.* 71, 181–192. doi: 10.1016/j.yebeh.2016.03.002

Musto, A. E., Rosencrans, R. F., Walker, C. P., Bhattacharjee, S., Raulji, C. M., Belayev, L., et al. (2016). Dysfunctional epileptic neuronal circuits and dysmorphic dendritic spines are mitigated by platelet-activating factor receptor antagonism. *Sci. Rep.* 6:30298. doi: 10.1038/srep30298

O'Donovan, K. J., Tourtellotte, W. G., Millbrandt, J., and Baraban, J. M. (1999). The EGR family of transcription-regulatory factors: progress at the interface of molecular and systems neuroscience. *Trends Neurosci.* 22, 167–173. doi: 10.1016/s0166-2236(98)01343-5

Oliver, D. L., Winer, J. A., Beckius, G. E., and Saint Marie, R. L. (1994). Morphology of GABAergic neurons in the inferior colliculus of the cat. *J. Comp. Neurol.* 340, 27–42. doi: 10.1002/cne.903400104

Pastor-Anglada, M., Cano-Soldado, P., Molina-Arcas, M., Lostao, M. P., Larráyoz, I., Martínez-Picado, J., et al. (2005). Cell entry and export of nucleoside analogues. *Virus Res.* 107, 151–164. doi: 10.1016/j.virusres.2004.11.005

Pattnaik, B. R., Asuma, M. P., Spott, R., and Pillers, D. A. M. (2012). Genetic defects in the hotspot of inwardly rectifying K+ (Kir) channels and their metabolic consequences: a review. *Mol. Genet. Metab.* 105, 64–72. doi: 10.1016/j.ymgme.2011.10.004

Pérez-Torras, S., Vidal-Pla, A., Cano-Soldado, P., Huber-Ruano, I., Mazo, A., and Pastor-Anglada, M. (2013). Concentrative nucleoside transporter 1 (hCNT1) promotes phenotypic changes relevant to tumor biology in a translocation-independent manner. *Cell Death Dis.* 4:e648. doi: 10.1038/cddis.2013.173

Planté-Bordeneuve, V., and Said, G. (2011). Familial amyloid polyneuropathy. *Lancet Neurol.* 10, 1086–1097. doi: 10.1016/S1474-4422(11)70246-0

Reimand, J., Isserlin, R., Voisin, V., Kucera, M., Tannus-Lopes, C., Rostamianfar, A., et al. (2019). Pathway enrichment analysis and visualization of omics data using g:Profiler, GSEA, cytoscape and enrichmentMap. *Nat. Protoc.* 14, 482–517. doi: 10.1038/s41596-018-0103-9

Richardson, F. C., and Kaczmarek, L. K. (2000). Modification of delayed rectifier potassium currents by the Kv9.1 potassium channel subunit. *Hear. Res.* 147, 21–30. doi: 10.1016/s0378-5955(00)00117-9

Roberts, D. S., Raol, Y. H., Bandyopadhyay, S., Lund, I. V., Budreck, E. C., Passini, M. A., et al. (2005). Egr3 stimulation of GABRA4 promoter activity as a mechanism for seizure-induced up-regulation of GABAA receptor 4 subunit expression. *Proc. Natl. Acad. Sci. U.S.A.* 102, 11894–11899. doi: 10.1073/pnas.0501434102

Robinson, M. D., McCarthy, D. J., and Smyth, G. K. (2010). EdgeR: a Bioconductor package for differential expression analysis of digital gene expression data. *Bioinformatics* 26, 139–140. doi: 10.1093/bioinformatics/btp616

Ross, K., and Coleman, J. (2000). Developmental and genetic audiogenic seizure models: behavior and biological substrates. *Neurosci. Biobehav. Rev.* 24, 639–653. doi: 10.1016/s0149-7634(00)00029-4

Saint Marie, R. L. (1996). Glutamatergic connections of the auditory midbrain: selective uptake and axonal transport of D-[3H]aspartate. *J. Comp. Neurol.* 373, 255–270. doi: 10.1002/(SICI)1096-9861(19960916)373:2<255::AID-CNE8>3.0.CO;2-2

Sánchez-Benito, D., Gómez-Nieto, R., Hernández-Noriega, S., Murashima, A. A. B., de Oliveira, J. A. C., Garcia-Cairasco, N., et al. (2017). Morphofunctional alterations in the olivocochlear efferent system of the genetic audiogenic seizure-prone hamster GASH:Sal. *Epilepsy Behav.* 71, 193–206. doi: 10.1016/j.yebeh.2016.05.040

Sánchez-Benito, D., Hyppolito, M. A., Alvarez-Morujo, A. J., López, D. E., and Gómez-Nieto, R. (2020). Morphological and molecular correlates of altered hearing sensitivity in the genetically audiogenic seizure-prone hamster GASH/Sal. *Hearing Res.* 392:107973. doi: 10.1016/j.heares.2020.107973

Scheffer, I. E., Berkovic, S., Capovilla, G., Connolly, M. B., French, J., Guilhoto, L., et al. (2017). ILAE classification of the epilepsies: position paper of the ILAE commission for classification and terminology. *Epilepsia* 58, 512–521. doi: 10.1111/epi.13709

Schmittgen, T. D., and Livak, K. J. (2008). Analyzing real-time PCR data by the comparative CT method. *Nat. Protoc.* 3, 1101–1108. doi: 10.1038/nprot.2008.73

Simler, S., Vergnes, M., and Marescaux, C. (1999). Spatial and temporal relationships between C-Fos expression and kindling of audiogenic seizures in Wistar rats. *Exp. Neurol.* 157, 106–119. doi: 10.1006/exnr.1999.7036

Soprano, D. R., Herbert, J., Soprano, K. J., Schon, E. A., and Goodman, D. S. (1985). Demonstration of transthyretin mRNA in the brain and other extrahepatic tissues in the rat. *J. Biol. Chem.* 260, 11793–11798.

Strehlow, V., Heyne, H. O., Vlaskamp, D. R. M., Marwick, K. F. M., Rudolf, G., de Bellescize, J., et al. (2019). GRIN2A -related disorders: genotype and functional consequence predict phenotype. *Brain* 142, 80–92. doi: 10.1093/brain/awy304

Suhr, O. B., Andersen, O., Aronsson, T., Jonasson, J., Kalimo, H., Lundahl, C., et al. (2009). Report of five rare or previously unknown amyloidogenic transthyretin mutations disclosed in Sweden. *Amyloid* 16, 208–214. doi: 10.3109/13506120903421587

Tachibana, M., and Kuriyama, K. (1974). No TiGamma-aminobutyric acid in the lower auditory brainstem of guinea pigstle. *Brain Res.* 69, 370–374.

Tchitchek, N., Safronetz, D., Rasmussen, A. L., Martens, C., Virtaneva, K., Porcella, S. F., et al. (2014). Sequencing, annotation and analysis of the Syrian hamster (*Mesocricetus auratus*) transcriptome. *PLoS One* 9:e112617. doi: 10.1371/journal.pone.0112617

Thiffault, I., Speca, D. J., Austin, D. C., Cobb, M. M., Eum, K. S., Safina, N. P., et al. (2015). A novel epileptic encephalopathy mutation in KCNB1 disrupts Kv2.1 ion selectivity, expression, and localization. *J. Gen. Physiol.* 146, 399–410. doi: 10.1085/jgp.201511444

Tomiyama, H., Hutson, J. M., Truong, A., and Agoulnik, A. I. (2003). Transabdominal testicular descent is disrupted in mice with deletion of insulin like factor 3 receptor. *J. Pediatr. Surg.* 38, 1793–1798. doi: 10.1016/j.jpedsurg.2003.08.047

Vaudry, D. (2002). Signaling pathways for PC12 cell differentiation: making the right connections. *Science* 296, 1648–1649. doi: 10.1126/science.1071552

Wada, J. A., Terao, A., White, B., and Jung, E. (1970). Inferior colliculus lesion and audiogenic seizure susceptibility. *Exp. Neurol.* 28, 326–332. doi: 10.1016/0014-4886(70)90240-2

Wagner, T. (1996). Lemniscal input to identified neurons of the central nucleus of mouse inferior colliculus: an intracellular brain slice study. *Eur. J. Neurosci.* 8, 1231–1239. doi: 10.1111/j.1460-9568.1996.tb01291.x

Walport, M. J. (2001). Complement. First of two parts. *N. Engl. J. Med.* 344, 1058–1066. doi: 10.1056/NEJM200104053441406

Wang, C., and Buolamwini, J. K. (2019). A novel RNA variant of human concentrative nucleoside transporter 1 (hCNT1) that is a potential cancer biomarker. *Exp. Hematol. Oncol.* 8:18. doi: 10.1186/s40164-019-0144-y

Wang, Z., Fan, Y., Xu, J., Li, L., Heng, D., Han, S., et al. (2014). Transcriptome analysis of the hippocampus in novel rat model of febrile seizures. *PLoS One* 9:e95237. doi: 10.1371/journal.pone.0095237.g001

Wang, Z., Gerstein, M., and Snyder, M. (2009). RNA-Seq: a revolutionary tool for transcriptomics. *Nat. Rev. Genet.* 10, 57–63. doi: 10.1038/nrg2484

Winden, K. D., Karsten, S. L., Bragin, A., Kudo, L. C., Gehman, L., Ruidera, J., et al. (2011). A systems level, functional genomics analysis of chronic epilepsy. *PLoS One* 6:e20763. doi: 10.1371/journal.pone.0020763

Wu, S. H. (2005). "Biophysical properties of inferior colliculus neurons," in *The Inferior Colliculus*, eds J. A. Winer, and C. E. Schreiner (New York, NY: Springer).

Ye, L., Allen, W. E., Thompson, K. R., Tian, Q., Hsueh, B., Ramakrishnan, C., et al. (2016). Wiring and molecular features of prefrontal ensembles representing distinct experiences. *Cell* 165, 1776–1788. doi: 10.1016/j.cell.2016.05.010

Yechikhov, S., Morenkov, E., Chulanova, T., Godukhin, O., and Shchipakina, T. (2001). Involvement of cAMP- and Ca2+/calmodulin-dependent neuronal protein phosphorylation in mechanisms underlying genetic predisposition to audiogenic seizures in rats. *Epilepsy Res.* 46, 15–25. doi: 10.1016/s0920-1211(01)00255-8

Conflict of Interest: The authors declare that the research was conducted in the absence of any commercial or financial relationships that could be construed as a potential conflict of interest.

frontiers | Frontiers in Molecular Neuroscience

TYPE Original Research
PUBLISHED 05 January 2024
DOI 10.3389/fnmol.2023.1322750

OPEN ACCESS

EDITED BY
Maria Eulalia Rubio,
University of Pittsburgh, United States

REVIEWED BY
Argel Estrada-Mondragon,
Linköping University, Sweden
Ping Dong,
Duke University, United States
Ciria Hernandez,
University of Michigan, United States

*CORRESPONDENCE
Ricardo Gómez-Nieto
✉ richard@usal.es

RECEIVED 16 October 2023
ACCEPTED 07 December 2023
PUBLISHED 05 January 2024

CITATION
Díaz-Rodríguez SM, Herrero-Turrión MJ, García-Peral C and Gómez-Nieto R (2024) Delving into the significance of the His289Tyr single-nucleotide polymorphism in the glutamate ionotropic receptor kainate-1 (*Grik1*) gene of a genetically audiogenic seizure model. *Front. Mol. Neurosci.* 16:1322750. doi: 10.3389/fnmol.2023.1322750

Delving into the significance of the His289Tyr single-nucleotide polymorphism in the glutamate ionotropic receptor kainate-1 (*Grik1*) gene of a genetically audiogenic seizure model

Sandra M. Díaz-Rodríguez[1,2,3], M. Javier Herrero-Turrión[1,2,4], Carlos García-Peral[1,2] and Ricardo Gómez-Nieto[1,2,3]*

[1]Institute of Neuroscience of Castilla y León (INCYL), University of Salamanca, Salamanca, Spain, [2]Institute for Biomedical Research of Salamanca (IBSAL), Salamanca, Spain, [3]Department of Cell Biology and Pathology, Faculty of Medicine, University of Salamanca, Salamanca, Spain, [4]Neurological Tissue Bank INCYL (BTN-INCYL), Salamanca, Spain

Genetic abnormalities affecting glutamate receptors are central to excitatory overload-driven neuronal mechanisms that culminate in seizures, making them pivotal targets in epilepsy research. Increasingly used to advance this field, the genetically audiogenic seizure hamster from Salamanca (GASH/Sal) exhibits generalized seizures triggered by high-intensity acoustic stimulation and harbors significant genetic variants recently identified through whole-exome sequencing. Here, we addressed the influence of the missense single-nucleotide polymorphism (C9586732T, p.His289Tyr) in the glutamate receptor ionotropic kainate-1 (*Grik1*) gene and its implications for the GASH/Sal seizure susceptibility. Using a protein 3D structure prediction, we showed a potential effect of this sequence variation, located in the amino-terminal domain, on the stability and/or conformation of the kainate receptor subunit-1 protein (GluK1). We further employed a multi-technique approach, encompassing gene expression analysis (RT-qPCR), Western blotting, and immunohistochemistry in bright-field and confocal fluorescence microscopy, to investigate critical seizure-associated brain regions in GASH/Sal animals under seizure-free conditions compared to matched wild-type controls. We detected disruptions in the transcriptional profile of the *Grik1* gene within the audiogenic seizure-associated neuronal network. Alterations in GluK1 protein levels were also observed in various brain structures, accompanied by an unexpected lower molecular weight band in the inferior and superior colliculi. This correlated with substantial disparities in GluK1-immunolabeling distribution across multiple brain regions, including the cerebellum, hippocampus, subdivisions of the inferior and superior colliculi, and the prefrontal cortex. Notably, the diffuse immunolabeling accumulated within perikarya, axonal fibers and terminals, exhibiting a prominent concentration in proximity to the cell nucleus. This suggests potential disturbances in the GluK1-trafficking mechanism, which could subsequently affect glutamate synaptic transmission. Overall, our study sheds light on the genetic underpinnings of seizures and underscores the importance of investigating the molecular mechanisms behind synaptic dysfunction in epileptic neural networks, laying

a crucial foundation for future research and therapeutic strategies targeting GluK1-containing kainate receptors.

KEYWORDS

animal models of epilepsy, GASH/Sal, GluK1, glutamatergic system, kainate receptor, neurotransmission, seizure susceptibility, synaptic dysfunction

1 Introduction

Normal brain functioning requires a complex molecular interplay to mediate the proper neuronal signaling between many distinct structures. This implies an orchestrated regulation and interaction of multiple intracellular signaling and gene expression pathways that dictate the overall neuronal responses. However, the normal neuronal signaling becomes aberrant in epilepsy that is characterized by elevated neuronal hyperactivity, enhanced synchrony, and altered neurotransmitter balance in restricted regions of the brain that might eventually spread throughout many other areas. Switch in molecular and cellular mechanisms leads to ictogenesis and epileptogenesis in those brain regions to finally drive a myriad of epilepsy symptoms, including seizures as the most notable behavioral manifestation of such neuronal network overactivity (Fisher et al., 2005; Pitkänen and Engel, 2014). The relationship between the glutamatergic system and epilepsy has stimulated broad public concern, and hence studies focusing on the role of glutamate receptors in epilepsy as well as the contribution of animal models to the understanding of epileptogenesis are of the greatest interest (reviewed in Wang et al., 2022). Glutamate, the predominant excitatory neurotransmitter in the mammalian central nervous system, acts on a variety of receptor proteins that are classified in NMDA (*N*-methyl-D-aspartate), AMPA (α-amino-3-hydroxyl-5-methyl-4-isoxazole-propionate), and kainate receptors based on the agonist that activates them (reviewed in Meldrum, 2000). AMPA and NMDA receptors serve as primary mediators of excitatory neurotransmission in the brain (Traynelis et al., 2010), playing a crucial role in both the initiation and spread of seizures (reviewed in Casillas-Espinosa et al., 2012). Kainate receptors are formed by tetrameric combinations of several subunits, namely GluK1, GluK2, GluK3, GluK4, and GluK5, formerly referred to as GluR5, GluR6, GluR7, KA1, and KA2, respectively. Of these, GluK1-3 may form functional homomeric or heteromeric receptors that included many and varied structural isoforms arising from the alternative splicing of the corresponding pre-mRNAs (Pinheiro and Mulle, 2006; Lerma and Marques, 2013). Kainate receptors are widely distributed pre- and postsynaptically on different cell types in the brain, taking part in the control of synaptic networking, regulation of neurotransmitter release, modulation of both excitatory and inhibitory transmission, and in enhancement of neuronal excitability (Contractor et al., 2011). There is clear evidence to strongly support that kainate receptors might be involved in the excitatory to inhibitory imbalances linked to epilepsy (reviewed in Lerma and Marques, 2013). Indeed, kainate is widely used in rodents to induce acute brain seizures and, after repetitive kainic injections, as a chronic model of temporal lobe epilepsy (reviewed in Ben-Ari, 2012). The proconvulsant actions of kainic acid are largely mediated by the activation of kainate receptors, in which their subunit composition and their possible action mechanisms has been widely studied and hotly debated (reviewed in Falcón-Moya et al., 2018). Thus, several studies suggested that the glutamate ionotropic receptor kainate type subunit 1 (GluK1) has a principal role in the activation of kainate receptors that favor the imbalance between excitation and inhibition in kainate-induced seizures (Rodríguez-Moreno et al., 1997; Fritsch et al., 2014; Falcón-Moya et al., 2018). Some studies suggest that kainate receptors containing the GluK1 subunit represent promising candidates for seizure prevention (Khalilov et al., 2002; Smolders et al., 2002; Rogawski et al., 2003), while others failed to confirm the pharmacological inhibition of GluK1-kainate receptors as an epilepsy treatment strategy (Fritsch et al., 2014). The uncontested fact is that bench to bedside ventures in epilepsy research cannot be accomplished without the contribution of preclinical animal models of seizures and epilepsy syndromes. Besides the experimental models induced by chemical means (e.g., the aforementioned model of kainate-induced seizures), the genetically audiogenic seizures models offers the following advantages: (1) The seizure susceptibility is inherited and there are no need of using exogenous chemicals or any experimental procedure to become susceptible, avoiding thus incompatibilities with experimental designs; (2) Seizures are induced on demand by the investigator when the animal is exposed to intense acoustic stimulation; (3) The overwhelming detailed information at the molecular, cellular and behavioral levels available for the research community that makes genetically audiogenic seizures models ideal to elucidate mechanisms and neuronal substrates underlying the seizure genesis and propagation (Ross and Coleman, 2000; Kandratavicius et al., 2014). Among the variety of genetically seizure-prone strains of rodents, the only scientifically available hamster that exhibits seizure susceptibility to sound is the genetic audiogenic seizure hamster from Salamanca (GASH/Sal) that presents an autosomal recessive inheritance pattern (Muñoz et al., 2017). In the GASH/Sal strain, high-intensity acoustic stimulation causes generalized tonic-clonic seizures that can be reduced or eliminated after administration of anticonvulsant compounds (Barrera-Bailón et al., 2013, 2017; Werner and Coveñas, 2017; Cabral-Pereira et al., 2021). There is currently a wide range of comprehensive knowledge regarding the neuroethological (Barrera-Bailón et al., 2013, 2017), electrophysiological (Carballosa-Gonzalez et al., 2013), neurochemical (Prieto-Martín et al., 2017;

Fuerte-Hortigón et al., 2021), molecular (López-López et al., 2017; Díaz-Casado et al., 2020; Díaz-Rodríguez et al., 2020; Bonet-Fernández et al., 2023) and morphological (Sánchez-Benito et al., 2017, 2020) features underlying the audiogenic seizures in the GASH/Sal model. At the molecular genetic level, a study using whole-exome sequencing in GASH/Sal and wild-type hamsters identified 3 high-impact and 15 moderate-impact genetic variants (Díaz-Casado et al., 2020). Among these missense single-nucleotide variants, it is noteworthy the substitution of C by T at position 9586732 of the *Grik1* gene that encodes the GluK1 protein, in which the His residue at position 289 is replaced for a Tyr (p.H289Y) (Díaz-Casado et al., 2020). This finding is extremely interesting since genetic variants of *Grik1* has been linked to epilepsy genetic risk in humans (Genome-wide association studies by the International League Against Epilepsy Consortium on Complex Epilepsies, 2018). Thus, *Grik1* polymorphisms confers susceptibility to juvenile absence epilepsy (Sander et al., 1997), and variations in the non-coding region of this gene, near regulatory sequences, could alter gene expression without affecting receptor structure (Izzi et al., 2002). Here, we explore for the first time the effects of the missense single-nucleotide polymorphism (C9586732T, p.His289Tyr) in the *Grik1* gene of the GASH/Sal model using an *in silico* 3D modeling protein structure. The brain structures that contribute to the seizure susceptibility, genesis, and propagation as well as those nuclei that might be recruited after repeated acoustic stimulation has been widely studied, coming out very similar among the different audiogenic seizure models (summarized in **Figure 1**). Activation of auditory pathways are required for the onset and progression of seizures in all audiogenic seizure models, and many studies pointed out that glutamate and glutamate receptors in the inferior colliculus (IC), a critical integration center in the auditory midbrain pathway, are essential to initiate, audiogenic seizures (Faingold, 2012; Faingold et al., 1992; Ross and Coleman, 2000; Garcia-Cairasco, 2002). In the GASH/Sal, the alterations at the morphological and molecular connectome level of the primary acoustic pathway form part of the GASH/Sal seizure-prone neural network that includes aberrant glutamatergic neurotransmission in the flow of sound processing from the inner ear to the cochlear nucleus to the IC (Sánchez-Benito et al., 2017, 2020). As a result, the IC is embedded in a web of pathologic connections that spread aberrant neuronal activity through multiple brain areas to finally drive the tonic-clonic convulsions (Sánchez-Benito et al., 2020). Despite these substantial advances to elucidate the glutamatergic system in genetic audiogenic seizure models (Ross and Coleman, 2000), the role of kainate receptors in the audiogenic seizure network is still waiting to be determined. As a novelty in the present article, we studied the *Grik1* gene expression as well as the protein levels of GluK1 in the GASH/Sal seizure network (**Figure 1**), using consolidated methodologies and tools available for the characterization of audiogenic seizures models (Bosque et al., 2021). The absence of specific antibodies against different kainate receptor subunits has limited the study of the receptor distribution in brain for a long time, however, new antisera are now available, and it is known that GluK1 is present in hippocampal and cortical interneurons (Lerma and Marques, 2013). The distribution of GluK1 in the audiogenic seizure network of genetic seizure-prone rodent models remains unknow and it has never been explored in the GASH/Sal strain. In the present study, we further conducted immunohistochemical analysis at bright-field and confocal scanning microscopy to examine the distribution of GluK1 in critical brain structures involved in the seizure neuronal network of the GASH/Sal (**Figure 1**). Since the outcomes of these experiments were based on the comparisons with age-matched wild-type Syrian hamsters, our study also provides valuable information of the GluK1 protein distribution in the brain of the *Mesocricetus auratus*. The overall goal of this study was to shed light on the effects of genetic alterations in a model organism with inherited propensity for developing seizures as well as delve into the knowledge of kainate receptors in the seizure-associated neural networks.

2 Materials and methods

2.1 *In silico* based protein 3D structure analysis and modeling

An *in silico* approach was used to analyze the impact of a missense single-nucleotide polymorphism in the *Grik1* gene of the GASH/Sal model. This computational method involved the utilization of diverse bioinformatics software tools for a comprehensive analysis of genetic variations within the context of protein 3D structures. Using the AlphaFold2 deep learning-based protein structure prediction system (Jumper et al., 2021), we investigated the impact of the specific gene variant p.H289Y on the structure of the GluK1 protein in *M. auratus* (sequence XP_005073900), while exploring various aspects of protein structure and organization. AlphaFold2 uses a two-step process to predict protein structures: it trains a deep learning model on known protein structures to predict amino acid distances, and then employs a second network to generate 3D coordinates for the atoms based on these distances, resulting in a predicted 3D structure (Jumper et al., 2021). Furthermore, interatomic interactions in the wild-type and mutated residues (p.H289Y) of the GluK1 subunit were calculated using the web server Arpeggio (Jubb et al., 2017), and their lengths were determined using the molecular viewer PyMOL (The PyMOL Molecular Graphics System, Version 1.8 Schrödinger, LLC). 3D images, depicting various views of the modeled protein structures, were generated using the PyMOL system. Additionally, we employed the Cortona Movie Maker software (Cortona; Parallel Graphics, Boston, MA, USA) to create video recordings at a resolution of 1024 × 768 pixels using the VRLM files of the corresponding 3D renderings. To assess the effect of the missense mutation on the thermodynamic stability of the protein ($\Delta\Delta G^{Stability}$), several protein stability predictors were employed: Dynamut2, INPS3D, FoldX, and MAESTRO. These computational stability predictors functioned as web interfaces that evaluated changes in protein folding or interaction energies due to mutations (expressed as $\Delta\Delta G$, representing the change in Gibbs free energy). DynaMut2 incorporated dynamics into the mutation analysis, enabling a precise evaluation of the mutation's impact on protein stability (Rodrigues et al., 2021). INSP3D considered sequence and physicochemical properties, as well as structure-derived features such as solvent accessibility and local energy differences (Savojardo et al., 2016). FoldX utilized an empirical force field to rapidly assess the effects of mutations on

10.3389/fnmol.2023.1322750

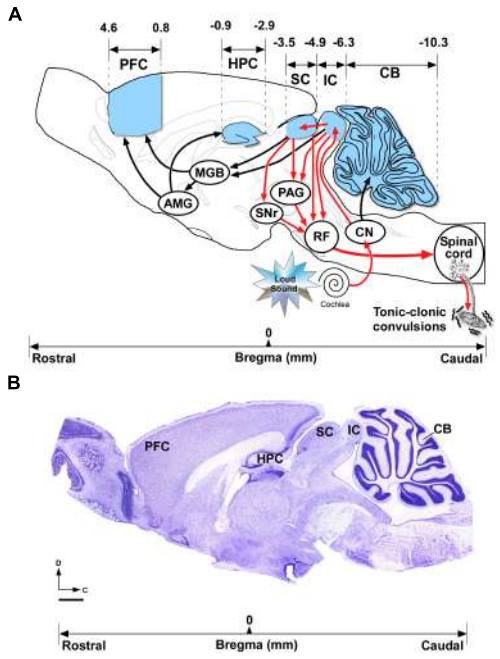

FIGURE 1
Brain areas included in the gene expression, immunoblotting and immunohistochemical analyses. **(A)** Overview of the brain structures that might be involved in the neuronal network associated with acute and chronic audiogenic seizures in genetically models of audiogenic seizures. The seizure-prone neuronal network (depicted with red arrows) involves alterations of bottom-up auditory inputs from the cochlea receptor, throughout the brainstem auditory pathway (cochlear nucleus) to the inferior colliculus (IC) (Faingold et al., 1992; Ribak and Morin, 1995; Sánchez-Benito et al., 2020). The aberrant neuronal activity in the IC initiates the audiogenic seizure that spreads throughout multiple projections targeting the superior colliculus to the substantia nigra, the periaqueductal gray, and the brainstem reticular formation, which in turn projects to the spinal cord, ultimately mediating the tonic-clonic convulsions (Garcia-Cairasco, 2002). During frequent repetitive audiogenic seizures, the seizure network might extend toward other brain regions (projections depicted with black arrows) such as the medial geniculate body, the amygdala, hippocampus, and prefrontal cortex (Faingold, 2012). The cerebellum that receives auditory inputs might be involved in the audiogenic seizure network (Mennink et al., 2020; Streng and Krook-Magnuson, 2021). The brain regions depicted in blue were selected for gene expression, immunoblotting and immunohistochemical analyses in the GASH/Sal model. **(B)** Representative Nissl-stained section of the sagittal section of the hamster brain, in which the sketch shown in **(A)** was based, shows the brain areas included in the present study. Bregma reference coordinates (in mm) were used for selection of those brain regions. Scale bar = 1 mm. AMG, amygdala; MGB, medial geniculate body; CB, cerebellum; CN, cochlear nucleus; PAG, periaqueductal gray; IC, inferior colliculus; HPC, hippocampus; PFC, prefrontal cortex; RF; reticular formation; SC, superior colliculus; SNr, substantia nigra (Image shown in (**B**) was adapted from the hamster brain atlas of Morin and Wood (2001), and the corresponding bregma data was obtained from the same source).

the stability, folding, and dynamics of proteins and nucleic acids (Schymkowitz et al., 2005). Lastly, MAESTRO employed statistical scoring functions and various machine learning approaches to generate multi-agent predictions (Laimer et al., 2016). For the Dynamut2 and INPS3D predictors, the mutation was considered stabilizing if the $\Delta\Delta G$ value was greater than 0 and destabilizing if it was less than 0, whereas for the FoldX and MAESTRO predictors, the mutation was considered stabilizing if the $\Delta\Delta G$ value was less than 0 and destabilizing if it was greater than 0.

2.2 Animal experiments and ethical statement

A total of 16 Syrian golden hamsters (*M. auratus*) were used in this study, specifically 8 wild-type hamsters (RjHan:AURA) from Janvier Labs (Le Genest-Saint-Isle, France) and 8 GASH/Sal animals from the inbred strain maintained at the vivarium of the University of Salamanca (USAL, Spain). The experimental design of the current study was based on comparisons with wild-type hamsters that were used as a control group. All control and GASH/Sal animals matched age (4 months old), gender (male), housing, handling, and care, in order that these variables can be ruled out as alternative explanations of any observed differences. The age of 4 months was selected as it was previously reported that the GASH/Sal strain exhibits the maximum susceptibility to seizures from 2 to 4 months of age (Muñoz et al., 2017). All GASH/Sal animals were naïve to sound-induced seizures, and hence, were not receiving any high-intensity sound stimulation to trigger audiogenic seizures. All procedures and experimental protocols were performed in accordance with the guidelines of the European Communities Council Directive (2010/63/UE) for the care and use of laboratory animals and approved by the Bioethics Committee of the University of Salamanca (approval number 375). All efforts were made to minimize the number of animals and their suffering. The animals were maintained in Eurostandard Type III cages (Tecniplast, Italy), with Lignocel bedding (Rettenmaier Iberica), 14/10 light/dark cycle, 22–24°C room temperature (RT) with *ad libitum* access to food (Tecklad Global 2918 irradiated diet) and water. Communities of 2–3 animals were housed in groups until the beginning of the study. A total of 10 animals (5 controls and 5 GASH/Sal) were processed for gene expression analysis of *Grik1* as well as immunoblotting to compare the levels of the corresponding encoded protein GluK1. The brain tissue from these 10 animals was obtained by inducing general anesthesia using 4% isoflurane (Forane, Abbott, IL, USA) vaporized in 100% oxygen at a flow rate of 1 L/min, followed by rapid decapitation for euthanasia. Subsequently, their brains were rapidly removed, hemisected, and frozen until use in downstream analysis (half of the brain for mRNA expression analysis and the other half for immunoblotting). In separate set of experiments, 6 animals (3 controls and 3 GASH/Sal) were processed for immunohistochemistry to determine the distribution of GluK1 in the brain tissue, following the procedure outlined below. In all animal experiments, the target study area included the following specific brain regions: cerebellum, inferior and superior colliculi, hippocampus, and prefrontal cortex (**Figure 1**). As indicated in the introduction, the selection of these specific brain areas was made based on their potential role in the seizure-associated neuronal network, in which the mRNA and protein expression patterns as well as the immunostaining may differ between wild-type and GASH/Sal animals. In each set of experiments, tissue samples were obtained and processed in parallel for both animal groups as previously done by our research team (Gómez-Nieto et al., 2014a; Sánchez-Benito et al., 2017, 2020). Hence, the disparities observed

were unrelated to the passage of time or any other experimental variables, including incubation periods, temperature, or sample manipulations.

2.3 Real-time quantitative reverse transcription PCR (RT-qPCR)

Total RNA was sequentially extracted using 30–70 mg of brain tissue and purified using a commercial kit (ReliaPrep™ RNA Tissue Miniprep, Z6112). The RNA was quantified, and its quality assessed by using an Agilent 2100 Bioanalyzer. Only samples with an RNA integrity number (RIN) >8.0 were used. The quantitative reverse transcription real-time polymerase chain reaction (RT-qPCR) procedure was carried out following the protocol routinely used by our research group (Díaz-Rodríguez et al., 2020; Sánchez-Benito et al., 2020; Cabral-Pereira et al., 2021). Briefly, complementary DNA (cDNA) was synthesized using messenger RNA (mRNA) contained in purified RNAs via a retrotranscription enzymatic reaction using the kit ImProm-II™ Reverse Transcription System (Promega). Total RNA (2 μg) was mixed with oligo-dT and random hexamer primers for reverse-transcription into cDNA at 37°C for 2 h into a 20 μL volume and stored at −20°C of temperature until use. In all cases, a reverse transcriptase negative control was used to test genomic DNA contamination. Subsequently, qPCR was conducted using the SYBR Green method with a 2 × Master Mix (#4367659, Applied Biosystems) as previously described (Herrero-Turrión et al., 2014). In brief, each reaction consisted of 10 μL of Master Mix, 0.4 μL of each primer (**Table 1**), 3 μL of the respective cDNA sample (ranging from 10 to 100 ng depending on the primer pair), in a different serial cDNA quantity for each gene, and MilliQ water (RNA-free) to reach a final volume of 20 μL. The amplification reaction was performed in the QuantStudio™ 7 Flex Real-Time PCR System (Applied Biosystems) under the following conditions: 10 min at 95°C followed by 40 cycles of 15 s at 95°C, and 30 s at 60°C depending on each pair of primers. RT-qPCR experiments were performed in replicates of 5 samples and conducted in triplicate. The comparative cycle threshold (Ct) method was used for presenting quantitative data (Schmittgen and Livak, 2008). Following removal of outliers (Burns et al., 2005), raw fluorescence data were used to determine PCR amplification efficiency (E) according to the equation $E = [10^{[-1/slope]} - 1] \times 100$. All amplifications had an *E*-value of 100 ± 10%, with an *E*-value close to 100% serving as an indicator of effective amplification. Before quantification of amplified DNA samples, E analysis for each primer (specific for each targeted gene) was performed (**Table 1**). These analyses allowed us to establish the expression dynamic range for each primer. To decide the most stable reference gene for RT-qPCR data normalization, two candidates [β-actin (*Actb*) and tubulin (*Tbp*)] were selected and their expression was measured by NormFinder software (Andersen et al., 2004) that calculates intra- and intergroup variations in gene expression. Our study identified *Actb* as the most suitable reference gene, and hence, the mean Ct value and primer *E*-value of *Actb* were used for data normalization. The relative gene expression value of each transcript was calculated following the comparative $2^{-\Delta\Delta Ct}$ method as used previously (Damasceno et al., 2020; Sánchez-Benito et al., 2020). Finally, a negative template-free (water) control reaction was used in all RT-qPCRs and the control group was used as the calibration sample.

2.4 Primary antibody against GluK1

In this study, we used immunoblotting to assess GluK1 protein levels and immunohistochemistry to visualize its distribution. The polyclonal anti-GluK1 antibody (catalog No. ab118891; Abcam) was generated in rabbits against a synthetic peptide corresponding to the central region of the human GluK1 within 380–430 amino acids, and the reactivity was validated in human and rat, showing the highest tissue specificity in the cerebellum. In Western blot analysis, the anti-GluK1 antibody recognizes a single band migrating at approximately 104 kDa (as per the manufacturer's technical information). In this study, we adhered to the manufacturer's guidelines and utilized this primary antibody for both Western blotting and immunocytochemistry. This primary antibody has been utilized successfully in prior immunohistochemical studies conducted by our research group (Díaz-Rodríguez et al., 2023) and by others (Perez-Ortiz et al., 2017). Nevertheless, as per the manufacturer's data sheets, hamster brain tissue reactivity remains untested. To tackle this concern, as illustrated in **Supplementary material 1**, we initiated a multi-sequence alignment analysis aimed at assessing the variability or conservation of epitopes in hamsters. For this, we retrieved the GluK1 protein sequence from the *Grik1* gene in the NCBI protein database[1] and conducted the analysis using the Jalview program (version 2.11.2)[2] (Troshin et al., 2011). The multiple sequence alignment showed that the antigenic region is highly conserved for all isoforms in the hamster, thereby indicating the suitability of employing the previously

1 http://www.ncbi.nlm.nih.gov/protein/

2 http://www.jalview.org/

TABLE 1 List of oligonucleotide primers used for RT-qPCRs.

Gene target	ID transcript Ensembl *Mesocricetus auratus* [a]	Primer forward	Primer reverse	Size of products (bp)	E[b] (%)
Grik1	*ENSMAUG00000000865*	TGTTCGCTTTAGATCTGGAACTC	TCATGCCATCAAGAAGACCA	165	93
Actb	*ENSMAUG00000008763*	AGCCATGTACGTAGCCATCC	ACCCTCATAGATGGGCACAG	105	97
Tbp	*ENSMAUG00000019343*	TGTATCCACGGTGAATCTTGG	GAAAATCAGCGCAGTTGTCC	139	95

"[a]"Indicates the identifier (ID) of each gene in the corresponding Ensembl sequences of the Syrian hamster (*M. auratus*). "[b]"Indicates percentage of qPCR primer efficiency (E).

mentioned Gluk1 antibody in the current study (**Supplementary material 1**).

2.5 Western blotting

Brain tissues containing each of the specific brain areas shown in **Figure 1**, with a weight between 30 and 75 mg, were collected from wild-type and GASH/Sal animals. Total protein extraction and isolation were carried out following homogenization of tissue samples in radioimmunoprecipitation assay (RIPA) buffer (catalog No. 9806S, Cell Signaling Technology) that contained a mixture of protease inhibitors (catalog No. 78442, Thermo Fisher Scientific Inc). Homogenates were centrifuged at ∼14,000 × *g* for 15 min to remove insoluble material. Protein concentration was determined using the Bio-Rad DC protein assay kit (catalog No. 500-0116, BIO-RAD). Next, the protein extracts were mixed with 10x NuPAGE™ Sample Reducing Agent (catalog No. NP0004, Thermo Fisher Scientific Inc) and 4x NuPAGE™ LDS Sample Buffer (catalog No. NP0007, Thermo Fisher Scientific Inc), and then boiled at 75°C for 10 min as indicated by the manufacturer's instructions. Equal amounts of protein (30 μg) were loaded into each lane of a Bolt 10% Bis-Tris gels (catalog No. NW00100BOX, Thermo Fisher Scientific Inc) and electrophoretically separated at RT using 90 V for 35 min and subsequently 200 V for 30 min with the PowerPac™ Basic power supply (catalog No. 1645050, BIO-RAD). The separated proteins were transferred to nitrocellulose membranes using the dry immunoblotting iBlot™ 2 system for approximately 7–8 min at 20–25 V (Invitrogen/Thermo Fisher Scientific Inc). To prevent non-specific antibody binding, all membrane blots were blocked for 1 h at RT with Tris-buffered saline/Tween (TBS-T), containing 5% bovine serum albumin (BSA, catalog No. A2153-100G, Sigma Aldrich). The membranes were subsequently incubated with the rabbit polyclonal anti-GluK1 antibody (10 ug/ml) overnight for 72 h at 4°C. Then, the membranes blots were washed with TBS-T and incubated with the horseradish peroxidase-conjugated secondary antibody (goat anti-rabbit antibody, catalog No. 7074S, Cell signaling technology) at a dilution of 1:250 for 2 h at RT. The membranes were stained with SuperSignal West Pico Chemiluminescent Substrate (catalog No. 34580, Thermo Fisher Scientific Inc) and detection was performed by an enhanced chemiluminescent method which combines the MicroChemi Unit and GelCapture image acquisition software. After image capturing, β-actin protein was used as internal loading control for comparative Western blot analysis of protein signals in the samples. To analyze protein loading, the membranes were washed extensively with TBS-T before treating with Restore™ Western Blot Stripping Buffer (catalog No. 21059, Thermo Fisher Scientific Inc) for 15 min at RT. Next, the membranes were re-blocked with a 5% BSA solution in TBS-T for 1 h at RT before being incubated with a 1:10,000 diluted rabbit anti-β-actin antibody (catalog No. 4967s, Cell Signaling Technology) for 1 h at RT, and this was followed by the application of horseradish peroxidase-conjugated anti-rabbit secondary antibodies (as previously mentioned). The membranes were then treated with chemiluminescent substrate and imaged as described above. Densitometric intensities of the digitalized membranes were measured and analyzed using the ImageJ software (WS, 1997). Band densities were normalized to the corresponding loading control densities and expressed as arbitrary density units.

2.6 Immunohistochemistry for bright-field and confocal scanning microscopy

Brain tissue employed for immunohistochemical analysis at bright-field and confocal scanning microscopy was collected and prepared following the established procedures described in our previous reports (Sánchez-Benito et al., 2017, 2020; Fuerte-Hortigón et al., 2021). Following the administration of a lethal dose of sodium pentobarbital (60 mg/kg) and subsequent perfusion through the heart with 4% paraformaldehyde in 0.1 M phosphate-buffered saline (PBS), the brains were removed from the skull. They were then cryoprotected through immersion in a 30% sucrose solution and coronal sections were sliced at a thickness of 40 μm using a freezing sliding microtome. Promptly, the serial sections were collected in 0.1 M PBS and organized into a set of 6. Sample labeling and visualization of the GluK1 protein were carried out following the steps of the immunohistochemistry method previously used by our research group (Gómez-Nieto et al., 2008a,b). Washes were made in Tris-buffered saline (TBS) pH 7.6 and dilutions of antisera in TBS pH 7.6 containing 0.2% Triton X-100 (catalog No. T9284; Sigma). All immunostaining steps were performed at RT (∼22°C), unless stated otherwise. For brightfield microscopy analysis, free-floating sections were blocked for 1 h with 6% normal goat serum (catalog No. S-1000, Vector Labs) and then incubated with the primary antibody, rabbit anti-GluK1 (dilution 1:1000) for 72 h at 4°C. Subsequently, sections were then washed and followed incubation with the goat anti-rabbit biotinylated secondary antibody (catalog No. BA-1000, Vector Laboratories) at 1:200 dilution for 2 h. After removal of secondary antisera, the visualization of epitope-antibody interactions was developed with the avidin-biotin-peroxidase complex procedure (catalog No. PK-4000, Vectastain, Vector Labs.), and diaminobenzidine histochemistry for peroxidase without heavy-metal intensification (DAB Kit, catalog No. SK-4100, Vector Labs.). All sections were mounted on slides, dehydrated and coverslipped with Entellan®Neu (catalog No. 107961, Merck). Histological sections containing the specified regions of interest were examined using a light microscope (Leitz DMRB, Leica Biosystem) equipped with a digital camera (DP50, Olympus). All microscope parameters and settings for digitizing the photomicrographs remained constant across both experimental groups and for each animal. Low-magnification images were taken with the 4x or 10x objective lens, and high magnification images were taken with a 40x or 100x objective lens (oil immersion). Morphometric measurements (diameter and area) of labeled structures were achieved analyzing high magnification images with the ImageJ software (version 1.53c) as described in our previous report (Gómez-Nieto et al., 2014b). For immunofluorescence analysis, non-specific binding sites were blocked for 1 h with 6% normal goat serum (catalog No. S-1000, Vector Labs) and then the sections followed incubation with a mixture of two primary antibodies, rabbit polyclonal anti-GluK1

(dilution 1:1000) and mouse monoclonal anti-NeuN (dilution 1:500, catalog No. MAB377, Millipore Sigma) for 72 h at 4°C. Thereafter, the sections were rinsed extensively and reacted for 2 h with the secondary antibodies using the VectaFluor™ Duet Immunofluorescence Double Labeling Kit [#DK-8818, DyLight® 488 Anti-Rabbit IgG (green)/DyLight® 594 Anti-Mouse IgG (red), Vector Labs]. Finally, sections were mounted on slides and coverslipped with VECTASHIELD® mounting medium for preserving fluorescence, containing the DAPI counterstain (4′,6-diamidino-2-phenylindole; catalog No. H-1200; Vector Labs.). The fluorescent DAPI dye, which labels the nuclear DNA of cells, and the NeuN-immunolabeling, which is specific to a nuclear protein expressed by nearly all neurons (with few exceptions like Purkinje Neurons as noted by Weyer and Schilling, 2003), were used to accurately delineate the cytoarchitecture of the brain nuclei. The sections processed for immunofluorescence were studied on a Leica Stellaris 8 confocal laser coupled to a Leica DMi8 inverted microscope, using the appropriate settings for detection of DyLight® 594 (red), DyLight® 488 (green) and DAPI fluorochromes. Representative images for illustration were collected as stacks with a z-step of 0.3 μm slices, using a 63x/NA1.4 oil-immersion objective lens and different digital zoom levels. The maximum intensity and stereo Z-projections of fluorescence confocal microscopy images (10–12 μm thickness) were used as methods of 3D visualization. We obtained images and animated-video documents from the 3D renderings using the image and movie editor in the Leica Application Suite X (LAS X software, version 4.2.0), and we completed the final composition of the videos using the Camtasia Studio software (version 8.3.0). In all immunohistochemical experiments, the absence of staining in the preparations was observed when the primary antibody was omitted. For visualization of the results, the stereotaxic atlas of the golden hamster brain (Morin and Wood, 2001) was used as an anatomical reference, in which histological sections were caudo-rostrally arranged. The photomicrographs were processed with minor modifications in contrast using Adobe Photoshop CS2 and the final composition of the figures was achieved with the Canvas 14 software.

2.7 Statistical analysis

Statistical analyses including relative values of gene expression and western blot-band intensities were performed using the SPSS-IBM software, version 20 (SPSS Inc., Chicago, IL, USA). For each statistical analysis, comparisons between control and GASH/Sal animals were performed with analysis of variance (*post-hoc* analysis with Fisher's test) and Student's *t*-test. The differences were considered statistically significant with a p-value < 0.05 (*), p-value < 0.01 (**) and p-value < 0.001 (***). All the quantitative data were presented as mean value ± standard error of the mean (SEM) and were plotted using GraphPad Prism (version 8). The GraphPad Prism software was further used to automatically create heatmaps, in which the squares were color coded according to the mean values of relative mRNA expression (RT-qPCR) or normalized densitometry (Western blot) for each brain structure, relative to the values obtained for the IC.

3 Results

3.1 Effect of the single-nucleotide polymorphism in the 3D protein structure

Our first approach to provide molecular insights into the potential consequences of the missense single-nucleotide polymorphism (C9586732T) in the *Grik1* gene of the GASH/Sal hamster was to generate a predicted 3D model of the corresponding protein structure. This single-nucleotide variant replaces in the amino acid sequence a histidine by a tyrosine at the codon 289 (p.H289Y, numbering according to the isoform X2; Uniprot A0A1U7QK31) in the GluK1 protein. The histidine residue at position 289 is in the amino-terminal domain (ATD) that together with the ligand binding domain form the extracellular moiety of the GluK1 protein (**Supplementary material 1**). To assess the potential impact of the p.H289Y polymorphism, we employed the protein structure prediction tool AlphaFold2, and subsequently analyzed the structural environment of the mutated residue. **Figure 2A** provides a visual representation of the ribbon structure, presenting the predicted monomeric form of the GluK1 receptor. Additionally, **Supplementary material 2**, which includes a video featuring dynamic rotations, offers a comprehensive and detailed visual depiction, highlighting the distinct domain organization of the receptor. Upon comparing the wild-type and mutated protein structures, we observed a consequential modification in the local environment of the regulatory region R2, located in the lower lobe of the ATD, which adopts a clamshell-like structure (**Figures 2B, C** and **Supplementary material 2**). Notably, our analysis revealed significant disparities between the wild-type and mutated structures, particularly in the emergence of new hydrophobic-proximal interactions and carbon-π interactions (atom ring interactions) in the mutated structure (**Figure 2D**; see video in **Supplementary material 2**). We further employed several computational stability predictors, including Dynamut2, INPS3D, FoldX, and MAESTRO, to assess the predicted change in fold stability ($\Delta\Delta G$ in kcal/mol). Our analysis consistently showed a favorable trend toward stabilization, as depicted in **Figure 2E**. Dynamut2 and INPS3D categorized $\Delta\Delta G$ values ≥ 0 as stabilizing, while FoldX and MAESTRO considered $\Delta\Delta G$ values ≤ 0 as indicative of stabilization. The specific predicted values for $\Delta\Delta G^{Stability}$ were as follows: 1.60 kcal/mol for Dynamut2, 0.36 kcal/mol for INPS3D, −0.43 kcal/mol for FoldX, and −0.26 kcal/mol for MAESTRO (**Figure 2E**). Notably, consistent results emerged across all stability predictors, indicating that the p.H289Y polymorphism presumably led to protein stabilization. Given the high percent identity (>97%, **Supplementary material 1D**) observed in the amino acid sequence of the GluK1 protein across various species such as mice, rats, and humans, it can be inferred that the presumed impact of this point mutation would be similar if it occurred in any of these species. Together, these results suggested that the single-point mutation p.H289Y leads to protein stabilization by increasing intermolecular interactions, as compared with the wild-type GluK1 receptor.

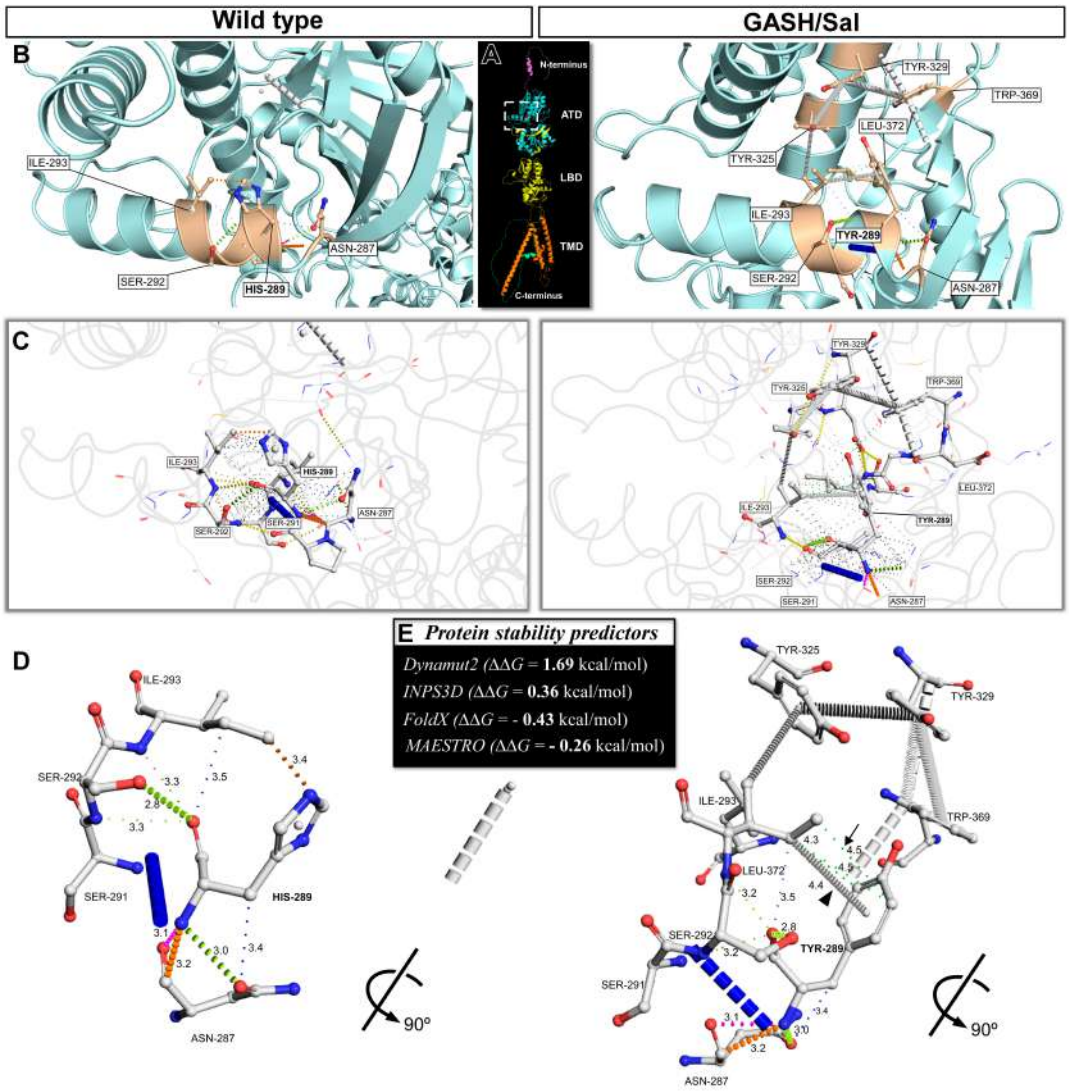

FIGURE 2
The missense single-nucleotide polymorphism p.H289Y provides new hydrophobic interactions that lead to improved GluK1 protein stability. **(A)** Ribbon representation of the predicted monomeric form of the GluK1 receptor illustrates its domain organization. These domains, namely the amino-terminal domain (ATD), ligand-binding domain (LBD), and transmembrane domain (TMD), are highlighted in different colors. **(B)** Close-up views corresponding to the white dashed box in **(A)** showcase the residual local environment in the ATD, in which the substitution of histidine-289 to tyrosine was found. The left panel shows the wild-type protein structure, and the right panel shows the mutated form in the *M. auratus* (structures predicted by AlphaFold). The highlighted residues with side-chain atoms shown with sticks are the mutated site and the neighboring residues. **(C)** Roving detail corresponding to the white dashed box in **(A)** features the molecular interactions between the mutated site and the neighboring residues. These interactions are represented by colored dashed lines, with thicker dashes indicating overlapping van der Waals' radii and the thinnest dashes representing "proximal" interactions beyond van der Waals' radius overlap but within 5 Å. **(D)** Protein backbone representations showcasing a 90° rotation of the 3D depictions shown in **(B,C)**. This 3D representation was simplified by hiding the undefined-proximal interactions to provide a clear visualization of the formation of new hydrophobic-proximal interactions (green dashed lines, arrow) and atom ring interactions (carbon–π, arrowhead) in the mutated structure, in comparison to the wild-type. The distances between atoms involved in each interaction are displayed in Å units. **(E)** Prediction of the change in fold stability (ΔΔG in kcal/mol) of the GluK1 protein due to the substitution of histidine-289 to tyrosine. ΔΔG values ≥0 were considered as stabilizing and ΔΔG values < 0 were destabilizing for Dynamut2 and INPS3D predictors, while ΔΔG values ≤0 were considered as stabilizing and ΔΔG values >0 were destabilizing for FoldX and MAESTRO predictors. Notice that all predictors consistently yielded stabilizing results.

3.2 Gene expression of *Grik1*

In a subsequent experimental approach, we quantified the transcriptional abundance of the *Grik1* gene in pivotal brain nuclei associated with the neuronal network involved in audiogenic seizures (Figure 3). Thus, brain tissue containing the specific brain areas shown in Figure 1 was freshly dissected from control and GASH/Sal animals. Quantitative gene expression data were normalized using *Actb* (β-actin) as internal reference gene. There were no significant differences in the number of cycles to reach the amplification threshold for *Actb* in both animal groups, indicating that the sample preparation was consistent. Raw gene expression data can be found in Supplementary material 3. Compared to controls, the mRNA expression levels of the

10.3389/fnmol.2023.1322750

Grik1 gene in the GASH/Sal was significantly higher in the cerebellum (p-value < 0.05; Figure 3A) as well as in the inferior and superior colliculi (p-value < 0.01 and p-value < 0.05, respectively; Figures 3B, C). On the other hand, comparison of gene expression/*Actb* ratios showed that expression of *Grik1* was significantly lower in the GASH/Sal hippocampus (p-value < 0.01; Figure 3D). In the prefrontal cortex, the gene expression of *Grik1* was not significantly different between control and GASH/Sal animals (Figure 3E). To determine the differences in relative transcript abundance between the structures of the seizure-associated neuronal network, we compared the results of the gene expression analysis in each structure with those obtained in the epileptogenic focus. The heatmap showed that the relative difference in mRNA expression levels of the *Grik1* gene was higher in the cerebellum and the superior colliculus, being this last the one with the highest increased differences as compared to the IC (Figure 3F). On the contrary, the brain structures exhibiting lower relative differences in mRNA expression levels than the IC were the prefrontal cortex, and in particular the hippocampus, that decreased notably over the epileptogenic focus (Figure 3F). In sum, these results indicated a disruption in the transcriptional profile of *Grik1* gene in the GASH/Sal model with differences in gene expression between the structures involved in the seizure neuronal network.

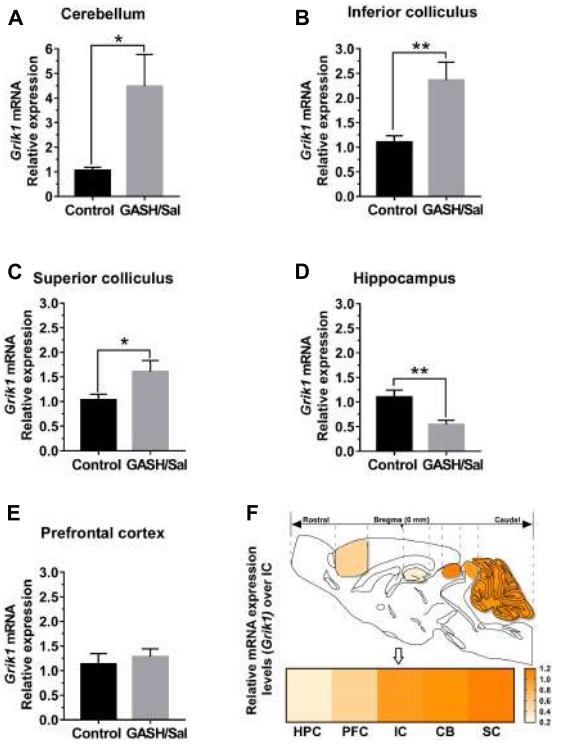

FIGURE 3
mRNA expression levels of *Grik1* gene within the seizure neural network of the GASH/Sal. Histograms show relative quantities of transcripts of the *Grik1* gene in the cerebellum [CB, **(A)**], the inferior colliculus [IC, **(B)**], the superior colliculus [SC **(C)**], the hippocampus [HPC, **(D)**], and the prefrontal cortex [PFC, **(E)**] of GASH/Sal animals. Notice that disruption of mRNA expression levels was found in the CB, the IC, the SC, and the HPC, whereas no differential gene expression was found in the PFC. Each bar in the histograms is an average ± S.E.M. Asterisks indicate statistical significance of gene expression in the brain regions of the GASH/Sal as compared to the control animals (*p-value < 0.05; **p-value < 0.01). **(F)** Sketch of the sagittal section of the GASH/Sal brain shows differences in relative transcript abundance between the structures of the seizure neuronal network. The color in the heat map represents the relative difference in mRNA expression levels of the *Grik1* gene between the control and GASH/Sal hamsters in each brain structure as compared to the IC (arrow), which were set equal to 1.0 in the heat map. For clarity the brain structures are ordered by the increasing color intensity in the lower part of the panel.

3.3 GluK1 protein levels

To further study the protein expression levels of the GluK1 receptor, we next detected the GluK1 protein levels by western blotting in the key brain structures (depicted in Figure 1) of the wild-type and GASH/Sal animals. The protein levels of GluK1 were normalized by calculating the intensity ratio of the bands according to the corresponding levels of the β-actin protein. As shown in Figure 4, compared with the controls, the protein content varied between the different brain regions, showing the band with the expected size (~104 kDa) in all the analyzed structures and, additionally, a second band of ~65 kDa in the inferior and superior colliculi of the GASH/Sal. This is in stark contrast with the control animals, in which the band of ~65 kDa was faint or absent in all brain structures (Figure 4). In the cerebellum, the analysis showed that the GluK1 proteins levels significantly decreased compared with the control group (p-value < 0.05; Figure 4A). The band of ~104 kDa showed no significant difference between control and GASH/Sal animals in the IC, whereas the 65-kDa band was remarkable detected in the GASH/Sal (Figure 4B). Bands of ~104 and ~65 kDa were also detected in the superior colliculus, showing a significant decrease and increase compared with the control group, respectively (p-value < 0.05; Figure 4C). In the hippocampus and the prefrontal cortex, there were no significant differences in the protein levels of GluK1 and the 65-kDa band had no signal (Figures 4D, E). To determine the differences in relative GluK1 levels between the structures of the seizure-associated neuronal network, we compared the normalized signal intensities of the GluK1 bands in each structure with those obtained in the epileptogenic focus. The heatmap showed that the total protein levels of GluK1 were higher in the prefrontal cortex and the superior colliculus, being this last structure with the highest increased differences as compared to the IC (Figure 4F). On the contrary, the brain structures exhibiting lower GluK1 levels than the IC were the hippocampus and the cerebellum (Figure 4F). Taken separately, the relative protein levels of the 104-kDa band were higher in the hippocampus and, particularly to a greater extend, the prefrontal cortex, whereas none of the structures exhibited greater intensity levels for the 65-kDa band than the IC (Figure 4F). The superior colliculus and the cerebellum presented lower relative protein levels of the 104-kDa band than the IC (Figure 4F). Together, the western blotting results suggested different sets and levels of GluK1 proteins expressed among the structures involved in the seizure neuronal network of the GASH/Sal model, showing an unexpected lower molecular weight band in the inferior and superior colliculi.

10.3389/fnmol.2023.1322750

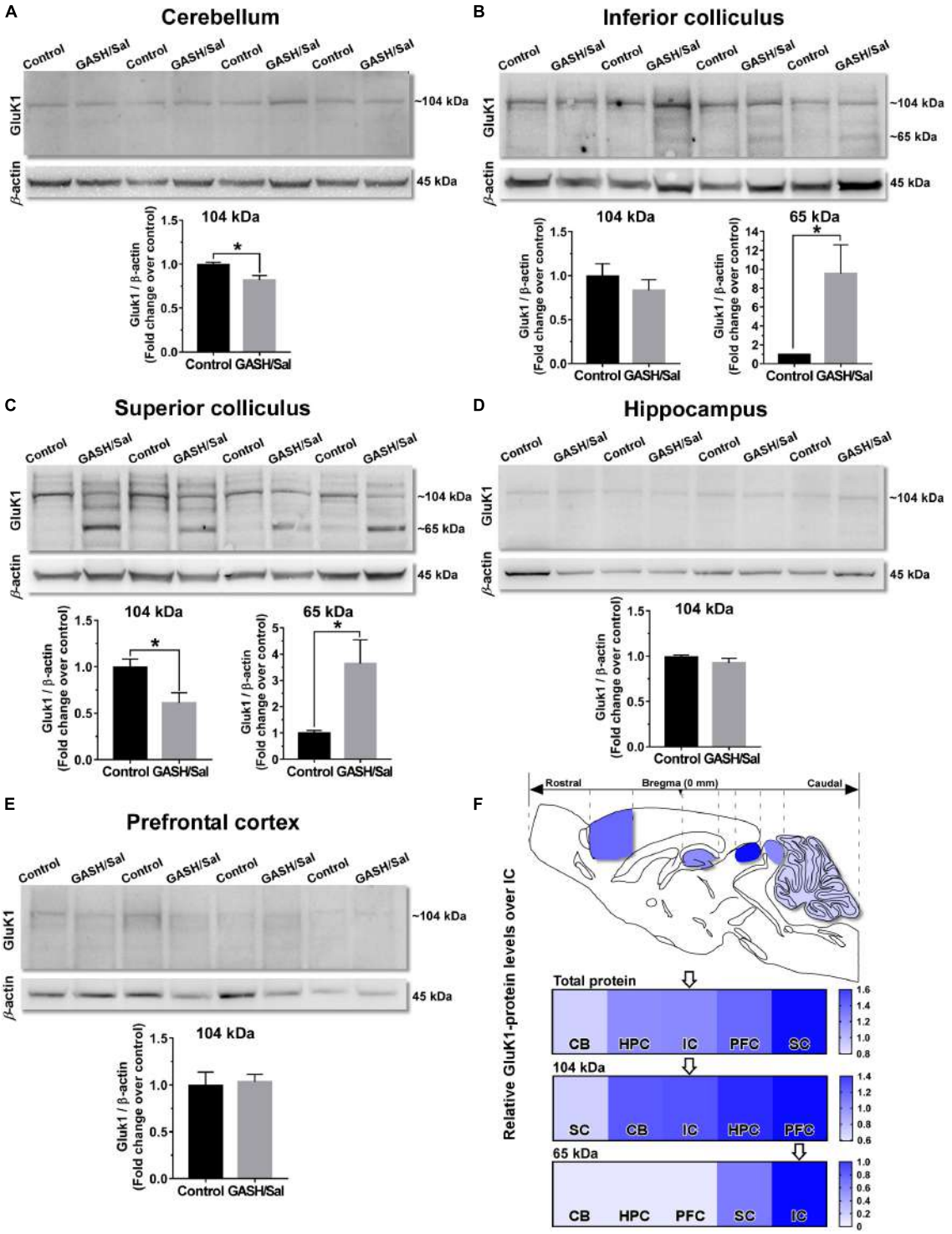

FIGURE 4
GluK1-protein levels within the seizure neural network of the GASH/Sal. Western blot analysis of relative GluK1-protein levels between the control and GASH/Sal hamsters in the cerebellum [CB, **(A)**], inferior colliculus [IC, **(B)**], superior colliculus [SC, **(C)**], hippocampus [HPC, **(D)**], and prefrontal cortex [PFC, **(E)**]. Representative western blot images of protein bands for the GluK1 receptor in each of the brain areas are depicted in the upper part of each panel. Histograms showing a quantitative analysis of GluK1-protein levels are depicted in the lower part of each panel. Each bar graph represents the mean ± standard deviation of the western blot-band intensities that were compared to wild-type values (control animals), which were set equal to 1.0. Notice that a band of the predicted molecular weight (~104 kDA) for GluK1 was detected in all the analyzed brain areas, and in addition a second band of ~65 kDA was observed in the IC and SC of the GASH/Sal. Note that protein levels of GluK1 was significantly different between control and GASH/Sal animals in the CB, the IC, and the SC. *p-value $\leq$ 0.05. **(F)** Sketch of the sagittal section of the GASH/Sal brain shows differences of total GluK1-protein levels between the structures of the seizure neuronal network. The color in the heat map represents the relative GluK1-protein levels between the control and GASH/Sal hamsters in each brain structure as compared to the IC (arrow), which were set equal to 1.0 in the heat map. Additional heat maps for the two detected GluK1 isoforms (~104 and ~65 kDa) are shown in the lower part of the panel. For clarity the brain structures are ordered by the increasing color intensity in all heat maps.

3.4 Distribution of GluK1-immunoreactivity

We next investigated the bright-field and confocal microscopic immunohistochemical localization of the GluK1 receptor in the brain structures associated with the seizure neuronal network of the GASH/Sal as compared to wild-type animals. The overall immunostaining with antibodies to GluK1 was light to moderate in many structures throughout the brain of both animal groups, with a regional distribution in each brain area rather heterogeneous (Figure 5). In general, GluK1-immunoreactivity was diffusely distributed and often concentrated in neuronal perikarya, axonal fiber tracts, and terminals as well as a punctate-like immunostaining in the neuropile (Figure 5). At the resolution of optical microscopy, no clear immunostaining was observed in postsynaptic elements, including dendrites, spines, and dendritic shafts, which was an unexpected finding that will be further discussed below. Thus, morphological features that distinguished axonal fibers from dendrites such as the constant diameter for most of its length, the branching pattern and the area covered from the soma were taken into consideration in the histological analysis. In most cases, the diffuse immunoreaction product was not sufficient for identification of the GluK1-immunolabeled processes at low magnifications, just becoming clearly visible using high objective lenses. A qualitative evaluation of the immunohistochemical distribution of the GluK1 receptor in the five brain areas of study is summarized in Figure 5, categorizing the immunolabeling of somata and visible processes with a description of the density as comparing one animal group to another. Differences between the immunostaining result, the distribution and density of GluK1-immunolabeled structures were noted between the tissue sampled from the control and GASH/Sal animals. Representative bright-field and confocal images as well as the details on the GluK1-immunoreactivity in the brain areas of interest are depicted at low and higher magnifications of coronal sections in Figures 6–10. To provide a more comprehensive description of GluK1 receptor distribution, we have included additional representative examples and supporting information in Supplementary materials 4–12, including high-resolution confocal micrographs, orthogonal analysis, and 3D videos of maximum and stereo projections of confocal microscope image stacks.

3.4.1 Cerebellum

The hamster cerebellum, like other rodent species, is a well-organized structure consisting of three distinct layers in its cortex: molecular, Purkinje cell, and granular layers, enabling the accurate coordination of movements and balance. In the cerebellum of control and GASH/Sal animals, conspicuous Gluk1-immunoreactivity was observed in neuronal perikarya, particularly in the Purkinje cell layer (Figures 6Aa, Ba). This immunoreactivity consisted of small and fine puncta, less than 1 μm in diameter, that cluster over the large cell bodies, presumably of Purkinje cells (Figures 6Ab, Bb). GluK1-immunolabeling was also evident within processes that were most likely to be axonal fibers following the criterion above mentioned. These fibers of varying calibers (0.2–0.5 μm in diameter) occurred in the vicinity of Purkinje neurons (Figures 6Ac, Bc). Those with such disposition and very thin diameter claims be identifiable as cerebellar parallel fibers. Axonal processes or fibers bundles were also intensely immunolabeled for GluK1 coursing throughout the white matter of the cerebellum (Figures 6Ad, Bd). At the confocal microscopy, GluK1-immunopositive axonal fibers were also detected through the layers of the cerebellar cortex, which were distinguishable through NeuN-immunostained and DAPI labeling (Figures 6Ae, Be). These GluK1-immunolabeled axons appeared coursing from the granular cell layer, ascending through the Purkinje cell layer to the lower molecular layer, in which the dendritic trees of the Purkinje neuron presumably distributed (Figures 6Ae, Be). The stereo view of confocal image sections showed that these GluK1-fibers bifurcated in the molecular layer as typically occurred in parallel fibers (Figures 6Af, Bf). Together, these results suggest that GluK1-immunoreactivity was intense in the cerebellar regions containing parallel fibers-Purkinje cells synapses. In addition, GluK1-immunoreactivity was observed as diffuse immunostaining of neuropile in the cerebellar cortex (Figures 6Ae, Be). As compared to controls, the cerebellum of the GASH/Sal exhibited less intensity of GluK1-immunoreactivity in the neuronal profiles (Figures 6A, B). The GluK1-immunopositive structures were less homogeneously distributed in the GASH/Sal, showing cerebellar lobules with absent or weak immunoreactivity (Figure 5). The number of cell bodies and axonal fibers immunolabeled for GluK1 were reduced in the GASH/Sal cerebellum, while the labeling of neuropile was seen similarly in diverse cerebellar regions (Figures 5, 6).

3.4.2 Inferior colliculus

Located in the midbrain, the IC is a vital paired structure serving as a relay center for auditory information and other non-auditory sources, with its main regions being the central nucleus, dorsal cortex, and external cortex. The distribution of GluK1-immunoreactivity in the IC was found to be heterogeneous in both animal groups, exhibiting variations across the three subdivisions. The observed density and intensity of the immunoreactive product was higher in the dorsal and external cortex compared to the central nucleus of the IC (Figures 5, 7Aa, Ba). In the dorsal and external cortex, the GluK1 distributed within small neuronal perikarya (Figures 7Ab, Bb) as well as axonal fibers that generate boutons near cell bodies (Figures 7Ad, Bd). While similar immunolabeled structures were observed in the central nucleus, the immunostaining was diffuse and weakly distributed, particularly in scarce cell bodies (Figures 7Ac, Bc). Using confocal microscopy, we observed specific GluK1-immunostaining in axonal fibers as well as in the neuropile in the external regions of the IC. These long fibers gave rise to endings on cell bodies, which we visualized with NeuN-immunostaining (Figures 7Ae, Be). Supplementary material 4 includes a 3D video with split-channel visualization of maximum projection of confocal images, providing a close-up view of the GluK1-immunopositive axonal fibers and endings. Upon comparison of GASH/Sal and controls, clear and significant differences were observed (Figure 5). In the external cortex, bright-field and confocal microscopic examination revealed a higher density of GluK1-immunopositive cell bodies and axonal fibers, with much more numerous axonal branches and endings in the GASH/Sal group compared to controls (Figures 5, 7Ae, Be and Supplementary material 4). Although GluK1-immunolabeled structures were sparse in the central nucleus in both groups, there was a slightly higher

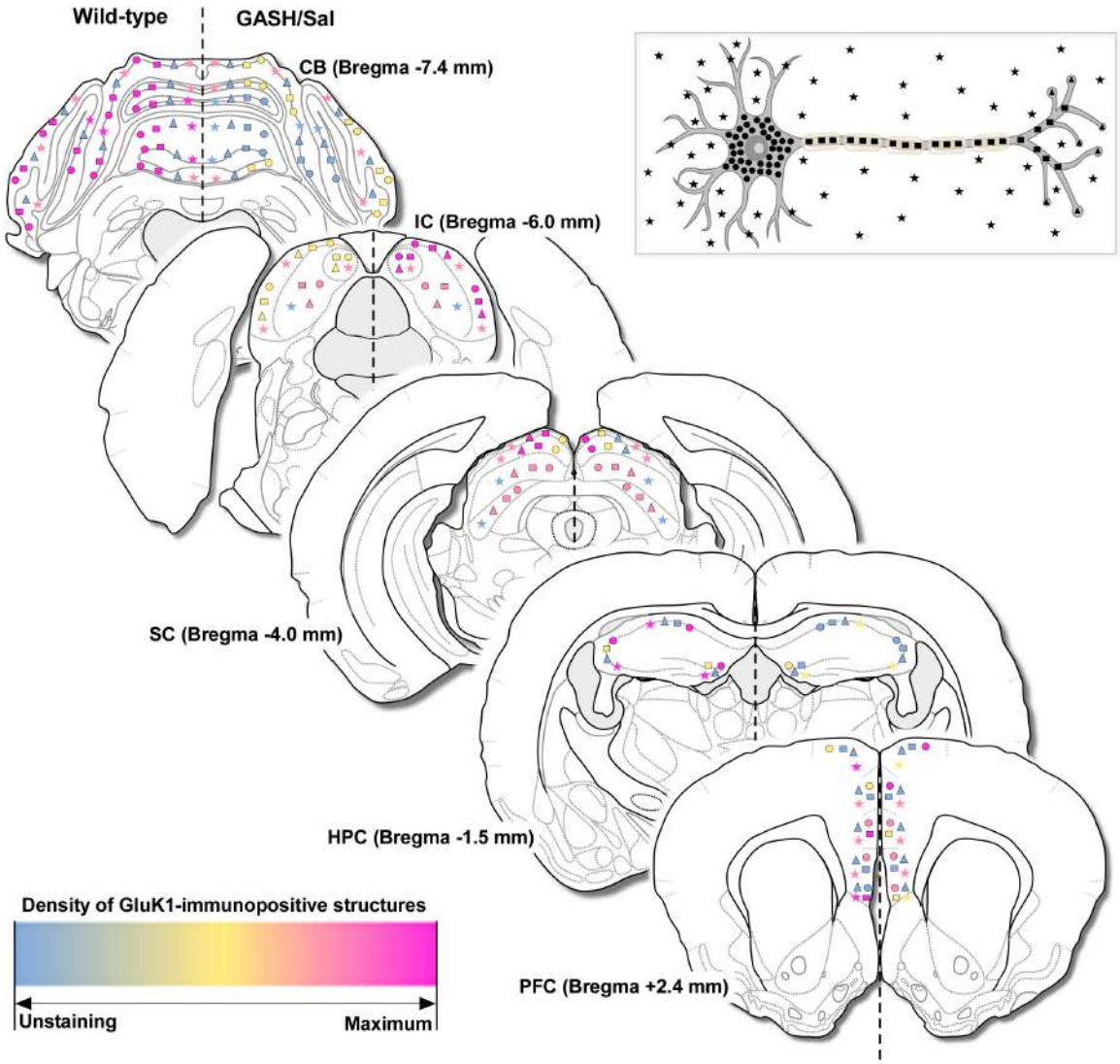

FIGURE 5
Overview of the immunohistochemical findings. Schematic representation of GluK1-immunopositive structures in the brain of the control and GASH/Sal hamsters corresponding to caudal-rostral levels (with respect to bregma) and based on visual qualitative observations. GluK1-immunoreactivity was categorized in cell bodies (circles), axonal fibers (rectangles), terminals (triangles) and punctate-like immunostaining nearby somata or in the neuropile (stars), according to the neuron diagram showed in the upper part of the figure. For comparative purposes, this classification was combined with a description of the density for GluK1-immunolabeling, ranging from unstained (in blue), to fewer (in yellow), similar (in pink), up to maximal immunostaining for numerous and dense immunoreactive structures (in magenta) as comparing one animal group to another. The information is provided in the left and right hemispheres for the wild-type and GASH/Sal hamsters, respectively. Bregma data from the hamster brain atlas of Morin and Wood (2001). CB, cerebellum; IC, inferior colliculus; SC, superior colliculus; HPC, hippocampus; PFC, prefrontal cortex.

density of GluK1-immunolabeled cell bodies in the GASH/Sal group compared to controls, while GluK1-immunolabeled axonal fibers and terminals were slightly more prominent in the control group (Figures 5, 7). Interestingly, GluK1-immunoreactivity was notably concentrated around the DAPI-stained nucleus with a higher frequency observed in the GASH/Sal group, especially within the external cortex, as vividly depicted in orthogonal confocal views (Supplementary material 5). In summary, the observed marked differences in GluK1-immunoreactivity between the regions of the IC in GASH/Sal animals suggest potential underlying glutamate synaptic transmission alterations that may be related to the role of the IC in seizure generation and propagation.

3.4.3 Superior colliculus

Neuroanatomically, the superior colliculus is comprised of a highly organized, six-layer structure. The three superficial layers are primarily responsible for receiving visual information, whereas the three deeper layers are interconnected with cortical and subcortical areas involved in auditory, somatosensory and motor function. Thus, GluK1-immunolabeling was compared between control and GASH/Sal hamsters, considering these two functionally distinct units, a superficial subdivision comprising the stratum zonale, stratum griseum superficiale, and stratum opticum, and a deep subdivision comprising stratum griseum intermediale, stratum album intermedium, and stratum profundum (Figure 8). The superficial subdivision exhibited

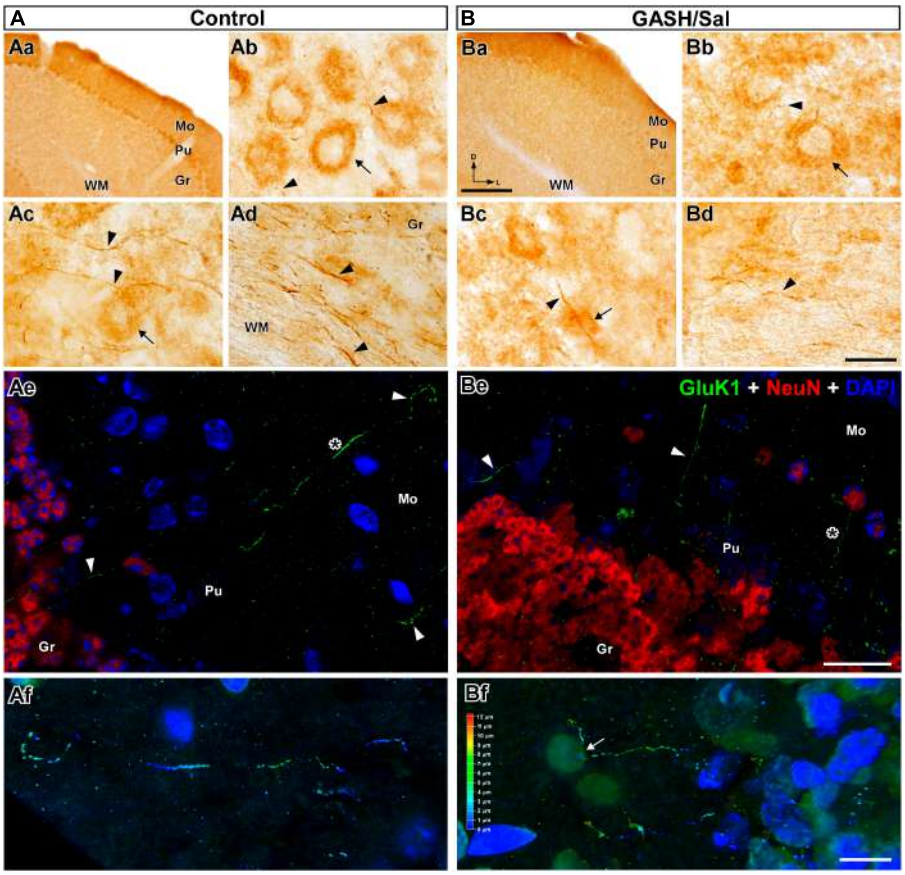

FIGURE 6
GluK1-immunolabeling in the cerebellum (CB) of the control **(A)** and GASH/Sal **(B)** hamsters. **(Aa,Ba)** Low magnification photomicrographs of representative coronal sections of the CB. Notice that Purkinje cells (Pu) were the cerebellar cell type most intensely immunolabeled for GluK1. GluK1-immunoreactivity was weaker in the GASH/Sal cerebellum as compared to controls. Photomicrographs showing details of GluK1-immunopositive cell bodies [arrow in **(Ab)** somatic size: 340.4 μm^2 with major and minor axes of 24.1 and 17.9 μm; arrow in **(Bb)** somatic size: 456.5 μm^2 with major and minor axes of 25.8 and 22.4 μm] and thin axonal fibers (arrowheads, diameter: ~ 0.5 μm) in the CB. Notice large neuronal perikarya heavily immunolabeled for GluK1 in the Pu layer. No staining of neuronal nuclei and dendrites was observed with anti-GluK1. **(Ac,Bc)** GluK1-immunoreactive axonal fibers (arrowheads) passing in proximity and through Purkinje neuronal somata (arrow). **(Ad,Bd)** GluK1-immunoreactive axonal fibers (arrowheads: diameter: ~ 0.7 μm) running into the white matter (WM) of the CB. Notice that fewer GluK1-immunopositive structures in the GASH/Sal cerebellum as compared to controls **(Ab–Bd)**. **(Ae,Be)** Confocal images show GluK1-immunopositive axonal fibers (in green, arrowheads) coursing into the three layers in the cerebellar cortex. DAPI (in blue) and the NeuN-immunolabeling (in red) were used to identify the cytoarchitecture of the brain nuclei. Purkinje cell layer was not labeled for NeuN. Notice the diffuse GluK1-immunolabeling in the cerebellar neuropile. **(Af,Bf)** Confocal micrographs of stereo projections corresponding to the area depicted with an asterisk in **(Ae,Be)** show details of GluK1-immunopositive fibers bifurcating in the cerebellar molecular layer (white arrow). Gr, cerebellar granular layer; Mo, cerebellar molecular layer; Pu, Purkinje cell layer. Scale bars = 200 μm in **(Aa,Ba)**; 20 μm in **(Ab–Be)**; 10 μm in **(Af,Bf)**.

robust GluK1-immunoreactivity in axonal fibers of varying thicknesses, as well as diffuse immunoreactivity in cell bodies in both animal groups (Figures 8Ab, Bb). Additionally, the GASH/Sal group displays a lower number of fibers and a higher number of GluK1-immunopositive cell bodies when compared to the control group (Figures 5, 8Ab, Bb). The deep subdivision, particularly the intermediate layers, exhibited GluK1-immunopositive axonal fibers that terminate in close proximity to GluK1-immunopositive cell bodies. In the wild-type animal, these fibers give rise to axonal terminals that are strongly GluK1-immunopositive (Figures 8Ac, Ad). However, a remarkable finding in the GASH/Sal animal was the absence of GluK1-immunopositive axonal terminals, despite exhibiting stronger GluK1-immunoreactivity in cell bodies (Figures 5, 8Bc, Bd). Although the deepest layers (striatum profundum) exhibited very weak immunostaining, punctate GluK1-immunolabeling was observed throughout the collicular neuropile in both animal groups (e.g., Figure 8Ad). All these findings agreed with those observed at confocal microscopy, which consistently revealed the presence of long axonal fibers exhibiting GluK1-immunoreactivity coursing throughout the external layers, passing over neuronal perikarya stained with anti-NeuN (Figure 8Ae and Supplementary material 6). Notably, the axonal fibers, including those observed through the dorso-ventral axis of the collicular lamination, exhibited weaker GluK1-immunolabeling in the GASH/Sal animal when compared to those of the control animal (Figures 8Ae, Be). Due to the critical role played by the superior colliculus in integrating diverse sensory modalities to generate appropriate behavioral responses and transforming this sensory information into motor commands, the observed differences in Gluk1-immunostaining between the two animal groups underscore its significance for seizure propagation in the GASH/Sal model.

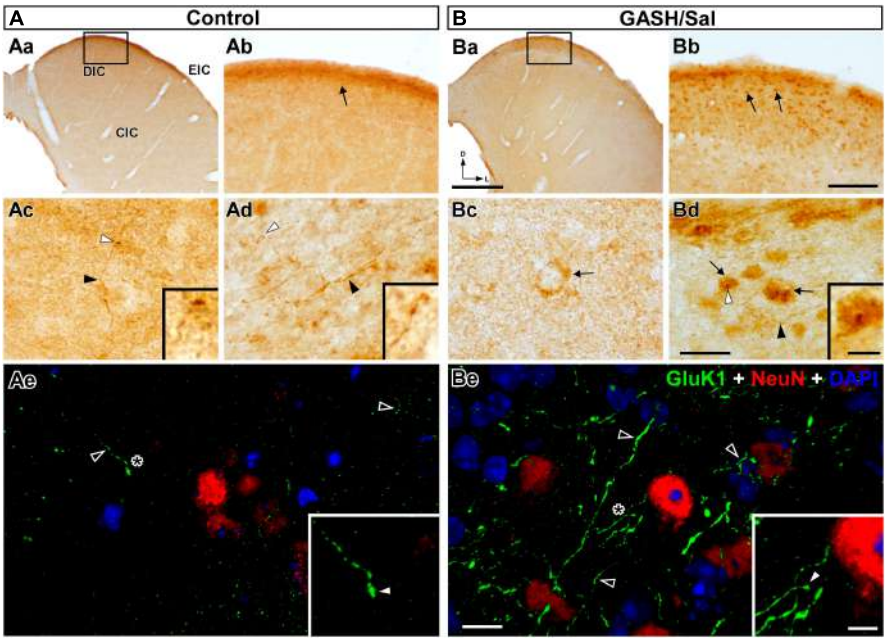

FIGURE 7
GluK1-immunolabeling in the inferior colliculus (IC) of the control **(A)** and GASH/Sal **(B)** hamsters. **(Aa,Ba)** Low magnification photomicrographs of representative coronal sections of the IC. Higher magnification of the dorsal cortex of the IC (DIC) corresponding to the frame in **(Aa,Ba)**. Notice greater number of GluK1-immunopositive neuronal somata (arrows; somatic size: ~ 50 μm^2 with major and minor axes of ~ 9.5 and ~ 6.8 μm) in the GASH/Sal as compared to controls. **(Ac,Bc)** Photomicrographs of the central nucleus of the IC (CIC) shows a GluK1-immunoreactive axonal fiber (black arrowhead) giving rise to an ending (white arrowhead) as well as diffuse GluK1-immunolabeling of neuronal somata (arrow). **(Ad,Bd)** High magnification photomicrographs of the external cortex of the IC (EIC) shows GluK1-immunopositive axonal fibers (black arrowheads) and endings (white arrowheads) in apposition to GluK1-immunopositive cell bodies (arrows). Insets show details of GluK1-immunopositive endings (corresponding to the white arrowheads in each panel). **(Ae,Be)** Confocal images of the DIC stained using anti-GluK1 (green), anti-NeuN (red), and DAPI (blue). Notice higher density of strong GluK1-immunopositive axonal fibers (black arrowheads) in the GASH/Sal as compared to controls. Insets show details of GluK1-immunopositive endings (white arrowheads) corresponding to the asterisk depicted in **(Ae,Be)**. The maximum projection of confocal images corresponding to the panels **(Ae,Be)** was displayed in the 3D video of Supplementary material 4. No staining of neuronal nuclei and dendrites was observed with anti-GluK1 in the IC. Scale bars = 500 μm in **(Aa,Ba)**; 100 μm in **(Ab,Bb)**; 20 μm in **(Ac,Bc)** and **(Ad,Bd)**; 10 μm in **(Ae,Be)**; and 5 μm for all insets.

3.4.4 Hippocampus

The hippocampus, a major limbic region in the brain, is composed of several subregions, including the dentate gyrus, CA1, CA2, and CA3 regions, which are interconnected via unidirectional pathways. As expected, strong Gluk1-immunoreactivity decorated the numerous cell bodies in the three hippocampal regions of the wild-type animals (Figure 9Aa). This immunostaining was found homogeneously distributed between the hippocampal regions as well as the rostro-caudal axis of the hippocampus. At higher magnification, the GluK1-immunostaining shows a characteristic subcellular distribution, with a prominent accumulation near the cell membranes of the somata, forming small and distinct punctate structures, as illustrated in Figures 9Ab–d as well as Supplementary materials 7, 8. Notably, the thin axons (with an approximate diameter of 1.5 μm) were found to be sparse in the hippocampal regions and were rarely detected in CA3 and dentate gyrus (Figure 9Ac and Supplementary materials 7, 8). In line with our findings in other brain regions, no dendrites were found to exhibit immunoreactivity with the anti-GluK1 antibody (Figures 9Ab–d). A comparison with control animals revealed a striking contrast in the hippocampus of the GASH/Sal animals, where a marked reduction in GluK1-immunostaining was observed (Figures 5, 9Ba). All hippocampal regions of the GASH/Sal animals displayed a remarkably weak, almost negligible level of GluK1-immunoreactivity (Figures 5, 9Bb–d), indicating a potential disruption in the expression or localization of this protein in the GASH/Sal model. In particular, the dentate gyrus, a relevant hippocampal area during seizures, exhibited a notable absence of strong GluK1 punctate-immunostaining in the neuronal perikarya of GASH/Sal animals, which contrasted with the observation in the wild-type animals (Supplementary material 7). Consistent results were obtained from both bright-field and confocal microscopy techniques, as a decrease in GluK1 punctate-immunolabeling was observed in the somata and neuropile of GASH/Sal animals. Notably, the confocal microscopy analysis showed that GASH/Sal animals exhibited sparse immunofluorescence for the GluK1 receptor in contrast to the control animals, which showed robust punctate GluK1-immunolabeling in the same regions (Figures 9Ae, Be and Supplementary material 7). Despite the weak immunolabeling of GASH/Sal hippocampus, the confocal microscopy analysis revealed that GluK1-immunostaining was gathered around the DAPI-stained nucleus, as observed in close-up orthogonal views in the dentate gyrus (Supplementary material 9). These findings suggest an alteration in the localization of GluK1 protein in the hippocampus, a limbic structure that indirectly receives auditory signals from the brainstem, which may be relevant in understanding the limbic recruitment during repeated audiogenic seizures in the GASH/Sal model.

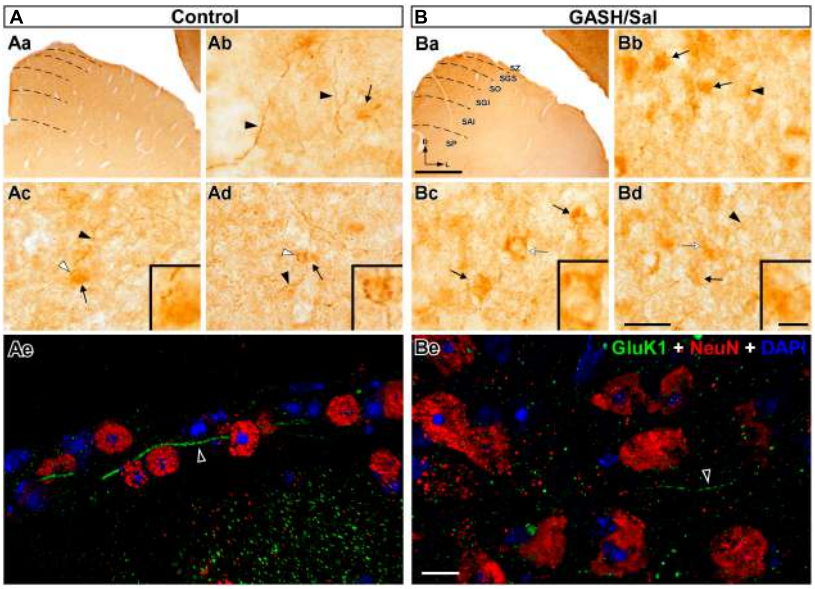

FIGURE 8
GluK1-immunolabeling in the superior colliculus (SC) of the control **(A)** and GASH/Sal **(B)** hamsters. **(Aa,Ba)** Representative photomicrographs of coronal sections of the SC show GluK1-immunolabeling in the superficial (SZ, SGS, and SO) and deep (SGI, SAI, and SP) subdivisions. Dashed lines indicate the collicular lamination. **(Ab,Bb)** Higher magnification of the external layers (SZ and SGS) show strong GluK1-immunoreactivity in axonal fibers (black arrowhead) of various thicknesses as well as diffuse immunoreactivity in the cell bodies (arrows). Notice fewer number of fibers and a greater number of GluK1-immunopositive cell bodies in the GASH/Sal as compared to controls. **(Ac,d,Bc,d)** Photomicrographs of the intermediate layers (SGI and SAI) show GluK1-immunopositive axonal fibers (black arrowheads) and endings (white arrowheads) in apposition to GluK1-immunopositive cell bodies (arrows). Insets show details of GluK1-immunopositive endings and somata (corresponding to the white arrowhead and arrow in each panel, respectively). Notice strong GluK1-immunopositive fibers give rise to axonal terminals, whereas in the GASH/Sal, there were no GluK1-immunopositive endings. Additionally, cell bodies in the GASH/Sal exhibited stronger GluK1-immunoreactivity. Punctate GluK1-immunolabeling was observed throughout the collicular neuropile, while no staining of neuronal nuclei and dendrites was detected with anti-GluK1. **(Ae,Be)** Confocal images of the superficial subdivision using anti-GluK1 (green), anti-NeuN (red), and DAPI (blue). Notice long axonal fibers with GluK1-immunoreactvity (black arrowheads) coursing throughout the collicular tissue and overcoming cell bodies. Notice weaker GluK1-immunolabeling in the axonal fiber of the GASH/Sal as compared to the wild-type animal. Punctate GluK1-immunolabeling was also observed in the neuropile. The maximum projection of confocal images corresponding to the panel **(Ae)** was displayed in the 3D video of Supplementary material 6. SAI, stratum album intermedium; SGI, stratum griseum intermediale; SGS, stratum griseum superficiale; SP, stratum profundum; SO, stratum opticum; SZ, stratum zonale. Scale bars = 500 μm in **(Aa,Ba)**; 20 μm in **(Ab–Bd)**; 10 μm in **(Ae,Be)**; and 5 μm for all insets.

3.4.5 Prefrontal cortex

The distribution of GluK1 was examined in sections taken from the middle portions of the prefrontal cortex, which encompass several discernible cytoarchitectural regions, including the cingulate cortex, prelimbic cortex, and infralimbic cortex, as well as neighboring areas such as the indusium griseum and the motor cortex. In control animals, the labeling for GluK1 was relatively heterogenous across the cortical laminae and made up of small puncta in the neuropile, axonal fibers, terminals, and perikarya (Figure 10A). At higher magnification, GluK1-immunoreactivity was seen in several compartments across the different regions of the prefrontal cortex (Figure 10Ab). In the cingulate cortex of control animals, we observed robust GluK1-immunopositive fibers that give off terminals, as well as abundant small puncta in the neuropile. Long axonal fibers, which were notably marked for GluK1, were observed coursing through the dorsoventral axis of layer I and giving off terminals (e.g., in Figure 10Ab). Diffuse punctate granular pattern of neuropile staining with labeling of neuronal cell bodies was observed in the prelimbic and infralimbic areas as well as strong GluK1-immunopositive axonal fibers in the cingulate cortex areas of control animals (Figure 10Ab). Similarly, strong axonal fibers were found in the indusium griseum, and diffuse labeling was detected in the cell bodies of the motor cortex (Figure 10Ab). As compared to controls, GASH/Sal animals exhibited strong GluK1-immunoreactivity in the cell bodies distributed in the motor and cingulate cortex (Figure 10Ba), while the prelimbic and infralimbic regions showed similar immunoreactivity in neuronal perikarya (Figures 5, 10Bb). Notably, axonal fibers of the GASH/Sal animals showed little to no immunoreactivity in the isidium griseum (Figure 10Bb). Furthermore, there was a marked difference in the intensity of the punctate immunostaining observed between the control and GASH/Sal animals, as well as between the selected brain regions. As in other examined brain areas, it is worth noting that the GluK1-immunoreactivity was found to be concentrated in the vicinity of nucleus-like organelles in both animal groups, but more frequently observed in the GASH/Sal (Figures 10A, B and Supplementary materials 11, 12). Consistent with the bright-field microscopy observations, confocal image analysis revealed that the same pattern of immunolabeling was observed in control animals, with numerous and lengthy GluK1-immunopositive axonal fibers as well as neuropile immunolabeling in the form of a fine dusting in the medial prefrontal cortex regions (Supplementary material 10). In the GASH/Sal animals, both microscopy techniques showed fewer and less intense GluK1-immunoreactivity in the same regions, and a closer examination revealed the presence

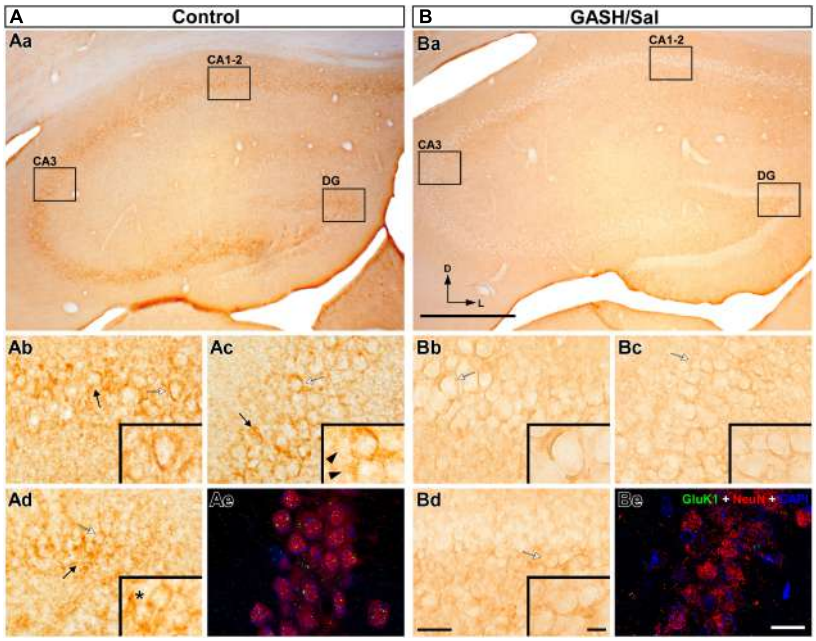

FIGURE 9
GluK1-immunolabeling in the hippocampus (HPC) of the control **(A)** and GASH/Sal **(B)** hamsters. **(Aa,Ba)** Representative low magnification images of the HPC, showing the three hippocampal regions. Notice the specific loss of GluK1-immunoreactivity in the hippocampal regions of the GASH/Sal. [High magnification photomicrographs of three hippocampal regions: CA1–2 **(Ab,Bb)**, CA3 **(Ac,Bc)**, and the dentate gyrus DG, **(Ad,Bd)**] corresponding to the black rectangles in **(Aa,Ba)**. Notice the strong GluK1-immunoreactivity in the cell bodies (black arrows) throughout the HPC of the control animal, whereas the GASH/Sal hippocampal regions show absence of GluK1-immunolabeling. The insets show details of GluK1-immunolabeling corresponding to the white arrow in each panel. Punctate GluK1-immunostaining (asterisk) and thin fibers (black arrowhead) immunolabeled for GluK1 were also observed in control animals. **(Ae,Be)** Confocal images of the CA3 region stained using anti-GluK1 (green), anti-NeuN (red), and DAPI (blue). Notice weaker punctate GluK1-immunolabeling in somata and neuropile of the GASH/Sal as compared to the wild-type animal. Scale bars = 500 μm in **(Aa,Ba)**; 40 μm in **(Ab,Bb)**, **(Ac–Bc,Ad,Bd)**; 20 μm in **(Ae,Be)**; and 10 μm for all insets.

of GluK1-immunopositive puncta weaky labeled in the somata and neuropile (see for comparison **Figures 10Ac, Bc** and **Supplementary materials 11, 12**). In sum, these results pointed out an altered distribution in GluK1 receptors that could lead to an increase in neuronal excitability and potentially alter synaptic plasticity in the medial prefrontal cortex of the GASH/Sal model.

4 Discussion

The GASH/Sal strain was previously analyzed using whole exome sequencing to identify and characterize its mutational landscape (Díaz-Casado et al., 2020). Moderate- and high-impact variants were validated using Sanger sequencing, including a single amino acid substitution from histidine to tyrosine in the GluK1 protein (Díaz-Casado et al., 2020). The impact of the p.H289Y polymorphism on the lifespan of the GluK1 protein and its potential effects on the function of the glutamatergic system in the GASH/Sal brain, if any, pose highly intricate and multifaceted inquiries. The present study explores the effects of this single-nucleotide polymorphism on brain structures involved in the neuronal network associated with audiogenic seizures in the GASH/Sal model. Through a predicted 3D model, we found that this missense mutation affects protein stabilization by increasing intermolecular interactions. Gene expression analysis revealed disturbances in the *Grik1* gene's transcriptional profile within the neuronal network associated to audiogenic seizures. Furthermore, variations in GluK1 protein patterns and levels were observed heterogeneously among the brain structures, including an unexpected lower molecular weight band in the inferior and superior colliculi. Immunohistochemical examination of GluK1 receptor distribution across the audiogenic seizure neuronal network revealed significant differences in GluK1-immunoreactivity, suggesting potential alterations in glutamate synaptic transmission in the GASH/Sal model. Overall, this study deepens our understanding of genetic alterations in seizure neural networks, particularly regarding the role of kainate receptors.

4.1 Potential protein stabilization caused by the p.H289Y polymorphism in the *Grik1* gene

To understand the functional and disease implications of genetic variations, it is crucial to have knowledge of the 3D structure of the gene product. In the context of utilizing predicted structures, such as in the present study, the question arises as to whether the predictions derived from a 3D model align with those obtained from an experimental structure and how the accuracy of the models impacts these findings. Nonetheless, evidence exists to support the notion that predicted protein 3D models are just as effective as experimental structures in determining the pathogenic impact of a variant (Ittisoponpisan et al., 2019). Changes at the amino acid level can affect the protein's shape, folding, function,

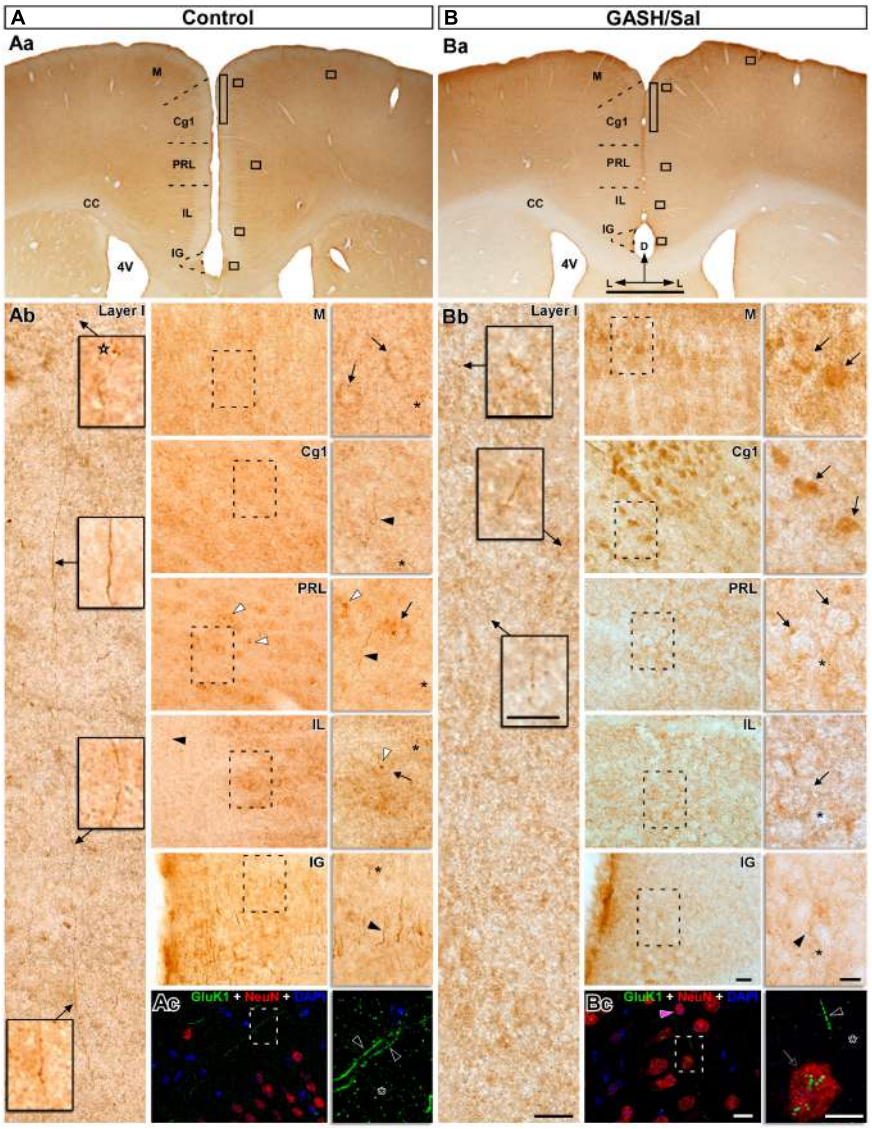

FIGURE 10
GluK1-immunolabeling in the prefrontal cortex (PFC) of the control **(A)** and GASH/Sal **(B)** hamsters. **(Aa,Ba)** Representative low-magnification images of coronal sections containing distinct cytoarchitectural regions of the medial PFC, including the cingulate cortex (Cg1), prelimbic cortex (PRL), and infralimbic cortex (IL), as well as adjacent areas such as the indusium griseum (IG) and the motor cortex (M). **(Ab,Bb)** High magnification photomicrographs corresponding to the squares in panels **(Aa,Ba)** show the GluK1-immunoreactivity pattern. Details of the selected brain areas corresponding to the dashed box are shown in zoomed-in images using 100x objective lens. Notice that strong GluK1-immunopositive fibers ran parallel to the long dorso-ventral axis through the layer I and give rise axonal terminals (star) in control animals, whereas the GluK1-immunopositive fibers were minimal in the GASH/Sal. Diffuse GluK1-immunopositive cell-like structures (arrows) were observed in M, PRL and IL areas as well as strong GluK1-immunopositive axonal fibers (black arrowheads) in the Cg1 and IG areas of control animals. In GASH/Sal animals, strong GluK1-immunoreactivity are found in the cell bodies (arrows) of the M and Cg1 areas, whereas GluK1-immunoreactive somata were low in PRL and IL areas. Low or absent immunoreactivity was detected in axonal fibers of the GASH/Sal (e.g., black arrowhead in the IG). Note the difference in the intensity of the punctate immunostaining (asterisk) between the control and GASH/Sal animals, as well as between the selected brain areas. GluK1-immunoreactivity concentrated nearby nucleus-like organelles (white arrowheads) in both animal groups (see **Supplementary material 11** for additional examples). Confocal merged images showing localization of GluK1 (green), NeuN (red), and DAPI (blue) in the layer I-II **(Ac)** and layer V **(Bc)** of the Cg1 area. Numerous and long GluK1-immunopositive axonal fibers (black arrows) and punctate immunostained (asterisks) were observed in control animals, whereas fewer and lower GluK1-immunoreactivity was present in the GASH/Sal. Notice detail of somata-showing GluK1-immunopositive puncta (arrow) in the GASH/Sal. The maximum projection of confocal images corresponding to the panel 10Ac was displayed in the 3D video of **Supplementary material 10**. The orthogonal analysis of the neuron highlighted with a magenta arrowhead in the panel **(Bc)** is shown in the **Supplementary material 12**. Scale bars = 1 mm in **(Aa,Ba)**; 20 μm in **(Ab,Bb)**, and 10 μm for all insets.

stability, ligand binding properties, catalysis, regulation, and post-translational modification, ultimately impacting the phenotype. While the structural context of each missense mutation can predict likely changes in molecular function, it is important to consider potential caveats, such as mutations that may be neutral in terms of phenotype rather than molecular function and effects that cannot be easily identified from structure alone (Wang and Moult, 2001). Therefore, each mutation can affect the various roles of a residue through modification of different types of interactions, including hydrophobic, hydrogen bond, van der

Waals, electrostatic interactions, and disulfide bonds (Wang and Moult, 2001). Taking this into consideration, our protein structure analysis revealed the emergence of new hydrophobic-proximal interactions resulting from the p.H289Y genetic variant, which differs from the wild-type structure, implying the likelihood of alterations in the intermolecular interactions within the GluK1 subunit. Histidine and tyrosine are distinct amino acids that differ significantly in their chemical structures and properties. Tyrosine, which possesses a large amphipathic side chain that can participate in non-polar, hydrogen-bonding, and cation-π interactions, is highly effective in mediating recognition in protein-protein interfaces in contrast to histidine, which lacks these features (Koide and Sidhu, 2009). However, considering its location in the ATD rather than the binding domain, the p.H289Y genetic variant is unlikely to directly compromise protein binding with glutamate. Consequently, it is anticipated to exert only a minimal or negligible effect on this activity. This leads us to argue on the potential implications of the substitution of histidine-289 to tyrosine in the ATD, specifically in the regulatory region R2, of the GluK1 receptor. One feasible possibility is that this point mutation may affect its assembly into tetramers from the pool of the five kainate receptor subunit types. Supporting this, research has shown that high-affinity interactions in the ATD are necessary for the biosynthesis of functional heteromeric kainate receptors (Ayalon and Stern-Bach, 2001; Kumar et al., 2011), and that the GluK1 subunit's ATD can form heteromeric receptors with all possible stoichiometries in an expression-dependent manner (Selvakumar et al., 2021). Although the inflexibility of the lower lobe (R2) interaction within the ATD is thought to be the cause of the lack of allosteric regulation in kainate receptors (Furukawa, 2012; Gangwar et al., 2023), the possibility that the p.H289Y polymorphism may impact this aspect cannot be dismissed, as the ATD contains extensive interactions with the ligand binding domains that allow for complex allosteric regulation, as observed in other ionotropic glutamate receptor subunits (Krieger et al., 2015). Interestingly, Matsuda et al. (2016) showed that complement proteins specifically bound the ATD of kainate receptors subunits, serving as master regulators of postsynaptic kainate receptor complexes. Although the role of the complement system in the GASH/Sal model remains unexplored, the dysregulation of complement proteins contributing to disease progression during synaptic pruning in development and disease (Stephan et al., 2012), underscores the importance of further exploring this potential influence. In line with this notion, the complement system has been implicated in the pathogenesis of epilepsy and may provide opportunities for developing better therapeutics and prognostic markers (Kopczynska et al., 2018). Duan et al. (2018) uncovered a trafficking mechanism for kainate receptors, suggesting that the cleaved signal peptide acts as a ligand for GluK1, binding with the ATD to repress receptor trafficking. Thus, a single point mutation in this domain could disrupt this crucial molecular function, leading to an alteration in the forward trafficking ability of the GluK1 receptor. Finally, our study employs several stability predictors to assess folding or protein interaction energy changes upon this mutation. The collective and convergence findings from all stability predictors utilized in our analysis consistently indicate that the p.H289Y polymorphism presumably leads to significant protein stabilization. Furthermore, the observed increase in total interactions within the protein carrying the p.H289Y genetic variant, compared to the wild-type structure, aligns with the predicted over-stabilization of the mutated GluK1 protein. Given the substantial amino acid sequence similarity of GluK1 protein among various species, as noted in **Supplementary material 1D**, it is plausible to extrapolate that the anticipated effect of this specific point mutation could be analogous. Computational stability predictors, such as those employed in our study, have become a widely adopted approach to assess the impact of missense mutations by evaluating changes in protein folding and interaction energy (Gerasimavicius et al., 2020). Although stability predictors were not specifically designed to identify pathogenic variants, their outputs are frequently included as supporting evidence for pathogenicity in publications reporting novel variants (Gerasimavicius et al., 2020). It is worth noting that although the previous emphasis was primarily on destabilizing mutations, it is now recognized that certain pathogenic missense mutations can stabilize protein structure. For instance, the histidine-to-glutamine substitution in the flexible loop of the chloride intracellular channel 2 (CLIC2) protein, which is associated with calcium ion signaling and epilepsy, is predicted to enhance protein stability (Takano et al., 2012). This prediction is supported by $\Delta\Delta G$ calculations indicating reduced flexibility and movement in the ATD as well as decreased membrane integration of the protein (Takano et al., 2012). In line with this rigidification argument, the heightened stability of the GluK1 protein's ATD could potentially result in adverse effects. Although the specific implications of increased stability depend on the protein's overall structure, function, and the context in which it operates, excessive stabilization of a protein might also prolong its half-life, elevate cellular concentration, and render it more resistant to denaturation or degradation. In the case of the GluK1 receptor, the over-stabilization of its ATD can affect folding, conformational dynamics, flexibility, and accessibility. This, in turn, may disrupt the intricate combinations of heteromeric kainate subunits and consequently impact the precise modulation of kainate receptor function within the GASH/Sal brain. Thus, the broader consequences of increased stability must not be disregarded, as they are closely intertwined with the protein's overall structure, function, and operational context.

4.2 Dysregulated *Grik1* gene expression within the GASH/Sal seizure network

The next step in exploring the potential consequences of a stability-altering point mutation was to examine the expression pattern of the *Grik1* gene in brain structures associated with the seizure neuronal network in the GASH/Sal model. Previous reports from our research group have identified alterations in the gene expression of the GASH/Sal under free-seizures condition and after audiogenic seizures (López-López et al., 2017; Prieto-Martín et al., 2017; Damasceno et al., 2020; Díaz-Casado et al., 2020; Díaz-Rodríguez et al., 2020; Sánchez-Benito et al., 2020; Fuerte-Hortigón et al., 2021). Examining baseline alterations in gene expression provides insights into inherent changes contributing to the epileptic phenotype of the GASH/Sal, enabling the identification of genes involved in seizure predisposition and the overall pathophysiology. Moreover, analyzing gene expression after seizures reveals immediate molecular changes associated with seizure activity, like the seizure propagation pathways. The

current study was conducted in GASH/Sal animals under free-seizures condition, showing significant differences in the mRNA expression levels of the *Grik1* gene between the GASH/Sal model and controls. Specifically, the cerebellum as well as the inferior and superior colliculi showed significantly higher expression of *Grik1* in the GASH/Sal, while the hippocampus exhibited downregulation. The consequences of dysregulation of the *Grik1* gene in these brain structures can vary depending on the context and the specific functions of that structure. Sánchez-Benito et al. (2020) investigated naïve GASH/Sal animals and discovered notably alterations in cochlear mechanotransduction, as evidenced by abnormal expression patterns in essential cochlear genes, including the vesicular glutamate transporters 1 and 2. Furthermore, they reported disrupted gene expression of these vesicular glutamate transporters in the cochlear nucleus. This observation hints at a disturbance in the normal glutamatergic transmission along the primary acoustic pathway, carrying significant implications for the potential propagation of abnormal transmission to the GASH/Sal inferior colliculus (Sánchez-Benito et al., 2020). As in other rodent models of epilepsy, seizure susceptibility corrupts acoustic integration in the IC, a critical structure involved in the initiation propagation of audiogenic seizures (Ribak and Morin, 1995; Pinto et al., 2019). Hence, our findings indicating the overexpression of *Grik1* in the IC suggest a potential contribution to heightened excitatory signaling and the potential disruption of neuronal activity balance, even in the absence of seizures. Furthermore, our results revealed that the *Grik1* gene expression was higher in the cerebellum and superior colliculus compared to the epileptogenic focus of the GASH/Sal model. This observation is noteworthy considering the role of the IC in transmitting epileptogenic events primarily through the deep layers of the superior colliculus to the motor nuclei of the brainstem (Faingold and Casebeer, 1999; Fuentes-Santamaría et al., 2007). Consequently, our findings have implications for sensory-motor integration pathways, potentially involving the cerebellum (McCandless and Schwartzenburg, 1982; Streng and Krook-Magnuson, 2021). Glutamate signaling, known for its significant dysregulation in epilepsy, was prominently characterized by layer-wise transcriptional alterations in multiple glutamate receptor genes (Pfisterer et al., 2020). Notably, newly identified genes including those encoding kainate receptor subunits and several AMPA auxiliary proteins, like the shisa9/cysteine-knot AMPAR modulating protein of 44 kDa (SHISA9/CKAMP44), were found dysregulated in epilepsy (Pfisterer et al., 2020). Consistent with these findings, the recent report by García-Peral et al. (2023) identified an altered expression of the SHISA9 protein within the IC of the GASH/Sal model. SHISA9, which is vital for proper brain development, function, and hearing, plays a crucial role in regulating glutamate receptor activity and synaptic transmission strength, potentially participating in tinnitus perception (Bhatt et al., 2022). Tinnitus and hyperacusis has been associated with hyperexcitability and increased spontaneous activity in auditory regions, including the cochlear nucleus (Auerbach et al., 2014) and the IC (Bauer et al., 2008). Consequently, the GASH/Sal model exhibits the morphological and molecular alterations that correlated with this hearing impairments as well as an inherited susceptibility to audiogenic seizure (Sánchez-Benito et al., 2017, 2020). Our results further suggest that the altered gene expression of *Grik1* may be a key factor contributing to the molecular correlates observed in the GASH/Sal model that led to elevated hyperactivity, enhanced synchrony, and disrupted neurotransmitter balance within seizure neuronal network. Indeed, the expression of immediate-early genes, which is part of the general neuronal response to natural stimuli, has been linked to the instability of homeostatic plasticity in tinnitus within the IC (Hu et al., 2014). This finding is consistent with our previous reports, demonstrating the overexpression of immediate-early genes in the IC of two genetically rodent models of audiogenic seizures (López-López et al., 2017; Damasceno et al., 2020; Díaz-Rodríguez et al., 2020). Certainly, the dysregulation of gene expression that influences the imbalance of neurotransmitters in the epileptogenic focus and the associated seizure neuronal network in the GASH/Sal is far more intricate. For instance, the cannabinoid system has been identified as playing a role in the regulation of auditory stimuli in the IC (Valdés-Baizabal et al., 2017). Additionally, glutamate can control inhibitory synaptic transmission through the simultaneous activation of presynaptic GluK1-containing kainate receptors and cannabinoid type 1 receptors (Kano et al., 2009; Lourenço et al., 2010). Therefore, it is plausible that any gene expression disruptions in those receptors could affect neuronal excitability. In a recent study, Fuerte-Hortigón et al. (2021) reported lower gene expression of cannabinoid type 1 receptors in the GASH/Sal inferior colliculus, as well as higher expression in the GASH/Sal hippocampus compared to wild-type counterparts. These findings, combined with our own observations of lower gene expression of *Grik1* in the GASH/Sal inferior colliculus and hippocampus, support the loss of this intrinsic synaptic modulation, contributing to the molecular basis of audiogenic seizure susceptibility. Notwithstanding, further investigations are necessary to understand the exact mechanisms by which dysregulation of kainate receptors and secondary neuromodulatory agents like the endocannabinoid system may alter neurotransmitter release in the GASH/Sal inferior colliculus and associated brain regions.

4.3 Alterations in Gluk1 protein levels within the GASH/Sal seizure neuronal network

Gene expression alterations do not always correlate directly with changes in protein levels due to the complex interplay of post-transcriptional, translational and protein degradation mechanisms (Vogel and Marcotte, 2012). Therefore, our study took a dual approach, examining both mRNA and protein levels, to thoroughly explore the implications of the *Grik1* polymorphism within the seizure neuronal network of the GASH/Sal model. Western blot analysis proved invaluable in exploring the molecular disparities between genetic rodent models of epilepsy and their wild-type counterparts, particularly for investigating altered protein abundance in specific brain regions (Bosque et al., 2021). Using the immunoblotting technique, we observed significant changes in GluK1 protein levels within the seizure associated structures of the GASH/Sal model. This finding prompts us to consider the interaction between GluK1 receptors and K^+/Cl^- cotransporters, in order to shed light on the potential impact of GluK1-protein level disruption. It is well-established that subunits of kainate-type glutamate receptors, including GluK1 and GluK2, play a crucial role in the oligomerization and surface expression of

K^+/Cl^- cotransporters (Mahadevan et al., 2014). Furthermore, recent studies on the GASH/Sal strain have reported reduced levels of cation-chloride cotransporters NKCC1 and KCC2 in epileptic brain regions, both at rest and following repeated sound-induced seizures (Prieto-Martín et al., 2017; Bonet-Fernández et al., 2023). These authors suggested impaired functionality of the GABAergic system in the GASH/Sal model, as neuron-specific K^+/Cl^- cotransporters NKCC1 and KCC2 are pivotal for maintaining low intracellular Cl^- levels, which are essential for facilitating rapid inhibitory synaptic transmission in the normal central nervous system (Prieto-Martín et al., 2017; Bonet-Fernández et al., 2023). Considering these facts, our observation of altered GluK1-protein abundance may indeed influence K^+/Cl^- cotransporters, potentially disrupting the delicate balance between inhibition and excitation, thus contributing to the heightened susceptibility of the GASH/Sal model to audiogenic seizures. An intriguing finding in our study was the presence of two distinct bands in the inferior and superior colliculi of the GASH/Sal model: the expected band size of ∼104 kDa and an additional band at ∼65 kDa. A well-established phenomenon is that alternative splicing in transcripts significantly enhances proteome diversity by enabling a single gene to produce multiple distinct isoforms. In this context, if the splicing events result in different protein isoforms that retain the epitope recognized by the antibody, then Western blotting can indeed show multiple bands corresponding to these isoforms. Our multiple sequence alignment confirmed that the GluK1-antibody we used in our study effectively recognized a highly conserved antigenic region across all isoforms in hamsters, and hence, the antibody can bind to each isoform, leading to distinct bands on the blot. Notably, our results in the GASH/Sal contrasts sharply with those obtained in wild-type animals, where the 65-kDa band consistently remained absent across all brain structures. This stark difference suggests that the presence of the 65-kDa band in the GASH/Sal collicular structures may likely be attributed to a splicing variant unique to the GASH/Sal strain. Nevertheless, verifying this hypothesis will require empirical investigation, as other factors, such as post-translational protein modifications and the regulation of protein degradation, can also contribute to the presence of multiple bands in Western blots. Regarding kainate receptors, alternative splicing significantly enhances the functional spectrum of GluK1 receptors as these splice variants differ in their tissue-specific expression, membrane delivery processes, and protein interactions (Jaskolski et al., 2004). Therefore, our observations gain significance considering recent studies suggesting that splicing events affecting the ATD of GluK1 receptors have the potential to impact receptor assembly, stability, and modulation by interacting with the corresponding auxiliary proteins neuropilin and tolloid-like (Neto) (Dhingra et al., 2023).

4.4 Abnormal distribution of Gluk1 receptors within the GASH/Sal seizure neuronal network

In line with the established workflow for comprehensively studying protein biology in genetic rodent models of epilepsy (Bosque et al., 2021), our study extended its scope by conducting an immunohistochemical analysis of the GluK1 protein in the hamster brain. Thus, we provided crucial spatial and anatomical information about GluK1 distribution within the GASH/Sal seizure neuronal network. Interpreting the GluK1-immunolabeling pattern in hamster brain tissue posed challenges, primarily because these immunolabeled structures only became discernible at high magnifications. The scattered and faint GluK1-immunolabeling could, in part, be attributed to the section thickness (40 μm), potentially affecting staining penetration and the sensitivity for identifying individual processes. Thus, to ensure accurate interpretation, our study utilized a combined analysis, using both bright-field and confocal microscopes. The confocal fluorescence microscopy enabled us to capture thin sections of the sample and acquire a series of images at multiple discrete focus levels, providing a 3D view of the samples that was subsequently presented in videos as in previous studies (Gómez-Nieto et al., 2008b). We observed diffuse GluK1-immunoreactivity spread throughout the hamster brain, with concentrations in subcellular compartments such as neuronal perikarya, axonal fiber tracts, and terminals. Surprisingly, we were unable to identify clearly postsynaptic elements, including dendrites, spines, and dendritic shafts, that were expected to contain GluK1 receptors (Vesikansa et al., 2012). This does not conclusively exclude the possibility of GluK1 receptors being present in postsynaptic elements within the hamster brain. Some of the diffuse punctate immunostaining in the neuropile may indeed indicate immunostaining of both postsynaptic elements and axons, a phenomenon that can be associated with the sectioning process during brain tissue preparation. Achieving a clearer view of these postsynaptic structures may require the use of higher-resolution imaging techniques like transmission electron microscopy that can confirm their identity and offer valuable insights into the distribution of GluK1 receptors in these subcellular regions. An additional constraint in our study arises from the presence of GluK1 receptors in glial cells, including astrocytes, as reported by Eyigor et al. (2005) and Vargas et al. (2013). We did not employ a specific marker for glial cells, which leaves open the possibility that some of the staining observed in the neuropile may have also encompassed glial cells. Indeed, as demonstrated by Vargas et al. (2013) in an immunohistochemistry study, reactive hippocampal astrocytes were shown to express GluK1 subunits in a chemically induced temporal lobe epilepsy model. In this model, astrocytes initiated the expression of kainate receptors in response to seizure activity (Vargas et al., 2013). Thus, it may be worthwhile to investigate a similar phenomenon in GASH/Sal animals following repeated seizure stimulations or under kindling conditions.

The pattern of GluK1-immunoreactivity observed in the wild-type hamster brain in our study closely resembles that reported in brain areas of other mammalian species, with certain disparities also noted. As in our results, GluK1-immunolabeling decorating neuronal perikarya has been reported in the arcuate nucleus, hypothalamus, and dorsal cochlear nucleus of the rat (Diano et al., 1998; Eyigor et al., 2005; reviewed in Wu and Tang, 2023) as well as in the neocortex and hippocampus of dogs and monkeys (Good et al., 1993; Huntley et al., 1993; Hof et al., 1996). Furthermore, a notable finding in hamsters was the robust GluK1-immunolabeling present in presynaptic terminals, including axonal fibers and terminals. This observation stands in contrast to previous studies on the immunocytochemical localization of GluK1 receptors, where antibodies recognizing all low-affinity kainate receptor subunits (GluR5/6/7) resulted in either no labeling or

very weak staining of axons (Good et al., 1993; Huntley et al., 1993; Diano et al., 1998). It is important to note that these earlier studies utilized antibodies that did not permit the individual and specific identification of the GluK1 subunit. Consequently, the previous conclusion that there was little or no definitive staining in presynaptic terminals may warrant reevaluation. Our study found significant GluK1 allocation in axonal fibers and terminals, aligning with latest research that demonstrates the role of Neto auxiliary proteins in regulating presynaptic kainate receptors and promoting the axonal recruitment of GluK1, thereby contributing to synaptic connectivity (Vesikansa et al., 2012; Orav et al., 2017).

Comparing wild-type and GASH/Sal hamsters, we observed significant differences in GluK1 distribution within crucial nuclei of the seizure neuronal network in the GASH/Sal model. Consistently with our findings, the presence of the GluK1 subunit has been previously documented in the cerebellar cortex, including within the granule and Purkinje cell layers (Bettler et al., 1990). In the GASH/Sal cerebellum, we observed a significant reduction in GluK1 protein levels and the corresponding immunoreactivity, particularly in the axons of cerebellar granule cells that form parallel fibers. This reduction implies an imbalance in excitatory signaling, leading to hyperexcitability and a higher likelihood of synchronous firing of neurons within the cerebellum. These observations lend support to the idea that the cerebellum actively participates in seizure events, rather than solely reflecting the motor aspects of seizures (Streng and Krook-Magnuson, 2021). Notably, one of the most striking distinctions in GluK1 distribution between wild-type and GASH/Sal hamsters was evident in the IC. The IC, with its distinct subdivisions, plays a critical role in audiogenic seizure activity, with the central subdivision involved in seizure initiation and the external/dorsal cortices contributing to seizure propagation (Ross and Coleman, 2000). Therefore, our findings, which reveal variations in GluK1 distribution between the central and dorsal/external regions of the IC, may correlate to the specific roles of these subdivisions in the mechanisms of audiogenic seizures in the GASH/Sal model. Our consistent results across the three employed methodological approaches (gene expression analysis, protein levels assessment, and immunohistochemistry) further support the notion that alterations in GluK1 receptors persist in the superior colliculus. This outcome is logically aligned with the interconnection of these two collicular structures and their role in audiogenic seizures (Garcia-Cairasco et al., 1993; Faingold, 1999, 2012; Ross and Coleman, 2000). The hippocampal formation is another structure closely associated with epileptogenicity (Reid et al., 1983; Ben-Ari, 1985) and the presence of GluK1 receptors, capable of co-assembling with other kainate receptor subunits in hippocampal neurons, suggests a previously underestimated diversity of these receptors and an enhanced functional complexity in this region (Paternain et al., 2000). In the GASH/Sal model, we observed a significant reduction in GluK1-immunoreactivity within the hippocampal regions, a finding that correlates with the decreased expression of the *Grik1* gene in this structure. The interpretation of these results is challenging, given the lack of consensus among studies focusing on the hippocampus and the role of GluK1 receptors in seizures. Some researchers showed that selective agonists of kainate receptors containing GluK1 induce seizure activity in preclinical models of epilepsy and observed that GluK1 knock-out mice exhibited reduced thresholds for behavioral arrest and clonic seizures (Fritsch et al., 2014). In contrast, Smolders et al. (2002) and Figueiredo et al. (2011) have shown that GluK1 antagonists inhibit seizure activity in various *in vitro* and *in vivo* models. Consequently, some authors have suggested that seizure protection can be achieved through inhibition of GluK1 receptors (Smolders et al., 2002; Figueiredo et al., 2011), while others propose that activating these receptors represents a promising antiepileptic strategy (Khalilov et al., 2002). In any case, genetically audiogenic seizure models are increasingly considered as prospective models for human temporal lobe epilepsy (Poletaeva et al., 2017; Kulikov et al., 2022), and hence, further investigation of the GASH/Sal hippocampus, particularly following audiogenic seizure stimulation, is warranted. The prefrontal cortex is involved in the generalized seizures of various genetic rodent models, in which a decline of histamine receptors has been reported in the lateral and medial prefrontal regions in the prefrontal cortex as well as the insular and cingulate cortices (Midzyanovskaya et al., 2022). However, as far as we are aware, there are no studies focused on GluK1 receptors in this context. Our results indicated GASH/Sal animals exhibited altered GluK1-immunoreactivity in the motor and cingulate cortices as well as the isidium griseum. The marked reduced immunoreactivity in the isidium griseum, a commissural hippocampal pathway that is targeted during palliative epilepsy surgery (Fauser and Zentner, 2012), might suggest a declined GluK1 receptor activity that can lead to an increase in glutamate release, which in turn enhance neuronal excitability in the afferent nuclei. An important observation from our image analysis in the prefrontal cortex was the concentrated presence of GluK1-immunoreactivity in close proximity to the cell nucleus. This peculiar subcellular distribution of GluK1 was consistently observed in the other brain areas such as the IC and hippocampus, and this pattern was more frequently seen in the GASH/Sal group compared to the wild type. The proper surface expression and synaptic trafficking of the GluK1 receptor depend on the presence of auxiliary Neto proteins (Sheng et al., 2015). Additionally, the signal peptide of GluK1 interacts directly with the ATD to inhibit the synaptic and surface expression of GluK1 (Duan et al., 2018). Considering the established influence of the extracellular ATD on the trafficking properties of GluK1 (Duan et al., 2018), it is plausible to suggest that the p.H289Y polymorphism within this domain could potentially affect the trafficking mechanism of GluK1 in the GASH/Sal model. Different isoforms of the GluK1 receptor (GluK1a, GluK1b, and GluK1c) have distinct patterns of cellular localization. While GluK1a and GluK1b can be found at the plasma membrane, the majority of GluK1c subunits predominantly remain confined in the endoplasmic reticulum (reviewed in Pahl et al., 2014). The predominant localization of GluK1-immunolabeling near the cell nucleus in the GASH/Sal model suggests that the p.H289Y polymorphism may disrupt the normal subcellular trafficking of GluK1, potentially contributing to the overall altered distribution of GluK1 protein in the GASH/Sal brain. In line with this observation, our research group concurrently conducted a functional analysis to assess the impact of the single-point mutation p.H289Y on GluK1 receptors through their expression in *Xenopus laevis* oocytes (Díaz-Rodríguez et al., 2023). Using confocal immunofluorescence microscopy to examine the distribution of GluK1 receptors within the oocytes and the two-electrode voltage-clamp technique to evaluate the mutation's functional implications, Díaz-Rodríguez et al. (2023) found that this genetic variant potentially modifies the

trafficking mechanism of GluK1, leading to increased expression and integration of mutated receptors into the oocyte membrane. Additionally, the study noted that the p.H289Y polymorphism enhances kainate-evoked currents without substantially altering the functional properties of the GluK1 receptor (Díaz-Rodríguez et al., 2023).

In summary, our study reinforces the substantial body of evidence implicating GluK1 receptors in the mechanisms underlying seizures. Human genetic studies involving families affected by idiopathic juvenile absence epilepsy have revealed elevated levels of *Grik1* polymorphisms (Sander et al., 1997). Moreover, patients with temporal lobe epilepsy exhibit modifications in GluK1 subunit expression, thereby impacting the kainate receptor function (Li et al., 2010). Rat models subjected to kainic acid-induced status epilepticus have documented disturbances in mRNA transcripts and concurrent alterations in GluK1 protein levels (Ullal et al., 2005). Notably, pharmacological investigations, particularly in the development of novel antiseizure medications, have increasingly emphasized the importance of GluK1 receptors. For instance, the anticonvulsant properties of the well-established antiepileptic drug topiramate are partly attributed to GluK1 receptor blockade (Kaminski et al., 2004). Additionally, it has been demonstrated that GluK1 receptor agonists can induce clonic seizures (Rogawski et al., 2003; Kaminski et al., 2004). Consequently, our study offers pivotal insights into the widespread alterations of GluK1 in various anatomical regions of the GASH/Sal model. This information is of paramount importance, as it lays the foundation for future experiments involving the administration of agonists or antagonists targeting kainate receptors containing GluK1 subunits. These investigations are indispensable for evaluating the potential antiseizure efficacy of GluK1 as a therapeutic target in epilepsy research.

Data availability statement

The original contributions presented in the study are included in the article/**Supplementary material**, further inquiries can be directed to the corresponding author.

Ethics statement

The animal study was approved by the Bioethics Committee of the University of Salamanca (approval number 375). The study was conducted in accordance with the local legislation and institutional requirements.

Author contributions

SD-R: Data curation, Formal analysis, Investigation, Methodology, Visualization, Writing – review and editing. MH-T: Formal analysis, Investigation, Writing – review and editing. CG-P: Formal analysis, Investigation, Methodology, Software, Visualization, Writing – review and editing. RG-N: Conceptualization, Data curation, Formal analysis, Funding acquisition, Investigation, Methodology, Project administration, Resources, Supervision, Validation, Visualization, Writing – original draft, Writing – review and editing.

Funding

The author(s) declare financial support was received for the research, authorship, and/or publication of this article. This study was supported by a grant from Consejería de Educación de la Junta de Castilla y León (#SA075P20, RG-N), and co-funded by ERDF: "A way of making Europe." SD-R held a JCyL predoctoral fellowship 2019 (BOCYL, EDU/556/2019).

Acknowledgments

The authors extend their heartfelt gratitude to Prof. Dolores E. López for securing funding (Project #SA075P20) and conceiving the original idea, as well as her invaluable insights and feedback during the manuscript's development. Special thanks are also due to Dr. Jose María de Pereda for his expert guidance in the preliminary analysis of protein 3D structures. We would like to acknowledge the dedicated technical assistance provided by Laura Zeballos and members of the Laboratory of Audiomotor Disorders at the Institute of Neuroscience of Castilla y León.

Conflict of interest

The authors declare that the research was conducted in the absence of any commercial or financial relationships that could be construed as a potential conflict of interest.

Publisher's note

Supplementary material

The Supplementary Material for this article can be found online at: https://www.frontiersin.org/articles/10.3389/fnmol.2023.1322750/full#supplementary-material

SUPPLEMENTARY MATERIAL 1
Topology of the GluK1 subunit, conserved epitope in GluK1 isoforms and sequence identity. **(A)** Scheme showing the topology of the GluK1 protein. The GluK1 subunit contains an extracellular amino-terminal domain (ATD) followed by a transmembrane domain (M1), a "p-loop" that dips in the lipid bilayer and forms the pore (M2), two successive transmembrane domains (M3 and M4) that delineate an extracellular loop, and an intracellular C-terminal domain (CTD). The glutamate-binding site is composed of two apposed segments (S1 and S2) in the ATD and the extracellular loop. The ATD of the kainate receptor have bi-lobed clamshell-like architectures

that are composed of two regulatory domains, named R1 and R2 in upper and lower lobe, respectively. The location of the p.H289Y polymorphism in the GASH/Sal model is in the ATD-R2 domains (depicted with a red asterisk). Scheme based in the information provided in Furukawa (2012) and Selvakumar et al. (2021). **(B)** Representation of the amino acid sequences encoded by the eight identified *Grik1* isoforms in the golden hamster (*M. auratus*, GenBank GCA_017639785.1). The conserved regions between the isoforms are depicted in blue-lilac color. The region shaded in red represents the location of the p.H289Y polymorphism in the ATD and the region shaded in green represents the epitope specifically recognized by the antibody against GluK1 used in this study (see the consensus amino acid sequence at the position 380–430 amino acids). **(C)** Multiple sequence alignment of the *Grik1* isoforms that corresponds to the region shaded in red [position 280–298 amino acids in panel **(B)**], in which the single nucleotide polymorphism (p.His289Tyr; red asterisk) was identified. The longest isoform (identified as canonical) was used as the consensus sequence. Level of each amino acid conservation is represented underneath as a bar chart, using Clustalx coloring (Jalview program 2.11.2 version; http://www.jalview.org/). The conserved columns with a score of 11 are indicated by "χ" (score of 11 with default amino acid property grouping), and columns with a score of 10 have mutations but all properties are conserved are marked with a " + ." **(D)** Multiple sequence alignment of GluK1 (at the positions 281–297 amino acids) in the golden hamster, mouse, rat, and human. Identity values (%) correspond to full-length sequences. Notice that the mutation site (indicated by a red asterisk) is conserved across species.

SUPPLEMENTARY MATERIAL 2
A video showcasing the dynamic rotation of the ribbon representation of the monomeric form of the GluK1 subunit. The 3D protein structures, predicted by AlphaFold, correspond to both the wild-type protein structure and the mutated form (histidine-to-tyrosine substitution at the position 289) found in the GASH/Sal model. This video corresponds to the results depicted in **Figure 2**.

SUPPLEMENTARY MATERIAL 3
Raw data of qPCR used for analyses. The qPCR data included a set of 5 biological replicates (sample cases) for each experimental group (wild-type and GASH/Sal animals), triplicate technical replicates as well as the Ct values of housekeeping genes (β-actin and tubulin) used for data normalization. Abbreviations of genes: *Grik1* (glutamate receptor ionotropic kainate-1); *Actb* (β-actin); *Tbp* (tubulin).

SUPPLEMENTARY MATERIAL 4
Animated video showing 3D renderings of the maximum projection of the confocal stacks depicting the GluK1-immunoreactivity in the inferior colliculus of the wild-type and GASH/Sal hamsters (video corresponding to **Figures 7Ae, Be**, respectively).

SUPPLEMENTARY MATERIAL 5
Confocal micrographs showing Gluk1-immunolabeling in the external cortex of the GASH/Sal inferior colliculus. Orthogonal view from different planes (x/y, x/z or y/z) of the confocal images illustrate GluK1-immunolabeling concentrated around the DAPI-stained nucleus. Scale bar = 10 μ m.

SUPPLEMENTARY MATERIAL 6
Animated video showing 3D renderings of the maximum projection of the confocal stacks depicting the GluK1-immunoreactivity in the superior colliculus of the wild-type hamsters (video corresponding to **Figure 8Ae**).

SUPPLEMENTARY MATERIAL 7
Bright field and confocal micrographs showing Gluk1-immunolabeling in the dentate gyrus of the wild-type and GASH/Sal hamsters. Notice the remarkable reduction of GluK1-punctate immunostaining (arrowheads) in the GASH/Sal hamster as compared to the wild-type animal. The maximum intensity projections of confocal Z-stack immunofluorescence images (depicted in lower part of the panel) show GluK1 (green), NeuN (red), and DAPI staining of DNA (blue). Scale bars = 10 and 5 μm for bright field and confocal images, respectively.

SUPPLEMENTARY MATERIAL 8
Confocal micrographs depicting Gluk1-immunolabeling in the dentate gyrus of the wild-type hamster brain. Maximum intensity projections of confocal Z-stack images show an axonal fiber immunostained for GluK1 (arrows). The panels below show higher magnification in separated channels GluK1 (green), NeuN (red), and DAPI staining of DNA (blue). Scale bars = 5 μm in the upper panel and 2 μm for lower panels.

SUPPLEMENTARY MATERIAL 9
Confocal micrographs showing Gluk1-immunolabeling in the dentate gyrus of the GASH/Sal brain. Orthogonal view from different planes (x/y, x/z or y/z) of the confocal images illustrate GluK1-immunolabeling concentrated around the DAPI-stained nucleus. Scale bar = 5 μ m.

SUPPLEMENTARY MATERIAL 10
Animated video showing 3D renderings of the maximum projection of the confocal stacks, highlighting the GluK1-immunoreactivity in the layer I-II of the cingulate cortex in wild-type hamsters (video corresponding to **Figure 10Ac**).

SUPPLEMENTARY MATERIAL 11
Animated video of the maximum projection of the confocal stacks shows details of GluK1-immunoreactivity in cells of the medial prefrontal cortex (prelimbic area) in the wild-type and GASH/Sal hamsters. Notice reduced punctate GluK1-immunostaining in cell bodies in the GASH/Sal as compared to the control animal.

SUPPLEMENTARY MATERIAL 12
Confocal micrographs showing Gluk1-immunolabeling in the medial prefrontal cortex (cingulate cortex) of the GASH/Sal brain. Orthogonal view from different planes (x/y, x/z or y/z) of the confocal images illustrate GluK1-immunolabeling concentrated around the DAPI-stained nucleus of the neuron depicted with a magenta arrowhead in **Figure 10Bc**. Scale bar = 5 μm.

References

Andersen, C. L., Jensen, J. L., and Ørntoft, T. F. (2004). Normalization of real-time quantitative reverse transcription-PCR data: A model-based variance estimation approach to identify genes suited for normalization, applied to bladder and colon cancer data sets. *Cancer Res.* 64, 5245–5250. doi: 10.1158/0008-5472.CAN-04-0496

Auerbach, B. D., Rodrigues, P. V., and Salvi, R. J. (2014). Central gain control in tinnitus and hyperacusis. *Front. Neurol.* 5:206. doi: 10.3389/fneur.2014.00206

Ayalon, G., and Stern-Bach, Y. (2001). Functional assembly of AMPA and kainate receptors is mediated by several discrete protein-protein interactions. *Neuron* 31, 103–113. doi: 10.1016/s0896-6273(01)00333-6

Barrera-Bailón, B., Oliveira, J. A. C., López, D. E., Muñoz, L. J., Garcia-Cairasco, N., and Sancho, C. (2013). Pharmacological and neuroethological studies of three antiepileptic drugs in the Genetic Audiogenic Seizure Hamster (GASH:Sal). *Epilepsy Behav.* 28, 413–425. doi: 10.1016/j.yebeh.2013.05.028

Barrera-Bailón, B., Oliveira, J., López, D., Muñoz, L., Garcia-Cairasco, N., and Sancho, C. (2017). Pharmacological and neuroethological study of the acute and chronic effects of lamotrigine in the genetic audiogenic seizure hamster (GASH:Sal). *Epilepsy Behav.* 71, 207–217. doi: 10.1016/j.yebeh.2015.11.005

Bauer, C. A., Turner, J. G., Caspary, D. M., Myers, K. S., and Brozoski, T. J. (2008). Tinnitus and inferior colliculus activity in chinchillas related to three distinct patterns of cochlear trauma. *J. Neurosci. Res.* 86, 2564–2578. doi: 10.1002/jnr.21699

Ben-Ari, Y. (1985). Limbic seizure and brain damage produced by kainic acid: Mechanisms and relevance to human temporal lobe epilepsy. *Neuroscience* 14, 375–403. doi: 10.1016/0306-4522(85)90299-4

Ben-Ari, Y. (2012). "Kainate and temporal lobe epilepsies: 3 decades of progress," in *Jasper's basic mechanisms of the epilepsies [Internet]*, 4th Edn, eds J. Noebels, M. Avoli, M. Rogawski, R. Olsen, and A. Delgado-Escueta (Bethesda, MD: National Center for Biotechnology Information).

Bettler, B., Boulter, J., Hermans-Borgmeyer, I., O'Shea-Greenfield, A., Deneris, E. S., Moll, C., et al. (1990). Cloning of a novel glutamate receptor subunit, GluR5: Expression in the nervous system during development. *Neuron* 5, 583–595. doi: 10.1016/0896-6273(90)90213-y

Bhatt, I. S., Wilson, N., Dias, R., and Torkamani, A. (2022). A genome-wide association study of tinnitus reveals shared genetic links to neuropsychiatric disorders. *Sci. Rep.* 12:22511. doi: 10.1038/s41598-022-26413-6

Bonet-Fernández, J. M., Tranque, P., Aroca-Aguilar, J. D., Muñoz, L. J., López, D. E., Escribano, J., et al. (2023). Seizures regulate the cation-Cl- cotransporter NKCC1 in a hamster model of epilepsy: Implications for GABA neurotransmission. *Front. Neurol.* 14:1207616. doi: 10.3389/fneur.2023.1207616

Bosque, J. R., Gómez-Nieto, R., Hormigo, S., Herrero-Turrión, M. J., Díaz-Casado, E., Sancho, C., et al. (2021). Molecular tools for the characterization of seizure

susceptibility in genetic rodent models of epilepsy. *Epilepsy Behav.* 121(Pt. B):106594. doi: 10.1016/j.yebeh.2019.106594

Burns, M. J., Nixon, G. J., Foy, C. A., and Harris, N. (2005). Standardisation of data from real-time quantitative PCR methods - evaluation of outliers and comparison of calibration curves. *BMC Biotechnol.* 5:31. doi: 10.1186/1472-6750-5-31

Cabral-Pereira, G., Sánchez-Benito, D., Díaz-Rodríguez, S. M., Gonçalves, J., Sancho, C., Castellano, O., et al. (2021). Behavioral and molecular effects induced by cannabidiol and valproate administration in the GASH/Sal model of acute audiogenic seizures. *Front. Behav. Neurosci.* 14:612624. doi: 10.3389/fnbeh.2020.612624

Carballosa-Gonzalez, M. M., Muñoz, L. J., López-Alburquerque, T., Pardal-Fernández, J. M., Nava, E., de Cabo, C., et al. (2013). EEG characterization of audiogenic seizures in the hamster strain GASH:Sal. *Epilepsy Res.* 106, 318–325. doi: 10.1016/j.eplepsyres.2013.07.001

Casillas-Espinosa, P. M., Powell, K. L., and O'Brien, T. J. (2012). Regulators of synaptic transmission: Roles in the pathogenesis and treatment of epilepsy. *Epilepsia.* 53(Suppl. 9), 41–58. doi: 10.1111/epi.12034

Contractor, A., Mulle, C., and Swanson, G. T. (2011). Kainate receptors coming of age: Milestones of two decades of research. *Trends Neurosci.* 34, 154–163.

Damasceno, S., Gómez-Nieto, R., Garcia-Cairasco, N., Herrero-Turrión, M. J., Marín, F., and Lopéz, D. E. (2020). Top common differentially expressed genes in the epileptogenic nucleus of two strains of rodents susceptible to audiogenic seizures: WAR and GASH/Sal. *Front. Neurol.* 11:33. doi: 10.3389/fneur.2020.00033

Dhingra, S., Chopade, P. M., Vinnakota, R., and Kumar, J. (2023). Functional implications of the exon 9 splice insert in GluK1 kainate receptors. *eLife* 12:R89755. doi: 10.7554/eLife.89755.1

Diano, S., Naftolin, F., and Horvath, T. L. (1998). Kainate glutamate receptors (GluR5-7) in the rat arcuate nucleus: Relationship to tanycytes, astrocytes, neurons and gonadal steroid receptors. *J. Neuroendocrinol.* 10, 239–247. doi: 10.1046/j.1365-2826.1998.00195.x

Díaz-Casado, E., Gómez-Nieto, R., de Pereda, J. M., Muñoz, L. J., Jara-Acevedo, M., and López, D. E. (2020). Analysis of gene variants in the GASH/Sal model of epilepsy. *PLoS One* 15:e0229953. doi: 10.1371/journal.pone.0229953

Díaz-Rodríguez, S. M., Ivorra, I., Espinosa, J., Vegar Saval, C., Herrero-Turrión, M. J., Lopéz, D. E., et al. (2023). Enhanced membrane incorporation of H289Y mutant GluK1 receptors from the audiogenic seizure-prone GASH/Sal model: Functional and morphological impacts on xenopus oocytes. *Int. J. Mol. Sci.* 24:16852.

Díaz-Rodríguez, S. M., López-López, D., Herrero-Turrión, M. J., Gómez-Nieto, R., Canal-Alonso, A., and Lopéz, D. E. (2020). Inferior colliculus transcriptome after status epilepticus in the genetically audiogenic seizure-prone hamster GASH/Sal. *Front. Neurosci.* 14:508. doi: 10.3389/fnins.2020.00508

Duan, G. F., Ye, Y., Xu, S., Tao, W., Zhao, S., Jin, T., et al. (2018). Signal peptide represses GluK1 surface and synaptic trafficking through binding to amino-terminal domain. *Nat. Commun.* 9:4879. doi: 10.1038/s41467-018-07403-7

Eyigor, O., Minbay, Z., Cavusoglu, I., and Jennes, L. (2005). Localization of kainate receptor subunit GluR5-immunoreactive cells in the rat hypothalamus. *Brain Res. Mol. Brain Res.* 136, 38–44. doi: 10.1016/j.molbrainres.2005.01.015

Faingold, C. L. (1999). Neuronal networks in the genetically epilepsy-prone rat. *Adv. Neurol.* 79, 311–321.

Faingold, C. L. (2012). "Brainstem networks: Reticulo-cortical synchronization in generalized convulsive seizures," in *Jasper's basic mechanisms of the epilepsies [Internet]*, 4th Edn, eds J. Noebels, M. Avoli, M. Rogawski, et al. (Bethesda, MD: National Center for Biotechnology Information).

Faingold, C. L., Naritoku, D. K., Copley, C. A., Randall, M. E., Riaz, A., Anderson, C. A., et al. (1992). Glutamate in the inferior colliculus plays a critical role in audiogenic seizure initiation. *Epilepsy Res.* 13:95e105.

Faingold, C., and Casebeer, D. (1999). Modulation of the audiogenic seizure network by noradrenergic and glutamatergic receptors of the deep layers of superior colliculus. *Brain Res.* 821, 392–399. doi: 10.1016/s0006-8993(99)01101-4

Falcón-Moya, R., Sihra, T. S., and Rodríguez-Moreno, A. (2018). Kainate receptors: Role in epilepsy. *Front. Mol. Neurosci.* 11:217. doi: 10.3389/fnmol.2018.00217

Fauser, S., and Zentner, J. (2012). Critical review of palliative surgical techniques for intractable epilepsy. *Adv. Tech.Stand. Neurosurg.* 39, 165–194. doi: 10.1007/978-3-7091-1360-8_7

Figueiredo, T. H., Qashu, F., Apland, J. P., Aroniadou-Anderjaska, V., Souza, A. P., and Braga, M. F. (2011). The GluK1 (GluR5) Kainate/{alpha}-amino-3-hydroxy-5-methyl-4-isoxazolepropionic acid receptor antagonist LY293558 reduces soman-induced seizures and neuropathology. *J. Pharmacol. Exp. Ther.* 336, 303–312. doi: 10.1124/jpet.110.171835

Fisher, R. S., Boas, W., van, E., Blume, W., Elger, C., Genton, P., et al. (2005). Epileptic seizures and epilepsy: Definitions proposed by the International League Against Epilepsy (ILAE) and the International Bureau for Epilepsy (IBE). *Epilepsia* 46, 470–472. doi: 10.1111/j.0013-9580.2005.66104.x

Fritsch, B., Reis, J., Gasior, M., Kaminski, R. M., and Rogawski, M. A. (2014). Role of GluK1 kainate receptors in seizures, epileptic discharges, and epileptogenesis. *J. Neurosci.* 34, 5765–5775. doi: 10.1523/JNEUROSCI.5307-13.2014

Fuentes-Santamaría, V., Alvarado, J. C., Herranz, A. S., García-Atarés, N., and López, D. E. (2007). Morphologic and neurochemical alterations in the superior colliculus of the genetically epilepsy-prone hamster (GPG/Vall). *Epilepsy Res.* 75, 206–219. doi: 10.1016/j.eplepsyres.2007.06.005

Fuerte-Hortigón, A., Gonçalves, J., Zeballos, L., Masa, R., Gómez-Nieto, R., and López, D. E. (2021). Distribution of the cannabinoid receptor type 1 in the brain of the genetically audiogenic seizure-prone hamster GASH/Sal. *Front. Behav. Neurosci.* 15:613798. doi: 10.3389/fnbeh.2021.613798

Furukawa, H. (2012). Structure and function of glutamate receptor amino terminal domains. *J .Physiol.* 590, 63–72. doi: 10.1113/jphysiol.2011.213850

Gangwar, S. P., Yen, L. Y., Yelshanskaya, M. V., and Sobolevsky, A. I. (2023). Positive and negative allosteric modulation of GluK2 kainate receptors by BPAM344 and antiepileptic perampanel. *Cell Rep.* 42:112124. doi: 10.1016/j.celrep.2023.112124

Garcia-Cairasco, N. (2002). A critical review on the participation of inferior colliculus in acoustic-motor and acoustic-limbic networks involved in the expression of acute and kindled audiogenic seizures. *Hear. Res.* 168, 208–222. doi: 10.1016/s0378-5955(02)00371-4

Garcia-Cairasco, N., Terra, V. C., and Doretto, M. C. (1993). Midbrain substrates of audiogenic seizures in rats. *Behav Brain Res.* 58, 57–67. doi: 10.1016/0166-4328(93)90090-d

García-Peral, C., Ledesma, M. M., Herrero-Turrión, M. J., Gómez-Nieto, R., Castellano, O., and López, D. E. (2023). Proteomic and bioinformatic tools to identify potential hub proteins in the audiogenic seizure-prone hamster GASH/Sal. *Diagnostics* 13:1048. doi: 10.3390/diagnostics13061048

Gerasimavicius, L., Liu, X., and Marsh, J. A. (2020). Identification of pathogenic missense mutations using protein stability predictors. *Sci. Rep.* 10:15387. doi: 10.1038/s41598-020-72404-w

Gómez-Nieto, R., Horta-Júnior Jde, A., Castellano, O., Millian-Morell, L., Rubio, M. E., and López, D. E. (2014a). Origin and function of short-latency inputs to the neural substrates underlying the acoustic startle reflex. *Front. Neurosci.* 8:216. doi: 10.3389/fnins.2014.00216

Gómez-Nieto, R., Horta-Junior, J. A., Castellano, O., Herrero-Turrión, M. J., Rubio, M. E., and López, D. E. (2008b). Neurochemistry of the afferents to the rat cochlear root nucleus: Possible synaptic modulation of the acoustic startle. *Neuroscience* 154, 51–64.

Gómez-Nieto, R., Rubio, M. E., and López, D. E. (2008a). Cholinergic input from the ventral nucleus of the trapezoid body to cochlear root neurons in rats. *J. Comp. Neurol.* 506, 452–468.

Gómez-Nieto, R., Sinex, D. G., Horta-Júnior Jde, A., Castellano, O., Herrero-Turrión, J. M., and López, D. E. (2014b). A fast cholinergic modulation of the primary acoustic startle circuit in rats. *Brain Struct. Funct.* 219, 1555–1573. doi: 10.1007/s00429-013-0585-8

Good, P. F., Huntley, G. W., Rogers, S. W., Heinemann, S. F., and Morrison, J. H. (1993). Organization and quantitative analysis of kainate receptor subunit GluR5-7 immunoreactivity in monkey hippocampus. *Brain Res.* 624, 347–353. doi: 10.1016/0006-8993(93)90102-s

Herrero-Turrión, M. J., Rodríguez-Martín, I., López-Bellido, R., and Rodríguez, R. E. (2014). Whole-genome expression profile in zebrafish embryos after chronic exposure to morphine: Identification of new genes associated with neuronal function and mu opioid receptor expression. *BMC Genomics* 15:874. doi: 10.1186/1471-2164-15-874

Hof, P. R., Vissavajjhala, P., Rosenthal, R. E., Fiskum, G., and Morrison, J. H. (1996). Distribution of glutamate receptor subunit proteins GluR2(4), GluR5/6/7, and NMDAR1 in the canine and primate cerebral cortex: A comparative immunohistochemical analysis. *Brain Res.* 723, 77–89. doi: 10.1016/0006-8993(96)00218-1

Hu, S. S., Mei, L., Chen, J. Y., Huang, Z. W., and Wu, H. (2014). Expression of immediate-early genes in the inferior colliculus and auditory cortex in salicylate-induced tinnitus in rat. *Eur. J. Histochem.* 58:2294. doi: 10.4081/ejh.2014.2294

Huntley, G. W., Rogers, S. W., Moran, T., Janssen, W., Archin, N., Vickers, J. C., et al. (1993). Selective distribution of kainate receptor subunit immunoreactivity in monkey neocortex revealed by a monoclonal antibody that recognizes glutamate receptor subunits GluR5/6/7. *J. Neurosci.* 13, 2965–2981. doi: 10.1523/JNEUROSCI.13-07-02965.1993

Ittisoponpisan, S., Islam, S. A., Khanna, T., Alhuzimi, E., David, A., and Sternberg, M. J. E. (2019). Can predicted protein 3D structures provide reliable insights into whether missense variants are disease associated? *J. Mol. Biol.* 431, 2197–2212. doi: 10.1016/j.jmb.2019.04.009

Izzi, C., Barbon, A., Kretz, R., Sander, T., and Barlati, S. (2002). Sequencing of the GRIK1 gene in patients with juvenile absence epilepsy does not reveal mutations affecting receptor structure. *Am. J. Med. Genet.* 114, 354–359. doi: 10.1002/ajmg.10254

Jaskolski, F., Coussen, F., Nagarajan, N., Normand, E., Rosenmund, C., and Mulle, C. (2004). Subunit composition and alternative splicing regulate membrane delivery of kainate receptors. *J. Neurosci.* 24, 2506–2515. doi: 10.1523/JNEUROSCI.5116-03.2004

Jubb, H. C., Higueruelo, A. P., Ochoa-Montaño, B., Pitt, W. R., Ascher, D. B., and Blundell, T. L. (2017). Arpeggio: A web server for calculating and visualising

interatomic interactions in protein structures. *J. Mol. Biol.* 429, 365–371. doi: 10.1016/j.jmb.2016.12.004

Jumper, J., Evans, R., Pritzel, A., Green, T., Figurnov, M., Ronneberger, O., et al. (2021). Highly accurate protein structure prediction with AlphaFold. *Nature* 596, 583–589. doi: 10.1038/s41586-021-03819-2

Kaminski, R. M., Banerjee, M., and Rogawski, M. A. (2004). Topiramate selectively protects against seizures induced by ATPA, a GluR5 kainate receptor agonist. *Neuropharmacology* 46, 1097–1104. doi: 10.1016/j.neuropharm.2004.02.010

Kandratavicius, L., Balista, P. A., Lopes-Aguiar, C., Ruggiero, R. N., Umeoka, E. H., Garcia-Cairasco, N., et al. (2014). Animal models of epilepsy: Use and limitations. *Neuropsychiatr. Dis. Treat.* 10, 1693–1705. doi: 10.2147/NDT.S50371

Kano, M., Ohno-Shosaku, T., Hashimotodani, Y., Uchigashima, M., and Watanabe, M. (2009). Endocannabinoid-mediated control of synaptic transmission. *Physiol Rev.* 89, 309–380.

Khalilov, I., Hirsch, J., Cossart, R., and Ben-Ari, Y. (2002). Paradoxical anti-epileptic effects of a GluR5 agonist of kainate receptors. *J. Neurophysiol.* 88, 523–527.

Koide, S., and Sidhu, S. S. (2009). The importance of being tyrosine: Lessons in molecular recognition from minimalist synthetic binding proteins. *ACS Chem. Biol.* 4, 325–334. doi: 10.1021/cb800314v

Kopczynska, M., Zelek, W. M., Vespa, S., Touchard, S., Wardle, M., Loveless, S., et al. (2018). Complement system biomarkers in epilepsy. *Seizur.* 60, 1–7. doi: 10.1016/j.seizure.2018.05.016

Krieger, J., Bahar, I., and Greger, I. H. (2015). Structure, dynamics, and allosteric potential of ionotropic glutamate receptor n-terminal domains. *Biophys. J.* 109, 1136–1148. doi: 10.1016/j.bpj.2015.06.061

Kulikov, A. A., Naumova, A. A., Dorofeeva, N. A., Ivlev, A. P., Glazova, M. V., and Chernigovskaya, E. V. (2022). Dynamics of neurodegeneration in the hippocampus of Krushinsky-Molodkina rats correlates with the progression of limbic seizures. *Epilepsy Behav.* 134:108846. doi: 10.1016/j.yebeh.2022.108846

Kumar, J., Schuck, P., and Mayer, M. L. (2011). Structure and assembly mechanism for heteromeric kainate receptors. *Neuron* 71, 319–331. doi: 10.1016/j.neuron.2011.05.038

Laimer, J., Hiebl-Flach, J., Lengauer, D., and Lackner, P. (2016). MAESTROweb: A web server for structure-based protein stability prediction. *Bioinformatics* 32, 1414–1416. doi: 10.1093/bioinformatics/btv769

Lerma, J., and Marques, J. M. (2013). Kainate receptors in health and disease. *Neuron* 80, 292–311. doi: 10.1016/j.neuron.2013.09.045

Li, J. M., Zeng, Y. J., Peng, F., Li, L., Yang, T. H., Hong, Z., et al. (2010). Aberrant glutamate receptor 5 expression in temporal lobe epilepsy lesions. *Brain Res.* 1311, 166–174. doi: 10.1016/j.brainres.2009.11.024

López-López, D., Gómez-Nieto, R., Herrero-Turrión, M. J., Garcia-Cairasco, N., Sánchez-Benito, D., Ludeña, M. D., et al. (2017). Overexpression of the immediate-early genes Egr1, Egr2, and Egr3 in two strains of rodents susceptible to audiogenic seizures. *Epilepsy Behav.* 71(Pt. B), 226–237. doi: 10.1016/j.yebeh.2015.12.020

Lourenço, J., Cannich, A., Carta, M., Coussen, F., Mulle, C., and Marsicano, G. (2010). Synaptic activation of kainate receptors gates presynaptic CB(1) signaling at GABAergic synapses. *Nat. Neurosci.* 13, 197–204.

Mahadevan, V., Pressey, J. C., Acton, B. A., Uvarov, P., Huang, M. Y., Chevrier, J., et al. (2014). Kainate receptors coexist in a functional complex with KCC2 and regulate chloride homeostasis in hippocampal neurons. *Cell Rep.* 7, 1762–1770. doi: 10.1016/j.celrep.2014.05.022

Matsuda, K., Budisantoso, T., Mitakidis, N., Sugaya, Y., Miura, E., Kakegawa, W., et al. (2016). Transsynaptic modulation of kainate receptor functions by C1q-like Proteins. *Neuron* 90, 752–767. doi: 10.1016/j.neuron.2016.04.001

McCandless, D. W., and Schwartzenburg, F. C. Jr. (1982). Audiogenic seizure-induced changes in energy metabolites in cerebral cortical and cerebellar layers. *Epilepsia* 23, 481–489. doi: 10.1111/j.1528-1157.1982.tb05436.x

Meldrum, B. S. (2000). Glutamate as a neurotransmitter in the brain: Review of physiology and pathology. *J. Nutr.* 130(4S Suppl), 1007S–1015S. doi: 10.1093/jn/130.4.1007S

Mennink, L. M., van Dijk, J. M. C., and van Dijk, P. (2020). The cerebellar (para)flocculus: A review on its auditory function and a possible role in tinnitus. *Hear Res.* 398:108081. doi: 10.1016/j.heares.2020.108081

Midzyanovskaya, I. S., Birioukova, L. M., Storvik, M., Luijtelaar, G. V., and Tuomisto, L. M. (2022). The prefrontal cortex shows widespread decrease in H3 histamine receptor binding densities in rats with genetic generalized epilepsies. *Epilepsy Res.* 182:106921. doi: 10.1016/j.eplepsyres.2022.106921

Morin, L. P., and Wood, R. I. (2001). *A stereotaxic atlas of the golden hamster brain*. New York, NY: Academic Press.

Muñoz, L. J., Carballosa-Gautam, M. M., Yanowsky, K., García-Atarés, N., and López, D. E. (2017). The genetic audiogenic seizure hamster from Salamanca: The GASH:Sal. *Epilepsy Behav.* 71(Pt. B), 181–192. doi: 10.1016/j.yebeh.2016.03.002

Orav, E., Atanasova, T., Shintyapina, A., Kesaf, S., Kokko, M., Partanen, J., et al. (2017). NETO1 guides development of glutamatergic connectivity in the hippocampus by regulating axonal kainate receptors. *eNeuro* 4, ENEURO.48–ENEURO.17. doi: 10.1523/ENEURO.0048-17.2017

Pahl, S., Tapken, D., Haering, S. C., and Hollmann, M. (2014). Trafficking of kainate receptors. *Membranes* 4, 565–595. doi: 10.3390/membranes4030565

Paternain, A. V., Herrera, M. T., Nieto, M. A., and Lerma, J. (2000). GluR5 and GluR6 kainate receptor subunits coexist in hippocampal neurons and coassemble to form functional receptors. *J. Neurosci.* 20, 196–205. doi: 10.1523/JNEUROSCI.20-01-00196.2000

Perez-Ortiz, A. C., Ramírez, I., Cruz-López, J. C., Villarreal-Garza, C., Luna-Angulo, A., Lira-Romero, E., et al. (2017). Pharmacogenetics of response to neoadjuvant paclitaxel treatment for locally advanced breast cancer. *Oncotarget* 8, 106454–106467. doi: 10.18632/oncotarget.22461

Pfisterer, U., Petukhov, V., Demharter, S., Meichsner, J., Thompson, J. J., Batiuk, M. Y., et al. (2020). Identification of epilepsy-associated neuronal subtypes and gene expression underlying epileptogenesis. *Nat. Commun.* 11:5038. doi: 10.1038/s41467-020-18752-7

Pinheiro, P., and Mulle, C. (2006). Kainate receptors. *Cell Tissue Res.* 326, 457–482.

Pinto, H. P. P., de Oliveira Lucas, E. L., Carvalho, V. R., Mourão, F. A. G., de Oliveira Guarnieri, L., Mendes, E. M. A. M., et al. (2019). Seizure susceptibility corrupts inferior colliculus acoustic integration. *Front. Syst. Neurosci.* 13:63. doi: 10.3389/fnsys.2019.00063

Pitkänen, A., and Engel, J. Jr. (2014). Past and present definitions of epileptogenesis and its biomarkers. *Neurotherapeutics* 11, 231–241. doi: 10.1007/s13311-014-0257-2

Poletaeva, I. I., Surina, N. M., Kostina, Z. A., Perepelkina, O. V., and Fedotova, I. B. (2017). The Krushinsky-Molodkina rat strain: The study of audiogenic epilepsy for 65years. *Epilepsy Behav.* 71(Pt. B), 130–141. doi: 10.1016/j.yebeh.2015.04.072

Prieto-Martín, A. I., Aroca-Aguilar, J. D., Sánchez-Sánchez, F., Muñoz, L. J., López, D. E., Escribano, J., et al. (2017). Molecular and neurochemical substrates of the audiogenic seizure strains: The GASH:Sal model. *Epilepsy Behav.* 71(Pt. B), 218–225. doi: 10.1016/j.yebeh.2015.05.025

Reid, H. M., Bowler, K. J., and Weiss, C. (1983). Hippocampal lesions increase the severity of unilaterally induced audiogenic seizures and decrease their latency. *Exp. Neurol.* 81, 240–244. doi: 10.1016/0014-4886(83)90171-1

Ribak, C. E., and Morin, C. L. (1995). The role of the inferior colliculus in a genetic model of audiogenic seizures. *Anat. Embryol.* 191, 279–295. doi: 10.1007/BF00534681

Rodrigues, C. H. M., Pires, D. E. V., and Ascher, D. B. (2021). DynaMut2: Assessing changes in stability and flexibility upon single and multiple point missense mutations. *Protein Sci.* 30, 60–69. doi: 10.1002/pro.3942

Rodríguez-Moreno, A., Herreras, O., and Lerma, J. (1997). Kainate receptors presynaptically downregulate GABAergic inhibition in the rat hippocampus. *Neuron* 19, 893–901. doi: 10.1016/S0896-6273(00)80970-8

Rogawski, M. A., Gryder, D., Castaneda, D., Yonekawa, W., Banks, M. K., and Lia, H. (2003). GluR5 kainate receptors, seizures, and the amygdala. *Ann. N.Y. Acad. Sci.* 985, 150–162.

Ross, K. C., and Coleman, J. R. (2000). Developmental and genetic audiogenic seizure models: Behavior and biological substrates. *Neurosci. Biobehav. Rev.* 24, 639–653.

Sánchez-Benito, D., Gómez-Nieto, R., Hernández-Noriega, S., Murashima, A. A. B., de Oliveira, J. A. C.„ Garcia-Cairasco, N., et al. (2017). Morphofunctional alterations in the olivocochlear efferent system of the genetic audiogenic seizure-prone hamster GASH:Sal. *Epilepsy Behav.* 71(Pt. B), 193–206. doi: 10.1016/j.yebeh.2016.05.040

Sánchez-Benito, D., Hyppolito, M. A., Alvarez-Morujo, A. J., López, D. E., and Gómez-Nieto, R. (2020). Morphological and molecular correlates of altered hearing sensitivity in the genetically audiogenic seizure-prone hamster GASH/Sal. *Hear Res.* 392:107973. doi: 10.1016/j.heares.2020.107973

Sander, T., Hildmann, T., Kretz, R., Fürst, R., Sailer, U., Bauer, G., et al. (1997). Allelic association of juvenile absence epilepsy with a GluR5 kainate receptor gene (GRIK1) polymorphism. *Am. J. Med. Genet.* 74, 416–421.

Savojardo, C., Fariselli, P., Martelli, P. L., and Casadio, R. (2016). INPS-MD: A web server to predict stability of protein variants from sequence and structure. *Bioinformatics.* 32, 2542–2544. doi: 10.1093/bioinformatics/btw192

Schmittgen, T. D., and Livak, K. J. (2008). Analyzing real-time PCR data by the comparative C(T) method. *Nat. Protoc.* 3, 1101–1108. doi: 10.1038/nprot.2008.73

Schymkowitz, J., Borg, J., Stricher, F., Nys, R., Rousseau, F., and Serrano, L. (2005). The FoldX web server: An online force field. *Nucleic Acids Res.* 33, W382–W388. doi: 10.1093/nar/gki387

Selvakumar, P., Lee, J., Khanra, N., He, C., Munguba, H., Kiese, L., et al. (2021). Structural and compositional diversity in the kainate receptor family. *Cell Rep.* 37:109891. doi: 10.1016/j.celrep.2021.109891

Sheng, N., Shi, Y. S., Lomash, R. M., Roche, K. W., and Nicoll, R. A. (2015). Neto auxiliary proteins control both the trafficking and biophysical properties of the kainate receptor GluK1. *Elife* 4:e11682. doi: 10.7554/eLife.11682

Smolders, I., Bortolotto, Z., Clarke, V., Warre, R., Khan, G., O'Neill, M., et al. (2002). Antagonists of GLUK5- containing kainate receptors prevent pilocarpine-induced limbic seizures. *Nat. Neurosci.* 5, 796–804.

Stephan, A. H., Barres, B. A., and Stevens, B. (2012). The complement system: An unexpected role in synaptic pruning during development and disease. *Annu. Rev. Neurosci.* 35, 369–389.

Streng, M. L., and Krook-Magnuson, E. (2021). The cerebellum and epilepsy. *Epilepsy Behav.* 121(Pt. B):106909. doi: 10.1016/j.yebeh.2020.106909

Takano, K., Liu, D., Tarpey, P., Gallant, E., Lam, A., Witham, S., et al. (2012). An X-linked channelopathy with cardiomegaly due to a CLIC2 mutation enhancing ryanodine receptor channel activity. *Hum. Mol. Genet.* 21, 4497–4507. doi: 10.1093/hmg/dds292

Traynelis, S. F., Wollmuth, L. P., McBain, C. J., Menniti, F. S., Vance, K. M., Ogden, K. K., et al. (2010). Glutamate receptor ion channels: Structure, regulation, and function. *Pharmacol. Rev.* 62, 405–496.

Troshin, P. V., Procter, J. B., and Barton, G. J. (2011). Java bioinformatics analysis web services for multiple sequence alignment–JABAWS:MSA. *Bioinformatics* 27, 2001–2002. doi: 10.1093/bioinformatics/btr304

Ullal, G., Fahnestock, M., and Racine, R. (2005). Time-dependent effect of kainate-induced seizures on glutamate receptor GluR5, GluR6, and GluR7 mRNA and Protein Expression in rat hippocampus. *Epilepsia* 46, 616–623.

Valdés-Baizabal, C., Parras, G. G., Ayala, Y. A., and Malmierca, M. S. (2017). Endocannabinoid modulation of stimulus-specific adaptation in inferior colliculus neurons of the rat. *Sci. Rep.* 7:6997. doi: 10.1038/s41598-017-07460-w

Vargas, J. R., Takahashi, D. K., Thomson, K. E., and Wilcox, K. S. (2013). The expression of kainate receptor subunits in hippocampal astrocytes after experimentally induced status epilepticus. *J. Neuropathol. Exp. Neurol.* 72, 919–932. doi: 10.1097/NEN.0b013e3182a4b266

Vesikansa, A., Sakha, P., Kuja-Panula, J., Molchanova, S., Rivera, C., Huttunen, H. J., et al. (2012). Expression of GluK1c underlies the developmental switch in presynaptic kainate receptor function. *Sci. Rep.* 2:310. doi: 10.1038/srep00310

Vogel, C., and Marcotte, E. M. (2012). Insights into the regulation of protein abundance from proteomic and transcriptomic analyses. *Nat. Rev. Genet.* 13, 227–232. doi: 10.1038/nrg3185

Wang, W., Gao, R., Ren, Z., Yang, D., Sun, K., Li, X., et al. (2022). Global trends in research of glutamate in epilepsy during past two decades: A bibliometric analysis. *Front. Neurosci.* 2022:1042642. doi: 10.3389/fnins.2022.1042642

Wang, Z., and Moult, J. (2001). SNPs, protein structure, and disease. *Hum. Mutat.* 17, 263–270. doi: 10.1002/humu.22

Werner, F. M., and Coveñas, R. (2017). Classical neurotransmitters and neuropeptides involved in generalized epilepsy in a multi-neurotransmitter system: How to improve the antiepileptic effect? *Epilepsy Behav.* 71(Pt. B), 124–129. doi: 10.1016/j.yebeh.2015.01.038

Weyer, A., and Schilling, K. (2003). Developmental and cell type-specific expression of the neuronal marker NeuN in the murine cerebellum. *J. Neurosci. Res.* 73, 400–409. doi: 10.1002/jnr.10655

Wu, Q. W., and Tang, Z. Q. (2023). Focusing on the emerging role of kainate receptors in the Dorsal Cochlear Nucleus (DCN) and cerebellum. *Int. J. Mol. Sci.* 24:1718. doi: 10.3390/ijms24021718

International Journal of
Molecular Sciences

MDPI

Article

Enhanced Membrane Incorporation of H289Y Mutant GluK1 Receptors from the Audiogenic Seizure-Prone GASH/Sal Model: Functional and Morphological Impacts on *Xenopus* Oocytes

Sandra M. Díaz-Rodríguez [1,2], Isabel Ivorra [3], Javier Espinosa [3], Celia Vegar [3], M. Javier Herrero-Turrión [1,2,4], Dolores E. López [1,2,*], Ricardo Gómez-Nieto [1,2] and Armando Alberola-Die [3]

1 Neuroscience Institute of Castilla y León (INCyL), University of Salamanca, E-37007 Salamanca, Spain; sdiazrodriguez@usal.es (S.M.D.-R.); mjaviht@usal.es (M.J.H.-T.); richard@usal.es (R.G.-N.)
2 Institute of Biomedical Research of Salamanca (IBSAL), E-37007 Salamanca, Spain
3 Department of Physiology, Genetics and Microbiology, University of Alicante, E-03690 Alicante, Spain; isabel.ivorra@ua.es (I.I.); javier.espinosa@ua.es (J.E.); celia.vegar@ua.es (C.V.); alberoladie.armando@ua.es (A.A.-D.)
4 Neurological Tissue Bank INCYL (BTN-INCYL), University of Salamanca, E-37007 Salamanca, Spain
* Correspondence: lopezde@usal.es

Abstract: Epilepsy is a neurological disorder characterized by abnormal neuronal excitability, with glutamate playing a key role as the predominant excitatory neurotransmitter involved in seizures. Animal models of epilepsy are crucial in advancing epilepsy research by faithfully replicating the diverse symptoms of this disorder. In particular, the GASH/Sal (genetically audiogenic seizure-prone hamster from Salamanca) model exhibits seizures resembling human generalized tonic-clonic convulsions. A single nucleotide polymorphism (SNP; C9586732T, p.His289Tyr) in the *Grik1* gene (which encodes the kainate receptor GluK1) has been previously identified in this strain. The H289Y mutation affects the amino-terminal domain of GluK1, which is related to the subunit assembly and trafficking. We used confocal microscopy in *Xenopus* oocytes to investigate how the H289Y mutation, compared to the wild type (WT), affects the expression and cell-surface trafficking of GluK1 receptors. Additionally, we employed the two-electrode voltage-clamp technique to examine the functional effects of the H289Y mutation. Our results indicate that this mutation increases the expression and incorporation of GluK1 receptors into an oocyte's membrane, enhancing kainate-evoked currents, without affecting their functional properties. Although further research is needed to fully understand the molecular mechanisms responsible for this epilepsy, the H289Y mutation in GluK1 may be part of the molecular basis underlying the seizure-prone circuitry in the GASH/Sal model.

Keywords: epilepsy; GluK1; genetic variant; kainate currents; membrane incorporation; *Xenopus* oocytes

Citation: Díaz-Rodríguez, S.M.; Ivorra, I.; Espinosa, J.; Vegar, C.; Herrero-Turrión, M.J.; López, D.E.; Gómez-Nieto, R.; Alberola-Die, A. Enhanced Membrane Incorporation of H289Y Mutant GluK1 Receptors from the Audiogenic Seizure-Prone GASH/Sal Model: Functional and Morphological Impacts on *Xenopus* Oocytes. *Int. J. Mol. Sci.* **2023**, *24*, 16852. https://doi.org/10.3390/ijms242316852

Academic Editors: Henry Hing Cheong Lee and Elek Molnár

Received: 6 October 2023
Revised: 21 November 2023
Accepted: 23 November 2023
Published: 28 November 2023

1. Introduction

Ionotropic glutamate receptors are ligand-gated ion channels permeable to cations which mediate most of the excitatory synaptic transmission in the central nervous system. They are divided into four functional classes, attending to their sequence identity and pharmacological properties: (i) α-amino-3-hydroxy-5-methyl-4-isoxazolepropionic acid (AMPA) receptors, (ii) kainate receptors (KARs), (iii) N-methyl-d-aspartate (NMDA) receptors, and (iv) glutamate delta (GluD) receptors [1–4]. More specifically, KARs are predominantly arranged in homomeric or heteromeric combinations of five different pore-forming subunits, known as GluK1-5, encoded by the KAR type 1-5 genes (*Grik1-5*) [5,6]. The low-affinity (named for the relative low affinity and agonist potency for glutamate) GluK1-3 subunits can assemble as functional homotetramers and heterotetramers, while the

high-affinity GluK4/5 subunits can only form functional heterotetrameric receptors with GluK1-3 subunits [3,6]. All KAR subunits have a shared architecture composed of (i) a large extracellular amino-terminal domain (ATD), which participates in assembly, trafficking, and the functional regulation of receptors; (ii) a ligand-binding domain (LBD); (iii) a transmembrane domain (TMD), comprising four membrane spanning-segments which form the cation-selective ion channel; and (iv) a cytoplasmic C-terminal domain (CTD), which mediates receptor localization and intracellular regulation [1,7–11]. Alternative splicing of GluK1 CTD can produce four different isoforms named GluK1-a, GluK1-b, GluK1-c [12], and GluK1-d (which is only found in humans [13,14]). GluK1-b is a larger isoform than GluK1-a, comprising an endoplasmic reticulum (ER) retention motif, whereas GluK1-c includes an additional sequence of 29 residues into the CTD of GluK1-b [15]. ATD can also undergo alternative splicing, resulting in GluK1-1 or GluK1-2 isoforms, the former with a 15-residue insertion in this domain. Moreover, RNA editing at the Q/R site, located in the M2 pore-loop of the TMD, drastically changes the properties of the ion channel. Thus, the unedited receptor GluK1(Q) is sensitive to polyamine channel-block and permeable to Ca^{2+}, unlike the edited form GluK1(R) [12,16].

KARs can localize in presynaptic neurons, modulating the release of excitatory and inhibitory neurotransmitters; in postsynaptic neurons, promoting excitatory neurotransmission; and in extrasynaptic ones, contributing to neuronal development and plasticity [2,17,18]. Remarkably, since these receptors have a pivotal role in excitatory neurotransmission, they constitute a key therapeutic target, as their dysfunction causes relevant disorders. Indeed, several alterations in *Grik* genes have been related to Alzheimer's disease, Huntington's chorea, amyotrophic lateral sclerosis, and epilepsy (reviewed in [1,19]). The latter is a chronic neurological disease with a multifactorial origin, including genetic mutations, and is defined by the appearance of sudden and recurrent seizures. Epilepsy has high epidemiological implications worldwide and, therefore, it is important to expand the knowledge on the genetic and functional basis of epilepsy to increasingly discover the inheritance patterns, genetic heterogeneity, and functional mechanisms responsible for this pathology [20]. Animal models of epilepsy serve as indispensable tools for discovering genes and pathways associated with seizures, offering potential avenues for the development of targeted treatments for this condition [21]. A noteworthy example is the genetically audiogenic seizure-prone hamster from Salamanca (GASH/Sal) strain, which exhibits sound-induced seizures (allowing a precise control of them by the experimenter) similar to the generalized tonic–clonic seizures observed in epileptic patients [22–24]. Recently, a whole-exome sequencing in GASH/Sal animals has been performed to identify and characterize the mutational landscape of this strain [25]. It has been described, among other findings, that GASH/Sal hamsters have a moderate-impact variant in the *Grik1* gene that causes a single-point mutation consisting of the substitution of a histidine for a tyrosine at residue 289 (SNP; C9586732T, p.H289Y), located in the ATD of GluK1 receptors (GluK1Rs) [25]. The important role played by GluK1Rs at excitatory synapses in the central nervous system might suggest their involvement in epileptogenesis [26]. Indeed, *Grik1* has been identified previously as an epilepsy-associated gene [27,28], and it has been described in relation to *Grik1* variants with juvenile absence epilepsy [29] and with sudden unexpected death in epilepsy [30]. However, to our knowledge, no epilepsy-related mutations located in the ATD of GluK1Rs have been reported.

In the present work, we studied, using confocal immunofluorescence microscopy, the effects of the single-point mutation H289Y in comparison with their wild-type (WT) on the expression and incorporation to the membrane of GluK1-2aRs that were heterologously expressed in *Xenopus laevis* oocytes. Moreover, to decipher the functional effects of this mutation, we used the two-electrode voltage-clamp technique, which is a well-established, highly robust, and versatile method for the functional evaluation of membrane proteins expressed in oocytes [31].

2. Results

2.1. Assessing the Impact of the H289Y Mutation on the Function and Stability of GluK1Rs using Sequence-Homology Based Tools

The H289Y mutation in GluK1R was subjected to analysis using the sequence homology-based tools Sorting Intolerant From Tolerant (SIFT) and iStable. Both are computational predictors that allowed us to evaluate the impact of the H289Y mutation on the function and thermodynamic stability of GluK1Rs. As a result, the prediction analysis for the H289Y mutation suggested that it was tolerant (SIF score > 0.05) and did not decrease the stability of the protein (iStable conf. score = 0.56).

The results obtained with these kinds of tools are a prediction and constitute a complementary instrument that cannot substitute experimental data obtained in the laboratory. Indeed, SIFT has been reported to perform well in predicting loss-of-function variants [32]. However, the ability to accurately identify variants with a normal function or gain-of-function is inferior, so that more than 40% of variants with altered receptor function demonstrated using biological tests were falsely predicted as benign [32]. Therefore, the expression, localization, and function of WT and H289Y GluK1Rs was evaluated using confocal immunofluorescence microscopy and electrophysiological techniques in *Xenopus* oocytes.

2.2. Expression and Localization of GluK1 Receptors in Xenopus Oocytes

Initially, we microinjected into *Xenopus* oocytes two expression vectors (WT, *Grik1*_WT; and with the mutation, *Grik1*_H289Y; see Figure 1) that contained the complete *Grik1* mRNA sequence, and we did not detect any type of immunolabeling of the corresponding translated GluK1 proteins (WT_GluK1-2b and H289Y_GluK1-2b; Figure 1). The work published by Han et al. [15] allowed us to find out that these GluK1s amino acid sequences translated with the microinjected *Grik1*-mRNAs contained a retention region in the ER and, consequently, GluK1-2bRs could not reach the oocyte plasma membrane. Based on these data, we microinjected two other types of expression vectors for these types of GluK1 proteins, but this time without containing in its sequence the ER retention region (*Grik1*_WT_nER and *Grik1*_H289Y_nER; Figure 1). On these experimental groups, we detected immunolabeling of these types of GluK1 proteins. Thus, both WT GluK1-2aR and H289Y GluK1-2aR reached the oocyte plasma membrane.

Then, we assessed the localization and distribution of WT and H289Y GluK1-2aRs throughout sections of whole oocytes, including the analysis of the distribution of receptors in the animal or vegetal hemispheres of the cells. In these sections, a lower immunoreactivity of WT GluK1-2aRs compared to H289Y GluK1-2aRs was detected (Figure 2A,B). Furthermore, the analysis of the immunoreactivity of GluK1-2aRs using RawIntDen in MATLAB matched the architecture of *Xenopus* oocytes. Therefore, our MATLAB mapping procedure provided a suitable reference for a visual analysis of the GluK1-2aRs' distribution (Figure 2C,D). Regarding the digital mapping of the oocyte-membrane expressing H289Y GluK1-2aRs, an increase in the red scale (larger staining) was calculated in the area of both the animal and vegetal hemispheres in comparison to the expression of WT GluK1-2aRs. The RawIntDen dataset is visually presented in Figure 2E to illustrate the quantitative distinctions between WT GluK1-2aRs and H289Y GluK1-2aRs, demonstrating a statistically significant difference (5654.0 $\pm$ 19.5 mean number of particles for WT GluK1-2a vs. 28764.0 $\pm$ 173.6 mean number of particles for H289Y GluK1-2a; $p < 0.01$). Therefore, there was an accumulation of labeling near the surface of the oocyte in both the animal and vegetal poles, suggesting a selective accumulation of H289Y GluK1-2aRs in this area, showing significant differences between the WT GluK1-2aRs compared to the H289Y GluK1-2aRs.

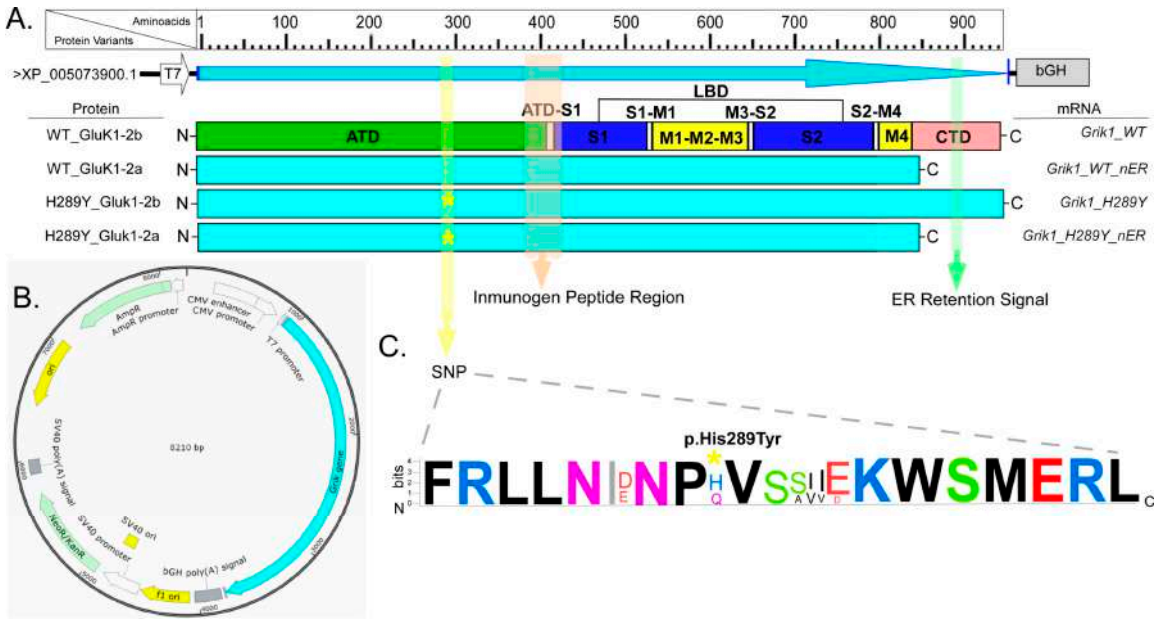

Figure 1. (**A**) Schematic representation of the protein sequences of GluK1, WT and mutated (H289Y). Protein domains are represented with colored bars in GluK1_WT: ATD (amino-terminal domain), S1 and S2 are two segments of the polypeptide chain that together form the ligand-binding domain (LBD), M1–M4 represent transmembrane domains, and CTD is the C-terminal domain. Color arrows show protein regions corresponding to the SNP (H289Y) in the ATD, immunogen peptide region (380–430 aa), and the ER retention sequence (amino acids 841–905). The asterisk (*) in yellow indicates the location of single-point mutation in the protein sequences. (**B**) Schematic representation of the plasmid for in vitro transcription of the distinct variants of *Grik1* gene. (**C**) WebLogo representation of the consensus alignment of the SNP containing region using 50 GluK1 ortholog proteins from different species (78% of conservation), including hamster and humans. It is important to note that the residue at position 289 in WT GluK1 receptor is a histidine (H) in *Mesocricetus auratus*, *Mus musculus*, *Rattus norvegicus*, and *Homo sapiens*. Color code: polar amino acids (G, S, T, Y, C, Q, N) shown in green, basic (K, R, H) in blue, acidic (D, E) in red, and hydrophobic amino acids (A, V, L, I, P, W, F, M) in black. Bits, in the y-axis, indicate the frequency of the corresponding amino acid with the overall height of each stack proportional to the sequence conservation.

Then, using a confocal laser microscope, we conducted a rigorous quantification of GluK1-2aR-immunoreactivity (for both the WT and the mutant) within the *Xenopus* oocyte membrane and the ER proximal to the oocyte membrane. Notably, we observed a significant decrease in immunoreactivity for WT GluK1-2aR (Figure 3A–F) when compared to the H289Y GluK1-2aR (Figure 3G–K) in both the animal (Figure 3M; 2845.0 ± 267.7 a.u. for WT GluK1-2a vs. 6030.0 ± 711.6 a.u. for H289Y GluK1-2a; $p < 0.01$) and vegetal hemisphere membranes (Figure 3N; 2543.0 ± 276.4 a.u. for WT GluK1-2a vs. 4879.0 ± 281.5 a.u. for H289Y GluK1-2a; $p < 0.01$). Furthermore, it is noteworthy that the immunoreactivity of H289Y GluK1-2aR seemed to exhibit a distinct pattern, showing a continuous overlay on the membrane, in contrast to the WT GluK1-2Ra, which displayed well-defined spherical accumulations of approximately 0.3 µm (Figure 3C,F,I,L). Additionally, we identified discernible differences between the animal and vegetal hemispheres within each experimental group. Remarkably, in both experimental groups (WT and mutated receptors), the expression of GluK1-2aRs was higher in some points of the animal hemisphere when shown juxtaposed with the vegetal hemisphere (Figure 3O,P; values at 140 µm for WT and H289Y, and values at 80, 120, and 140 µm for H289Y).

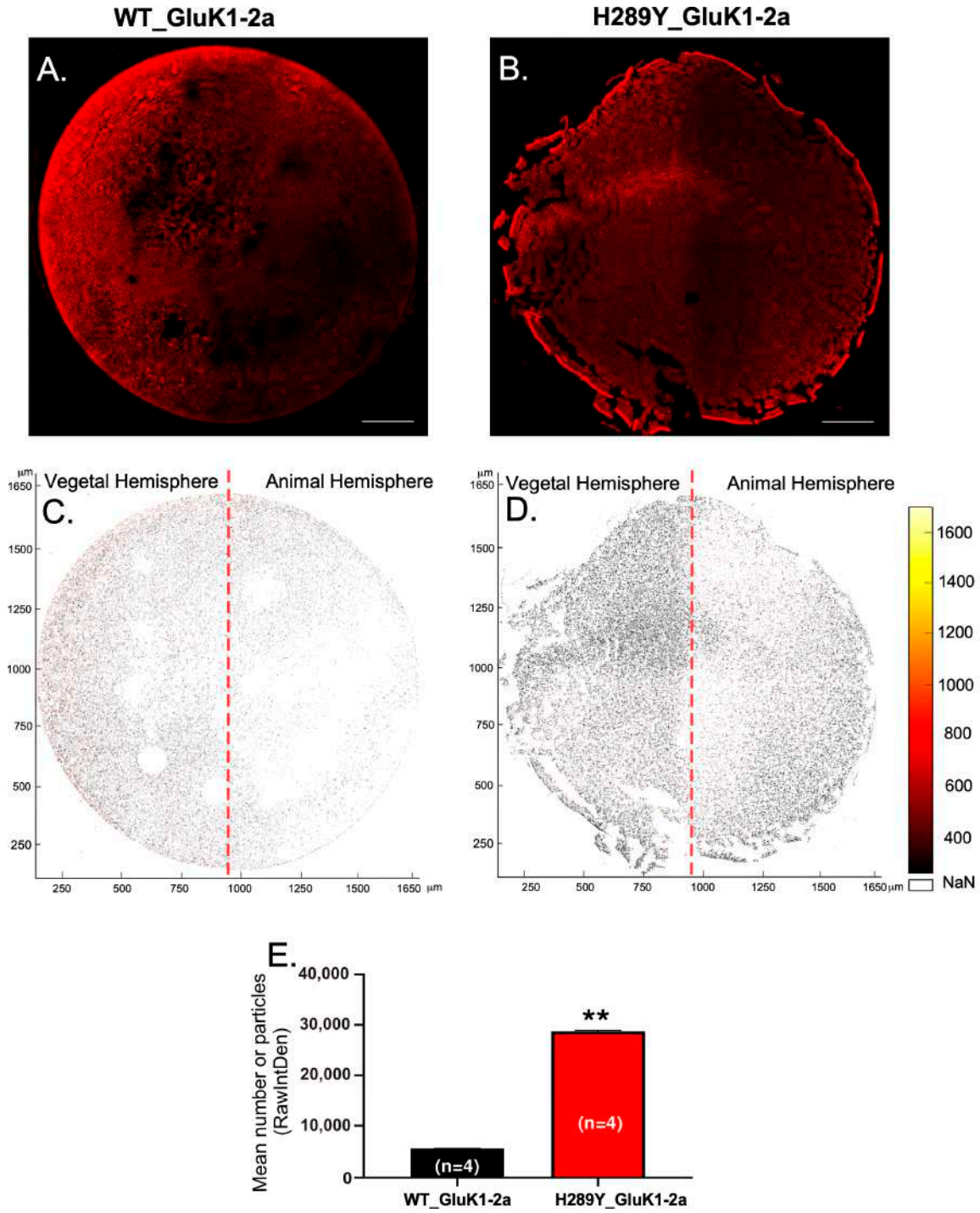

Figure 2. Distribution of GluK1-2a-immunolabeling in *Xenopus* oocytes containing WT GluK1-2a and H289Y GluK1-2a receptors. Representative confocal microscopy images showing GluK1-2a-immunolabeling in cross-sections of oocytes expressing WT GluK1-2a (**A**) and H289Y GluK1-2a (**B**) receptors. Scale bar = 200 µm. MATLAB maps of the oocyte cross-sections corresponding to panels A and B showing comparison of GluK1-2a-immunolabeling between WT GluK1-2a (**C**) and H289Y GluK1-2a (**D**) receptors. Inset in the right of the maps show the optical density-to-color calibration bars. NaN stands for not-a-number values. (**E**) Comparative levels of the sum of the values of the pixels (RawIntDen) corresponding to images (**C**,**D**). Each bar represents the mean number of particles ± hemistandard deviation (SEM). Statistical significance: ** $p < 0.01$.

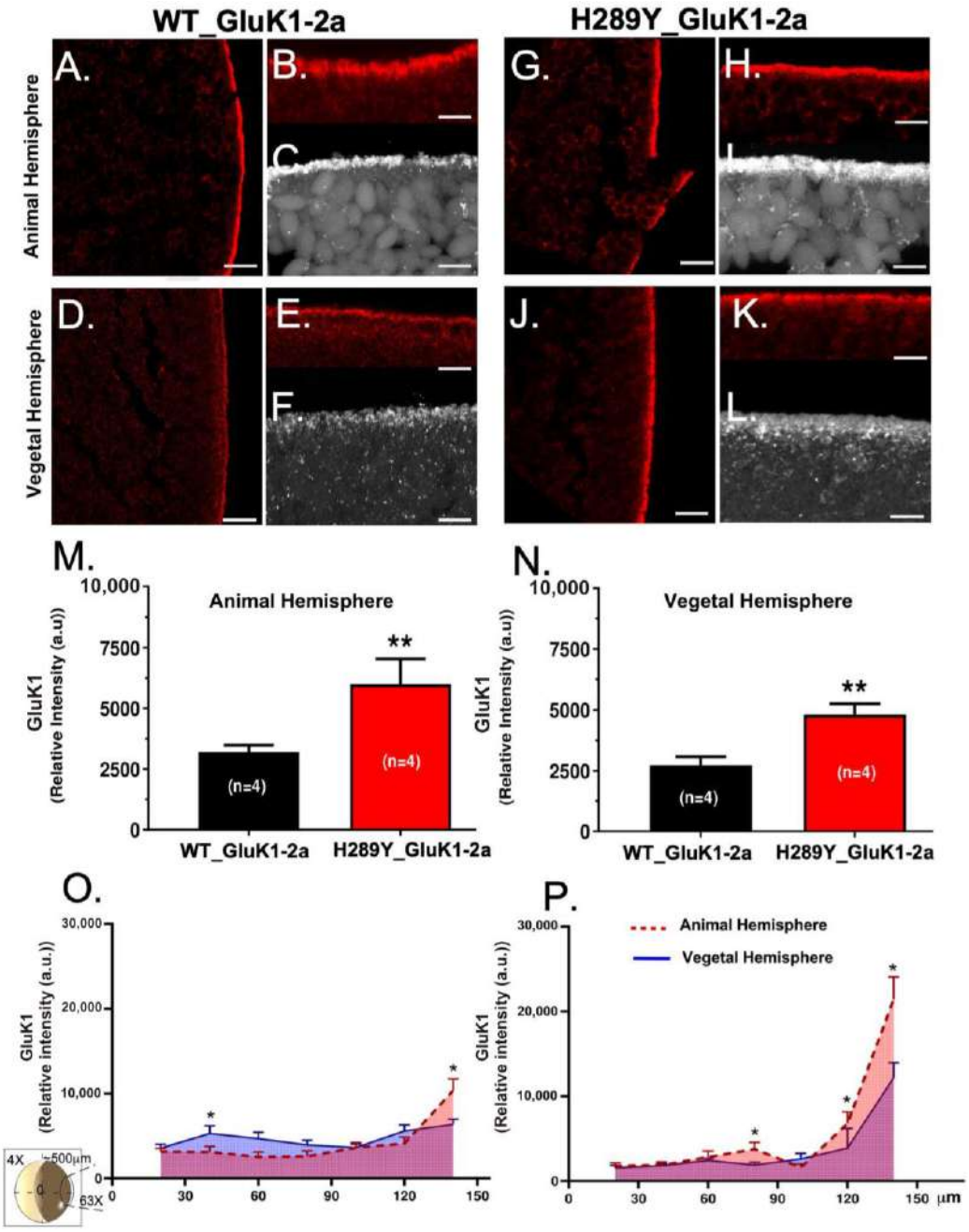

Figure 3. Confocal immunofluorescence micrographs showing representative cross-sections of animal and vegetal oocyte hemispheres. Immunolabeling for WT GluK1-2a (**A**–**F**) and H289Y GluK1-2a (**G**–**L**) receptors. Scale bar = 50 µm in (**A**,**D**,**G**,**J**) and 10 µm in (**B**,**C**,**E**,**F**,**H**,**I**,**K**,**L**). (**M**,**N**) Relative emission intensity levels (a.u.—arbitrary units—) of immunofluorescence for WT GluK1-2a and H289Y GluK1-2a receptors in the animal (**M**) and vegetal (**N**) oocyte hemispheres. Each bar represents the relative intensity ± SEM. (**O**,**P**) Expression levels vs. distribution of WT GluK1-2a (**O**) and H289Y GluK1-2a (**P**) receptors across 150 µm of the oocyte membrane (as indicated in the oocyte drawing in the left part of the panel). Each bar represents the relative intensity ± SEM. Statistical significance: * $p < 0.05$, ** $p < 0.01$.

2.3. The H289Y Mutation Enhances Kainate Currents in Oocytes Expressing GluK1-2aRs

The membrane conductance of uninjected oocytes was unaffected by bathing the cells for 5 s with Ka (up to 500 µM) while holding the membrane potential at −60 mV, in accordance with previous data [33]. Similarly, no Ka currents (I_{Ka}s) were evoked in oocytes previously microinjected with mRNAs coding for WT and H289Y GluK1-2b as

expected, due to the presence of the ER retention motif in these mRNAs [15]. However, the application of 100 µM Ka for 5 s elicited an inward I_{Ka} (Figure 4A, WT_GluK1-2a, black recording) in oocytes previously microinjected with WT GluK1-2a-encoding mRNA. Thus, these WT GluK1-2aRs were functionally incorporated in the membrane of 23 oocytes out of 51 (from four different donors), that is, 45.1% of the cells. A statistically significant increase in functional expression (χ^2-test, $p < 0.05$) was observed when the oocytes were microinjected with H289Y GluK1-2a-encoding mRNA. Actually, I_{Ka}s were evoked in 30 cells of 46 (63.2%; from four donors); see a representative I_{Ka} in Figure 4A (H289Y_GluK1-2a, red recording). The average amplitudes of the I_{Ka}s from oocytes incorporating either WT or H289Y GluK1-2a receptors were of -37.8 ± 8.3 nA and -61.0 ± 11.0 nA, respectively. No significant differences were found between both groups (Mann–Whitney rank-sum test, $p > 0.05$), most likely due to the large variability in I_{Ka}s among oocytes from different donors. For this reason, the I_{Ka} amplitude for each oocyte was normalized to the maximum I_{Ka} evoked in its corresponding donor. As shown in Figure 4B, the average percentage of the maximum I_{Ka} was significantly larger for oocytes that incorporated H289Y GluK1-2a receptors (40.5 ± 5.9%, red column; Mann–Whitney rank-sum test, $p < 0.05$) than those expressing WT GluK1-2a receptors (22.7 ± 4.1%, black column).

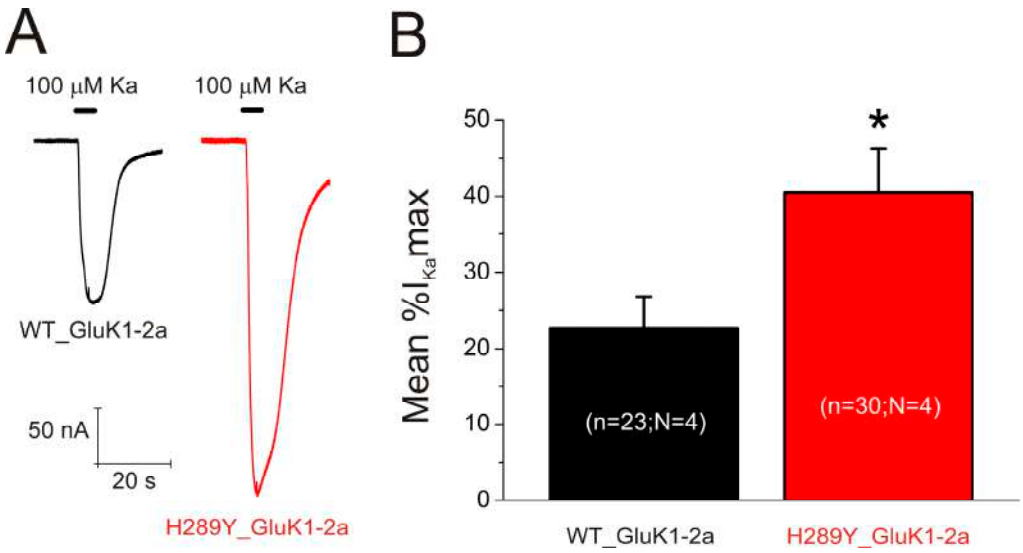

Figure 4. (**A**) Representative I_{Ka}s obtained through application of 100 µM kainate (Ka) for 5 s in two oocytes from the same donor, one injected with WT GluK1-2a-coding mRNA (left, black recording) and the other with H289Y GluK1-2a-coding mRNA (right, red recording). Henceforth, bars above the traces show the timing of agonist application, downward deflections represent inward currents, and, unless otherwise stated, the holding potential was −60 mV. (**B**) Bar diagram showing the average percentage of the normalized I_{Ka}s for cells incorporating either WT or H289Y GluK1-2a receptors. The asterisk (*) indicates significant differences between the two values ($p < 0.05$ in Mann–Whitney rank-sum test). "n" and "N" specify the number of oocytes and donors (frogs), respectively.

2.4. The H289Y Mutation Does Not Significantly Modify the Functional Properties of GluK1-2aRs

Firstly, to assess the possible effects of the H289Y single-point mutation in the functional properties of GluK1-2aRs, I_{Ka}s were obtained through the subsequent superfusion of different concentrations of Ka (1, 5, 10, 50, 100, and 500 µM) to oocytes bearing either WT (Figure 5A, black recordings) or H289Y (Figure 5A, red recordings) GluK1-2aRs. Figure 5B shows the relationship between the Ka concentration and I_{Ka} amplitude for WT (black solid symbols) and H289Y (red solid symbols) GluK1-2aRs after fitting the Hill equation curve to the experimental data. The estimated EC_{50} and n_H values of the fitted curve were 23 µM (CI = 9–26 µM) and 1.3 ± 0.3 for WT GluK1-2aR, respectively, and 12 µM (CI = 10–16 µM) and 1.3 ± 0.2 for H289Y GluK1-2aRs, respectively. Therefore, despite the slight shift to

the left of the curve of H289Y Gluk1-2aR, which could indicate an increase in the affinity and/or efficacy of Ka for these receptors, this was not a statistically significant effect.

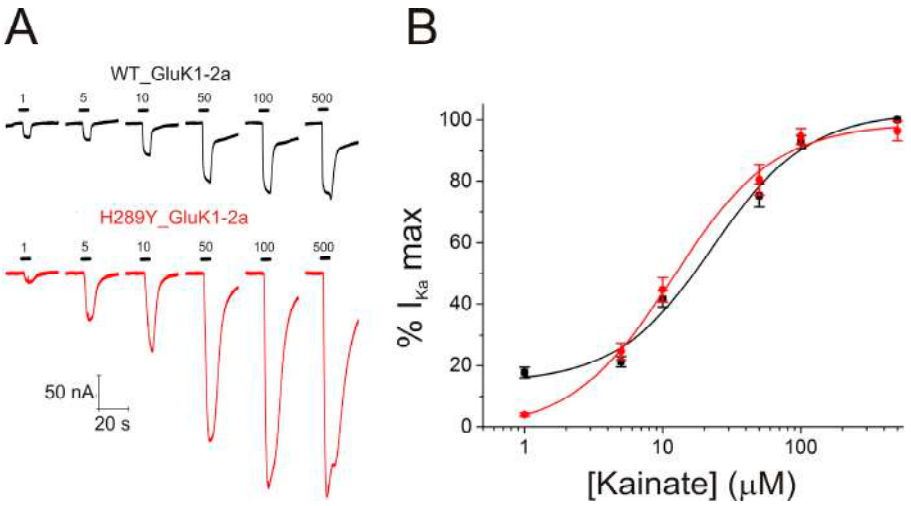

Figure 5. (**A**) Recordings obtained by applying 1, 5, 10, 50, 100, and 500 μM Ka to an oocyte bearing either WT (black recordings) or H289Y (red recordings) GluK1-2aRs. (**B**) Averaged Ka concentration–I_{Ka} amplitude curves for WT (black solid symbols; n = 4, N = 3) and H289Y (red solid symbols; n = 7, N = 3) GluK1-2aRs. Data were normalized to the maximal I_{Ka} elicited and the Hill equation was fitted to them (continuous lines).

Furthermore, we obtained current–voltage (I–V) relationships at the steady-state component of I_{Ka}s. For this, voltage jumps (from −120 to +60 mV, in 20 mV steps) were imposed on oocytes bearing either WT (Figure 6A, black recordings) or H289Y (Figure 6A, red recordings) GluK1-2aRs, while superfusing normal Ringer (NR) solution at the I_{Ka} plateau elicited by adding 100 μM Ka to the NR solution. The I–V curves of net I_{Ka}s elicited in both WT (Figure 6B, solid black symbols) and H289Y (Figure 6B, solid red symbols) GluK1-2aR groups showed a reversal potential close to 0 mV, indicating that channel-permeability properties were unaffected by the single point mutation H289Y. Likewise, the characteristic inwardly rectifying I–V shape of unedited forms of GluK1-2aR was maintained.

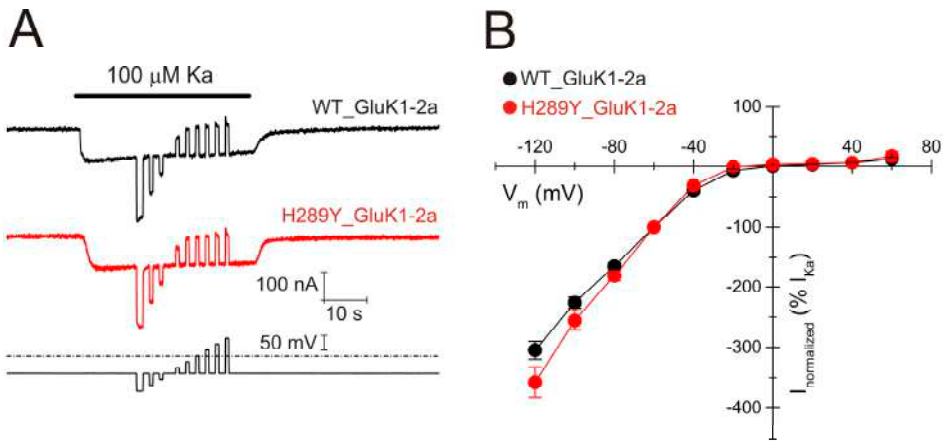

Figure 6. (**A**) I_{Ka}s evoked using 100 μM Ka when applying voltage pulses from −120 to +60 mV, as shown underneath, in oocytes bearing WT (black recording) or H289Y (red recording) GluK1-2aRs. (**B**) Net I–V relationship of I_{Ka}s elicited through the protocol shown in A. Black and red symbols are for I_{Ka}s elicited in oocytes that expressed WT (n = 7; N = 3) or H289Y (n = 6; N = 3) GluK1-2aRs, respectively. Net I_{Ka}s were normalized as the percentage of the I_{Ka} obtained at −60 mV.

3. Discussion

An SNP in the *Grik1* gene (C9586732T, p.H289Y) [25] has been previously reported in GASH/Sal hamsters, causing the GluK1Rs encoded by that gene to show the H289Y mutation located in the ATD (shown in Figure 1). Thus, in the present work, we evaluated the effects of this mutation on GluK1-2aRs through their heterologous expression in *Xenopus* oocytes. These receptors, after the microinjection of their coding mRNA, were expressed by the oocytes and incorporated in their membrane as homotetramers. We found differences between WT and H289Y GluK1-2aRs in terms of their incorporation and targeting to the oocyte membrane, as well as in the amplitude of the responses evoked with Ka, their agonist. The main results were as follows: (i) the H289Y mutation increases the expression and incorporation of GluK1-2aRs into an oocyte's membrane, as determined using confocal immunofluorescence microscopy, and this was higher in the animal hemisphere; (ii) this outcome was consistent with the increase in the functional expression and the percentage of maximum I_{Ka} obtained using the two-electrode voltage-clamp technique in oocytes bearing H289Y GluK1-2aRs; (iii) to our knowledge, we have characterized, for the first time, some of the electrophysiological properties of the GluK1-2aR from *Mesocricetus auratus*; and (iv), as predicted using sequence-homology based tools, the H289Y mutation does not modify the functional properties of GluK1-2aRs, and this result was confirmed in accordance with the results obtained from dose–response curves and I–V relationships.

Most of the disease-associated genetic variants affecting human *Grik* genes have been described for the *Grik2* gene, altering ATD (five variants) and TMD-linker domains (seven variants), while only two variants have been described for the *Grik1* gene, both of which affect the CTD [1]. Our results suggest that the H289Y gain-of-function mutation, located in the ATD of the GluK1-2aR from the GASH/Sal hamster, may be related with an important mechanism for the control of GluK1-2aR surface expression and, in particular, for regulating GluK1-2aR levels at synapses, even though this should be demonstrated in further research. Indeed, although many previous studies have already indicated the importance of the intracellular CTD for KARs trafficking and retention in the ER [34–37], as stated above (see Section 1), it is known that alterations in the ATD would contribute to changes in the regulation of the synaptic and surface expression of KARs [7]. However, the scarce studies describing the role of ATD regulating the membrane trafficking of KARs have been carried out by replacing a large number of amino acids in the ATD or even the whole domain [7,10], but not by a single-point mutation. Studies carried out in CA1 neurons hippocampus showed that the GluK1 receptors are completely excluded from synapses when a signal peptide interacts with ATD, but the replacement of either a signal peptide or the ATD domain with the corresponding GluK2 sequences enables GluK1 to appear on the neuronal surface and at the synapse [7]. Further research is needed to understand in detail the molecular mechanisms through which the H289Y mutation increases the expression and incorporation of GluK1-2a receptors into the plasma membrane. This should include studies to analyze the functional relevance of this mutation in a native system to know whether the increased protein expression will contribute to the diseased phenotype or not. Other studies are needed to decipher the possible effects of the H289Y mutation in the GluK1-2a receptor and its interaction with certain proteins, such as Neuropilin Tolloid-like 1 and Neuropilin Tolloid-like 2 (NETO1 and NETO2, respectively), among others, since GluK1 and GluK2 ATDs have been described to have a differential dependence on NETO proteins, which regulate extrasynaptic and synaptic trafficking [2,10].

In relation with the distribution of GluK1-2aRs in an oocyte's membrane, we observed that there was a higher presence of receptors in some points of the animal hemisphere plasma membrane. Oocytes were microinjected with mRNAs coding for GluK1-2aRs in the vegetal hemisphere close to the equator, as this is the best procedure reported [38]. It is known that native muscarinic acetylcholine receptors, ρ1 γ-aminobutyric acid (GABA) receptors, α7 nicotinic receptors, and GluA3 glutamate receptors expressed in the oocyte plasma membrane after the injection of their respective mRNAs, are all located mainly in the animal hemisphere [39–41]. However, cat and *Torpedo* nicotinic receptors, incorporated

in oocytes after mRNA microinjection, were preferentially inserted in the vegetal site [42]. Besides these heterogeneous expressions in the oocyte plasma membrane, which were more often in the animal hemisphere, another reported difference in the location has been whether the heterologous proteins were evenly distributed or by contrast were found in patches. In fact, when injecting membranes containing nicotinic receptors, they were incorporated in the oocyte membrane in patches; in contrast, a homogeneous distribution was found when the same receptors were incorporated after the injection of the corresponding mRNA [31,38]. The differential distribution of receptors between oocyte's hemispheres, like those now reported for WT and H289Y GluK1-2aRs, could be due to an uneven distribution of the translation machinery and subsequent translocation of the proteins to the plasma membrane, or to a pre-existence of some components which facilitate the binding of receptors to the plasma membrane [42].

As stated above, the H289Y mutation does not modify the functional properties of WT GluK1-2aRs, but this fact is not unexpected as the ATDs in KARs seem to minimally regulate their function, mainly due to the limited ATD–LBD interaction [1,43]. However, an improvement in the functional expression of mutated GluK1-2aRs in oocytes was observed, which was shown as an increase in the percentage of maximal I_{Ka}; this was in accordance with the results obtained using confocal immunofluorescence microscopy. Furthermore, the electrophysiological features of both WT and H289Y GluK1-2aRs from *M. auratus* resembled those of GluK1-2aRs from other species: (i) the EC_{50} values obtained in the dose-response curves matched those previously obtained by other authors. Sommer et al. [12] and Alt et al. [44] reported an EC_{50} of 33.6 and 21.3 μM using a whole-cell patch-clamp technique in HEK293 cells that transiently expressed rat and human GluK1-2aRs, respectively. (ii) We obtained a Hill coefficient (n_H) close to 1 for hamster GluK1-2aRs, suggesting that the binding of a single molecule of Ka to the LBD of a GluK1-2aR is enough to open its ion channel, in strong concordance with previously published data [44] ($n_H = 0.82 \pm 0.09$). (iii) The hamster GluK1-2aRs' I–V relationships showed the characteristic inwardly rectifying shape of unedited forms of GluK1-2aRs, which are sensitive to a polyamine blockade due to the presence of a glutamine (Q) within the pore, unlike when it is absent and a charged arginine is present in edited forms of GluK1-2aRs [12,16]. (iv) The reversal potential at 0 mV indicated that the ion channel was also similar to that described previously [12].

Several genetic variants associated with disease in humans have been described for *Grik* genes such as schizophrenia, intellectual disability, bipolar and movement disorders, autism, and epilepsy [1]. It is established that epilepsy is caused by an imbalance between inhibitory and excitatory neuronal signaling within the brain [45]. The main neurotransmitter mediating the excitatory conductance of nerve cells in the central nervous system is glutamate, which binds to AMPARs and NMDARs, which are present at most glutamatergic synapses, or KARs, which are much more selectively expressed, e.g., GluK1Rs are mainly expressed in the hippocampus, cortical interneurons, Purkinje cells, and sensory neurons [7,19,46]. Moreover, it has been described that KARs are related to epileptogenesis, as the net effect of their activation in vivo causes a decrease in GABA release, which, in turn, leads to an increase in excitability and thus epileptiform activity [47]. In this context, the use of the GASH/Sal strain as an animal model to study epilepsy is fundamental because it enables progress in the knowledge of the cellular and molecular bases that cause this disease in the animal under study, but also because it could be used to determine mechanisms equivalent to those that occur in humans [24].

In addition to the study presented here, our research group conducted in silico experiments utilizing protein 3D-structure modelling and various computational stability predictors. These experiments indicated, in accordance with the in silico predictions and functional data obtained in the present work, that the single-point mutation H289Y likely leads to protein stabilization by increasing the number of intermolecular interactions, as compared to the wild-type GluK1 receptor [48]. Concurrently, we observed a concentration of GluK1 immunoreactivity near the cell nucleus in brain structures associated with the GASH/Sal seizure neuronal network [48]. These combined findings support the asser-

tion made in our study that the mutation has the potential to alter the GluK1 trafficking mechanism while exerting a relatively minor influence on the functional properties of the receptor. The precise genetic alterations and molecular mechanisms contributing to audiogenic susceptibility in the GASH/Sal strain remain an ongoing area of investigation, necessitating further research. Nevertheless, our present study unequivocally demonstrates an increase in the expression and incorporation of functional GluK1 receptors into the oocyte's membrane, and this finding is supported by our immunolabeling and electrophysiological data. Probing the existence of functional receptors incorporated into the membrane is of paramount importance in determining whether the mutation present in the GASH/Sal hamster could have a genuine implication for epileptogenesis and other techniques, such as immunoblotting, which is used as a valuable tool for confirming protein levels, cannot surpass that given by the two techniques we have used in this work. On that basis, our hypothesis centers on the notion that the H289Y mutation in GluK1-2aRs may lead to an increased trafficking of these receptors to neuronal membrane sites within the circuit responsible for seizures, thereby favouring an excitatory imbalance of the neuronal activity in critical brain regions within the GASH/Sal model.

4. Materials and Methods

4.1. In Silico Prediction Tools

Two highly reliable in silico prediction tools, SIFT version 6.2.1 and iStable, were employed to evaluate the potential functional impact of the H289Y mutation on the GluK1 receptor. SIFT 6.2.1 assesses evolutionary conservation, predicting the tolerability or adverse effects of amino acid substitutions, thereby shedding light on functional alterations. Additionally, iStable utilizes machine-learning algorithms to forecast stability changes resulting from mutations, providing invaluable insights into structural modifications. These tools were specifically selected for their robustness in predicting both functional and stability alterations induced by mutations. The in silico assessment utilized the online sequence homology-based tools: SIFT version 6.2.1 (accessible at https://sift.bii.a-star.edu.sg/index.html, accessed on 8 November 2023) and iStable (accessible at http://predictor.nchu.edu.tw/iStable/, accessed on 8 November 2023).

4.2. Design of the Vector and Synthesis of mRNA Coding for Wild-Type and Mutant GluK1 Receptors

A cDNA fragment of *M. auratus* encompassing the gene encoding the GluK1 receptor (GenBank accession XM_005073843.3, *Grik1* subunit 1 isoform X1) was synthesized and cloned using GenScript Biotech (Rijswijk, The Netherlands). *Grik1* cDNA fragments, bearing either the WT sequence or the missense point mutation H289Y, were both synthesized and cloned into the pcDNA3.1 vector (Invitrogen, Waltham, MA, USA) using GenScript gene synthesis service, and yielded the plasmids pcDNA_*Grik1_WT* and pcDNA_*Grik1_H289Y*, respectively. The final constructs were verified using automated dideoxy DNA sequencing.

The plasmids were used as templates to obtain, using primer pairs T7ultra + Glu2R or T7ultra + Glu-trunca-1R, four PCR products: full-length *Grik1_WT* and *Grik1_H289Y*, and two truncated derivatives lacking the region coding for the ER retention motif described previously, namely, *Grik1_WT_nER* and *Grik1_H289Y_nER* [15,49–52].

Each of these purified PCR amplicons was then employed as a template in an in vitro transcription reaction using the mMessage mMachine T7 Transcription kit (Invitrogen, Waltham, MA, USA, AM1340) following the manufacturer's recommendations. After visualization through agarose gel electrophoresis, transcripts were subjected to polyadenylation using the Poly(A) Tailing kit (Invitrogen, Waltham, MA, USA, AM1350) to enhance stability. The effective increase in size for all four mRNA transcripts was verified through gel electrophoresis. Finally, a purification step was carried out using the MEGAclear™ Transcription Clean-Up Kit (Invitrogen, Waltham, MA, USA, AM1909) and quantification of purified mRNA was performed using Qubit (Invitrogen, Waltham, MA, USA).

4.3. Oocyte Microinjection with mRNA Coding for GluK1 Receptors

Adult female *Xenopus laevis* (purchased from European *Xenopus* Resource Centre at the University of Portsmouth, Portsmouth, UK) were immersed, during 15–20 min, in 0.17% tricaine methanesulfonate (MS-222) and a piece of ovary was removed under aseptic conditions. The study was conducted in accordance with the guidelines for the care and use of experimental animals adopted by the European Union (European Communities Council Directive of 22 September 2010, 2010/63/UE), and the animal protocol was approved by the Ethic Committee of Universidad de Alicante (protocol codes 2019/VSC/PEA/0097 type 2 from 25 April 2019, and 2023-VSC-PEA-0114 type 2 from 31 May 2023). The surrounding layers of isolated Dummont stage V and VI oocytes were removed manually with tweezers. Before use, cells were maintained inside an incubator at 15–16 °C in a modified Barth's solution (88 mM NaCl, 1 mM KCl, 2.40 mM $NaHCO_3$, 0.33 mM $Ca(NO_3)_2$, 0.41 mM $CaCl_2$, 0.82 mM $MgSO_4$, 10 mM HEPES (pH 7.4), 100 U/mL penicillin, and 0.1 mg/mL streptomycin). A total of 50 nL of solution, containing 30 ng of WT or H289Y GluK1-2a or GluK1-2b mRNAs, was microinjected in oocytes.

4.4. Oocyte Preparation, Processing, Immunostaining, and Imaging

4.4.1. Immunohistochemistry

Firstly, oocytes previously microinjected with mRNAs coding for full-length and truncated WT and mutant GluK1 receptors were fixed in 0.1 M phosphate-buffered saline (PBS) with 4% paraformaldehyde. Cells were then stored in this PBS until being embedded in paraffin. The oocytes were then serially sectioned at 10 µm using a sliding microtome (the total number of slides per cell was 12). Slides containing oocyte sections in the equatorial plane were selected for histological processing.

After selection of the slides, deparaffinization and antigen recovery were performed at 90 °C in 10 mM sodium citrate buffer at 0.05% with Tween 20 (pH 6.0). Slides were washed in Tris-buffered saline solution (TBS 0.5 M and then TBS 0.05 M), continuing with endogenous peroxidase inactivity. The samples were blocked for 2 h with 6% normal goat serum (Catalog No. S –1000, Vector Labs) in TBS-Tx dilutions of antisera in TBS 0.05 M containing Triton X-100 at 0.1% (Catalog No. T9284; Sigma, St. Louis, MO, USA). The washes were again realized with the TBS 0.5 M and then TBS 0.05 M. This technique included a simple procedure to quench autofluorescence of *Xenopus* and to remove surface pigment from oocytes which may have interfered with fluorescence imaging [53,54]. We followed a procedure previously described [55] to perform the preparation of 1% H_2O_2, 5% formamide (Catalog N°199837, Merk, Darmstadt, Germany) and 0.5 × SSC (0.75 M NaCl, 0.075 M Sodium Citrate) (Catalog N°51804, Sigma; Catalog N°7647-14-5, Panreac, Barcelona, Spain). To decolorize the oocytes they were depigmented in the photobleaching solution for 2 h under fluorescent light (~488–570 nm). Subsequently, the samples were washed in TBS 0.5 M and then TBS 0.05 M, and incubated with the primary antibodies rabbit anti-GluK1 (Catalog N°ab118891; Abcam, Cambridge, UK) in TBS-T × 0.1% at 1:1000 dilution for 72 h at 4 °C. This antibody has been effectively employed in our ongoing research on the GASH/Sal brain [48]. However, despite the fact that their reactivity was not tested in oocytes, a multisequence alignment analysis of GluK1 of distinct species demonstrated the high conservation of epitopes. The sections were then washed and this was followed by incubation with Alexa Flour™ 647 Goat anti-Rabbit IgG (catalog N°A21244; ThermoFisher, Waltham, MA, USA) at 1:750 dilution for 2 h. Finally, Vectashield® mounting medium was used to cover the sections and preserve their fluorescence, containing DAPI stain (4,6-diamidino-2-phenylindole, catalog N°H-1200, Vector Labs., Newark, CA, USA). Negative controls were not treated with primary antibodies, and this resulted in no immunolabeling.

4.4.2. Observation and Study of Histological Samples

A Leica Stellaris confocal laser coupled to a Leica DMI8 microscope (Leica Microsystems, Wetzlar, Germany) was used to study the sections processed for immunofluorescence. DyLight® 647 (red) and DAPI (violet) fluorochromes (Invitrogen, Waltham, MA, USA) were

detected sequentially, stack by stack, using the 647 and 405 nm laser spectral lines, respectively, and an acousto-optic beam splitter as a tunable dichroic filter system. In addition, the following lenses were used: ×4, ×10, and oil-immersion ×63/numerical aperture 1.40. With the aim of generate a maximal intensity z projection of stacks, a series of 10–15 confocal images was obtained to determine the distribution of the immunolabeled terminals.

4.5. Mapping of WT and H289Y GluK1-2a Proteins in Xenopus Oocytes

4.5.1. Image Analysis

The image analysis was conducted using ImageJ software (version 1.51g-v1.51n; Fiji package), an open-source tool routinely employed by our research group [56]. In this current image analysis, a comprehensive assessment of various parameters was undertaken. This encompassed the quantification of the product of area and mean gray value (IntDen), the summation of pixel values (RawIntDen), determination of particle area, and computation of mean and mode values for both X and Y coordinates. To ensure uniform visual comparisons among samples, all image processing operations were executed simultaneously. Notably, the original captured images remained unaltered in terms of brightness and contrast, preserving the integrity of the data.

4.5.2. MATLAB Maps

Employing MATLAB software (© MATLAB R-2017, MathWorks, Natick, MA, USA), extensive full-sections maps which encoded the location, area, and density of segmented particles were made. Using *Scatterplot* function and the MATLAB color scale "Hot", the RawIntDen was converted to color.

4.6. Two-Electrode Voltage-Clamp Recordings in Xenopus Oocytes

As previously described [57], oocyte membrane currents were recorded 48–72 h after mRNA microinjection. The solution that continuously superfused oocytes was a normal frog Ringer's (NR) solution composed of 2 mM KCl, 1.8 mM $CaCl_2$, 115 mM NaCl, and 5 mM HEPES, and it had pH 7.0. Unless otherwise stated, the membrane potential of oocytes was clamped at −60 mV. The currents elicited by Ka (I_{Ka}s) were sampled at five-fold the filter frequency (Digidata series 1440A and 1550; Axon Instruments, Foster City, CA, USA), low-pass filtered at 30–1000 Hz, and then recorded on two PCs using two appropriate software, WCP v. 4.8.6 (Strathclyde Electrophysiology Software, University of Strathclyde, Scotland, UK) and AxoScope v. 10.0.0.60 (Molecular Devices Corporation, Sunnyvale, CA, USA).

4.7. Experimental Design and Data Analysis of Functional Experiments

To characterize the functional profile of either WT or H289Y GluK1-2a receptors, Ka concentration–I_{Ka} amplitude curves were obtained by bathing GluK1-2a receptor-bearing oocytes with increasing Ka concentrations. I_{Ka}s were normalized to the maximum I_{Ka} and a sigmoid curve was fitted to these values (see equation 1 below). An interval of at least 3 min between consecutive Ka applications was maintained in order to avoid GluK1-2aRs desensitization. The current–voltage (I–V) curves were obtained by giving series of 800–1200 ms voltage pulses (from −120 to +60 mV, in 20 mV steps) to the oocyte before ligand superfusion and during the I_{Ka} plateau elicited by 100 µM Ka.

To obtain Ka concentration–I_{Ka} amplitude curves, GluK1-2a receptors were activated with different concentrations of Ka. The following form of the Hill Equation (1) was used to fit dose–response data:

$$I/I_{Ka}max = \left[1 + (EC_{50}/[Ka])^{n_H}\right]^{-1} \quad (1)$$

where I is the I_{Ka} amplitude elicited at a given concentration of Ka ($[Ka]$); EC_{50} is the agonist concentration required to halve the maximum I_{Ka}; $I_{Ka}max$ is the maximum I_{Ka} recorded; and n_H is the Hill coefficient.

Steady-state currents attained in NR (measured at the last 100 ms of the pulse) and recorded at each voltage were subtracted from the corresponding currents obtained in presence of 100 µM Ka, in order to compute net I–V curves for I_{Ka}. These values were then normalized to the I_{Ka}s recorded at −60 mV for each cell.

4.8. Statistical Analysis

Statistical analysis was performed to compare the number of immunoreactive particles between oocyte samples using GraphPad Prism 7 (GraphPad Software, Boston, MA, USA). A $p < 0.05$ was considered statistically significant. All quantitative data were expressed as mean value ± SEM. Asterisks indicate significant differences between experimental groups (* = p-value < 0.05; ** = p-value < 0.01; ***= p-value < 0.001).

For functional experiments, mean ± SEM are presented; the number of oocytes and oocyte donor (frogs) from which the data were obtained is indicated by "n" and "N", respectively. A Student's t-test was used when contrasting two group means of normally distributed values; otherwise, the Mann–Whitney rank-sum test was applied. When comparing two population proportions, an χ^2-test was used. A significance level of $p < 0.05$ was adopted in all cases.

4.9. Drugs

Reagents of general use were purchased from Scharlau Chemie S.A. (Barcelona, Spain); HEPES was purchased from Acros Organics (Geel, Belgium); and MS-222, penicillin, streptomycin, and Ka were purchased from Sigma-Aldrich (St. Louis, MO, USA).

Author Contributions: Conceptualization, S.M.D.-R., I.I., D.E.L. and A.A.-D.; methodology, S.M.D.-R., J.E., C.V. and A.A.-D.; software, S.M.D.-R., J.E. and A.A.-D.; validation, S.M.D.-R., I.I. and J.E. and A.A.-D.; formal analysis, S.M.D.-R. and A.A.-D.; investigation, S.M.D.-R., I.I., J.E., C.V. and A.A.-D.; resources, D.E.L. and A.A.-D.; data curation, S.M.D.-R. and A.A.-D.; writing—original draft preparation, S.M.D.-R. and A.A.-D.; writing—review and editing, S.M.D.-R., I.I., J.E., C.V., M.J.H.-T., D.E.L., R.G.-N. and A.A.-D.; visualization, S.M.D.-R., I.I., J.E., M.J.H.-T., D.E.L., R.G.-N. and A.A.-D.; supervision, I.I., M.J.H.-T., D.E.L. and A.A.-D.; project administration, D.E.L.; funding acquisition, D.E.L. All authors have read and agreed to the published version of the manuscript.

Funding: This study was supported by the Junta de Castilla y León SA075P20 (D.E.L.), co-financed by the ERDF "a way of making Europe", and by the Universidad de Alicante VIGROB-058. S.M.D.-R. held a predoctoral research fellowship in 2019 from JCyL (BOCYL, EDU/556/2019).

Institutional Review Board Statement: The study was conducted in accordance with the guidelines for the care and use of experimental animals adopted by the European Union (European Communities Council Directive of 22 September 2010, 2010/63/UE), and the animal protocol was approved by the Ethic Committee of Universidad de Alicante (protocol codes 2019/VSC/PEA/0097 type 2 from 25 April 2019, and 2023-VSC-PEA-0114 type 2 from 31 May 2023).

Data Availability Statement: Immunofluorescence and electrophysiological data are available on request.

Acknowledgments: We thank Andrés Morales for his valuable advice, his help with preliminary experiments, and his review of the draft; Cristóbal Almendros for his assistance with the *Grik1* vector; and Simón Moya for his expert technical assistance.

Conflicts of Interest: The authors declare no conflict of interest.

References

1. Hansen, K.B.; Wollmuth, L.P.; Bowie, D.; Furukawa, H.; Menniti, F.S.; Sobolevsky, A.I.; Swanson, G.T.; Swanger, S.A.; Greger, I.H.; Nakagawa, T.; et al. Structure, Function, and Pharmacology of Glutamate Receptor Ion Channels. *Pharmacol. Rev.* **2021**, *73*, 1469–1658. [CrossRef]
2. Lerma, J.; Paternain, A.V.; Rodríguez-Moreno, A.; López-García, J.C. Molecular Physiology of Kainate Receptors. *Phys. Rev.* **2001**, *81*, 971–998. [CrossRef]
3. Traynelis, S.F.; Wollmuth, L.P.; McBain, C.J.; Menniti, F.S.; Vance, K.M.; Ogden, K.K.; Hansen, K.B.; Yuan, H.; Myers, S.J.; Dingledine, R. Glutamate Receptor Ion Channels: Structure, Regulation, and Function. *Pharm. Rev.* **2010**, *62*, 405–496. [CrossRef]

4. Watkins, J.C.; Jane, D.E. The glutamate story. *Br. J. Pharm.* **2006**, *147*, S100–S108. [CrossRef] [PubMed]
5. Collingridge, G.L.; Olsen, R.W.; Peters, J.; Spedding, M. A nomenclature for ligand-gated ion channels. *Neuropharm.* **2009**, *56*, 2–5. [CrossRef] [PubMed]
6. Contractor, A.; Mulle, C.; Swanson, G.T. Kainate receptors coming of age: Milestones of two decades of research. *Trends Neurosci.* **2011**, *34*, 154–163. [CrossRef] [PubMed]
7. Duan, G.-F.; Ye, Y.; Xu, S.; Tao, W.; Zhao, S.; Jin, T.; Nicoll, R.A.; Shi, Y.S.; Sheng, N. Signal peptide represses GluK1 surface and synaptic trafficking through binding to amino-terminal domain. *Nat. Commun.* **2018**, *9*, 4879. [CrossRef]
8. Karakas, E.; Simorowski, N.; Furukawa, H. Structure of the zinc-bound amino-terminal domain of the NMDA receptor NR2B subunit. *EMBO J.* **2009**, *28*, 3910–3920. [CrossRef]
9. Rossmann, M.; Sukumaran, M.; Penn, A.C.; Veprintsev, D.B.; Babu, M.M.; Greger, I.H. Subunit-selective N-terminal domain associations organize the formation of AMPA receptor heteromers. *EMBO J.* **2011**, *30*, 959–971. [CrossRef] [PubMed]
10. Sheng, N.; Shi, Y.S.; Nicoll, R.A. Amino-terminal domains of kainate receptors determine the differential dependence on Neto auxiliary subunits for trafficking. *Proc. Natl. Acad. Sci. USA* **2017**, *114*, 1159–1164. [CrossRef] [PubMed]
11. Straub, C.; Noam, Y.; Nomura, T.; Yamasaki, M.; Yan, D.; Fernandes, H.B.; Zhang, P.; Howe, J.R.; Watanabe, M.; Contractor, A.; et al. Distinct Subunit Domains Govern Synaptic Stability and Specificity of the Kainate Receptor. *Cell Rep.* **2016**, *16*, 531–544. [CrossRef]
12. Sommer, B.; Burnashev, N.; Verdoorn, T.A.; Keinänen, K.; Sakmann, B.; Seeburg, P.H. A glutamate receptor channel with high affinity for domoate and kainate. *EMBO J.* **1992**, *11*, 1651–1656. [CrossRef] [PubMed]
13. Gregor, P.; O'Hara, B.F.; Yang, X.; Uhl, G.R. Expression and novel subunit isoforms of glutamate receptor genes GluR5 and GluR6. *Neuroreport* **1993**, *4*, 1343–1346. [CrossRef]
14. Barbon, A.; Barlati, S. Genomic organization, proposed alternative splicing mechanisms, and RNA editing structure of GRIK1. *Cytogenet. Cell Genet.* **2000**, *88*, 236–239. [CrossRef] [PubMed]
15. Han, Y.; Wang, C.; Park, J.S.; Niu, L. Channel-Opening Kinetic Mechanism of Wild-Type GluK1 Kainate Receptors and a C-Terminal Mutant. *Biochemistry* **2012**, *51*, 761–768. [CrossRef]
16. Bowie, D. Polyamine-mediated channel block of ionotropic glutamate receptors and its regulation by auxiliary proteins. *J. Biol. Chem.* **2018**, *293*, 18789–18802. [CrossRef] [PubMed]
17. Carta, M.; Fièvre, S.; Gorlewicz, A.; Mulle, C. Kainate receptors in the hippocampus. *Eur. J. Neurosci.* **2014**, *39*, 1835–1844. [CrossRef]
18. Sihra, T.S.; Flores, G.; Rodríguez-Moreno, A. Kainate Receptors. *Neuroscientist* **2014**, *20*, 29–43. [CrossRef]
19. Lerma, J.; Marques, J.M. Kainate Receptors in Health and Disease. *Neuron* **2013**, *80*, 292–311. [CrossRef]
20. Lucarini, N.; Verrotti, A.; Napolioni, V.; Bosco, G.; Curatolo, P. Genetic Polymorphisms and Idiopathic Generalized Epilepsies. *Pediatr. Neurol.* **2007**, *37*, 157–164. [CrossRef]
21. Kandratavicius, L.; Balista, P.A.; Lopes-Aguiar, C.; Ruggiero, R.N.; Umeoka, E.H.; Garcia-Cairasco, N.; Bueno-Junior, L.S.; Leite, J.P. Animal models of epilepsy: Use and limitations. *Neuropsychiatr. Dis. Treat.* **2014**, *10*, 1693. [CrossRef]
22. Muñoz, L.J.; Carballosa-Gautam, M.M.; Yanowsky, K.; García-Atarés, N.; López, D.E. The genetic audiogenic seizure hamster from Salamanca: The GASH:Sal. *Epilepsy Behav.* **2017**, *71 Pt B*, 181–192. [CrossRef]
23. Carballosa-Gonzalez, M.M.; Muñoz, L.J.; López-Alburquerque, T.; Pardal-Fernández, M.J.; Nava, E.; de Cabo, C.; Sancho, C.; López, D.E. EEG characterization of audiogenic seizures in the hamster strain GASH:Sal. *Epilepsy Res.* **2013**, *106*, 318–325. [CrossRef] [PubMed]
24. Díaz-Rodríguez, S.M.; López-López, D.; Herrero-Turrión, M.J.; Gómez-Nieto, R.; Canal-Alonso, A.; Lopéz, D.E. Inferior Colliculus Transcriptome After Status Epilepticus in the Genetically Audiogenic Seizure-Prone Hamster GASH/Sal. *Front. Neurosci.* **2020**, *14*, 508. [CrossRef] [PubMed]
25. Díaz-Casado, E.; Gómez-Nieto, R.; de Pereda, J.M.; Muñoz, L.J.; Jara-Acevedo, M.; López, D.E. Analysis of gene variants in the GASH/Sal model of epilepsy. *PLoS ONE* **2020**, *15*, e0229953. [CrossRef] [PubMed]
26. Lipsky, R.H.; Goldman, D. Genomics and variation of ionotropic glutamate receptors. *Ann. N. Y. Acad. Sci.* **2003**, *1003*, 22–35. [CrossRef] [PubMed]
27. Wang, J.; Lin, Z.J.; Liu, L.; Xu, H.Q.; Shi, Y.W.; Yi, Y.H.; He, N.; Liao, W.P. Epilepsy-associated genes. *Seizure* **2017**, *44*, 11–20. [CrossRef] [PubMed]
28. International League Against Epilepsy Consortium on Complex Epilepsies. Genome-wide mega-analysis identifies 16 loci and highlights diverse biological mechanisms in the common epilepsies. *Nat. Commun.* **2018**, *9*, 5269. [CrossRef] [PubMed]
29. Sander, T.; Hildmann, T.; Kretz, R.; Fürst, R.; Sailer, U.; Bauer, G.; Schmitz, B.; Beck-Mannagetta, G.; Wienker, T.F.; Janz, D. Allelic association of juvenile absence epilepsy with a GluR5 kainate receptor gene (GRIK1) polymorphism. *Am. J. Med. Genet.* **1997**, *74*, 416–421. [CrossRef]
30. Friedman, D.; Kannan, K.; Faustin, A.; Shroff, S.; Thomas, C.; Heguy, A.; Serrano, J.; Snuderl, M.; Devinsky, O. Cardiac arrhythmia and neuroexcitability gene variants in resected brain tissue from patients with sudden unexpected death in epilepsy (SUDEP). *NPJ Genom. Med.* **2018**, *3*, 9. [CrossRef]

31. Ivorra, I.; Alberola-Die, A.; Cobo, R.; González-Ros, J.M.; Morales, A. Xenopus Oocytes as a Powerful Cellular Model to Study Foreign Fully-Processed Membrane Proteins. *Membranes* **2022**, *12*, 986. [CrossRef] [PubMed]
32. Min, L.; Nie, M.; Zhang, A.; Wen, J.; Noel, S.D.; Lee, V.; Carroll, R.S.; Kaiser, U.B. Computational Analysis of Missense Variants of G Protein-Coupled Receptors Involved in the Neuroendocrine Regulation of Reproduction. *Neuroendocrinology* **2016**, *103*, 230–239. [CrossRef] [PubMed]
33. Schmidt, C.; Klein, C.; Hollmann, M. *Xenopus laevis* oocytes endogenously express all subunits of the ionotropic glutamate receptor family. *J. Mol. Biol.* **2009**, *390*, 182–195. [CrossRef]
34. Coussen, F. Molecular determinants of kainate receptor trafficking. *Neuroscience* **2009**, *158*, 25–35. [CrossRef] [PubMed]
35. Jaskolski, F.; Coussen, F.; Mulle, C. Subcellular localization and trafficking of kainate receptors. *Trends Pharmacol. Sci.* **2005**, *26*, 20–26. [CrossRef] [PubMed]
36. Ren, Z.; Riley, N.J.; Garcia, E.P.; Sanders, J.M.; Swanson, G.T.; Marshall, J. Multiple trafficking signals regulate kainate receptor KA2 subunit surface expression. *J. Neurosci.* **2003**, *23*, 6608–6616. [CrossRef]
37. Yan, S.; Sanders, J.M.; Xu, J.; Zhu, Y.; Contractor, A.; Swanson, G.T. A C-terminal determinant of GluR6 kainate receptor trafficking. *J. Neurosci.* **2004**, *24*, 679–691. [CrossRef]
38. Eusebi, F.; Palma, E.; Amici, M.; Miledi, R. Microtransplantation of ligand-gated receptor-channels from fresh or frozen nervous tissue into Xenopus oocytes: A potent tool for expanding functional information. *Prog. Neurobiol.* **2009**, *88*, 32–40. [CrossRef]
39. Kusano, K.; Miledi, R.; Stinnakre, J. Cholinergic and catecholaminergic receptors in the *Xenopus* oocyte membrane. *J. Physiol.* **1982**, *328*, 143–170. [CrossRef]
40. Martinez-Torres, A.; Miledi, R. Expression of gamma-aminobutyric acid rho 1 and rho 1 Delta 450 as gene fusions with the green fluorescent protein. *Proc. Natl. Acad. Sci. USA* **2001**, *98*, 1947–1951. [CrossRef]
41. Palma, E.; Mileo, A.M.; Martinez-Torres, A.; Eusebi, F.; Miledi, R. Some properties of human neuronal alpha 7 nicotinic acetylcholine receptors fused to the green fluorescent protein. *Proc. Natl. Acad. Sci. USA* **2002**, *99*, 3950–3955. [CrossRef] [PubMed]
42. Miledi, R.; Sumikawa, K. Synthesis of cat muscle acetylcholine receptors by Xenopus oocytes. *Biomed. Res.* **1982**, *3*, 390–399. [CrossRef]
43. Meyerson, J.R.; Chittori, S.; Merk, A.; Rao, P.; Han, T.H.; Serpe, M.; Mayer, M.L.; Subramaniam, S. Structural basis of kainate subtype glutamate receptor desensitization. *Nature* **2016**, *537*, 567–571. [CrossRef] [PubMed]
44. Alt, A.; Weiss, B.; Ogden, A.M.; Knauss, J.L.; Oler, J.; Ho, K.; Large, T.H.; Bleakman, D. Pharmacological characterization of glutamatergic agonists and antagonists at recombinant human homomeric and heteromeric kainate receptors in vitro. *Neuropharmacology* **2004**, *46*, 793–806. [CrossRef]
45. Chen, T.-S.; Huang, T.-H.; Lai, M.-C.; Huang, C.-W. The Role of Glutamate Receptors in Epilepsy. *Biomedicines* **2023**, *11*, 783. [CrossRef]
46. Ojanen, S.; Kuznetsova, T.; Kharybina, Z.; Voikar, V.; Lauri, S.E.; Taira, T. Interneuronal GluK1 kainate receptors control maturation of GABAergic transmission and network synchrony in the hippocampus. *Mol. Brain* **2023**, *16*, 43. [CrossRef] [PubMed]
47. Falcón-Moya, R.; Sihra, T.S.; Rodríguez-Moreno, A. Kainate Receptors: Role in Epilepsy. *Front. Mol. Neurosci.* **2018**, *11*, 217. [CrossRef]
48. Díaz-Rodríguez, S.M.; Herrero-Turrión, M.J.; García-Peral, C.; Gómez-Nieto, R. Delving into the Significance of the His289Tyr Single-Nucleotide Polymorphism in the Glutamate Ionotropic Receptor Kainate-1 (Grik1) Gene of a Genetically Audiogenic Seizure Model. *Front. Mol. Neurosci.* **2023**, *in press*.
49. Hayes, D.M.; Braud, S.; Hurtado, D.E.; McCallum, J.; Standley, S.; Isaac, J.T.; Roche, K.W. Trafficking and surface expression of the glutamate receptor subunit, KA2. *Biochem. Biophys. Res. Commun.* **2003**, *310*, 8–13. [CrossRef]
50. Nasu-Nishimura, Y.; Hurtado, D.; Braud, S.; Tang, T.T.; Isaac, J.T.; Roche, K.W. Identification of an endoplasmic reticulum-retention motif in an intracellular loop of the kainate receptor subunit KA2. *J. Neurosci.* **2006**, *26*, 7014–7021. [CrossRef]
51. Ren, Z.; Riley, N.J.; Needleman, L.A.; Sanders, J.M.; Swanson, G.T.; Marshall, J. Cell Surface Expression of GluR5 Kainate Receptors Is Regulated by an Endoplasmic Reticulum Retention Signal. *J. Biol. Chem.* **2003**, *278*, 52700–52709. [CrossRef]
52. Vivithanaporn, P.; Yan, S.; Swanson, G.T. Intracellular trafficking of KA2 kainate receptors mediated by interactions with coatomer protein complex I (COPI) and 14-3-3 chaperone systems. *J. Biol. Chem.* **2006**, *281*, 15475–15484. [CrossRef] [PubMed]
53. Lee, C.; Kieserman, E.; Gray, R.S.; Park, T.J.; Wallingford, J. Whole-Mount Fluorescence Immunocytochemistry on *Xenopus* Embryos. *Cold Spring Harb. Protoc.* **2008**, *2008*, pdb.prot4957. [CrossRef] [PubMed]
54. Kumar, S.; Dunsby, C.; De Beule, P.A.; Owen, D.M.; Anand, U.; Lanigan, P.M.; Benninger, R.K.; Davis, D.M.; Neil, M.A.; Anand, P.; et al. Multifocal multiphoton excitation and time correlated single photon counting detection for 3-D fluorescence lifetime imaging. *Opt. Express* **2007**, *15*, 12548. [CrossRef] [PubMed]
55. Paulina, R.H.; Manuel, K.P. Produccion de Anticuerpos Policlonales Contra el Silenciador de la Transcripcion del Elemento Represor (Rest) de *Xenopus laevis*. Bachelor's Thesis, Universidad de Chile, Santiago de Chile, Chile, 2005.